The Role Of HPV E6 Protein In The Induction Of Autophagy

Ghadir Almuhaini

Hertford College

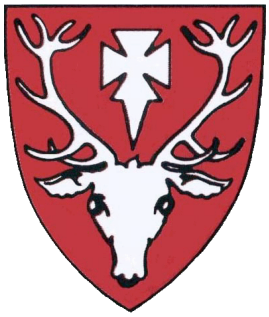

A thesis submitted to the Medical Sciences Division of the University of Oxford in partial fulfilment of the requirements for the Degree of Doctor of Philosophy

Michaelmas Term 2014

Department of Oncology
The Weatherall Institute of Molecular Medicine
University of Oxford

Abstract

Non-Melanoma skin cancer is the most common cancer in Caucasians. Accumulating evidence suggest a strong role for β-HPV (mainly HPV5 and HPV8) in the development of NMSC alongside UV, the main etiologic agent. The HPV genome encodes two potent oncoproteins, E6 and E7. HPV E6 protein has been shown to inhibit mitochondrial apoptosis following UVB exposure by specifically targeting BAK, a key apoptotic protein for proteolysis. A cross talk exists between the apoptotic pathway and the cellular survival pathway, autophagy. Where both autophagy and apoptosis can be triggered by common upstream signals. Additionally, cell lacking BAK and BAX respond with autophagy following the receipt of an apoptotic stimulus.

The aim of this work was to investigate if HPV E6 may induce autophagy in response to an apoptotic stimulus.

Cells expressing HPV5 E6 protein were exposed to UVB and autophagy levels, as well as autophagic flux, were investigated using endogenous LC3 staining, LC3 immunoblots and electron microscopy. Results showed an increase in autophagic flux and autophagy levels in HPV5 E6 expressing cells upon UV irradiation. Furthermore, the modulation of autophagy was demonstrated to be a conserved function amongst high-risk HPV (8, 20, 38 and mucosal HPV 16 and 18). Moreover, inhibition of autophagy resulted in a marked decrease in the viability of cells expressing E6 from HPV types 5 and 8. Furthermore, examining the respiration status of HPV5 E6 expressing cells showed a marked increase in both the glycolytic and the oxidative phosphorylation pathways.

These results indicate that HPV E6 may promote autophagy following an apoptotic stimulus allowing the cells to survive in the background of DNA damage and that may contribute towards tumorigenesis.

Acknowledgements

First, I would like to express my deepest appreciation for my supervisor Dr. Alan Storey, for providing me with the opportunity me to work on this D.Phil. project, and allowing me to travel and present this work at multiple conferences. His mentorship, guidance and encouragement were truly valuable and have allowed me to grow as a research scientist. My deepest gratitude also goes for my supervisor Dr. Katja Simon for her continuous support, encouragement and for including me in a wonderful lab retreat. My appreciation goes to Dr. Peter McHugh for welcoming me in to his lab (by that I mean allowing me to take over a whole area!), for all the useful discussions and for tolerating my endless questions.

My gratitude goes to my collaborators Dr. Baki Akgül and Dr. Martin Hufbauer for their help with the *in vivo* experiments and for inviting me to Koln to present my work. I would also like to thank Dr. Ioannis Roxanis for his help with scoring immunohistochemistry slides and professor David Ferguson for electron microscopy work.

Working with three different research groups has allowed me to interact with a great number of talented people, many of whom have become good friends. First, I would like to thank all the past members of the Storey lab: Abul Azad, Joanna Fox for their continued help and great company and particularly Amy Holloway for a healthy dose of cynicism and casual dance in the lab Thursdays. I would also like to thank all the members of the McHugh lab and the Simon lab for their entertaining company and valuable scientific discussions.

I am mostly grateful for all the friends I made in Oxford who have made the past few years quite an adventure! I am especially thankful for Marta for her willingness

to part-take in ‘fun-times’, even a slow-motion fight! I am also thankful for my dear friend Ulrike, for her support, great company and for always asking WHY?
I would like to thank all my friends back home and particularly Rawa and Mesheal, your friendship is truly valuable. I would also like to thank all the members of Gahwat Alsa’ada for good entertainment value whenever I go to visit home.

I am thankful most of all for my wonderful family, I wouldn’t have done It without them. I am grateful for my mother, who has always provided financial and emotional support and encouraged me to peruse this D.Phil., thank you mum you make my dreams a reality. I am very thankful for, Ghada, Noura, Ibrahim, Munera, Sara, Saud and Nany for their love and continued support. I would also like to thank Ghada and Noura for producing such wonderful offspring that always made me laugh and gave an excuse to watch Disney movies.
Lastly, I would have never gotten this far in my career if it wasn’t for my late father Abdulaziz, whose words of wisdom still inspire me.

Table of Contents

List of Figures

List of Tables

Abbreviations

Atg	Autophagy related
AMBRA1	Autophagy/beclin-1 regulator 1
ACD	Autophagic cell death
BAK	Bcl-2-antagonist/killer 1
BAF	Bafilomycin A1
BCC	Basal cell carcinoma
Bcl-2	B cell lymphoma 2
BAX	Bcl-2 associated X protein
CER	Complete early region
CIS	Carcinoma *in situ*
CQ	Chloroquine
DDR	DNA damage response
DISC	Death inducing signalling complex
ER	Endoplasmic reticulum
EV	*Epidermodysplasia verruciformis*
FACS	Fluorescence-activated cell sorting
FADD	Fas associated death domain
HGSIL	High Grade Intra-epithelial Lesion
HPV	Human papillomaviruses
LC3	Microtubule- associated protein 1 light chain 3
LGSIL	Low Grade Intra- epithelial Lesion

MOMP	Mitochondrial outer membrane permeabilisation
mTORC	Mammalian target of rapamycin complex
NMSC	Non-melanoma skin cancer
NER	Nucleotide excision repair
PM1	Premalignant keratinocytes
PI	Propidium iodide
SCC	Squamous cell carcinoma
TCA	Tri-carboxylic acid cycle
TEM	Transmission electron microscopy
TG	Thapsigargin
UV	Ultraviolet light irradiation
ULK1	Unc51-like kinase 1

Chapter 1 Introduction

1.1 Human Papillomaviruses

Human papillomaviruses are small DNA viruses of the *Papillomaviridea* family that strictly infect the stratified epithelial tissue and cause different epithelial lesions. They are non-enveloped viruses with an icosahedral capsid about 55nm in diameter and contain a small dsDNA with cellular histones. The HPV genome is about 8kb and is divided into three regions, the upstream non-coding region (NCR) that contains the origin of replication but does not encode for any proteins. The late region encodes for two capsid proteins L1 and L2, and the early region codes for E1, E2, E4, E5, E6 and E7, who's functions are discussed in 1.1.3.

There are more than 150 different types of HPV and they are divided into five different genera based on DNA sequence analysis of the L1 gene: Alpha, Beta, Gamma, Mu and Nu. These HPV types harbor different epithelial tropisms and disease associations Figure 1-1 (Bernard et al. 2010). α-HPVs have a particular tropism for mucosal epithelium, and generally do not cause cutaneous squamous cell carcinomas outside of the anogenital area. The mucosal HPVs are further divided into high and low risk based on their oncogenic potential. High-risk α-HPV types are identified as the main causative agent for cervical cancer, with HPV DNA detected in more than 99% of the disease. In contrast, low risk HPVs cause benign genital warts. The β-group are cutaneous HPVs that are typically associated with asymptomatic cutaneous lesions. However, accumulating evidence suggest that β-genus HPV have a co-factorial role in the development of non-melanoma skin cancer (NMSC) alongside UV (the main focus of this work and are described in more detail in (1.2.2). Gamma, Mu and Nu are also cutaneous HPV types that cause benign cutaneous lesions and are rarely found in skin cancer.

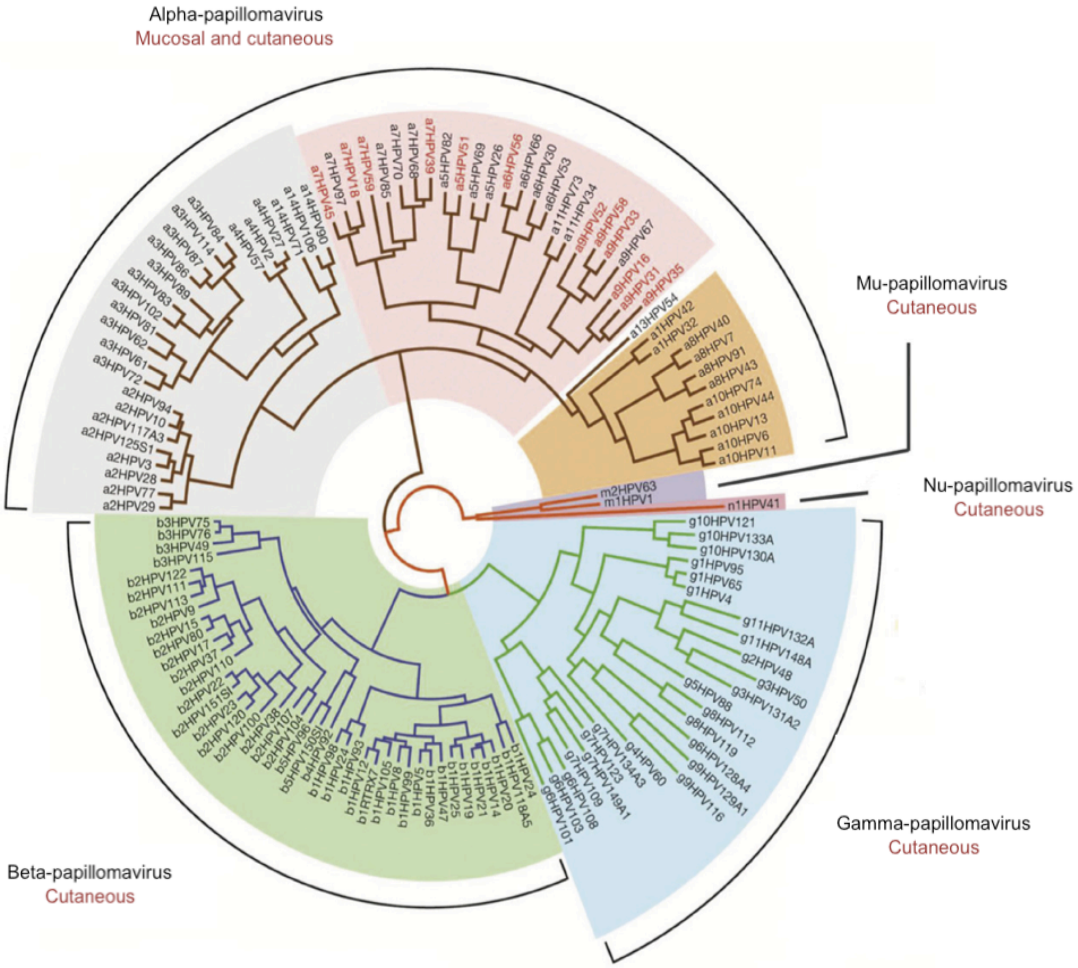

Figure 1-1 Phylogenetic tree of HPV

HPV consisting of five different groups based the L1 gene nucleotide sequence. Alpha-HPVs are mostly mucosal with some types infecting cutaneous tissue. Beta-HPVs are cutaneous viruses that are associated with the development of non-melanoma skin cancer. Gamma, Mu and Nu HPVs are typically associated with benign cutaneous lesions. Adapted from (Doorbar et al. 2012)

α-HPV of the high-risk types include; 51 (α5); 56, 66 (α6); 18, 39, 45, 59 (α7); 16, 31, 33, 35, 52, and 58 (α9), and are the causative agents of cervical cancer (Muñoz 2000), with HPV16 and 18 being the most frequently detected (around 70% of the cases). In addition to cervical cancer, HPV16 and 18 are also detected in about 50% of penile carcinomas, 43% vulvar carcinomas and 70% of vaginal cancers

(Forman et al. 2012; Gillison et al. 2013). Additionally HPV16 is found in 50% of head and neck cancers in America (Jayaprakash et al. 2011).

Low-risk α-HPVs include; 6, 11, 44 (α10); 40, 43 (α8); 42 (α1); 61, 72, 81 (α3). These types typically cause benign genital warts with HPV6 and 11 being the most predominant. HPV 11 also causes Recurrent Respiratory Papillomatosis (RRP), a disease in which tumours grow in the air passages leading from the nose and mouth into the lungs (Tjon Pian Gi et al. 2014).

HPVs are transmitted by contact and in the case of cervical cancer, the virus is sexually transmitted. Although infection with high-risk HPVs is a prerequisite for cervical cancer development, not all HPV infections proceed to malignancy. In most cases, infection with HPV results in the development of Low Grade Intra-epithelial Lesion (LGSIL), these are flat and inconspicuous lesions, where infectious viral particles are produced. These lesions spontaneously regress within 18 months (Stockman 2006). However, the persistence of HPV infection drives cell proliferation at the sites of infection in the basal and the suprabasal layers, resulting in cellular abnormality and the formation of High Grade Intra-epithelial Lesion (HGSIL) that is the precursor lesion for invasive carcinoma (Schiffman & Kjaer 2003).

The burden of cervical cancer was greatly reduced due to the introduction of organised Papanicolaou cervical cancer-screening programs in the developed world. However, cervical cancer remains the third most common cancer in women world wide; 530,000 cases per year with 275,000 deaths, 80% of which are in the developing world (Forman et al. 2012).

The focus of this work is on the β-HPVs that infect the cutaneous epithelium. Aiming to shed light on the transformation potential of β-HPVs and their possible role in NMSC, the structure of the skin, NMSC carcinogenesis and the life cycle of the virus are further described below.

1.1.1 The skin

1.1.1.1 Structure and function

The HPV life cycle is closely associated with the keratinocytes life cycle and differentiation, thus this section aims to describe the structure and function of the skin.

The skin is the largest organ, comprising 16% of the total body. The skin mainly functions as a protective barrier to the inner and more vulnerable organs; additionally the skin has many regulatory functions such as regulating body temperature through sweat and hair, maintaining homeostasis, Vitamin D synthesis, protection from ultraviolet light irradiation (UV) and microbial and mechanical insults (Zmijewski & Slominski 2011; Slominski et al. 2003).The skin is divided into two main layers: the outer epidermis and the inner dermis that includes hair, nails, sensory nerve receptors and sweat and sebaceous glands.

The epidermis is separated from the dermis by a basement membrane, and is comprised primarily of non-vascularised keratinising stratified squamous epithelium. Alongside keratinocytes, the epidermis also contains: Langerhans cells (dendritic cells), Merkel cells (sensory cells) and melanocytes (melanin producing cells). In the epidermis keratinocytes undergo a distinct form of cell death termed: terminal differentiation where proliferative cells are converted into highly differentiated non-dividing cells that ultimately give rise to a thick non-living cornified envelope (Eckhart et al. 2013). Keratinocytes at different stages of differentiation make up four distinct layers in the epidermis: stratum basale, stratum spinosum, stratum granulosum and stratum cornuem (Figure 1-2).

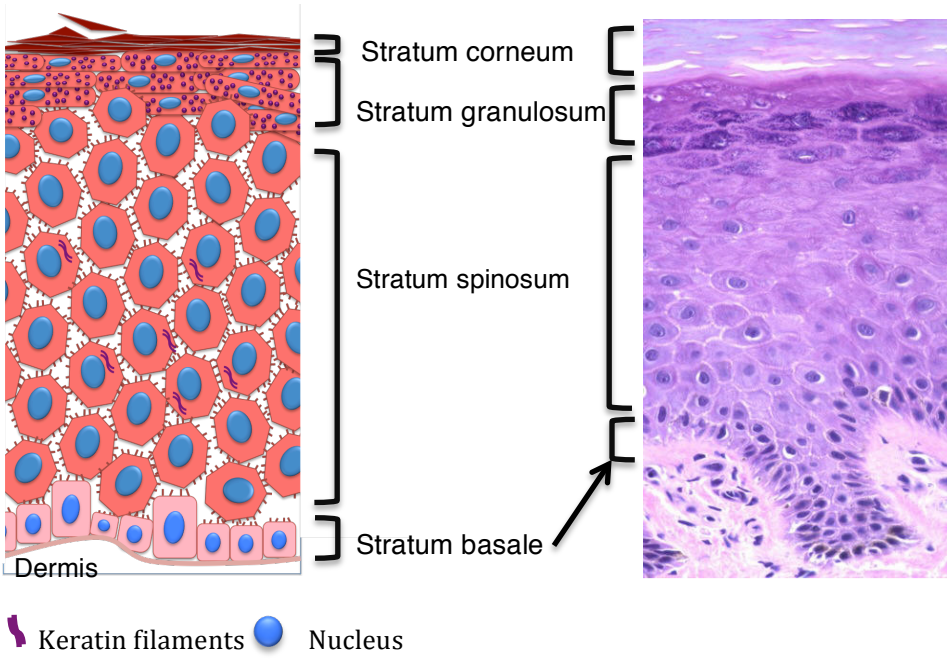

Figure 1-2 Layers of the epidermis

The epidermis consists of four layers that are characterised by keratinocytes at different stages of differentiation: stratum basale stratum spinosum, stratum granulosum and stratum corneum. The stratum basale is comprised of dividing basal cells that are attached to the basement membrane. As the cells differentiate they lose their proliferative capacity and move towards the outmost stratum cornuem where they detach. Adapted from (Eckhart et al. 2013)

1.1.1.2 Keratinocyte differentiation

The continuous self-renewal of the epidermis is dependent on keratinocyte stem cells residing in the interfollicular epidermis (Pincelli & Marconi 2010). Through asymmetric cell division keratinocytes stem cells produce transiently proliferating basal cells that reside on the basement membrane (stratum basale), which ultimately undergo terminal differentiation (Jones & Watt 1993; Lechler & Fuchs 2005). One of the key factors in epithelial stratification and keratinocytes differentiation is calcium gradient throughout the epidermis that is sustained predominantly by extracellular calcium concentration and intracellular calcium stores localized in the ER and the Golgi. A low calcium concentration is observed in the stratum basale whilst higher concentrations are observed in the stratum granulosum (Elias et al. 2002).

Once the cells commit to terminal differentiation key morphological and transcriptional changes occur. The morphological changes are a result of migration through changing calcium gradient and are associated with changes in keratin expression. Additionally, keratinocyte fate is mediated by transcriptional changes such as Notch signalling and p300 (factors regulating keratinocytes differentiation are reviewed in (Koster & Roop 2007).

Basal cells in the stratum basale are characterised by their high proliferative potential and their expression of K5 and K14. Upon the decision to undergo differentiation, cells detach from the basement membrane, exit the cell cycle and migrate upward to form the post-mitotic spinosum layer (Fuchs & Raghavan 2002). Keratinocytes in this layer express K1 and K10, strengthening cell-cell junctions and providing resistance to mechanical stress (Eckhart et al. 2013).

Non-dividing keratinocytes then flatten. keratinohyalin help break down organelles and nuclei and produce additional structural filaments below the plasma membrane resulting in an impermeable barrier. These cells exectrete the lipid bilayer into the outercelluar matrix resulting in waterproofing the skin and also preveting the pathogens from entering.

The stratum corneum, is formed from approximately 30 sheets of keratinocytes that have completed the terminal differentiation and are now known as corneocytes. Corneocytes are strengthened by densely packed keratin filaments and surrounded by lipids. Corneocytes briefly form the outer protective layer of the skin before sloughing from the skin (desquamation) to be replaced by the differentiating cells below.

1.1.2 The HPV life cycle

The study of HPV life cycle is complicated by the fact that vial particles are only produced in the terminally differentiated cells, and the production of viral particles *in vitro* has proved challenging. However, despite some differences based on infection site and virus type, generally most HPV infections result in productive 'normal' infections as a result of well-regulated gene expression, leading to shedding of progeny virus (the HPV life cycle is reviewed in (Doorbar et al. 2012).

To initiate an infection HPV viral particles (composed of viral DNA and two capsid proteins L1 and L2, (Finnen et al. 2003) must gain access to the dividing basal cells residing on the basement membrane, such entry may be the result of micro-trauma of the epithelium. It is proposed that in the cutaneous skin, slow cycling keratinocyte stem cells existing in the hair follicles provide the access site for β-HPVs. This is supported by the recurrent detection of HPV DNA in plucked hair (Iannacone et al. 2014).

Current evidence suggests that cellular entry by HPV can be mediated by the attachment to the heparan sulphate proteoglycan that are expressed on the surface of keratinocytes, and the subsequent entry by clathrin or cavelolin, depending on HPV types (Johnson et al. 2009; Culp et al. 2006).

Upon entry to the cell, the capsid is disassembled and is subjected to endosomal transport, the viral DNA is transported to the nucleus via the action of the minor capsid protein L2, while the L1 protein is retained in the endosome and ultimately subjected to lysosomal degradation (Kines et al. 2009; Schiller et al. 2010) (Bergant Marušič et al. 2012). The viral entry is followed by an initial phase of genome amplification and then maintenance of the viral episome at low copy number (20-100 copies per cell) (McBride 2008; Maglennon et al. 2011). The E1 and E2 proteins are proposed to have an important role in the amplification of viral DNA. E2

regulates viral transcription and during viral DNA replication E2 recruits the viral E1 helicase to the origin of replication. (Hughes & Romanos 1993)

As the cells detach from the basement membrane, they withdraw from the cell cycle and enter the terminal differentiation program. In virally infected cells this activates the expression of E6 and E7, which reactivate the cell cycle program and drive proliferation allowing cellular DNA polymerase activity and therefore viral genome amplification. Additionally E4 and E5 (E5 is only present in genus α) proteins are also expressed in these cells and they function mainly to regulate viral genome replication (R. Wilson et al. 2007). The HPV life cycle completion and release of viral particles occurs at the upper layers of the epithelium and involves the expression of the minor coat protein (L2), the exit of the cell from the cell cycle and the expression of the major coat protein L1 to allow genome packaging. Figure 1-3 shows a schematic representation of the HPV life cycle in the skin (Day et al. 1998; Finnen et al. 2003).

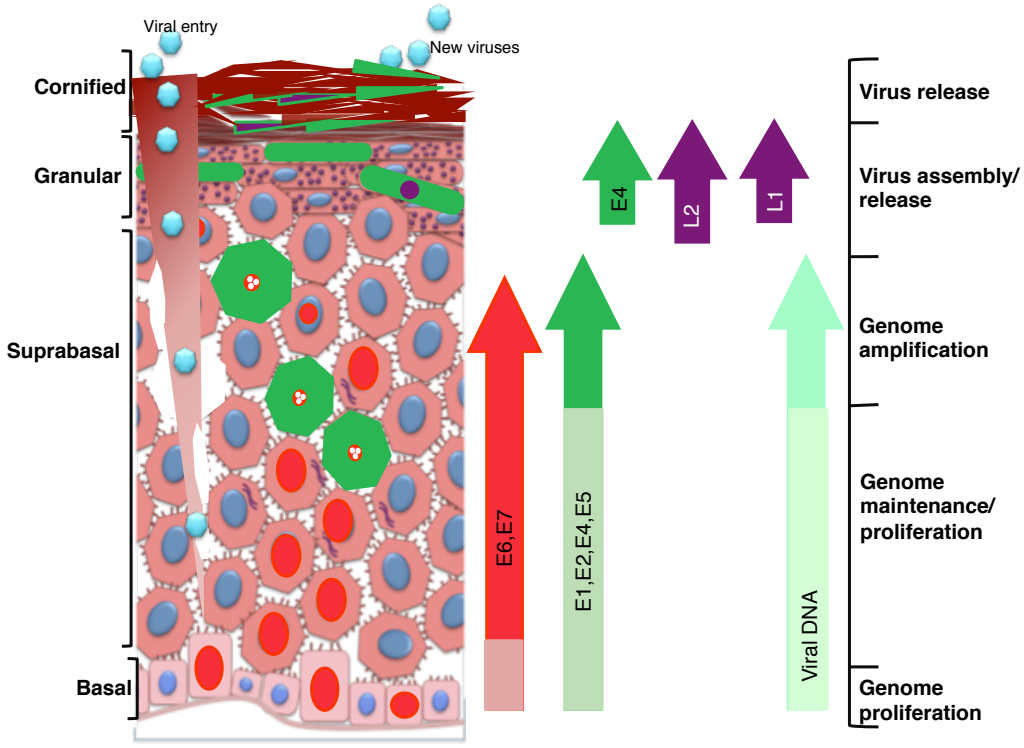

Figure 1-3 Schematic representation of the HPV's life cycle

HPV virus infections depend on the virus gaining access to the dividing basal cell layer as a result of microaberasion. Red nuclei marks actively dividing cells, their presence in the suprabasal cell layer is a result of E6 and E7 expression. Cells expressing viral proteins that are essential for viral genome amplification are labelled with green. Adapted from(Quint et al. 2015)

1.1.3 HPV genome and encoded proteins

The HPV genomic template is conserved across HPV species, it encodes similar proteins with the exception of α-HPV only E5 protein. The HPV genome is divided into three regions, the upstream non-coding region (NCR) contains the origin of replication but does not encode for any proteins. The late region encodes for two capsid proteins L1 and L2, and the early region codes for E1, E2, E4, E5 (only found in α-HPV), E6 and E7 (Figure 1-4). Generally, the encoded proteins by different HPV genera have similar functions. However, many functional differences exist between early region proteins of α and β-HPV. The role of each of the viral proteins is described below.

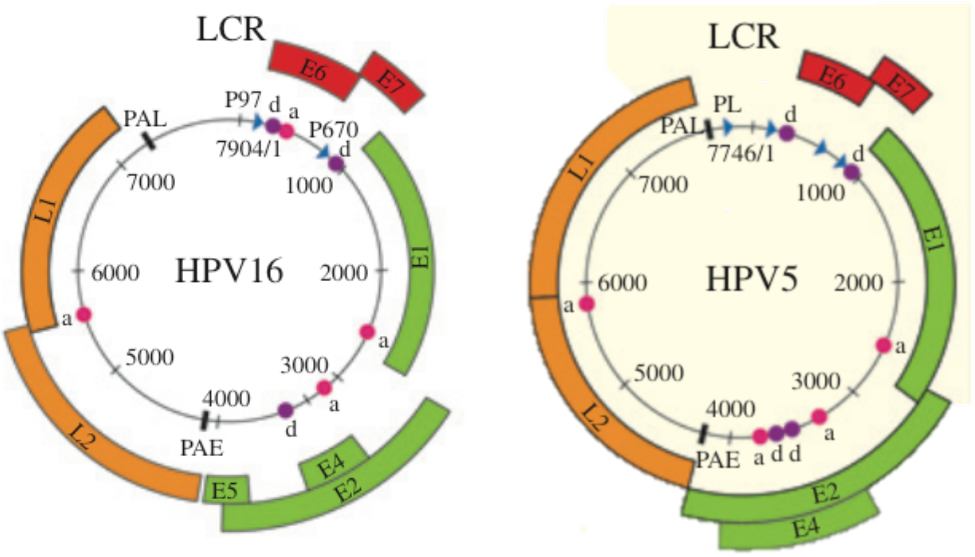

Figure 1-4 HPV genome organisation from α-HPV16 and β-HPV5

Genome organisation of α-HPV16 and β-HPV5. The positions of the major open reading frames and the long control region are indicated. β-HPV types lack an E5 ORF and have a much longer E4 ORF than the α-HPV types. The positions of major promoters and splice donor/acceptor sites are indicated by arrows (promoters) and circles (d, donor; a, acceptor), respectively, alongside the positions of the early (PAE) and late polyadenylation sites (PAL). Infection and life cycle, and lesion formation, by β-HPV types are shown in the right panels. To initiate infection, HPV virions must gain access to the epithelial basal cells and probably an epithelial stem cell (coloured purple), either through a wound or possibly through the hair follicle Taken from (Quint et al. 2015)

1.1.3.1 E1 and E2

E1 and E2 are amongst the first proteins to be expressed upon viral entry to the cell and are involved in viral replication and the regulation of viral transcription.

E1 is the most conserved and largest of the ORF, coding for 70kDa protein. E1 has been demonstrated to be essential for the viral replicative cycle by promoting viral DNA replication upon infection and the maintenance of viral DNA episomally in the more differentiated keratinocytes (V. G. Wilson et al. 2002). E1 is a hexameric DNA helicase with 3' to 5' directionality and it demonstrates ATPase activity (Hughes & Romanos 1993). A key step in viral DNA replication is the recognition of the origin of DNA replication "ori" by E1 through the recognition of AT-rich sequences that

contain six E1-binding sites (E1BS 1–6) of the consensus sequence 5'-ATTGTT-3' (Chen & Stenlund 2002; Morin et al. 2011; Titolo et al. 2000). The recognition of these specific elements by E1 requires the binding of E2, which enhances the E1 binding affinity to ori. E1 interacts with several members of the cellular DNA replication machinery such as the DNA polymerase α-primase (Pol α-prim) complex, the single-stranded DNA binding protein replication protein A (RPA), making E1 a key replication factor (V. G. Wilson et al. 2002). Moreover, it has been demonstrated that E1 is able to interact with other cellular proteins to assist and regulate viral DNA replication such as p80 and p56 (Côté-Martin et al. 2008; Terenzi et al. 2008).

In addition to E1, E2 is also required for viral replication. E2 is a 50kDa protein composed of approximately 360 amino acids, and it consists of a conserved N-terminal "transactivation" domain that is linked to a C terminal DNA binding domain, the two domains are connected by a flexible linker sequence (Giri & Yaniv 1988; McBride et al. 1989). As described above, in viral genome replication, E2 tethers E1 to the ori and then is displaced after E1 is converted to a hexameric helicase. Additionally, viral replication occurs in nuclear foci and the formation of these foci is dependent on E2. The E2 protein is the main transcription regulator and it functions by the recruitment of cellular factors to the viral genome that activate or repress the transcriptional process (Steger et al. 1996; Fujii et al. 2001). E2 has been shown to interact with transcription co-factors such as p300/CBP (Peng et al. 2000) and the histone acetyl transferase NuA4/TIP60. E2 also ensures viral genome partitioning during mitosis by tethering replicated HPV episomes to the host cell chromosome (Bastien & McBride 2000; McBride 2013).

1.1.3.2 E4 and E5

The viral E4, and α-HPV E5 in proteins are expressed in the stratum spinosum and granular layers.

The E4 open reading frame (ORF) lies within the larger E2 ORF, and the E4 protein is expressed as a fusion with the first few amino acids of E1, this fusion protein is described as E1^E4 (Nasseri et al. 1987). E4 is highly abundant in the productive HPV lesions and serves as a marker for active HPV infection, unlike E1 and E2 however, E4 is believed to be required for the later stages of the viral life cycle (Fang et al. 2006; Doorbar 2013). This is supported by studies demonstrating that depletion of E4 in HPV16, 18 and 31 does not affect their ability to be maintained in proliferating 'basal-like' keratinocytes in monolayer culture. The precise mechanism by which E4 supports genome amplification and viral assembly is yet to be elucidated. However, E1^E4 from high risk α-HPV16 and low risk β-HPV1 was demonstrated to cause a cell cycle arrest in G2, this involves the sequestration of CyclinB/Cdk1 to the cytoplasm which prevents its nuclear translocation and mitotic progression (Davy et al. 2005; Nakahara et al. 2002). For high-risk types, this G2 arrest may inhibit E6/E7 mediated cell proliferation in the mid epithelial layers, and in this way contribute to the vegetative viral genome amplification (Knight et al. 2011). Moreover, E4 associates with cytokeratin filaments leading to the reorganisation of the cytokeratin filament network and this may facilitate the production of viral particles. (Doorbar 2013).

E5 is encoded only by α-HPV and is an 84 amino acid, highly hydrophobic, membrane-bound protein (reviewed in (DiMaio & Petti 2013). E5 is found to differ from low and high-risk HPVs where low-risk HPV11 and 6 encode two E5 proteins known as E5A and E5B, whilst high-risk HPV16 encodes E5. Moreover, HPV16 E5 predominantly localises to the ER, and is less frequently associated with Golgi

apparatus and the nuclear membrane, whilst HPV6 E5 is found primarily in the Golgi apparatus (Bravo et al. 2013). This difference in E5 between high and low risk α-HPV suggests that E5 might play a role in the oncogenic transformation of the virus. *In vitro* studies demonstrated that E5 works with E7 to enhance the proliferation of keratinocytes. Furthermore the N-terminal hydrophobic domain of HPV16 E5 is required for its ability to induce anchorage independent growth and invasiveness of human keratinocytes. However, E5 is found in precancerous LGSIL and seems to be deleted upon integration of the viral genome (Venuti et al. 2011). HPV16 E5 was shown interact with the heavy chain component of the human MHC1 antigen and impede its transport to the cell surface and thus E5 allows for immune system evasion (Ashrafi et al. 2006).

1.1.3.3 E6

The oncogenic transformation of HPV is largely attributed to the functions of the viral oncoproteins E6 and E7. During the viral life cycle both E6 and E7 drive cellular proliferation, survival and differentiation. E6 and E7 contribute to the malignant transformation of cells by interacting with multiple cellular targets and disturbing cell functions, as described below.

E6 is a small multifunctional protein approximately 18kDa in size, that has been found to localise in the cytoplasm and the nucleus of the infected cell (Cornet et al. 2012). The E6 protein consists of two zinc binding domains formed by the conservation of four Cys-XX-Cys that are connected by an inter domain linker (Nominé et al. 2006). E6 protein has no enzymatic activity of its own but it functions by interacting with multiple cellular proteins (reviewed in (Vande Pol & Klingelhutz 2013). The E6 proteins from diverse HPV types exhibit different physical and chemical properties, for example surface residue analysis revealed that HPV5 E6 is more hydrophobic than the hydrophilic E6 from high-risk mucosal HPV16 (Nominé

et al. 2006). These differences translate to different interacting partners between E6 encoded by mucosal and cutaneous HPV genera. It is important to mention that the cellular targets of E6 from high-risk mucosal HPV are more characterised than those of E6 from the cutaneous HPV types.

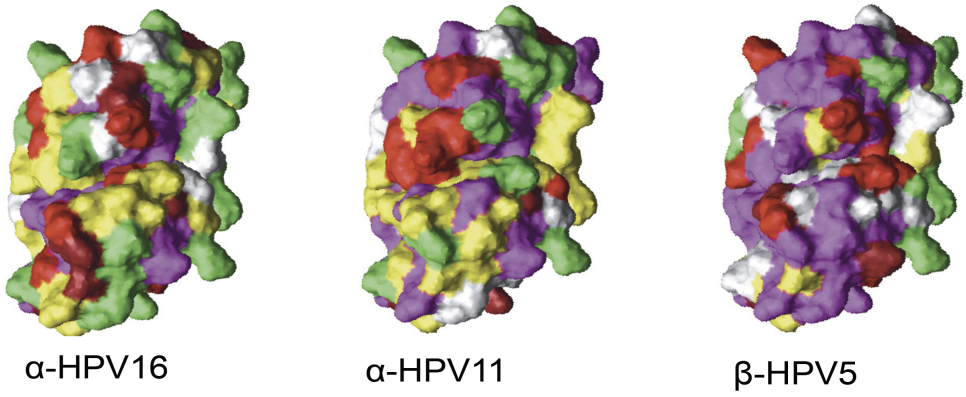

Figure 1-5 surface properties of E6 from different HPV types

E6 protein encoded by different HPV types show conserved overall structure but display different amino acid residues on the surface. Color codes: A, G, P, white; R, K, H, green; D, E, red; N, Q, S, T, yellow; M, V, L, I, F, W, Y, purple. Taken from (Nominé et al. 2006)

The replication of the viral genome within the cell promotes the up-regulation of cellular genes involved in programmed cell death and growth arrest as a host defence mechanism. One of the key functions of HPV E6 is the abrogation of cellular apoptosis, evasion of apoptosis is one of the hallmarks of human cancers (Hanahan & Weinberg 2011). E6 from high-risk α–HPV types (16, 18 and 33) mediates the degradation of p53 through its association with E6AP (E6 associated protein), a HECT domain E3 ligase (Scheffner et al. 1990; Huibregtse et al. 1993; Huibregtse et al. 1991). E6 binds with E6AP via its LXXLL motif, thus promoting the ubiquitination of p53 by the 26S proteasome. Studies have demonstrated that this function of E6 reduces the half-life of p53 to less than 20 min. This LXXLL motif is used by E6 to interact with a number of substrates, including tuberous sclerosis complex 2 (TSC2) that is an upstream regulator of mTORC1 (Lu et al. 2004). Recently it was demonstrated that E6 from cutaneous HPV is also able to bind

LXXLL containing proteins. HPV8 E6 binds to MAML1 (transcriptional co-activator of Notch1) via its LXXLL motif to repress Notch1 signalling in keratinocytes, and thus interferes with the keratinocyte differentiation (Tan et al. 2012; Meyers & Münger 2013; Brimer et al. 2012). SCC that arises from the skin and head and neck has been shown to have a loss of Notch signalling (Stransky et al. 2011). Additionally, the loss of Notch upregulates Wnt5a signalling in keratinocytes, which is implicated in skin carcinogenesis (Kang et al. 2012).

The p53 degradation by E6 abrogates p53-mediated apoptosis and contributes towards genomic instability by impeding p53 DDR and this contributes towards tumour formation (Kessis et al. 1993). Albeit, p53 degradation by E6 is not the only mechanism of apoptosis inhibition, HPV16 E6 is capable of inhibiting apoptosis that is stimulated by the Fas and TRAIL pathways by the degradation of FADD adapter and caspase 8 (Filippova et al. 2004), (Garnett et al. 2006). Contrastingly, E6 from cutaneous HPV types such as 5 and 8 does not promote the degradation of p53 (Steger & Pfister 1992; Jackson & Storey 2000). This phenomena was thought to be conserved amongst cutaneous HPVs, however it is observed that the expression of HPV49 E6/E7 resulted in the degradation of p53 in an E6AP dependent manner (Cornet et al. 2012).

E6 from β-HPV 5 and 8 can abrogate cellular apoptotic responses via the targeted degradation of the pro-apoptotic protein BAK (for description of the apoptotic pathway refer to 1.3.2) following UV DNA damage (Sarah Jackson & Storey 2000). This function is conserved amongst different cutaneous and mucosal HPV types (Thomas & Banks 1999; Underbrink et al. 2008). A recent report by Holloway et al. described the mechanism of BAK degradation by HPV5 E6. The researchers showed that upon UV DNA damage, BAK undergoes an N-terminal conformational change and becomes dephosphorylated and this exposes a hydrophobic groove, HPV5 E6 then recruits HERC1, an E3 ligase to activated BAK where HERC1 binds

BAK via a BH3 domain:groove interaction (Holloway et al. 2014). Moreover, high-risk HPV E6 proteins target the pro-apoptotic protein BAX (pro-apoptotic protein, described in 1.3.2) for degradation and lead to the repression of *bax* mRNA expression in cervical cancer. In addition, expression of the HPV5 and 8 E6 proteins has been observed to correlate with reduced BAX steady state levels (Struijk et al. 2008). The different cellular targets of E6 from β-HPV and α-HPV described above demonstrate how the E6 protein can modulate common pathways using different mechanisms.

In addition to apoptosis inhibition by BAK degradation, the E6 protein of β-HPVs may exacerbate the mutagenic effects of UV irradiation by delaying the repair of UV-induced thymine dimers (the DNA damage induced by UV is described in more detail in 1.2.1) through targeting of the DNA damage-response proteins ATR and XRCC1 and elimination of the apoptotic response to irreparable DNA damage, which may increase genomic instability to promote tumourigenesis (Wallace et al. 2012; Giampieri & Storey 2004).

One of the major differences between cutaneous and mucosal E6, is the lack of a four amino acid motif at the C-terminal PDZ motif, which enables the binding of PDZ containing proteins. Such proteins are involved in an array of cellular functions such as cellular migration, adhesion, polarity and proliferation (Vande Pol & Klingelhutz 2013). E6 from high-risk mucosal HPV types can promote the degradation of PDZ domain containing protein such as MUPP1, hDLG, hScrib and the MAGI protein family (S. S. Lee et al. 2000; Nakagawa & Huibregtse 2000). The binding of PDZ proteins by E6 has been linked to cell immortalisation. Intriguingly, some β-HPV E6 proteins associated with the highest risk of malignancy, including those of HPV5 and 8, have a conserved C-terminal motif of YHDW. E6 from high-risk β-HPV5, 8 and 20 interact with β1-integrin through this YHDW motif, resulting

in increased cell migration (Holloway & Storey 2014). A list of some of E6 interacting proteins is in Table 1 List of HPV E6 interacting partners.

Table 1 List of HPV E6 interacting partners.

Target	E6 types	Effect
p53	Predominantly high-risk α-HPV	Inhibit p53-mediated DDR, cell cycle arrest and apoptosis.
XRCC1	HPV1, 8, 16	Inhibit DNA Repair
p300	HPV5, 18, 16	Inhibit DDR and gene transcription
Mastermind 1	HPV8, 17, 38	Disrupts the Notch pathway required for cell differentiation
hTERT	HPV16	Increases cell lifespan
BAK	β-type HPV5, 8, 10, 20, 22, 38, 76, 92, and 96 α-type HPV16, 18, 77	Inhibit the intrinsic apoptotic pathway
BAX	High-risk α-HPV	
FADD	HPV16	Inhibit the extrinsic apoptoticpathway
Caspase-8	HPV16	
PDZ domain containing proteins	High-risk α-HPV with an ETQV motif	Disrupt cell polarity and adhesion. Such proteins include Scribble, the MAGI family, Dlg and MUPP1
E6AP	α-HPV	Used to target host cell substrates for degradation
Paxillin	BPV1 and HPV16	Disruption of focal adhesions
E6BP	High-risk α-HPV	Calcium binding protein
TSC2	High-risk α-HPV	Activation of mTOR signalling
MCM7	High and low-risk α-HPV	DNA replication
HIPK2	HPV23 and 38	Prevent p53 activation
β1-integrin	β-type HPV5, 8 and 20	Increased cell migration
TIP60	HPV8, 11, 16 and 18	Inhibit p53-dependent activation of apoptotic pathways

Another function of E6 is the ability to increase cell proliferation. This is achieved through the upregulation of a cellular telomerase enzyme, which consists of four-subunits, containing an hTERT catalytic domain that once activated by E6, adds

hexamer repeats to the telomeric ends. The majority of tumour cells have increased expression of hTERT and the induction of telomerase by E6 contributes to the immortalization of cells together with pRB inactivation by E7 (Klingelhutz et al. 1996; Oh et al. 2001; Kiyono et al. 1998). α-HPV, along with some β-HPV, E6 proteins are capable of activating telomerase. The β-HPV E6 proteins are able to upregulate hTERT mRNA to varying degrees. HPV38 E6 shows the most significant hTERT mRNA upregulation through mechanisms similar to that of HPV16 E6 whilst HPV5 and 8 E6 have moderate activity towards hTERT and HPV20 E6 has none (Amy, Holloway 2013,Bedard et al., 2008).

1.1.3.4 E7

The HPV E7 oncoprotein of both low and high-risk types is located in the nucleus and cytoplasm. It is a 98 amino acid protein consisting of three domains, termed CR1, CR2 and CR3, based on sequence homology to the E1A oncoprotein of adenovirus. The CR2 and CR3 regions contain a LXCXE and carboxy-terminal zinc binding domains respectively (Phelps et al. 1992). The latter is similar in structure to the zinc-binding domain in E6. The E7 protein, like E6, is pleiotropic and has many functions that are determined by its ability to bind a number of different cellular proteins (Mavromatis et al. 1997). Many of these affect cell growth and, more specifically, progression from the G_1 to S phase of the cell cycle. The main function of the HPV E7 proteins is generally thought to be to retain differentiating cells in a DNA synthesis competent state. However, for at least some of the viruses, E7 is also required for maintenance of the viral genome in undifferentiated cells (Roman & Münger 2013).

The cellular targets of the E7 protein from the mucosal HPV types are more characterised than those of the cutaneous HPVs. Essentially, three groups of

proteins are bound by E7: the pRb family members, cyclins and cyclin-dependent kinases and histone deacetylases, which will be described below.

The high-risk HPV E7 proteins can disrupt cell cycle control by degrading the tumour suppressor protein retinoblastoma (pRb) (Munger & Howley 1991) (Gonzalez et al. 2001). Hypo-phosphorylated pRb binds and inactivates the E2F family of transcription factors, therefore the E7- mediated degradation of pRb releases E2F to transcribe genes required for DNA synthesis driving cells into S-phase. An LXCXE motif in the E7 protein is required for pRb binding. The E7 proteins use the Cullin 2 ubiquitin ligase complex to degrade pRb (Huh et al. 2007). Whilst β-HPV E7 proteins also interact with pRb the strength of the interaction is much weaker. Human keratinocytes in monolayer cultures expressing the HPV8 E7 gene have lower levels of pRb, correlating with cell cycle defects and increased proliferation. Additionally, the expression of HPV8 E7 protein results in invasion of human keratinocytes into the epidermis of organotypic cultures (Akgül et al. 2005). Moreover, the expression of HPV8 E7 in keratinocytes increased clonogencity and resulted in an increase in the number of cells with stem-cell markers EpCAM and CD44 (Hufbauer et al. 2013).

1.1.3.5 L1 and L2

The late proteins 1 and 2 are the structural components of the viral capsid, and thus their expression is confined to terminally differentiated cells located at the upper most layers of the epithelium (Buck et al. 2013; Wang & Roden 2013). Each virion contains 360 L1 proteins that assemble into star-shaped structures of 5 called capsomers, and the capsid is then created by the association of the 72 capsomers and it also contains up to 72 L2 proteins (Buck et al. 2008; Buck & Trus 2012). The L1 protein has the ability to self assemble into virus-like particles (VLP),

which are the basis of the HPV vaccine (Schiller & Lowy 2012). L1 is essential for virus entry as it interacts with the heparan sulfate (HS) carbohydrates displayed on proteoglycans. The L2 protein is just under 500 amino acids in length (Doorbar & Gallimore 1987) and is required for the transfer of the viral genome to the nucleus after un-coating.

1.2 Non-Melanoma Skin Cancer

Non-Melanoma Skin Cancer (NMSC) is the most common cancer in caucasians with more than 100,000 new cases each year in the UK (http://www.cancerresearchuk.org). NMSC can be divided into different types according to the cell it originates from; 1) basal cell carcinoma (BCC) arises from membrane attached basal cells and accounts for 74% of the cases, 2) squamous cell carcinoma (SCC) arises from the keratinocytes superficial to the basal cells and accounts to for 23% of cases 3) and Merkel cell carcinoma that is the least frequent and is associated with polyomavirus infection (H. Feng et al. 2008). BCC and SCC often occur in older people (over 50) and are more common in men (due to outdoor work) however, use of tanning beds has decreased the age of the disease presentation (Wehner et al. 2012). The focus of this work is mainly on SCC as their development is associated with HPV.

SCC development is viewed as a multistep process. SCC is usually preceded by actinic keratosis (thickened patches of skin) (Figueras et al. 2014) and Bowen's disease (squamous cell carcinoma in situ) (Bhambri & Del Rosso 2010). Some SCC can metastasise to other strata of the epidermis and the lymph nodes (less than 5%), however, the rate of metastasis increases to 20% in the immunosuppressed population (Veness, 2007).

Surgical excision of BCC and SCC remains the only effective treatment with low risk of perineural invasion in BCC (3%) and a higher risk in SCC (up to 14%). Treatment of BCC and SCC is often successful, resulting in low mortality. However NMSC has a high morbidity owing to invasion of surrounding tissue and resultant damage from treatment (Madan et al. 2010).

There are several factors contributing to the metastatic potential of these tumours including; host immunosuppression, the histologic grade and subtype and tumour vasculature. Although the risk of development of NMSC depends on various factors such as environmental factors, genetic predisposition and HPV infection, the main etiological agent is DNA damage resulting from prolonged exposure to ultraviolet light. This is evidenced by the development of NMSC in sun-exposed body sites and the increased incidence of NMSC in countries with higher UV indices. For example, Australia has a higher incidence of NMSC compared to the UK (Lomas et al. 2012).

1.2.1 Effects of UV on the skin

The UV spectrum of sunlight is divided into UVA (320-400nm), UVB (290-320nm) and UVC (200-290nm). The solar UV rays that reach the earth are 95% UVA and 5% UVB, whereas UVC is mostly absorbed through the ozone layer. UVA penetrates deep into the stratified epithelium of the skin and leads to indirect DNA damage through the formation of free radicals and reactive oxygen species (ROS) as well as exhibiting immunosuppressive effects (Agar et al. 2004). UVB is known to be a potent mutagenic, it permeates the epidermis and is able to damage DNA indirectly through the production of ROS and directly via the formation new bonds between DNA bases. The DNA photoproducts created by UVB are cyclobutane pyrimidine dimers (CPD) between adjacent thymine (T) or cytosine (C) residues, and pyrimidine 6,4 photoproducts (6,4PPs), occurring between the 5-prime 6 position

and the 3-prime 4 position of two adjacent pyrimidines, most often between TC and CC residues (Figure 1-6) (Besaratinia et al., 2008). If unrepaired, these lesions lead to mutations in the DNA sequences in the form of C to T and CC to TT transitions, known as UVB signature mutations (Tessman et al. 1992; de Gruijl et al. 2001; Pustišek & Šitum 2011).

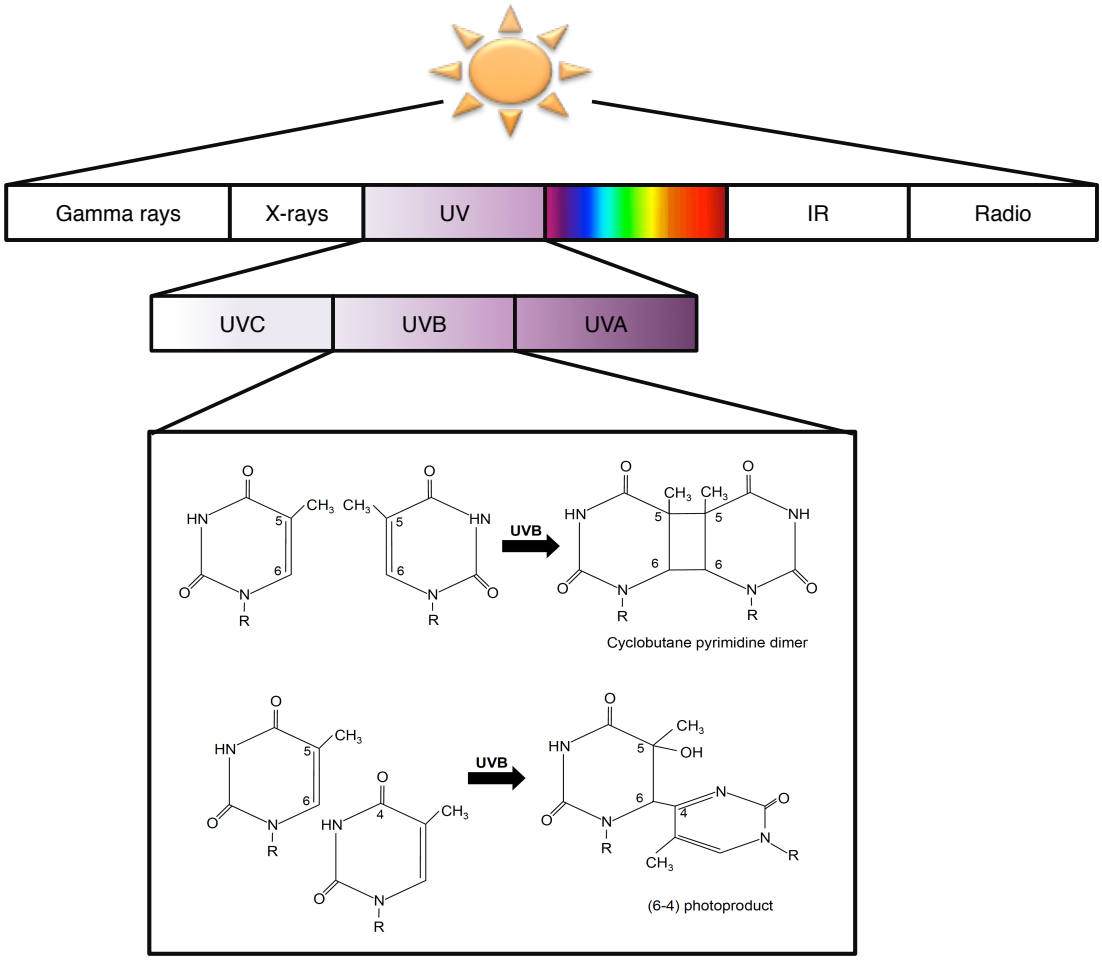

Figure 1-6 DNA damage by UV

Adapted from (Pfeifer & Besaratinia 2012)

UVB damage activates the cellular DNA Damage Response (DDR) that is orchestrated by p53 (Dai and Gu, 2010). Activation of p53 by UV results in G1 arrest that allows for DNA repair to occur before proceeding to S phase. CPD and 6,4PPs resulting from UVB are primarily repaired via the nucleotide excision repair (NER) pathway, a highly conserved repair pathway that uses the product of around

30 genes to remove a damage-containing oligonucleotide from cellular DNA. The removal of 6,4PPs by NER is much more effective than that of CPD, rendering these lesions to be more toxic (Sinha & Häder 2002). The importance of the NER pathway in skin cancer is demonstrated by increased sensitivity to skin cancer formation in patients suffering from from Xeroderma pigmentosum type C (XPC), which is a rare autosomal recessive disorder (XPC is a crucial component of the NER apparatus) (Cleaver, 2000). In some cases the sunlight exposure results in DNA damage that is too severe and cannot be repaired, this results in an apoptotic cell death and the formation of sunburn cells. The UVB mediated apoptosis can be a result of p53 activation. Upon the receipt of damage signals, p53 can translocate to the cytoplasm and activate the pro-apoptotic proteins BAK and BAX leading to cytochrome *c* release and cell death (described in more detail in 1.3.2). Expression of Fas and FasL can be induced in response to UVB and mice lacking active FasL have a reduced number of apoptotic keratinocytes and increased frequency of p53 mutation (Hill 1999). Thus an apoptotic response to UV is believed to be an anti-tumour mechanism, facilitating the elimination of DNA damaged cells and preventing the accumulation of genetic mutations that can lead to cancer development.

p53 is found to be mutated and inactivated in at least 50% of NMSC cases, and in SCC p53 mutations often follow the UV-induced signature (Kraemer 1997; Pfeifer & Besaratinia 2012). However the contribution of p53 mutation to the progression of NMSC is uncertain given that healthy skin is found to have patches with p53 mutations. These appear to have normal morphological appearance and exhibit very little, pre-cancerous potential (Giglia Mari & Sarasin 2003; Olivier et al. 2004). In addition, Li–Fraumeni patients, who have a germline mutation in the p53 gene, have an increased risk of developing any soft tissue cancer with the exception of NMSC (Lustbader et al. 1992).

1.2.2 HPV and NMSC

β-genus HPVs have a cutaneous tropism and, analogous to the α-HPV, some of them are considered as potentially high-risk due to their isolation in SCC lesions. Specifically, these are HPV 5, 8, 9, 12, 14, 15, 17, 19-25, 36-38, 47, and 50.

The link between β-HPV and NMSC was first observed in patients suffering from *Epidermodysplasia verruciformis* (EV), a rare autosomal recessive disorder that may be linked to mutations in the EVER1 or EVER2 genes. EV patients have impaired cell mediated immunity and are predisposed to infections with β-HPV (Ramoz et al. 2002; Majewski & Jabłońska 1995; Ramoz et al. 1999). EVER1/EVER2 proteins are located in the ER of keratinocytes forming a complex with zinc transporter-1 (ZnT-1), it was therefore proposed that zinc homeostasis plays a role the viral life cycle (Lazarczyk et al. 2008). EVER proteins were also suggested to regulate the immune system, supporting this notion a recent study revealed that EVER proteins are abundantly expressed in T cells. Additionally excess zinc concentrations blocked T-cell activation and proliferation (Lazarczyk et al. 2012).

EV patients develop flat warts that can undergo malignant transformation to SCC in approximately 30–50% of cases, usually in sun-exposed body sites. HPV5 and 8 are the most frequently detected types in EV patients, up to 90% of cases and were previously identified as EV types (Orth et al. 1978).

The immune status of EV patients drew attention to the relationship between HPV and SCC in the immunocompromised individuals, in particular organ transplant recipients (OTR). Although β-HPV is detected in OTR with no history of skin cancer, studies showed that OTR have about 200-fold increased risk of SCC development compared to the immunocompetent population (Stockfleth et al. 2001, Hartevelt et al. 1990). Interestingly, in contrast to the general population the incidence of SCC in OTR is much higher compared to BCC (Moloney et al. 2006, Pfister, 2003).

A study by (Borgogna et al. 2014) examined the presence of HPV in 111 tumour samples taken from kidney transplant patients, 85% of the tumours were positive for HPV with 71% positive for β-HPV (65% HPV5 and 8). Moreover, β-HPV was detected in 94% in OTR with no history of skin cancer and 97% in SCC patients, however concordant detection of both seropositivity and DNA in patients increased risk of SCC. This study also noted a borderline significant association between SCC and infection with HPV5, 9, 24 and 36 (Proby et al. 2011). Like α-HPV, multiple cutaneous HPV are detected in single tumours from transplant recipients (Harwood et al. 2000, Borgogna et al. 2014), making epidemiological associations between specific HPV and malignancy difficult to delineate. However β-HPV associated with greatest risk for malignancy, such as HPV5, have been identified in the centre of a carcinoma, whilst other HPV types have been identified surrounding it (Pfister et al. 1983).

A link between β-HPVs and non-melanoma skin cancer has also been identified in the immunocompetent population (Masini et al. 2003, Bavinck et al. 2010). β-HPV DNA has been identified in 50% of SCCs in immunocompetent individuals (Asgari et al., 2008) whilst seropositivity to β-HPV, especially HPV5, 8 and 20 is also associated with risk of SCC (Karagas et al. 2006, Feltkamp et al. 2003). A multicenter study revealed that the presence of β-HPV infection correlated with a 3-fold increased risk for SCC in the Netherlands (Bavinck et al. 2010).

The highest risk of SCC is associated with infection by multiple HPV types, a 2 fold risk of SCC was observed in patients with seropositivity against >4 types of HPV (Iannacone et al., 2014). Individuals with tumours on sun-exposed sites were also found more likely to be seropositive for β-HPV types than individuals with SCC at other anatomic sites (Karagas et al. 2006). This correlates with a poor tanning ability, supporting a sun exposure component (Shamanin et al. 1996, Iannacone et al. 2012). Increased sun exposure appears to correlate with an increase in

cutaneous HPV infection (Chen et al., 2008), possibly through UV-induced immune suppression (Ullrich, 2005).

The role of β-HPV in the development of NMSC is under debate, this due to the detection β-HPV in up to 80% of healthy skin showing no signs of pre-malignancy in the immunocompetent population (Alotaibi et al. 2006, Antonsson et al. 2003, Antonsson et al. 2000, Astori et al. 1998, de Koning et al. 2009). Furthermore, β-HPV DNA is not ubiquitously detected in all NMSC (Arron et al. 2011) and β-HPV DNA does not appear to persist in SCC: higher viral loads are detected in actinic keratosis compared to SCC (Pfister et al. 2003, Weissenborn et al. 2005).

In addition to epidemiological studies, experiments with mouse models provide supportive evidence to the role of β-HPV in the development of NMSC. Expression of the early coding region of HPV8 in mice leads to the spontaneous development of papilloma within 90 days, a subset of which progress to SCC (Schaper et al. 2005). Moreover, exposing HPV8 transgenic mice to UV accelerates the carcinogenesis dramatically (Marcuzzi et al. 2009), supporting the role of HPV as a co-factor in NMSC. In agreement with this mice expressing the HPV38 E6 and E7 genes under a keratin-14 promoter showed reduced cell cycle arrest and p21 accumulation, development of actinic keratosis, a proportion of which progressed to SCC, in response to chronic UV exposure whilst wild type animals did not (Dong et al. 2005; Viarisio et al. 2011)

As discussed in 1.1.3.3 and 1.1.3.4 E6 and E7 are potent oncogenes that can impinge on all the defined hallmarks of cancer such as, cell cycle check points overrides, inhibition of apoptosis, prevention of differentiation and the compromise of genome integrity, all of which may contribute to the promotion of NMSC. Figure 1-7

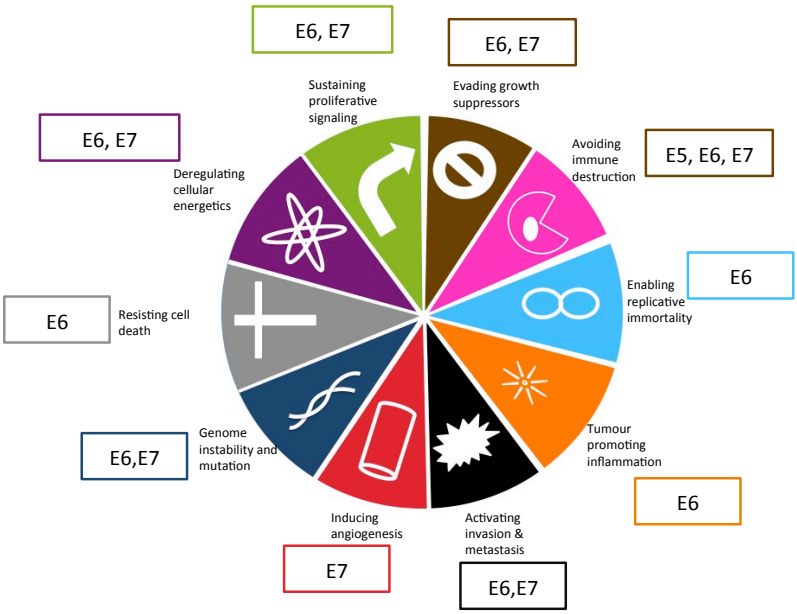

Figure 1-7 Oncogenic potential of E6 and E7

A schematic representation of the hallmarks of cancer and how E6 and E7 can function to promote oncogensis. Adapted from (Mesri et al. 2014).

1.3 Apoptosis

The cellular response to genotoxic stress is complex, but signals from diverse pathways are integrated resulting in either cell death or survival.

There are different modalities of programmed cell death including necroptosis and apoptosis. Apoptosis is a highly conserved mechanism of programed cell death, the term was first coined in the 1972 (Kerr et al. 1972). The morphological features of apoptosis were described in many cell types and these include: nuclear condensation, DNA fragmentation, membrane blebbing and the formation of apoptotic bodies (Häcker 2000). Apoptosis has different important functions during development and the maintenance of tissue homeostasis and the deregulation of apoptosis is involved in many pathologic conditions including cancer.

The human apoptotic cascade can be activated by two main ways: the extrinsic or death receptor pathway and the intrinsic or the mitochondrial pathway.

1.3.1 Extrinsic apoptotic pathway

The extrinsic apoptotic pathway is triggered through signal transduction cascades activated by ligand-bound death receptors of the tumour necrosis factor (TNF) superfamily. Of the TNF super family the apoptosis inducing ligands include: Fas Ligand (FasL/CD95) and TNF-related apoptosis inducing ligand (TRAIL) (Nagata & Golstein 1995; Wiley et al. 1995). In mammals there are eight known plasma membrane death receptors (DR) that are recognised by a sequence of 80 amino acids known as the death domain (DD) (Gao et al. 2011). The binding of FasL and TRAIL to their respective receptors (Fas and DR4 and DR5 respectively) results in receptor trimerization and subsequent recruitment of adaptor protein Fas associated death domain (FADD) (Schneider-Brachert et al. 2013). FADD interacts with DR via its DD, additionally FADD contains a death effector domain (DED) that can recruit DED containing proteins such as pro-caspase 8 and 10 and this forms a

complex known as the death inducing signalling complex (DISC) (Chinnaiyan et al. 1995) (Hongmei 2012) (Sessler et al. 2013). Binding of pro-caspase 8 and 10 to FADD leads to their activation, which in turn activates effector caspase 3 thus leading to apoptotic cell death (Sprick et al. 2002). FLIP, a protein with a caspase 8 sequence homology, that does not show protease activity, can compete with caspase 8 and bind to the DISC complex thereby inhibition of apoptosis (Scaffidi et al. 1999).

In some cells (Type I) the activation of caspase 8 is sufficient to induce apoptosis in the absence of MOM. However in so called type II cells, the extrinsic activation of caspase 8/10 is not sufficient to stimulate the activation of effector caspases and thus mitochondrial apoptosis is initiated by the cleavage and activation of BID (BCL-2 homology 3 (BH3)-interacting domain death agonist) via active caspase 8. Activated BID translocates to the mitochondria where it activates the pro-apoptotic proteins BAK and BAX leading to mitochondrial membrane permeabilization and the release of cytochrome *c* (H. Li et al. 1998). A summary of the extrinsic apoptotic pathway is shown in Figure 1-8.

1.3.2 Intrinsic apoptotic pathway

The intrinsic or mitochondrial apoptotic pathway can be initiated in response to different triggers such as chemotherapeutic agents, reactive oxygen species (ROS) and DNA damage. The cellular demise is achieved by mitochondrial outer membrane permeabilization (MOMP) and the subsequent release of proteins into the cytoplasm that leads to the activation of executioner caspases and cell death, reviewed in (Tait & Green 2013).

Upon the receipt of an apoptotic signal, pro-apoptotic proteins BAK and BAX (described in more details below) are activated and oligomerised. This leads to the formation of pores in the mitochondrial outer membrane, resulting in MOMP and

the release of mitochondrial factors such as cytochrome *c*, Smac and Omi. The release of cytochrome *c* is considered a point of no return (Goldstein et al. 2000). Cytochrome *c* promotes APAF1 conformational changes, leading to its oligomerisation and assembly into a heptameric wheel-like structure known as the apoptosome. The apoptosome then recruits pro-caspase 9, promoting its dimerization and activation (Bratton & Salvesen 2010). This leads to the activation of executioner caspases 3 and 7 resulting in rapid cell death (Malladi et al. 2009). In addition to cytochrome *c,* Smac and Omi are released from the mitochondrial inter-membrane space. Their main function is to mainly inhibit the action of the caspase inhibitor X-linked inhibitor of apoptosis protein (XIAP) (Du et al. 2000; Verhagen et al. 2000; Y. Suzuki et al. 2001). Figure 1-8

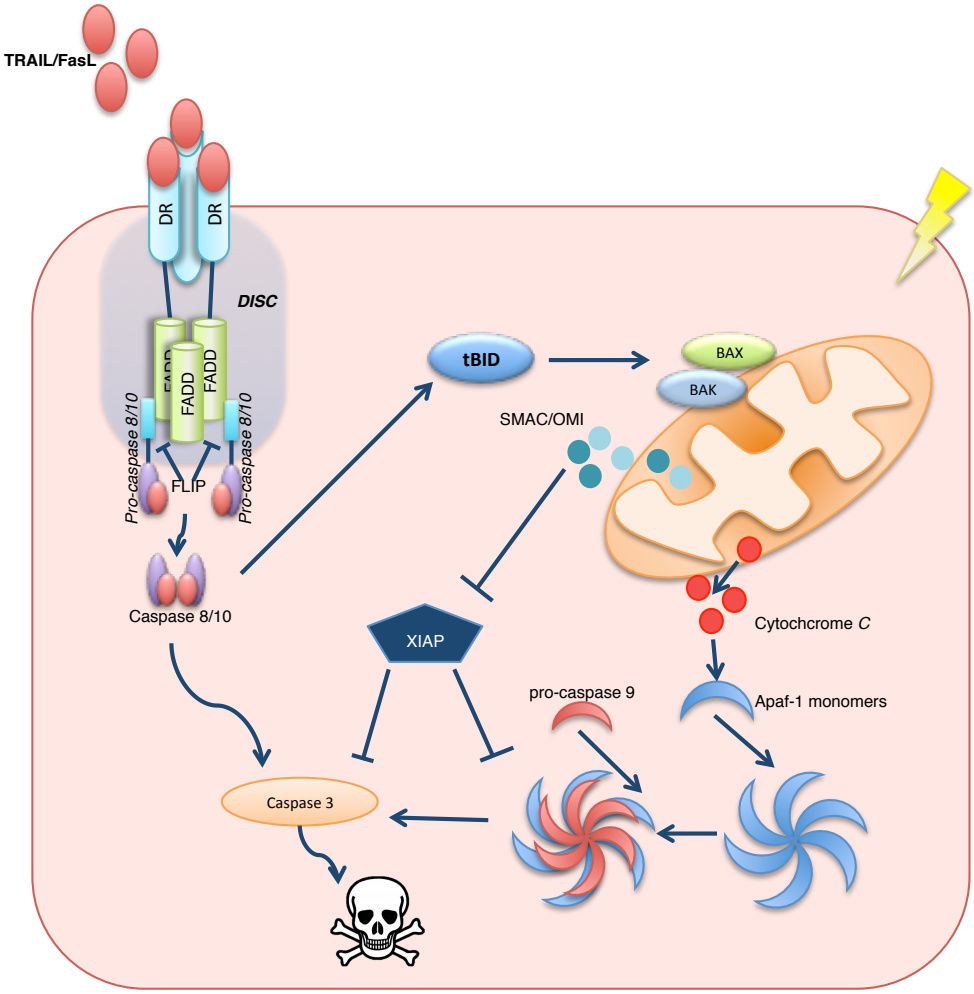

Figure 1-8 Summary of the extrinsic and the intrinsic apoptotic pathways

A Schematic summary of the extrinsic and intrinsic apoptotic pathways.

The extrinsic pathway is activated by ligand binding to death receptors, such as TRAIL and FasL. This binding to the cytoplasmic tail of the receptors recruits FADD which then initiates the formation of the death inducing signalling complex (DISC) and binds pro-caspase 8/10. This activates caspase 8/10 which can activate the effector caspase-3 to cleave cellular substrates and induce cell breakdown. Caspase-8 can also cleave BID to an active form to initiate the intrinsic apoptotic pathway.

The intrinsic apoptotic pathway is regulated by the Bcl-2 pro apoptotic proteins that can activate BAK and BAX effector proteins. This activation results in the permeabilisation of the outer mitochondrial membrane and the release of mitochondrial factors such as Cytochrome *C*, Smac and Omi. Cytochrome *C* binds to the Apaf-1 monomer leading to its oligomerisation and the formation of the apoptosome, this in turn recruits caspase 9 and activation of effector caspases 3 and 7. The release of Samc and Omi neutralises the function of XIAP thus facilitating caspase activation. Adapted from (Vucic et al. 2011)

The MOMP is regulated by B cell lymphoma 2 (Bcl-2) family proteins, that can be recognised by the presence of homology in Bcl-2 domains (BH domains 1-4) (Tsujimoto et al. 1985). The Bcl-2 family can be divided into two main subclasses:

pro-apoptotic and anti-apoptotic and it's the interaction between these two groups that dictates the fate of the cell. The pro-apoptotic Bcl-2 proteins can be further categorised according to the number of BH domains they harbour. First, the BH3 only proteins with only one BH domain. The interaction of the BH3 only proteins with the anti-apoptotic Bcl-2 repertoire or both the anti-apoptotic proteins and the effectors divides them into two groups: a) sensitizers/de-repressors and those include: BAD (BCL-2 antagonist of cell death), p53-upregulated modulator of apoptosis (PUMA) and NOXA. b) Direct activators such as BID (Bcl-2- interacting domain death agonist) and BIM (BCL-2-interacting mediator of cell death) interact with the anti-apoptotic repertoire as well as the effectors (reviewed in (Chipuk et al. 2010).

Secondly the pro-apoptotic effector proteins BAK (Bcl-2 antagonist killer) and BAX (Bcl-2 associated x protein) contain BH domains (1-3). The MOMP is dependent on the activation and homo-oligomerisation of the effector pro-apoptotic proteins BAK and BAX. There are two main models explaining the activation of BAK and BAX by the pro-apoptotic proteins; the direct and indirect model. In the direct model, BAK and BAX activation can be achieved via the direct interaction with activator BH3 only proteins such as BID (Eskes et al. 2000). Whilst the BH3 only sensitizers such as PUMA and NOX act by binding the anti-apoptotic proteins and thus decreasing the threshold required for the activation of BAK and BAX. For example PUMA binds Bcl-2 and therefore prevents its inhibitory function of BIM, allowing BIM to directly activate BAX and resulting in MOMP and cell death. However, the indirect model proposes that BAX and BAK are bound in a constitutively active state by the anti-apoptotic Bcl-2 proteins. Upon an apoptotic stimulus the BH3 domains of the BH3 only proteins bind to the BH3 domain binding hydrophobic pocket of the anti-apoptotic Bcl-2 proteins. This relieves inhibition of the effector proteins permitting

effector protein activation and subsequent mitochondrial outer membrane permeabilization (Tait & Green 2010).

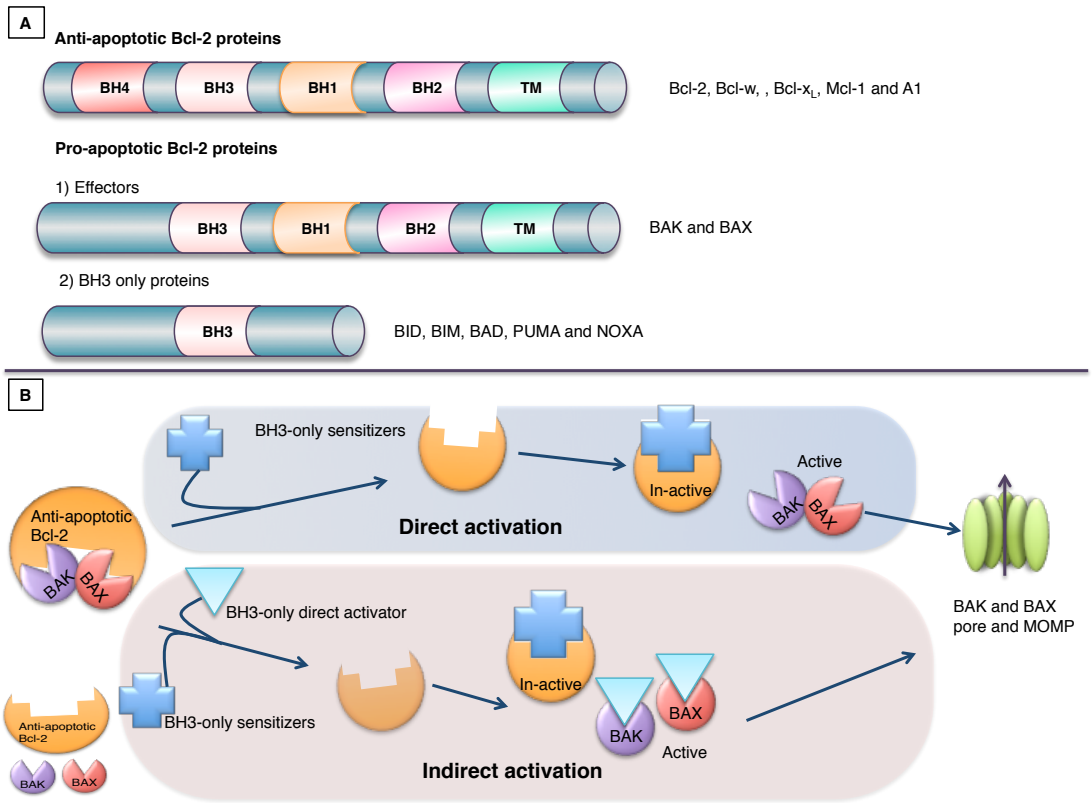

Figure 1-9 The Bcl-2 protein family and models of BAK/BAX activation

A. The BCL-2 family of proteins are classified as i) anti-apoptotic members, ii) pro-apoptotic proteins. The pro-apoptotic proteins are further classified into 1) the effector proteins such as BAK and BAX that permeabilise the outer mitochondrial membrane, 2) the BH3 only family members retain only the BH3 domain.

B. The direct and indirect models of effector proteins activation. It is proposed that in healthy cells the effector BCL-2 proteins, BAK and BAX, are sequestered and inactivated by binding to anti-apoptotic BCL-2 proteins. Upon apoptosis induction the 'indirect' model postulates that BH3 only proteins bind the anti-apoptotic proteins, relieving BAK and BAX inhibition, freeing the effector proteins to permeabilise the mitochondria. For BAK and BAX activation to occur in the 'direct' model 'sensitiser' BH3 only proteins sequester the anti-apoptotic BCL-2 proteins but the free BAK and BAX must then be activated by transient binding to 'activator' BH3 only proteins, BIM and tBID, before mitochondrial permeabilisation can occur. Adapted from (Tait & Green 2010)

Both BAK and BAX are globular proteins comprising of 9 helices. Inactive BAX is localised to the cytoplasm as inactive monomer where the α9 helix is sequestered to the hydrophobic groove. Upon transient binding of BH3 only proteins, BAX undergoes a number of conformational changes including the exposure of the α9

helix, thus facilitating its translocation and insertion into the mitochondria (Wolter et al. 1997). The newly exposed regions allow new interactions and thus oligomerisation and MOMP (Nechushtan et al. 2001; M. Suzuki et al. 2000).

In contrast, BAK is localised to the outer mitochondrial membrane. Upon receipt of an activating signal, BAK is transiently bound by a BH3 only protein stimulating an N-terminal conformational change to expose a BH3 domain in a BAK monomer. This BH3 domain then binds the exposed hydrophobic pocket of another BAK monomer resulting in BAK dimer formation (Dewson et al. 2008). These dimers oligomerise to form homo-oligomers comprising at least 18 BAK molecules through an interface of α6 helices which permeabilise the OMM (Fox et al. 2011; Azad & Storey 2013).

1.4 Autophagy

The apoptotic cell death pathway is closely associated with the cell survival pathway, autophagy.

Autophagy is a highly conserved catabolic process that results in the degradation and recycling of cytoplasmic proteins and organelles. Autophagy is required for cellular homeostasis under physiologic conditions where it is active at basal levels. On the other hand autophagy is part of the cellular stress response system leading to cell survival during sub-lethal stress and its disregulation has been implicated in many pathological conditions.

To date three distinct types of autophagy have been identified. First, macroautophagy where a double membrane vesicle called the autophagosome engulfs cytoplasmic contents and fuses with the lysosome for degradation. Second, microautophagy that is an inward invagination of the lysosomal membrane and third, chaperon mediated autophagy that involves a direct translocation across the lysosomal membrane. The focus of this project is macroautophagy that herein

after will be referred to as autophagy (reviewed in (Kroemer et al. 2010; Esclatine et al. 2009; Wirawan et al. 2011; Rubinsztein et al. 2010). The autophagic pathway involves the following key steps: 1) initiation or phagophore formation (also called isolation membrane formation), 2) elongation, 3) maturation and fusion of the autophagosome with the lysosome (Figure 1-10). The core pathway of mammalian autophagy involves the proteins of more than 30 autophagy related genes (ATG). The Atg proteins function at several steps in autophagy and orchestrate much of the process (Y. Feng et al. 2014).

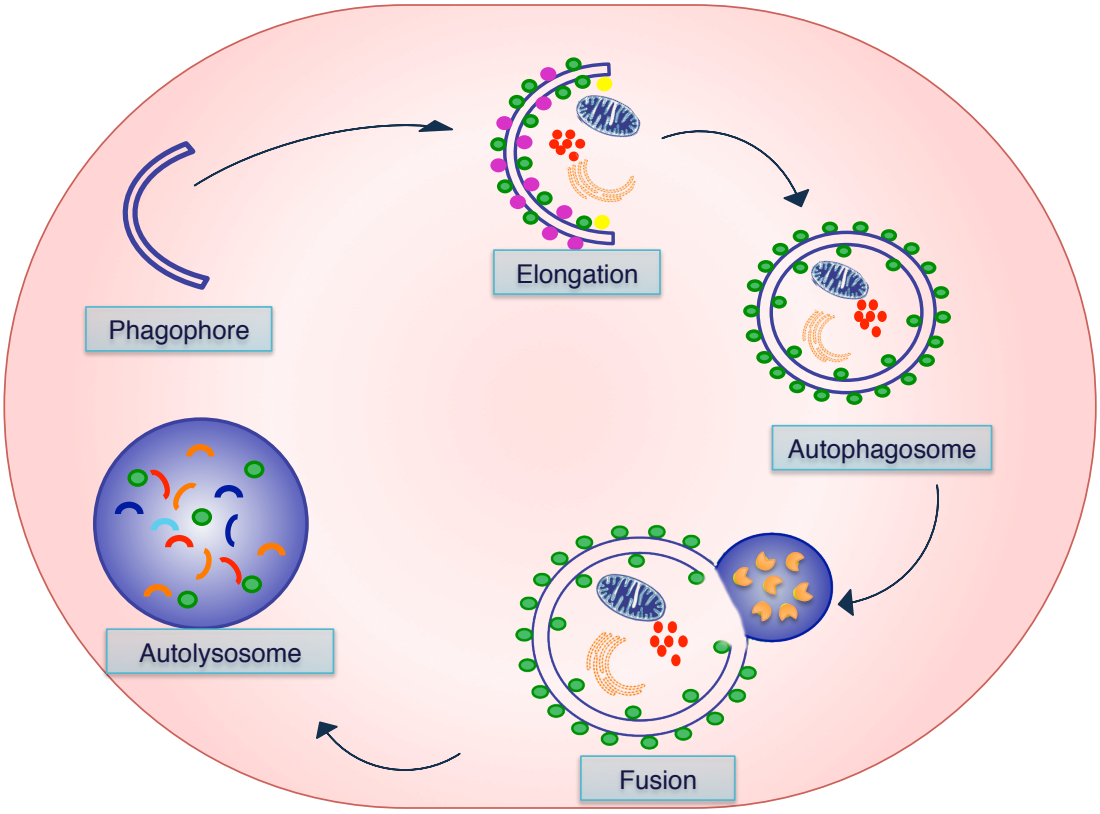

Figure 1-10 Key steps in the autophagic pathway and its machinery

Mammalian autophagy proceeds through a series of steps including initiation and the formation of the phagophore, elongation of the pahgophore and sequestration of cargo followed by maturation and the formation of a full autophagosome, which subsequently fuse with the lysosome to form an autolysosome for cargo degradation. Adapted from (Y. Feng et al. 2014)

1.4.1 Mechanism of autophagy

The induction of autophagy requires the action of Unc51-like kinase 1 (ULK1) complex (Chan et al. 2007). ULK1 is a downstream target of the nutrient of the cell sensor mTORC1 (mammalian target of rapamycin complex 1). Under nutrient low conditions, mTORC1 dissociates from ULK1, resulting in its dephosphrylation and its association with Atg13, FIP200 (focal adhesion kinase (FAK) family interacting protein of 200 kD) and Atg101 (Chang & Neufeld 2009). This core complex is essential for autophagy induction as it facilitates the recruitment of other Atg proteins such as the trans-membrane Atg9 protein that may provide lipids to the isolation membrane. Although the ULK1 complex is an mTORC1 target, it is also

important for mTORC1 independent autophagy (Orsi et al. 2012; Mizushima 2010). The isolation membrane can be generated from multiple sources in the cell including the endoplasmic reticulum (ER), the outer mitochondrial membrane, plasma membrane and de novo from precursor cellular proteins (Tooze & Yoshimori 2010; Ravikumar et al. 2010; Hayashi-Nishino et al. 2009). The formation of the phagophore requires another complex known as the class III PI3K complex. This protein complex includes: Beclin1 (Bcl2 interacting protein), Vps15 and class III PI3K. Beclin1 is an essential autophagy protein and is proposed to have different roles in diseases such as pathogen infection, cancer and neurodegeneration. In the class III PI3K complex, Beclin1 acts as a platform for the recruitment and binding of proteins that can positively or negatively regulate autophagy (He & Levine 2010). The formation of the class III PI3K complex is essential for the generation of phosphatidylinositol-3-phosphate (PI3P) that is required for the formation of the omegasomes, the Ω−shaped structures that bud from the ER during the initial steps of autophagosome formation (Axe et al. 2008). Figure 1-11 provides a summary of the mechanism of autophagy.

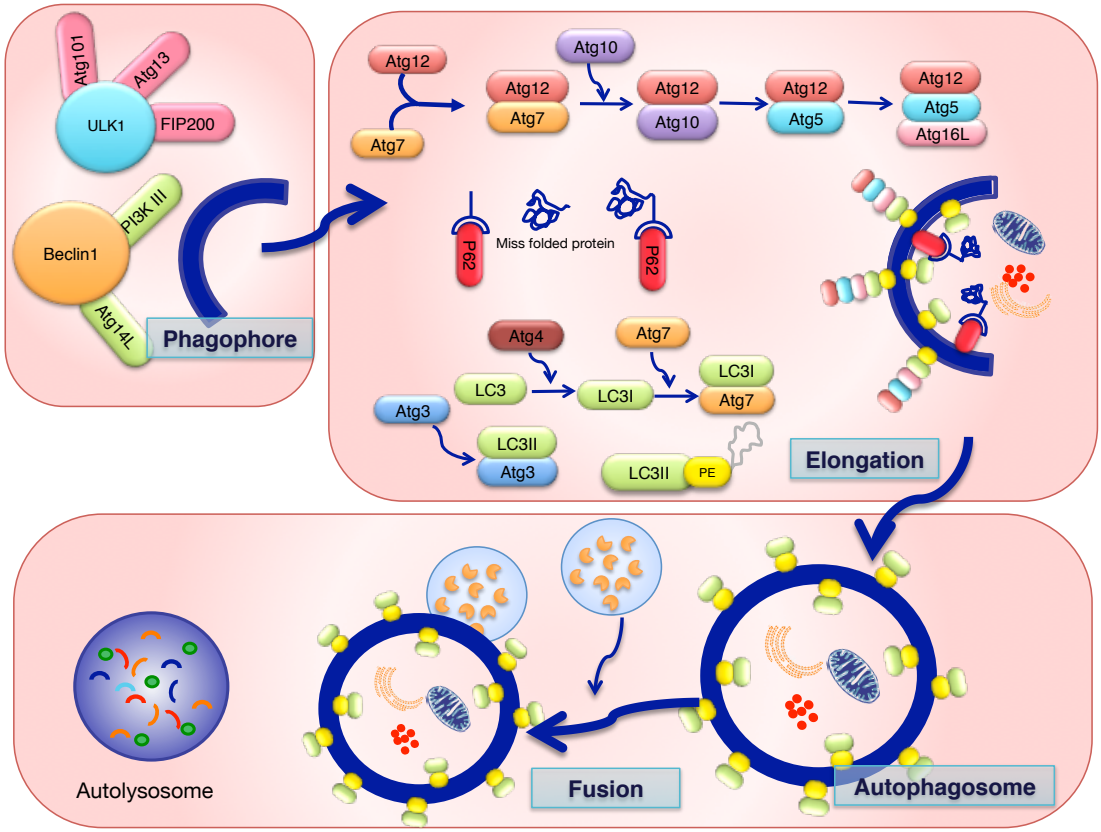

Figure 1-11 Mechanism of autophagy

The first step of the pathway is the formation of the phagophore. Execution of this step requires two essential complexes: first, a class III PI3K complex (PI3K3C) that is formed by the activation of class III PI3K that subsequently binds to Beclin-1. The second macrocomplex contains ULK1 and it is formed by the activation of ULK1 and its subsequent binding to Atg13 and FIP200. The second step in the pathway is vesicle elongation and sequestration of cytoplasmic contents, where two ubiquitin like systems are involved. The first involves the covalent binding of Atg12 to Atg5 with the help of the E1 like enzyme Atg7 and the E2 like Atg10. The second system entails the conjugation of phosphatidylethanolamine (PE) to LC3-1 by the action of the Atg4, Atg7 and Atg3. The lipid conjugation leads to the conversion of the soluble form of LC3 to the autophagosome-associated form (LC3-II). LC3-II is the only protein that remains bound to the autophagosomal membrane until fusion with the lysosome, making it a useful marker for autophagy. Other proteins are also recruited to the autophagosomes in addition to LC3 such as p62, a protein that is degraded upon autophagy induction. The third step is maturation to a full autophagosome and finally fusion with the lysosome where contents are degraded. Adapted from (Kroemer et al. 2010)

The elongation step involves two ubiquitin like conjugation systems (Z. Yang & Klionsky 2010). The first conjugation system is the Atg12-Atg5-Atg16L that is essential for the formation of the pre-autophagosomes. The E1 like Atg7 activates the carboxy-terminal glycine residue of Atg12, Atg12 is then transferred to E2-like Atg10 and is then bound to Atg5 through an isopeptide bond. The Atg12-Atg5

conjugate then interacts non-covalently with Atg16L1 to form the multimeric Atg12-Atg5-Atg16 protein complex through the homo-oligomerization of Atg16. The Atg12-Atg5-Atg16L protein complex is recruited to the pre-autophagosomal membrane but disassociates fully from the mature autophagosome (Walczak & Martens 2013). The second conjugation system involves the microtubule-associated protein 1 light chain 3 (LC3). LC3 is cleaved at the carboxy terminal by Atg4 to form LC31. LC31 is conjugated to phosphatdylethanolamine (PE) at a glycine (Gly) residue by the action of the E1-like enzyme Atg7 and the E2-like enzyme Atg3 to form LCII (Kabeya et al. 2000). LC3 is specifically recruited to the membrane of the growing autophagosome where it remains bound until fusion with the lysosomes. LC3 plays a vital role in the selective recruitment of cargo into autophagosomes, and serve as a docking site for adaptor proteins. There are at least six orthologs of LC3 in mammals that contribute redundantly in the autophagic pathway, the most studied include; LC3B, GABARAP and GATE16 (Weidberg et al. 2010).These proteins are expressed ubiquitously in all tissues and display only slight variations between each family member. A cross talk exists between the two conjugation systems, studies have demonstrated that Atg16 complex acts as an E3 ligase and determines the sites of LC3 lipidation on the autophagosomes (Fujita et al. 2008). Other proteins are also recruited to the autophagosomes such as sequestosome 1 (SQSTM1/p62) that functions by driving the damaged or unfolded proteins to the autophagic pathway for degradation. Unlike LC3 however, p62 is degraded upon autophagy induction (Pankiv et al. 2007; Bjørkøy et al. 2005).

Mature autophagosomes move in the cytoplasm along the microtubule network with the function of the dynein motor proteins (Köchl et al. 2005). Autophagosomes then fuse with the lysosomes to form autolysosomes. The contents of which are degraded by the action of lysosomal hydrolases. In mammals several proteins have

been described to be essential for the maturation and fusion of the autophagosomes and those include: UVRAG, Robicon and syntaxin-5 SNARE complex proteins (Itakura et al. 2012). Additionally, the inhibition of vacuolar H^+ ATPase (V-ATPase) by the use of pharmaceutical inhibitors such as BafilomycinA1 prevents the fusion between the autophagosomes and the lysosomes indicating a role for lysosomal PH in the fusion step of autophagy.

Autophagy is a dynamic process; the turnover of autophagosomes by lysosomes is termed the autophagic flux and serves as in indication of autophagy induction or activation. The use of inhibitors to block the fusion of the autophagosomes and lysosomes is used to assess the dynamic autophagic flux (Klionsky et al. 2014).

1.4.2 Signaling pathways regulating autophagy

Autophagy is induced in response to various stimuli including nutrient and growth factor depletion, hypoxia, genotoxic stress that is mediated by radiation and chemotherapy. There are many signaling pathways that tightly regulate autophagy and many of these pathways converge mTORC (Figure 1-12). mTORC is regulated by diverse signals such as growth factors, amino acids, glucose and energy status, it serves as a master negative regulator of the autophagic pathway (Hosokawa et al. 2009). The presence of growth factors stimulates class 1 PI3K that in turn phosphorylates the plasma membrane lipid phosphatidylinositol-4,5-bisphosphate (PIP_2) to produce phosphatidylinositol-3,4,5-trisphosphate (PIP_3), which recruits and binds AKT. Activated AKT can activate mTORC1 through the tuberous sclerosis complex 1/2 (TSC1/2) and Rheb (Y. Li et al. 2004). Activated mTORC1 then phosphorylate ULK1 at S757 thus preventing the formation of the ULK1-Atg13-FIP200 complex. The phosphatase PTEN, which hydrolyzes PIP_3, has a stimulatory effect on autophagy by abolishing class I PI3K/AKT inhibition. Although the mTORC1 pathway is the most investigated autophagy regulator, there are

various signaling molecules that can regulate the pathway for example; the energy sensor AMPK can regulate autophagy in an mTORC1 dependent and independent manner. AMPK is activated by a decreased ATP/AMP ratio through the upstream LKB1 kinase. Activated AMPK leads to the phosphorylation and activation of TSC1/TSC2 resulting in the inhibition of mTORC1 and the induction of autophagy. Moreover, when energy is limited AMPK can directly activate autophagy by the phosphorylation and activation of ULK1 at S317 and S77 (Kim et al. 2011). Furthermore, AMPK stimulates autophagy in response to glucose starvation by the phosphorylation of Beclin1, thus promoting its incorporation into the PI3K complex. AMPK can also be activated via the action of p53 upon its oncogenic activation or in response to genotoxic stress. p53 can stimulate the autophagic pathway through the up regulation of the damage-regulated autophagy modulator (DRAM), a lysosomal protein that functions at the crossroad between p53-induced autophagy and cell death (Crighton et al. 2006). Moreover, p53 can induce the transcription of autophagy related proteins and activate autophagy. Other transcription factors have also been implicated in autophagy regulation such as FOXOs. In nutrient rich conditions, PI3K/AKT pathway sequesters FOXOs into the cytoplasm and upon nutrient depletion FOXOs translocate to the nucleus and mediate the transcription of autophagy related genes such as LC3 and ULK1 (Mammucari et al. 2007). Autophagy is induced in response to low oxygen levels via the action of HIF1. HIF is a key transcription factor that allows rapid adaptation to and survival in a large range of reduced oxygen concentrations. HIF1 can activate autophagy and stimulate cell survival through the activation of BCL2/adenovirus E1B 19kDa interacting protein 3 (BNIP3). FOXO can also mediate the transcription of BNIP3 leading to autophagy induction (K. Guo et al. 2001).

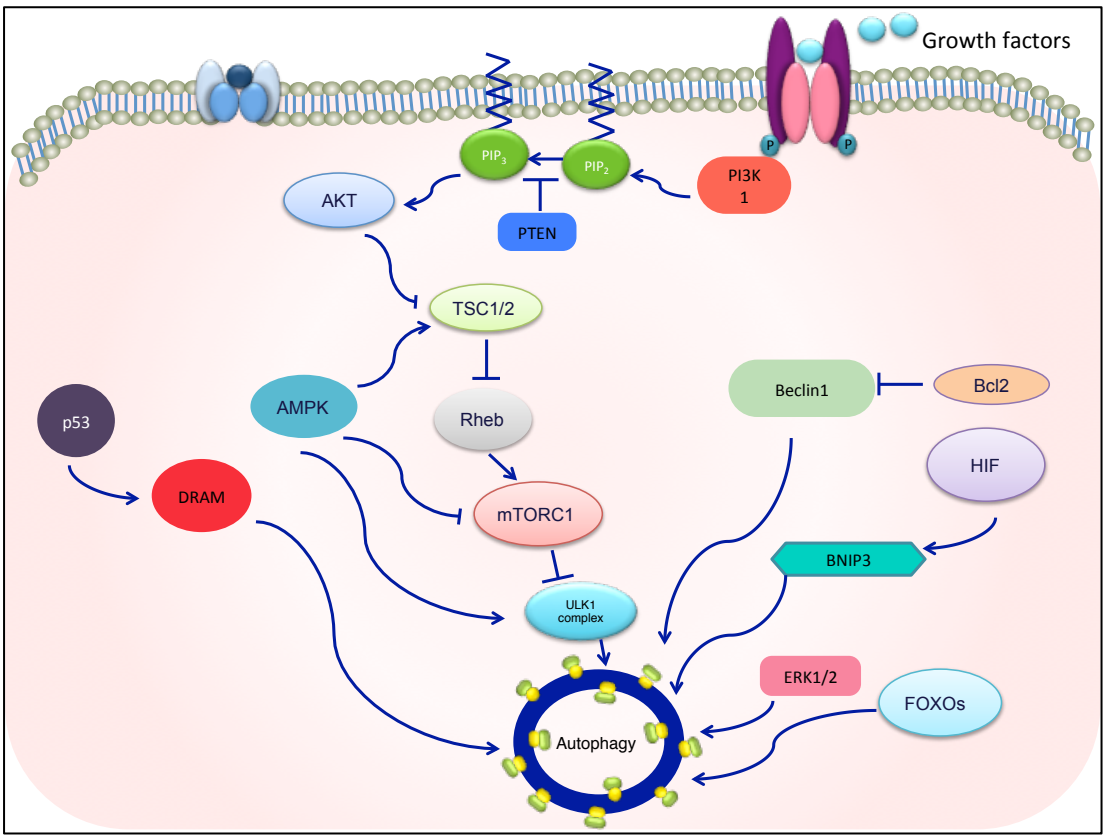

Figure 1-12 Regulation of autophagy

A schematic representation of the different signalling molecules regulating autophagy.
In nutrient rich conditions, class I PI3K facilitates the formation of PIP_3 that in turn activates AKT. AKT inhibit autophagy by abolishing the inhibitory effect of TSC1/2 and activating mTORC1. AMPK can activate autophagy through direct interaction with ULK1 or through inhibition of mTORC1 activity. Although mTORC1 serves as the main regulator other signalling molecules can activate autophagy in an mTORC1 independent manner such as ERK1/2, p53, HIF and Bcl2 proteins. Adapted from (Rubinsztein et al. 2010).

Additionally, The Bcl-2 protein family plays a dual role in autophagy regulation through Beclin1. The anti-apoptotic proteins Bcl- 2, Bcl-XL, and Mcl-1, can inhibit autophagy, by binding to Beclin1 and decreasing its association to class III PI3K (Zhou et al. 2011). On the other hand pro-apoptotic BH3-only proteins, such as BNIP3, Bad, Bik, Noxa, Puma, and BimEL, can induce autophagy (Kroemer et al. 2010).

The accumulation of misfolded proteins in the ER can stimulate autophagy by activating PERK (protein kinase R-like endoplasmic reticulum kinase), which upregulates Atg12, and activates the Atg5–Atg12–Atg16 complex (Kouroku et al.

2006). Additionally studies have demonstrated that the activation of extracellular signal-regulated kinases (ERK1/2), activates autophagy in different cell types (Ogier-Denis et al. 2000).

1.4.3 Divergent roles of autophagy

Autophagy has been shown to be essential in a number of physiological processes ranging from adaptation to starvation, cell differentiation and development, the degradation of aberrant structures, turnover of superfluous or damaged organelles, tumour suppression, innate and adaptive immunity, lifespan extension and cell death. Additionally autophagy is implicated in many pathological conditions such as cancer, neurodegenerative diseases metabolic dysfunctions and vascular instability. The roles of autophagy relevant to this work are discussed in details in the introduction of each chapter.

1.4.3.1 Physiologic roles of autophagy

Autophagy is one of the most evolutionary conserved cellular processes that promote cell survival. Autophagy plays a critical role under physiologic conditions of nutrient depletion of reduced growth factor signalling. The autophagic degradation of cytoplasmic organelles and proteins yields free amino acids, fatty acids and other substrates that can be used by the tricarboxylic acid cycle (TCA) to maintain cellular ATP production (discussed in more detail in 4.1) (Rabinowitz & White 2010). Additionally the elimination of defective proteins and organelles prevents of abnormal protein aggregate accumulation and makes autophagy an important cellular quality control mechanism. All ageing cells accumulate damaged proteins and organelles, even in the absence of any mutations that predispose the cells to a pathogenic phenotype such as aggregate prone mutant proteins. It is

observed that the autophagic activity decreases with age and thus it is proposed that autophagy plays a major role in aging (Schneider & Cuervo 2014).

Moreover, autophagy acts as a cell remodeling mechanism during differentiation and development. For example, autophagic degradation of components of the oocyte cytoplasm (maternal mRNAs and paternal mitochondria) is vital for the pre-implantation period after oocyte fertilization. Additionally, Atg7 was shown to be an essential regulator of hematopoietic stem cell maintenance (Vessoni et al. 2012).

Autophagy constitutes a stress adaptation pathway that promotes cell survival. An apparent paradox is that autophagy is also considered a form of nonapoptotic programmed cell death called “type II” or “autophagic” cell death (ACD), and it is identified by extensive accumulation of autophagosomes. This form of cell death is matter of debate in the autophagy field, it is believed that an autophagic process occurs in dying cells and this does not constitute a cell death modality. Additionally much evidence of ACD was produced in model organisms and the evidence for the existence of ACD in mammals is scarce (Kroemer & Levine 2008; Shen et al. 2014).

1.4.3.2 Autophagy in diseases

Autophagy is considered a cellular housekeeping process and defects in autophagy are implicated in many pathological conditions such as viral infections (discussed in detail in 3.1.1) and cancer (discussed in 5.1.2).

1.5 Summary and study aims

Different types HPVs have various associations with human diseases. Low risk HPVs such as HPV1 and 4 cause *verrucae vulgares*, a benign wart lesion of the skin. Human Papilloma Viruses of the high-risk types are typically associated with the development of dysplastic epithelial lesions and cancer. Alpha high-risk HPV types 16 and 18 are established as the etiological agents for cervical cancer and are also attributed to head and neck cancers. Accumulating evidence suggests that high-risk beta HPV types (5, 8, 20 and 38) play a co-factorial role in the development of non-melanoma skin cancer alongside UV.

The HPV genome encodes two major oncoproteins: E6 and E7. E6 from different high-risk HPV types can abrogate UVB induced apoptosis, partly by targeting the pro-apoptotic protein BAK for proteolysis. This allows the cells to survive the milieu of genomic stress, which can be a potential mechanism of oncogenesis.

Several studies highlighted a cross talk between the apoptosis and the autophagy pathways, in which both pathways can be stimulated by common upstream signals such as stress. Additionally, an autophagic response is triggered in $BAK^{-/-}BAX^{-/-}$ mouse embryonal fibroblasts in response to Etoposide, a DNA damaging agent (Shimizu et al. 2004).

Having noted that E6 can inhibit apoptosis, the purpose of the studies conducted here was to investigate whether E6 protein of cutaneous HPVs impinges upon or activates autophagy and to investigate the underlying mechanism.

Chapter 2 Materials and Methods

2.1 Tissue Culture

2.1.1 Media

Dulbecco's Modified Eagle's Medium (DMEM)

500ml High glucose, L-Glutamine DMEM (#11965-092, Gibco, Life Technologies) supplemented with 50ml Foetal Calf Serum (FCS, #A15-151, PAA).

Rheinwald Media (RM+)

3:1 (vol/vol) DMEM Ham's F12 media (US Biologicals, #D9811-14D), high bicarbonate, pH 7.5 with 10% FCS (#FB-1001, Biosera) supplemented with RM+ supplement to give the final concentrations listed in Table 2.

An RM+ concentrated supplement was prepared so that upon 100-fold dilution in media gave the final concentrations indicated below.

Table 2 Contents of RM+ Media

Component	Final Concentration in Media
Hydrocortisone	0.4µg/ml
Cholera toxin	10^{-10}M
Transferrin	5µg/ml
Liothyronine	2 x 10^{-11}M
Insulin	5µg/ml
Epidermal Growth Factor (EGF)	10ng/ml

2.2 Cell Lines and Maintenance

2.2.1 Cell Lines

HT1080 Fibrosarcoma cell lines (Rasheed et al. 1974) PT67 and 293T cells maintained at 37ºC, 10% CO_2 in DMEM + 10% FCS. See supplementary files for cell line authentication report.

PM1 cells (Proby et al. 2000) were cultured in RM+ media at 37ºC, 10% CO_2.

All cell lines used are adherent, therefore for passage the media was aspirated and cells washed with Phosphate Buffered Saline (PBS). The cells were detached using a volume of 1x Trypsin-EDTA solution in PBS (from 10X stock, #15400-054, Life Technologies) sufficient to cover the flask surface. Once cells were detached the trypsin was neutralised with an equal volume of DMEM + 10% FCS. A fraction of this was then resuspended in the relevant growth media. Specific cell densities were acquired by counting live cells using a haemocytometer.

2.2.2 Mycoplasma Testing

Cell lines were periodically tested for mycoplasma using the PCR based Venor GeM kit. The primers provided are specific to the 16S rRNA coding region in the mycoplasma genome. Internal control primers are also included as a positive control for the PCR reaction.

Testing was performed according to the manufacturer's instructions. Briefly, cell culture supernatant was heated at 95°C for 5 minutes and cell debris pelleted by centrifugation. Two microliters of this supernatant, water as a negative control or positive control DNA was added to a 25µl PCR reaction and the PCR reaction performed as described by the manufacturer. PCR products were analysed on a 2% agarose gel, loading 10µl of the PCR reaction. A PCR product of 191bp indicated a successful PCR reaction and a product of 270bp indicated mycoplasma contamination.

2.2.3 UVB Irradiation of Cells

Cells were seeded in 60mm-150mm dishes at approximately 70% confluence. After 24 hours the media was removed and cells washed in PBS. Cells were then irradiated with indicated doses using either a UVP CL-1000 Ultraviolet Crosslinker (F875 bulbs, spectral peak at 312nm) or a calibrated lamp (UV source MRL 58

lamp). Fresh media was then added and cells incubated for the indicated time points.

2.2.4 Storage and Recovery of Cell Lines

Cells were detached using trypsin and neutralised with DMEM + 10% FCS as described above (chapter 2.2.1). Cells were pelleted by centrifugation at 1,000rpm for 5 minutes (Heraeus Biofuge Primo), resuspended in FCS + 10% dimethylsulphoxide (DMSO) at a density of 10^6/ml and 1ml aliquoted to cryovials. Vials were wrapped in 5 layers of tissue paper and frozen at -80°C. They were later transferred to liquid nitrogen for long term storage.

To revive from liquid nitrogen cells were rapidly thawed at 37°C and diluted in 5ml of DMEM + 10% FCS and pelleted by centrifugation at 1,000rpm for 5 minutes (Heraeus Biofuge Primo). The media was aspirated to remove the DMSO, the cell pellet resuspended in appropriate culture media and transferred to a 75cm^2 flask for culture.

2.2.5 Pharmaceutical drugs used

Name	Concentration
Bafilomycin A1	100nM
Thapsigargin	3μM
Doxycycline	1μg/ml

2.3 Transfection of Mammalian Cells

2.3.1 DNA Transfections

XtremeGene 9

HT1080 and PT67 cells were seeded at $3x10^5$ cells in a 6 well plate. Twenty-four hours later cells were transfected using XtremeGene 9 (Roche). Transfection reagent (3:1 transfection reagent [µl] to DNA [µg]) was diluted to a total volume of 100µl using serum free media. One to two micrograms of DNA were added and mixed by pipetting. After incubation at room temperature for 15 minutes the mixture was added to 2ml of culture media on cells.

2.3.2 Retrovirus Production and Transduction

In order introduce HPV E6 expression into keratinocyte lines (PM1), which have a low transfection efficiency, cells were retrovirally transduced with recombinant viruses encoding the genes of interest using the pLXSN vector (Clontech). pLXSN also contains a neomycin resistance gene enabling selection of transduced cells with G418. The plasmids were transfected into the viral packaging cell line PT67 ($1x10^5$ cells per well of a 6 well plate) using XtremeGene9 (Roche, see chapter 2.3.1). Twenty-four hours after transfection cells were selected using 500µg/ml G418. Cells were maintained in G418 selection and passaged until untransfected control cells were dead. Selected cells were grown to confluence in T180 flasks. Sixteen millilitres of fresh media was added and cells maintained overnight at 32°C to package RNA into replication incompetent retroviral particles. Media containing the viral particles was collected in 4ml aliquots and frozen at -80°C.

For infection, cells were seeded 24 hours previous at $2x10^5$ cells per well of a 6 well plate. The culture media was aspirated and cells incubated with 2ml serum free

DMEM containing 5μg/ml polybrene (Hexadimethrine bromide) previously mixed in glass (as polybrene adheres to plastic) for 10 minutes at 37°C then removed by aspiration. Polybrene was added to viral supernatant to a final concentration of 5μg/ml and 2ml added to each well of cells. Cells were centrifuged with the viral supernatant for 1 hour at room temperature at 350rpm (Beckman Coulter, AllegraX-12R) to increase efficiency of infection. The supernatant was removed and fresh media added to the cells. Twenty-four hours later 500μg/ml G418 selection was added to the cells and cells were passaged to sufficient number under G418 selection.

2.3.3 shRNA ULK1 Transduction

The lentivirus was obtained from Open Biosystems (Table 3 shRNA sequences for ULK1). The mir-30 shRNA sequences were sub-cloned from pGIPZ into pTRIPZ using XhoI and MluI digestion. Lentivirus was packaged in HEK-293T cells by CaPO4 co-transfection of pTRIPZ vectors with psPAX2 and pMD2.G. Titers calculated from transduction of A431 cells were 1.0E5 and 1.7E5 for ULK1 and NS, respectively.

PM1 cells transduced with HPV5 E6 and pLXSN were seeded in a 6 well plate ($2x10^5$ cells per well of a 6 well plate). 24 hours later, culture media was aspirated and cells were incubated with 2ml serum free DMEM containing 5μg/ml polybrene (Hexadimethrine bromide) previously mixed in glass (as polybrene adheres to plastic) for 10 minutes at 37°C then removed by aspiration. Polybrene was added to viral supernatant to a final concentration of 5μg/ml and 2ml added to each well of cells. Cells were centrifuged with the viral supernatant for 1 hour at room temperature at 350rpm (Beckman Coulter, AllegraX-12R) to increase the efficiency of infection. The supernatant was removed and fresh media added to the cells. Cells were then selected by puromycin (1g/ml) for one week. Cell death

experiments, the cells were incubated in media containing 1µg/ml Doxycycline and the experiment was initiated 24 hours later.

Table 3 shRNA sequences for ULK1

Gene	Number	Sequence
ULK1	V2LHS_33057	CCCTTTGCGTTATATTGTA
Non-silencing control	RHS4743	

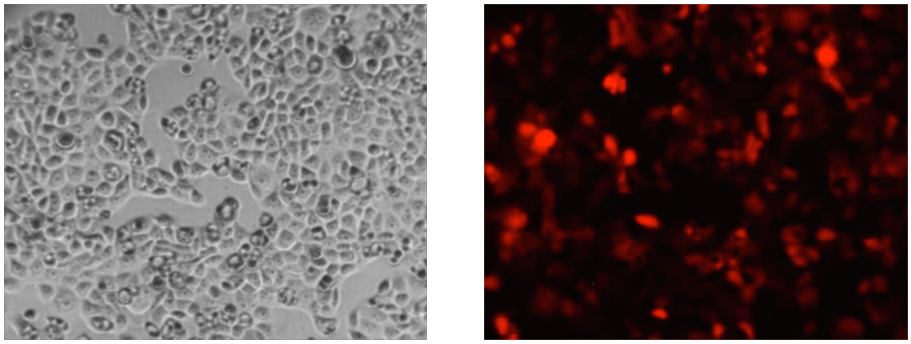

Figure 2-1 Example of RFP expression following 24 hours of Dox 1ug/ml

2.4 Protein Techniques

2.4.1 Whole Cell Extracts

The media was removed from cells, were washed once with PBS on ice. Cells were then scraped into microcentrifuge tubes and washed once with PBS. Cells were pelleted by microcentrifugation at 4,000rpm for 5 minutes at 4ºC and the PBS removed. Unless indicated otherwise microcentrifugation at 4ºC was performed using an Eppendorf centrifuge 5415R. Pellets, if not immediately lysed, were snap frozen on dry ice for 10 minutes and stored at -80ºC.

For lysis, frozen cell pellets were first thawed on ice. Pellets were resuspended in 80-200µl (dependent on pellet size) of appropriate lysis buffer and incubated on ice for at least 30 minutes with occasional vortexing. Samples microcentrifuged at 4ºC at 13,000rpm for 5 minutes to pellet cell debris. The protein lysate supernatant was

transferred to a clean microcentrifuge tube and the protein content quantified by NanoDrop at A_{280} or by Bradford protein assay described below.

2.4.2 Bradford protein quantification

Bradford protein quantification was performed using Bio-Rad Protein Assay Dye Reagent Concentrate #500-0006. Briefly, the reagent was diluted to 1x in distilled water, and then 1µl of protein lysate was mixed with 200µl of 1x Bradford reagent and incubated for 15 min at room temperature. Absorbance was read at 595 nm. The protein concentration was calculated based on a standard curve, which was prepared for each assay, a standard curve using a serial dilution of 2 mg/ml BSA (Sigma- Aldrich, MO, USA). Samples were kept at -20 °C. Figure 2-2

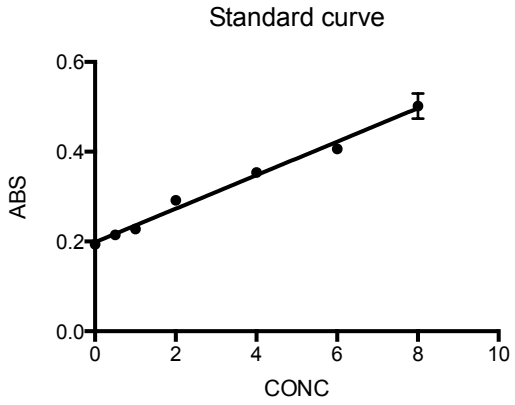

Figure 2-2 Example of obtained standard curve

2.4.3 Protein Extraction Buffers

RIPA buffer: 20mM Tris-HCl pH 7.5, 1mM EDTA, 150mM NaCl, 1% Triton X-100, 0.5% sodium deoxycholate, 0.1% SDS, 1 x protease inhibitors (Roche, cOmplete Protease Inhibitor Cocktail Tablets).

2.4.4 Sodium Dodecyl Sulphate Polyacrylamide Gel Electrophoresis

Protein lysates containing 1x Laemmli sample buffer (Table 4 5x Laemmli buffer) were denatured at 90ºC for 4 minutes and run on 16 or 12% acrylamide gels depending on the size of the proteins to be analysed. 1.5mm thick gels were used for transfer to membrane for western blotting. Gels were cast (Table 5 Gel components and concentrations) and run using standard equipment. Gels were electrophoresed in SDS-PAGE running buffer (25mM Trizma base, 192mM glycine, 0.1% SDS) at 35mA. Proteins were transferred to PVDF membrane (GE Healthcare), PVDF membrane were pre-wetted in methanol and equilibrated in transfer buffer for at least 20 minutes before transfer. After membrane equilibration, gels were transferred onto PVDF membrane in transfer buffer (25mM Tris-base, 192mM glycine, 20% [v/v] methanol) for 2 hours at 150mA.

For SDS-PAGE of samples to be analysed for large molecular weight proteins, the Life Technologies NuPAGE system was used. Samples were run on precast 1.5mm 3-8% NuPAGE Tris-Acetate gels in Tris-Acetate SDS Running Buffer using the XCell SureLock system (Life Technologies) according to manufacturer's instructions. Proteins were then transferred to PVDF membrane, again using the SureLock system with NuPAGE Transfer Buffer according to manufacturer's instructions.

Table 4 5x Laemmli buffer

Component	Concentration in 5x stock
Tris-HCl pH 6.8	625mM
Sodium Dodecyl Sulphate	5%
Glycerol	25%
β-mercaptoethanol	100mM
Bromophenol blue	0.025%

Table 5 Gel components and concentrations

The resolving mix was made and APS and TEMED added immediately before use and poured into a 10x8cm gel cast (1.0 or 1.5mm thick). The gel was covered by a thin layer of isopropanol to ensure even setting. The isopropanol was removed by rinsing with water. The stacking gel was then poured.

Volume per gel	4ml	10ml	
Component	4% stacking	16% resolving	12% resolving
Distilled water (ml)	2.72	1.96	3.3
30% acrylamide (ml)	0.68	5.33	4
1.5M Tris pH 8.8 (ml)	-	2.5	2.5
1M Tris pH 6.8 (ml)	0.5	-	-
10% SDS (ml)	0.04	0.1	0.1
10% APS (ml)	0.04	0.1	0.1
TEMED (ml)	0.004	0.004	0.006

2.4.5 Western Blotting

Following successful transfer, PVDF membranes were rinsed with H_2O and then methanol. To reduce non-specific binding membranes were incubated in 10% fat free milk (w/v) TBST (50mM Tris-base, 150mM NaCl, pH 7.5, 0.1% Tween-20) overnight at 4°C or at room temperature for 1 hour. Primary antibodies were incubated with the membrane in 0.1% milk TBST for over night at 4°C at the concentrations described (Table 6 List of antibodies and concentrations)

The primary antibody solution was discarded and membranes washed three times for at least 5 minutes with TBST before incubating with appropriate goat anti-rabbit or rabbit anti-mouse secondary horseradish peroxidise conjugated antibody used at 1/2000 in 0.1% milk TBST for 1 hour at room temperature. Membranes washed as previous and developed by the addition of electrochemical luminescence reagent (GE Healthcare, #RPN2106). Membranes exposed to X-ray film (Fuji Super RX) or Amersham Hyperfilm ECL for higher sensitivity detection (GE Healthcare #28906837) and the films were developed using X-ray developers (Xograph Imaging).

Table 6 List of antibodies and concentrations

The antibodies and dilutions used in western blots and immunoprecipitations are indicated in the table. All antibodies were monoclonal except where indicated otherwise.

Antibody	Company and catalogue number	Dilution and application	Species
ULK1	Cell Signalling, #4773	1/250	Rabbit
LC35F10	Nanotools, #0231-100/LC3-5F10	1/1000 WB	Mouse
Atg5/12	NB110-53818	1/250 WB	Rabbit
Beclin1	Santa cruz #Sc-11427	1/250 WB	Rabbit
Atg7	Cell Signalling, #2631	1/250 WB	Rabbit

GAPDH [6C5]	Millipore, #MAB374	1/5000 WB	Mouse
β-Actin	Abcam, #ab8227	1/1000 WB	Mouse

2.5 Molecular Biology Techniques

2.5.1 Polymerase Chain Reaction

2.5.1.1 RNA Isolation from Cells

RNA longer than 200 nucleotides was extracted and purified from cell pellets (less than $1x10^7$ cells) using the Qiagen RNeasy mini kit spin protocol (Qiagen). Briefly, cells were removed from the plate by trypsinisation as previously described and excess media removed by washing with PBS. Cells were lysed with appropriate amount of RLT lysis buffer, which contains guanidine-thiocyanate to inactivate RNases, according to protocol. One volume of 70% ethanol was added and the mixture was placed in the RNeasy spin column. Columns were centrifuged for 1 minute at 8,000x *g* to allow binding of RNA to the silica column under high salt conditions and the flow through was discarded. Contaminants were removed by washing as per manufacturer's instructions. The flow through was again discarded and the column spun for an additional minute to remove any residual buffer. Thirty microliters of water was placed on the column and incubated at room temperature for 1 minute. RNA was eluted in water by centrifugation as above.

2.5.2 Reverse Transcription of RNA

Reverse transcription reaction was performed using Finnzymes Dynamo Sybr Green 2 Step RT-QPCR kit (Thermo Scientific, #F430) to generate complementary DNA (cDNA) templates from mRNA.

In a 20µl reaction: 10µl 2x Reverse Transcriptase Buffer, 1µl random hexamers, 2µl M-MuLV RNase H+ reverse transcriptase containing RNase inhibitor, 7µl RNA eluted.

2.5.3 Real Time Quantitative Polymerase Chain Reaction

A real time quantitative Polymerase Chain Reaction (RT-QPCR) was used to measure the mRNA levels of target genes. mRNA was extracted as described in chapter 2.5.1.1 and cDNA generated by reverse transcription as described in chapter 2.5.2 using random hexamers. The cDNA templates were used in RT-QPCR reactions with primers against the target gene designed to span exon junctions in order to quantitate only mRNA, and not contaminating genomic DNA The same cDNA templates were also used in control reactions with primers against a reference gene (*gapdh*) in order to control for DNA loading and quality. RT-QPCR was performed using a DNA Engine Opticon 2 Continuous Fluorescence Detector (MJ Research) and the Finnzymes Dynamo Sybr Green 2 Step QRT-PCR kit (Thermo Scientific, #F430).

In a 20µl reaction: 10µl 2x mastermix, 0.5µM forward primer, 0.5µM reverse primer and 0.5µg cDNA, water to 20µl.

Table 2.7 RT-QPCR primers

Primer name	**Sequence (5'→3')**
ULK1 Fwd	TCATCTTCAGCCACGCTGT
ULK1 Rev	CACGGTGCTGGAACATCTC
GAPDH Fwd	GAGTCAACGGATTTGGTCGT
GAPDH Rev	TTGATTTTGGAGGGATCTCG

The reaction specificity was checked by the melting curve, with a narrow, single peak, overlaying curves indicating a specific reaction product. The RT-qPCR was

performed using 7900HT Fast Real-Time PCR system (Applied Biosystems) as follows: 2 minutes at 50°C, 10 minutes at 95°C followed by 40 cycles of 15 seconds at 95°C and 1 minutes at 60°C. A dissociation stage was performed after a complete amplification: 15 seconds at 95°C, 20 seconds at 60°C and 15 seconds at 95°C. Each experiment was repeated three times, in triplicate each time. The gapdh expression was used for normalization as an internal control. The relative expression of the transcript was determined by quantifying target transcript compared to control gene actin, using the ΔΔCt method:

Relative expression $_{transcript} = 2^{- \Delta\Delta Ct}$

Where $\Delta\Delta Ct_i$ = Transcript $_{normalized\ (i)}$ = (Ct $_{(i)}$ - Ct $_{gapdh\ (i)}$) - (Ct $_{(cont)}$ - Ct $_{gapdh\ (cont)}$) and, for sample i, "Ct $_{(i)}$" is the mean of the instrument Ct triplicate results for sample i; and "Ct $_{gapdh\ (i)}$" is the mean of ACTIN Ct triplicate results.

Taq Polymerase Chain Reaction

The confirmation of E6 expression in cell lines was performed using recombinant Taq polymerase (Fermentas, #EP0402).

In a 50µl reaction: 5µl 10x Taq buffer with $(NH_4)_2SO_4$, 1µl 10mM dNTP (Promega), 0.2µM forward primer, 0.2µM reverse primer, 1.5µM $MgCl_2$, 10ng DNA template, 1.25 units of Taq Polymerase, water to 50µl.

Table 2.8 Taq polymerase reaction primers

Primers were designed in order to detect cellular expression of the indicated genes by PCR.

Primer	**Sequence (5'→3')**
GAPDH Fwd	GAGTCAACGGATTTGGTCGT
GAPDH Rev	TTGATTTTGGAGGGATCTCG
HPV5 E6 Fwd	ATGGCTGAGGGAGCCGAACACC
HPV5 E6 Rev	TTACCAATCATGATAAAAATGC
HPV8 E6 Fwd	ATGGACGGGCAGGACAAGGC
HPV8 E6 Rev	TTACCAATCATGATACAAAT

Agarose Gel Electrophoresis

DNA products (PCR and plasmids) were typically separated on a 1% agarose mini gel (30ml) at 70V in 1x TBE buffer (0.4nM EDTA, 18mM Boric acid, 18 mM Tris Base pH 8.2) until adequate resolution was achieved. DNA was loaded in dye (6x, Fermentas) and stained using Webgreen DNA stain (WebScientfic). Markers used were O'Gene Ruler 100bp or 1kb (Fermentas, #SM0241 and #SM0312 respectively).

2.6 Plasmid DNA Preparation

2.6.1 Bacterial Transformation

Fifty microliters of DH5α *E. coli* subcloning efficiency competent bacteria (Life Technologies) were aliquoted into pre-chilled microcentrifuge tubes on ice. For some bacterial strains (SURE2 supercompetent, XL-10 Gold Ultracompetent, Stratagene), 1µl of β-mercaptoethanol was added and incubated for 10 minutes on ice with occasional agitation. Up to 10µl of ligation or mutagenesis reactions or 10ng of DNA were added and incubated for 30 minutes on ice. Bacteria were subsequently heat shocked for 20 seconds at 42°C and then cooled on ice for 2 minutes. Five hundred microliters of Luria Bertani (LB) media with 2% glucose was added and the bacteria were incubated with agitation at 37°C for 1 hour before plating on selective agar plates containing the appropriate antibiotic.

2.6.2 Plasmid Purification

Four millilitres of LB medium with selection was inoculated with a single bacterial colony and grown in a shaking incubator at 37°C overnight. 1.5ml of the 4ml bacterial culture was pelleted by centrifugation at 16,000x *g* for 2 minutes. The

plasmid was extracted according to manufacturer's instructions using the QIAprep Spin Miniprep Kit (Qiagen).

For plasmid amplification, after 8 hours of incubation, 200µl of the 4ml starter culture was used to inoculate a larger 200ml culture that was incubated overnight. Two hundred millilitre bacterial cultures were pelleted by centrifugation at 6000x *g* for 15 minutes at 4°C. Pellets were either frozen at -80°C or the plasmid extracted immediately using the Qiagen Plasmid Maxi Kit (#12163) according to manufacturer's instructions. Briefly, the Qiagen Plasmid DNA Isolation protocols lyse bacteria under alkaline conditions with SDS and RNase A to solubilise the cell membrane, denature proteins and DNA and to digest any RNA. Addition of acidic potassium sulphate precipitates chromosomal DNA, proteins and debris and re-natures in-solution plasmid DNA. The insoluble debris is removed by centrifugation. The plasmid DNA is extracted from the supernatant by binding to a silica membrane under high salt conditions. Following washing the plasmid DNA is eluted with distilled water.

2.7 Flow Cytometry

2.7.1 Annexin V/PI

Cells were harvested after UVB exposure at indicated times. Floating cells were included by centrifuging media at 1200 rpm for 5 minutes at 4°C. Adherent cells were then rinsed with PBS and removed from the plate with trypsin. When all cells were detached the trypsin was deactivated with an equal volume of appropriate media and cells were then pelleted with those collected from the media by centrifugation of 1200 rpm for 5 minutes. Cells were washed in PBS, and resuspended in Annexin V binding buffer (Becton Dickinson 10x stock Annexin V binding buffer) and AnnexinV- AlexaFluor 647. Propidium iodide (PI) (P4864

SIGMA-ALDRICH, Propidium iodide solution,1.0 mg/ml in water) was then added to the cells. Cells were kept on ice in the dark and analysed within 1hr on (Becton Dickinson) or CYAN with Summit software (Dako).

2.7.2 Annexin V/ Live Dead Aqua

The LIVE/DEAD® Fixable Dead Cell Stain was reconstituted with 50µl DMSO, as per manufacturer recommendation. Cells were then harvested as in 2.7.1. Then 1µl of reconstituted dye was added to 1ml of cell/PBS suspension. The cells were then incubated at room temperature in a dark place for 30 minutes. Stained cells were then washed twice with PBS and stained for annexin V using AnnexinV- AlexaFluor 647 as previously described. Cells were then analysed within 30min on (Becton Dickinson) or CYAN with Summit software (Dako).

2.7.3 Mitotracker

To determine the mitochondrial load, the mitochondria was labelled using MitoTracker® Green FM. First MitoTracker® 1mM was prepared according to manufacturers protocol. Following UVB irradiation, the culture media was aspirated and cells were washed with PBS. Adherent cells were detached using trypsin which was then neutralised using the appropriate cell culture media. Cells were washed again to remove any media contaminants. The cells were then incubated with 200nM MitoTracker® for 15 minutes. After staining was complete the cells were pelleted by centrifugation and staining solution was aspirated, cells were then resuspended in PBS and then analysed immediately (Becton Dickinson) or CYAN with Summit software (Dako).

2.7.4 GLUT1

To check the levels of the glucose transporter 1 (GLUT1), flowcytometric analysis was carried out using Human GLUT1 PerCP-conjugated antibody from R&D (FAB1418C) systems. After indicated treatment, the cells were washed with PBS and detached from plates using trypsin. Conjugated antibody was then added at a concentration of 10 µL/10^6 cells and incubated 30 minutes at room temperature in the dark. Following incubation, the cells were washed with PBS twice and were resuspended in PBS. The samples were analysed immediately using (Becton Dickinson) or CYAN with Summit software (Dako).

2.7.5 2NDBG glucose

To check for glucose uptake is a fluorescent glucose analog 2-NBDG was used. Culture media was aspirated from cells and the cells were washed with PBS. Cells were then incubated with a culture media containing 50 µg/ml 2-NBDG for 1 hour at 37°C. After incubation the cells were washed twice with PBS and analysed immediately using (Becton Dickinson) or CYAN with Summit software (Dako).

2.7.6 Measurement of internal ROS

Following UVB irradiation the cells where washed with PBS and MitoSOX Red (Invitrogen) was added to the cells to give a final concentration of 5µM and left on for 10 minutes at 37°C. Cells were harvested as described in Apoptosis assays and analyzed by FACS. Antimycin A (10mM) was used as a positive control and was added to the cells 2 hours prior to harvesting.

2.8 ImageStream

PM1 cells stably expressing HPV5 E6 and pLXSN were cultured in high glucose RM+ media supplemented with 10% FCS and treated with UV. 24 hours later, adherent cells were detached from plates by trypsin that was deactivated with an equal volume of keratinocytes media containing 10% serum and RM+. Cells were then pelleted by centrifugation at 1500 rpm for 5 minutes at 4°C. Cells were washed in PBS and re-suspended in a 96 wells round bottom plate in 100 µl of FACS buffer (PBS + 1%FCS + 0.2% sodium azide). Cells where centrifuged at 1500 rpm for 5 minutes at 4◦C and FACS buffer was aspirated. Lyso-ID® Red (Enzo Life Sciences), was added to the cells (1/1000) and left on for 10 minutes at 37°C. Cells were then washed using cold Lyso-ID® assay buffer (provided with the kit) and spun for 1500 rpm 5 minutes at 4°C. 4% Para-formaldehyde (PFA) was added to fix the cells and left on for 20 minutes at room temperature. Cells were then washed with FACS buffer twice and spun for 1500 rpm 5 minutes at 4°C. Anti-LC3 antibody (mouse monoclonal nanotools clone 5F10) diluted 1/1000 was added to the cells and left on for 20 minutes at room temperature on shaker. Cells where then washed using FACS buffer as previous. Anti-mouse Alexaflour 488 (Invitrogen probes) diluted 1/1000 was added to the cells and left on for 20 minutes at room temperature protected from light. Cells were then washed as previous, and re-suspended in 50µl of FACS buffer in 0.5 ml eppendorf tubes and analyzed using Image Stream.

2.9 Immunoflurescent microscopy assays

2.9.1 LC3 foci staining

Cells were seeded at $3x10^5$ in 60mm dishes on cover-slips. The following day cells were treated as required, the media was aspirated and the cells were washed with ice-cold PBS once. The cells were then fixed in methanol at -20°C for 20 minutes then methanol was aspirated and the cells were washed twice in PBS. Non-specific binding sites were blocked with 10%FCS/PBS for 2 hours at room temperature. Blocking solution was aspirated and Anti-LC3 (mouse monoclonal nanotools clone 5F10) diluted 1/1000 in 0.01% FCS/PBS was added onto the cells and left on overnight at 4°C. The following day the cells were washed in PBS three times for 5 minutes. Anti-mouse Alexaflour 488 Invitrogen probes was diluted 1/1000 in 0.01% FCS/PBS and added onto the cells and left on for 2 hours at room temperature in the dark. Cells were then washed with PBS three times for 5 minutes. Excess PBS was aspirated and cover slips were mounted on glass slides using flouromount. DAPI was used to visualize the nucleus. Slides were left to dry overnight in the dark, then images were obtained using Ziess confocal microscope.

2.9.2 Mitotracker staining

Cells were cultured on cover-slips in keratinocytes media with 10% FCS. The following day cells were exposed to UV and after indicated time, the media was aspirated and cells were washed once in PBS. MitoTracker Red FM (Invitrogen molecular probes) was diluted to 200nm in PBS. The MitoTracker/PBS mix was added to the cells and left on for 30 minutes at 37°C in the dark. Cells were then processed for LC3 staining as described below.

2.9.3 Time-Lapse analysis of necrosis

PM1 keratinocytes were seeded to 70% confluency on glass bottom 4 well dishes. Twenty-four hours later, the media was aspirated and the cells were irradiated with 7mJ/cm^2 UVB. Cell culture media containing 100nM Bafilomycin A1 was added to cells. To stain for annexin V, 2.5 mM of $CaCl_2$ was added and FITC-conjugated annexin V (5 µl/1 ml medium). 1.5 µM PI was then added to each well. The DeltaVision controlled chamber was set to 37°C and 10% CO_2. In each well 2 fields of views were randomly selected, and the microscope was set to acquire images every hour for 24 hours. The video series was then exported to Fiji (Image J). Then in each field of view the % of apoptotic and necrotic cells were counted. Apoptotic cells were defined by annexin V positivity alone for at least 3 hours. Necrotic cells were defined by the rapid uptake of PI and annexin V (double positive) or the uptake of PI alone.

2.10 Metabolism Assays

The Seahorse XFe analyzer (Seahorse Bioscience, Denmark) was utilized to measure the extracellular oxygen concentration or extra cellular acidification rate in a 96-well format. The assay was set up and optimized with the help of Dr. Simon Wigfeild.

Briefly, 16 h prior to the assay, a XF96 sensor cartridge (Seahorse Bioscience, Denmark) was transferred in XF calibration buffer (Seahorse Bioscience, Denmark) and placed into an incubator at 37 °C.

HT1080 cells transfected with pcDNA or pcDNA-5E6 were seeded to 70% confluence in 60mm dishes. The following day, the cells were irradiated with UVB of 10mJ/cm^2 and left to recover for 2 hours. Cells were then lifted and re-seeded in Seahorse 96 well plates (120,000 cells per well in 80 µl DMEM) and left to attach for 2 hours. The culture media was then aspirated and replaced with Seahorse custom

media without glucose and the basal non-glycolytic ECAR was measured by the XF Seahorse analyser. The first injection is a saturating concentration of glucose (10mM). Glucose is taken up by the cells and catabolized through the glycolytic pathway to lactate, producing ATP and protons. The extrusion of protons into the surrounding medium produces a rapid increase in ECAR. This glucose-induced response is reported as the rate of glycolysis (or Glycolytic Flux) under basal conditions. The second injection is oligomycin, an ATP synthase inhibitor. Oligomycin inhibits mitochondrial ATP production and thus shifts the energy production to glycolysis, with the subsequent increase in ECAR revealing the maximum glycolytic capacity of the cells.

The final injection is 2-DG, a glucose analog, which inhibits glycolysis through competitive binding to glucose hexokinase, the first enzyme in the glycolytic pathway. The resulting decrease in ECAR further confirms that the ECAR produced in the experiment is due to glycolysis (but it is not required for calculating Glycolytic Flux or Glycolytic Capacity). The difference between Glycolytic Capacity and Glycolysis rate defines Glycolytic Reserve. ECAR prior to glucose injection is referred to non-glycolytic acidification, which includes CO2 evolution (from the TCA cycle and other biochemical pathways) followed by its hydration to carbonic acid and bicarbonate, as well as proton extrusion.

2.10.1 Glycolysis Assay

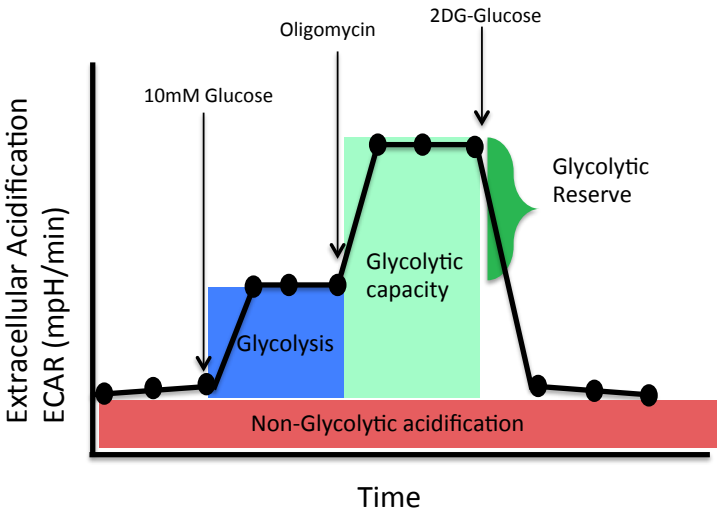

Figure 2-3 The different parameters as measured by Glycolysis stress test

2.10.2 Mitostress Test

The MitoStress Test (Seahorse Bioscience, Denmark) was performed according to the manufacturer's instructions. The cells were seeded and treated as described in Glycolysis Assay. Just before the assay, the drug dilutions were prepared at the appropriate concentrations as determined during optimisation experiments (see Appendix I, Fig. 2) and taking into account the change of volume after pneumatical sequential addition of the drugs into each well.

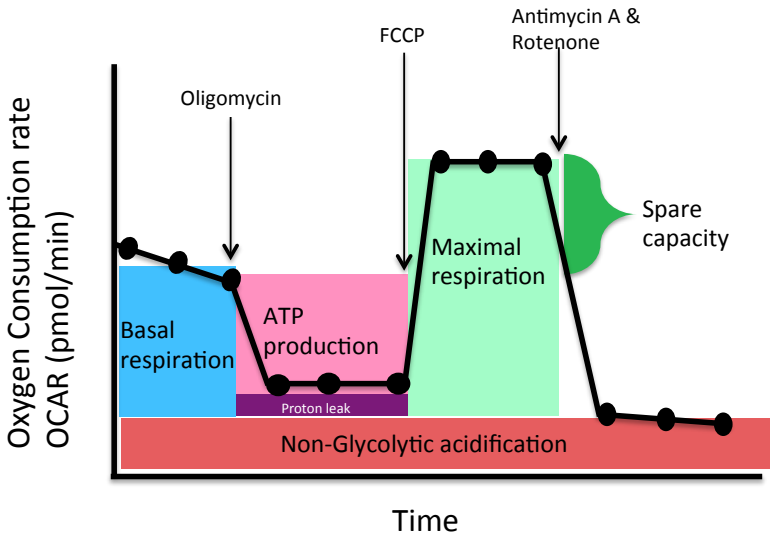

Figure 2-4 Parameters measured by MitoStress kit

Drugs used were oligomycin (inhibits ATP synthase), FCCP (uncouples OxPhos), and antimycin A (inhibits OxPhos) and rotenone (inhibits OxPhos). Indicated are final concentrations. For more information on the effect of the drugs please see section 4.3.4. 25 µl of the drug dilutions were added into the injection ports of the XF96 sensor cartridge, prior to transferring the cartridge into the Seahorse XFe analyser to start calibration of the sensors. Then, the media of the cells was removed, the cells were washed, and 175 µl assay media (Seahorse media), free of glucose, glutamine or pyruvate, with appropriate supplements as indicated in section 3.2) was added. The cell plate was placed into the machine, and the calibrated sensor cartridge automatically placed above it. The assay was started and measurements of oxygen levels were taken every 5 min and media was mixed each time before the measurements were taken. This first cycle of measurements determines the basal oxygen consumption (rate 0). After this first cycle, oligomycin was added through injection port A, and the measurements were taken again for three times (rate A). Then, the cycle was repeated after injection of FCCP through injection port B (rate B). AA and rotenone were then injected through port C, and

the measurement cycle repeated (rate C). The difference between the basal oxygen consumption and oxygen consumption after oligomycin injection is the ATP production-linked oxygen consumption rate (Rate 0 minus rate A). The maximal oxygen consumption rate was determined after FCCP addition as the difference of rate A and rate B. The spare capacity was determined by addition of AA and rotenone, by subtracting rate C from rate B. The proton leak is determined by subtracting rate C from rate A.

2.11 Electron Microscopy

Following UVB treatment, the cell culture media was aspirated and the cells were washed with PBS (for analysis of cell death, floating cells were also collected by centrifugation of media). The cells were then detached using Trypsin, then media was added to neutrilize the Trypsin. The cells were pelleted and washed with PBS. Cells were then fixed using 4% gluteraldeyde and pelleted. Pellets were washed, post-fixed in 1% osmium tetroxide, pre-embedding stained with 2% uranyl acetate, dehydrated and embedded in Spurr's resin (all from Agar Scientific, UK). Ultrathin sections were cut onto nickel grids, contrast enhanced with 2% uranyl acetate and lead citrate and viewed using a Joel 1010 electron microscope. Please note that images were taken by Prof David Ferguson (Professor of ultrastructural morphology).

2.12 Immunohistochemistry

The formalin-fixed and paraffinembedded tissue sections were retrieved, dewaxed, and rehydrated. Briefly, slides were heated to 65 °C for 10 min. Then, sections were dewaxed in Citroclear (HD, supplies, UK) twice for 5 min and rehydrated in graded industrial methylated spirit solutions of 100% (twice, 5 min each), followed by 50% (once, 5 min), before placing the slides into PBS. The antigen retrieval was performed in the 1X citrate buffer (Lab Vision™ Citrate Buffer for Heat-Induced Epitope Retrieval 10X). The slides were placed in PBS to cool down. The sections were then blocked in 10% normal horse serum (Vector Laboratories, UK) for 30 min. The primary antibody incubation was performed over night at 4°C in humidified champer. Following the primary antibody incubation, the slides were washed in PBS, and the secondary antibody (Anti-Rabbit IgG, Vector laboratories

UK) was applied and incubated for 30 minutes at room temperature in humidified chamber . Visualisation was performed by using the DAB (3, 3'-diaminobenzidine) Peroxidase (HRP) Substrate Kit (Vector Laboratories, UK) for 5-8 min. The slides were washed in tap water, before immersing them in heamatoxylin solution (Gill No3, Sigma-Aldrich, MO, USA) for 1 minute, and rinsing them in tap water. The slides were mounted with Aquamount (Fisher Scientific, UK) and visualized and photographed on a BX51 microscope (Olympus, Japan) attached to a DP40 digital camera (Olympus, Japan).

Chapter 3 HPV and Autophagy

3.1 Introduction

Autophagy is a highly conserved cellular degradation process though which cytoplasmic components are sequestered into double membrane vesicles and delivered to the lysosomes for degradation. Autophagy plays fundamental roles in physiological processes such as maintaining cellular haemostasis, ageing, development, tumour suppression, innate and adaptive immunity and adaptation to stress. Moreover, deregulation of the autophagic pathway is implicated in different pathological conditions such as viral infections and cancer (reviewed in (Z. Yang & Klionsky 2010b).

3.1.1 Autophagy and viruses

Generally, in viral infections, autophagy is triggered by viral replication or entry as a part of the host defence mechanism. The antiviral roles of autophagy are suggested by at least three different observations: First, by the degradation of viral particles through the autophagosomes (virophagy). For example, studies demonstrated that Sindbis virus nucleocapsids are selectively targeted for autophagic degradation by a mechanism that involves p62/SQSTM1 (Orvedahl et al. 2010). Additionally, Epstein Barr Virus (EBV) can be subjected to degradation by autophagy in epithelial cells (Valencia & Hutt-Fletcher 2012). Second, the delivery of viral nucleic acids to endosomal toll-like receptors (TLRs) such as in the case of vesicular stomatitis virus, where autophagy delivers cytosolic PAMPs to their cognate endosomal TLRs, activating an innate immune response (H. K. Lee et al. 2007). Third, studies showed that autophagy can participate in viral antigen presentation to the major histocompatibility complex (MHC) class I and class II molecules and leading to adaptive immunity. For example, macrophages infected with herpes simplex virus type 1 (HSV-1) show increased autophagy levels at the late infection stages and

this correlated with an increase in the presentation of a peptide of HSV-1 glycoprotein B (gB) to CD8+ T (English et al. 2009).

Given the role of autophagy in immunity, it can be expected that several viruses have developed strategies and mechanisms to subvert and utilize the autophagic pathway and use it to promote the viral life cycle, evade the immune system and promote the survival of virally infected cells. Several studies showed that Huh7.5-cells infection with Hepatitis B virus (HBV) resulted in an autophagy increase, and inhibition of autophagy led to a dramatic decreased in viral DNA replication, suggesting a role for autophagy in viral replication (McFarlane et al. 2011). Moreover, the overexpression of Kaposi Sarcoma associated Herpes Virus (KSHV) replication and transcription activator (RTA) increased autophagic flux in 293T cells. Additionally, inhibition of autophagy decreased KSHV lytic replication and expression of viral lytic genes in the PEL cell line (Primary effusion lymphoma) (Wen et al. 2010). However, v-Bcl-2, another protein that is encoded by KSHV can bind to and inhibit the key autophagy protein, Beclin-1 and that leads to autophagy inhibition. This suggests that KSHV can tightly control its replication by modulating autophagy (reviewed in Pratt & Sugden 2012).

3.1.2 Autophagy and apoptosis crosstalk

The studies on autophagy and HPV are limited. However, it is known that one of the major functions of HPV E6 oncoprotein is the abrogation of cellular apoptosis.

Cells respond to stresses such as DNA damage, nutrient depletion or hypoxia by engaging different pathways, including autophagy and/or apoptosis. Although, autophagy and apoptosis lead to different outcomes for the cell, they can be triggered by a common stress signal. Recent work demonstrated that in $BAK^{-/-}$ $BAX^{-/-}$ mouse embryonic fibroblasts (MEF) autophagy is triggered in response to etoposide, a DNA damaging agent (Shimizu et al. 2004). This could be due to the

existence of numerous signal transduction molecules which can regulate both pathways such as p53. Cytoplasmic p53 interacts with FAK family kinase-interacting protein 200 (FIP200) and blocks the activation of ULK1-Atg101-Atg13-FIP200 complex (for more details on the autophagy pathway refer to 1.4) and therefore inhibiting autophagy initiation (Morselli et al. 2011). However, p53 nuclear translocation leads to the transactivation of many autophagy-related genes that induce autophagy, for example DNA damage-regulated autophagy modulator1 (DRAM) (Crighton et al. 2006). p53 can also induce apoptosis by directly activating pro-apoptotic proteins BAK and BAX resulting in to MOMP permeabilisation and the release of cytochrome C leading to cellular demise (Perfettini et al. 2004). Furthermore, BH3 only apoptotic proteins such as BAD, BID and BNIP3 (BCL-2 and adenovirus E1B 19 kDa protein-interacting protein 3) can regulate autophagy by interfering with the interaction of BCL-2 with Beclin-1, a tumour suppressor protein that possesses a BH3 homology domain and has a key role in autophagy initiation (Zhang & Ney 2009).

In addition to upstream regulators, different proteins are in the signal transduction intersection between autophagy and apoptosis leading to either mutual inhibition or induction. In autophagy Beclin-1 acts as a platform that binds the proteins that are essential for the allosteric activation of the class III PI3K Vps34 to generate phosphatidylinositol-3-phosphate (PI3P), to mediate the initial stages of vesicle nucleation/autophagosome formation (for more details on autophagy induction refer to (Mukhopadhyay et al. 2014). Recent studies demonstrated that Beclin-1 is a novel substrate for caspases 3, 6 or 9. Activated caspases cleave Beclin-1 and generate a carboxyl-terminal fragment, downstream of the BH3 domain that localizes to the mitochondria and *in vitro* leads to cytochrome *c* release (Mariño et al. 2014).

3.2 Hypothesis and study aims

Taken as a whole, these examples of the role of autophagy in the cell stress response and immunity highlight the significance of this pathway in determining cell fate. HPV proteins have developed mechanisms to manipulate cellular pathways including apoptosis. As described previously in chapter 1.1.3.3 E6 proteins from different HPV types can specifically target the pro-apoptotic protein BAK after the receipt of a death signal such as UV DNA damage and thus altering the fate of the cell. It was postulated that E6 might modulate autophagy in this context. Moreover, since its been demonstrated that HPV E7 expression results in increased autophagy in response to nutrient stress, it is important to investigate whether E6 expression may impinge upon the autophagy pathway following an apoptotic stimuli.

The following studies focus mainly on high risk cutaneous HPV5 and 8 and their involvement in the development of NMSC, and in this chapter the postulated hypothesis is tested in using HPV5 first.

Initial aims:

1) To establish whether HPV early oncoproteins can affect host autophagy after UVB, a physiologically relevant DNA damaging signal for HPV5.

2) To determine which HPV oncoproteins affect autophagy.

3) To investigate whether different HPV types show a similar phenotype to HPV5.

3.3 Results

Since HPV E6 specifically targets and degrades BAK as a result of UVB exposure, and studies showed that autophagy is induced in cells lacking BAK and BAX following an apoptotic stimulus, the effects of HPV E6 on autophagy were studied first.

3.3.1 The generation of cell line models to study autophagy

Studies characterising the behaviour of HPV E6 expressing cells have been carried out in different cell lines. Throughout this study two cell line models were used: the HT1080 cell line and a pre-malignant keratinocyte (PM1) cell line. HT1080 is a fibrosarcoma cell line that expresses wt p53. Additionally, several studies on HPV E6 mediated evasion of UVB induced apoptosis have been published using this cell line. However, since keratinocytes are the natural host for HPV, it was essential to answer the questions of this study in a biologically relevant model alongside HT1080 cell lines. Here a pre-malignant keratinocytes cell line that was isolated from a dysplastic foreskin lesion (PM1) was chosen as a model to study effects of HPV E6 protein on autophagy. These keratinocytes serve as a good model to test the hypothesis that HPV plays a role in the initial transformation of cells, since they retained a normal keratin profile relatively and the ability to differentiate *in vitro* (Proby et al. 2000).

HT1080 cells were seeded at $3x10^5$ cells/well in a 6 well plate. After 24 hours cells were transfected with 1µg of DNA to express either HPV5 E6 or pcDNA using Fugene transfection reagent at a ratio of 3:1 (Fugene volume µl : DNA volume µg). Twenty-four hours later, successfully transfected cells were selected by culturing them in media containing G418 for two weeks.

Stable PM1 lines expressing HPV5 E6 protein or pLXSN empty vector control, were generated by retroviral transduction as described in (2.3.2). Briefly, cells were seeded at $2x10^5$ per well in 6 well plates. Twenty-four hours later the media was removed and 4ml of media was placed in a small glass bottle and 4µl of polyberene (5mg/ml) added; this mixture was added directly onto the cells and left for 10 minutes at 37°C. The media/polybrene mixture was then aspirated and 4ml of retroviral supernatant and 4ul polybrene mixed in a glass bottle and placed on the

cells and centrifuged for 1 hour at 350rpm. The cells were then washed once in warm PBS and fresh media was added. After 24 hours cells were selected and expanded using 0.5μg/ml G418 for two weeks.

Following successful drug selection, mRNA was extracted from HT1080 and PM1 cell lines transfected with either empty vector control or HPV5 E6 and cDNA was generated by reverse transcription PCR (refer to materials and methods for more details). A PCR reaction using the Taq polymerase with primers specific to the HPV5 E6 sequence or the cell housekeeping gene Glyceraldehyde 3-phosphate dehydrogenase (*gapdh*) was then performed and the products resolved by agarose gel electrophoresis. Figure 3-1A shows that HPV5 E6 PCR DNA fragment at the correct size can only be detected in HT1080-pcDNA 5E6 at 474bp product. Figure 3-1B shows similar results in PM1 keratinocytes; these results indicated successful generation of cell lines expressing HPV5 E6 and empty vector control in the two cell line models chosen for this study.

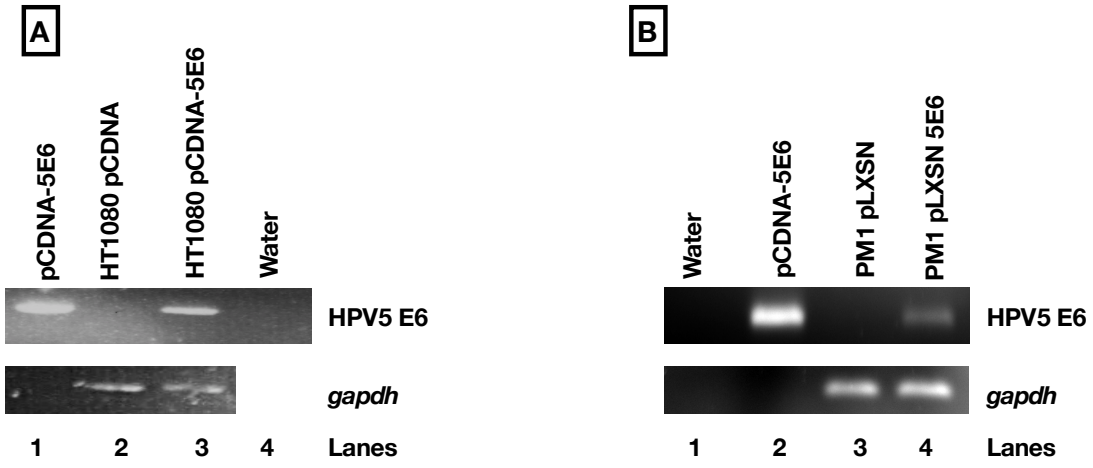

Figure 3-1 Expression of HPV5 E6 in HT1080 and PM1 cell lines

mRNA was extracted using the Qiagen RNeasy kit from HT1080 and PM1 cell lines expressing either empty vector control or HPV5 E6. cDNA was generated by reverse transcription and used in PCR reactions with the Taq polymerase and primers specific to the HPV5 E6 sequence (474bp product) or the house keeping gene *gapdh* (261bp product). PCR products were analysed by agarose gel electrophoresis. **A)** Lane 1 and 2; 10ng of the pcDNA vector encoding the HPV5 E6 gene was used in place of the cDNA template respectively, Lane 2 and 3; template cDNA generated from HT1080 cells expressing pcDNA-5E6 or pcDNA respectively. Water was used in lane 4 was used as a control instead of DNA to monitor contamination. **B)** Lane 1 and 2; water and 10ng of pCDNA-5E6, lanes 3 and 4; template cDNA generated from PM1 keratinocytes transduced with pLXSN or pLXSN 5E6.

3.3.2 Establishing a UVB dose in HT1080 and PM1 cell lines

UVB is a strong inducer of apoptosis following DNA damage. Prior to addressing the main aims of this study, it was important to determine the UVB dose that is sufficient to promote apoptotic cell death in the non-transfected cell lines without killing all the cells. Different cell types can tolerate different doses of UVB, therefore it was necessary to demonstrate a UVB dose response in both HT1080 and PM1 cell lines.

Levels of apoptosis were determined by annexin V positivity as measured by flow cytometric analysis. Annexin V is an anticoagulant protein that binds to the phosphatidylserine located on the external cellular membrane of apoptotic cells with high affinity. In this assay Alexa Fluor® 647 conjugate (Invitrogen) antibody was used to label apoptotic cells. HT1080 or PM1 cell lines were seeded to 70% confluency, and 24 hours later HT1080 cells were exposed to 5, 10 or 15mJ/cm^2

UVB while PM1 keratinocytes were irradiated with 7, 10, 15 or 20mJ/cm^2. Cells were collected at the times indicated in Figure 3-2A&B, stained for annexin V and analysed by flow cytometry. Briefly, an annexin V positive gate was created in the untreated control of each cell line, 3% in HT1080 and 5% in PM1. This was done based on the assumption that the untreated cells should have a low percentage of the cell death, and hence low annexin V staining. The percentage of cells that fell within the gate after UVB was then recorded. Figure 3-2A shows that upon irradiation with 5mJ/cm^2 UVB there is a slight increase in annexin V positive cells after 24 hours and at 10mJ/cm^2 of UVB a higher increase in the percentage of apoptotic cells is observed at both 16 and 24 hours. However a dose of 15mJ/cm^2 UVB led to a high percentage of apoptotic cell death as measured by annexin V positivity, indicating a large decrease in cell viability. These results indicate that a UVB dosage of 10mJ/cm^2 is sufficient to induce DNA damage and an apoptotic response that is not completely lethal to the cells and this is in line with previous studies done using this cell line (Jackson & Storey 2000)

Similar to HT0180 Figure 3-2B shows annexin V levels in PM1 keratinocytes following UVB exposure. From these results it is noted 15mJ/cm^2 induces an apoptotic response comparable to that of HT1080 cells; this dose was therefore chosen for these cells.

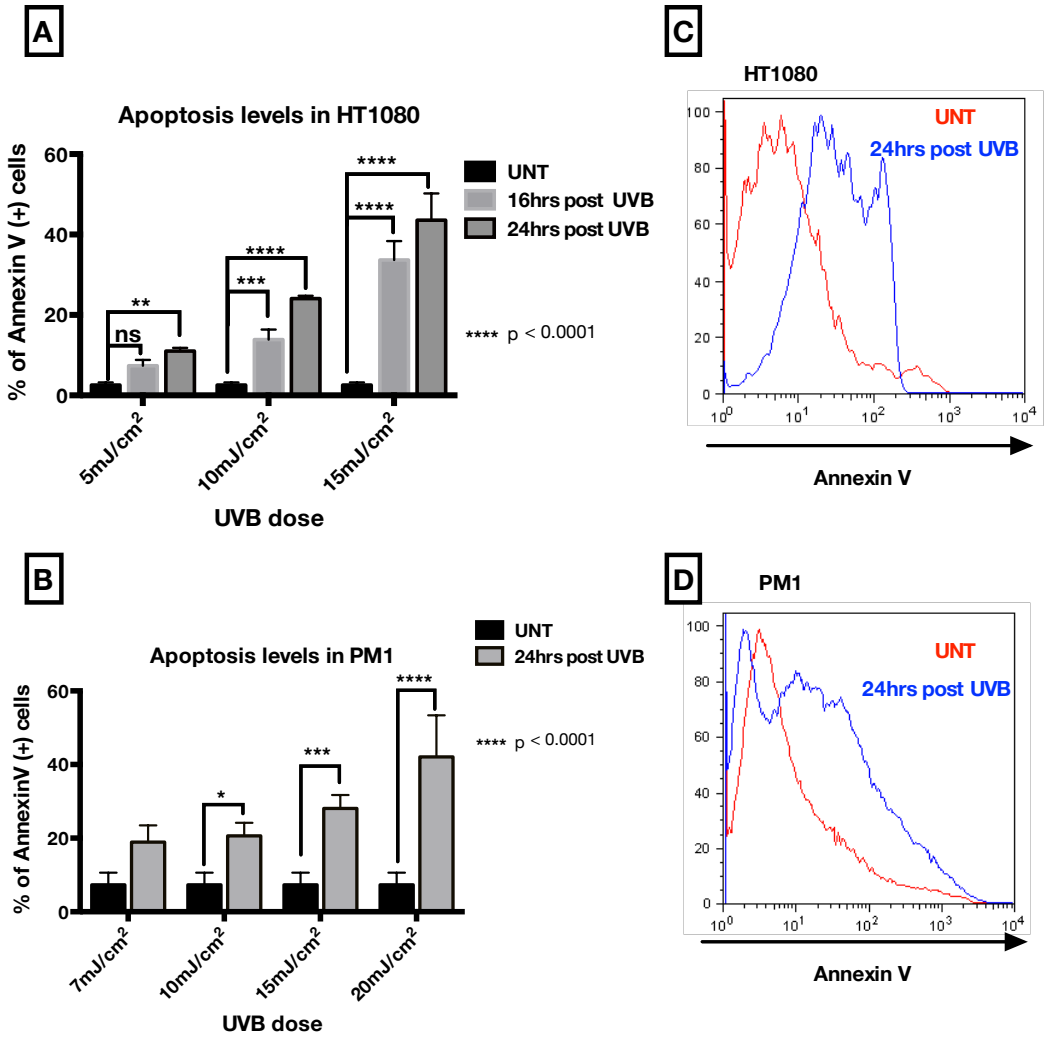

Figure 3-2 Levels of apoptosis after UVB irradiation in HT1080 and PM1 cells

A) HT1080 cells were irradiated with 5,10, or 15mJ/cm^2. Cells were then collected at 16 and 24hrs and stained for annexin V Alexa Fluor® 647 conjugate (Invitrogen) and analysed by FACS. Percentage increase in annexin V from the untreated baseline is plotted. n=3 ± SEM. Statistical significance calculated using two way ANOVA with Bonferroni's multiple comparison test. * p<0.05, ** p<0.01, and ***p<0.001, and ****p<0.0001

B) PM1 keratinocytes were irradiated with 7,10, 15 or 20mJ/cm^2. Cells were then collected at 24hrs and stained for annexin V Alexa Fluor® 647 conjugate (Invitrogen) and analysed by FACS. Percentage increase in annexin V from the untreated baseline is plotted. n=3 ± SEM. Statistical significance calculated using two way ANOVA with Bonferroni's multiple comparison test. * p<0.05, ** p<0.01, and ***p<0.001, and ****p<0.0001

C/D) Example FACS histogram of annexin V peak shift after UVB in HT1080 and PM1 cells respectively.

3.3.3 Effect of HPV5 E6 expression on UVB induced apoptosis in HT1080 and PM1 keratinocytes

Having delineated the UVB dose required to promote an apoptotic response in both HT1080 and PM1, it was important to demonstrate HPV E6 abrogation of apoptosis at the selected dosages as previously reported. HT1080 and PM1 cell lines transfected or transduced with either empty vector control or HPV5 E6 were seeded at 70% confluency and 24 hours later exposed to UVB irradiation at 10mJ/cm^2 or 15mJ/cm^2 for HT1080 and PM1 cell lines respectively. Cells were harvested at the times indicated in Figure 3-3 AnnexinV levels in HT1080 cells HPV5 E6 following UVB, stained for annexin V and analysed as previously described in 3.3.2. Figure 3-3A shows an increase in apoptotic cell death over time after UVB exposure in HT0180-pcDNA demonstrated by an increase in annexin V positivity. Meanwhile HT1080-HPV5 E6 expressing cells showed only a small increase in annexin V positive cells after UVB. PM1 cell lines respond more slowly to UVB, therefore different times were used for these cell lines (personal observation). Figure 3-3B demonstrate that PM1 cells expressing HPV5 E6 show a small increase in apoptotic cells after UVB, by contrast to cells transduced with pLXSN. These results indicate that HPV5 E6 protects the cells from apoptosis in HT1080 and PM1 cell lines at the UVB doses used making these doses suitable for further studies.

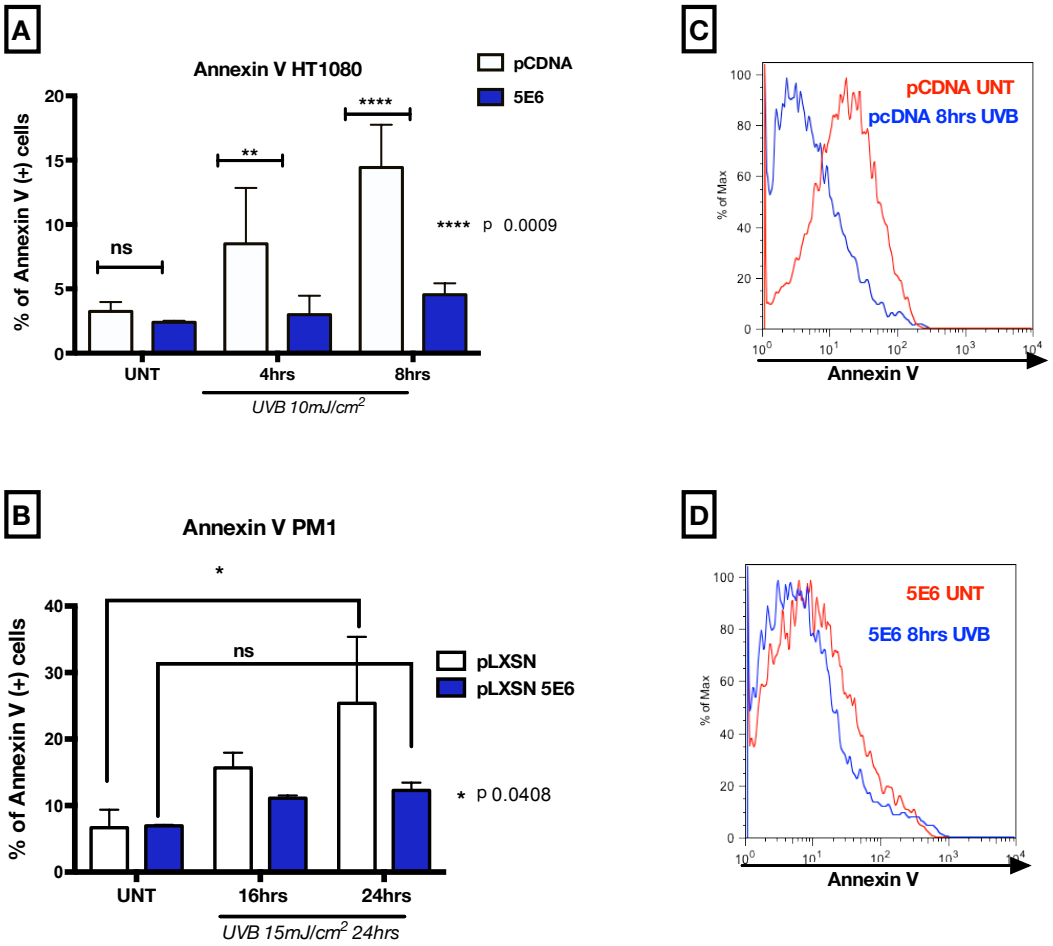

Figure 3-3 AnnexinV levels in HT1080 cells HPV5 E6 following UVB

A) HT1080 cells expressing pCDNA or HPV5 E6 were exposed to 10mJ/cm^2 UVB and harvested at 4 or 8 hours later. Cells were then stained with Annexin V, Alexa Fluor® 647 conjugate (Invitrogen) and levels measured by FACS. Results were analysed by two way ANOVA. S.E.M ± three biological replicates are shown (**p<0.01).

B) PM1-pLXSN or PM1-pLXSN 5E6 expressing cells were irradiated with 15mJ/cm^2 UVB. Cells were collected after 16 or 24 hours and stained with annexinV and analysed by FACS. Results were analysed by two way ANOVA and S.E.M ± n=3 (*p<0.0408).

C/D) Example FACS histogram of annexin v peak shift in HT1080 cells expressing pCDNA and HPV5 E6 respectively.

3.3.4 Levels of p53 in PM1 keratinocytes expressing HPV5 E6 or pLXSN

As previously mentioned in 3.1.2 p53 acts as an important regulator of autophagy and apoptosis. Therefore, having delineated the conditions under which HPV5 E6 inhibits apoptosis in PM1 keratinocytes, it was interesting to determine whether expression of HPV5 E6 did not alter p53 behaviour in PM1 cells and that the dose of UVB determined in 3.3.3 caused sufficient DNA damage to stimulate p53. PM1

cells expressing either pLXSN or pLXSN-5E6 were seeded as previously described and exposed to 15mJ/cm^2 UVB. 8 hours later cell pellets were collected and lysed using RIPA buffer, and protein concentrations were determined using the Biorad Bradford protein assay. Levels of proteins were then normalised across samples. Protein samples were resolved on a SDS-PAGE gels that were transferred onto a PVDF membrane. Antibodies specific to p53 and GAPDH were used to immunoprobe the membrane. Figure 3-4 shows that in both pLXSN and pLXSN-5E6, p53 levels were increased after UVB, indicating that HPV5 E6 expression in PM1 keratinocytes did not affect p53 behaviour in PM1 keratinocytes.

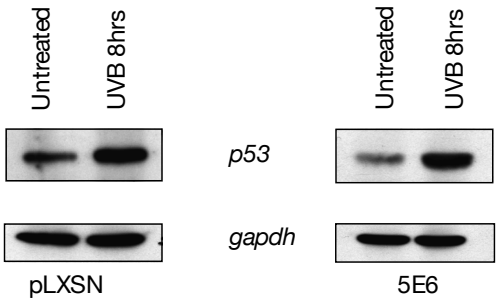

Figure 3-4 Levels of p53 in PM1 cell lines

Western blot of p53 (~53kDa) in PM1 keratinocytes expressing pLXSN on the left or 5E6 on the right. PM1 cells were irradiated with 15mJ/cm^2 UVB and 8 hours later, cells were lysed and protein lysates were resolved on SDS-PAGE. GAPDH (~36kDa) was used as a loading control.

3.3.5 Investigating autophagy levels in E6 expressing cells

Having established UVB doses and cell culture conditions in which HPV5 E6 inhibits apoptosis, the induction of autophagy was investigated next.

LC3 serves as a marker for autophagy levels in cells. The lipid conjugation and specific recruitment to the growing autophagosomal membrane changes the staining pattern of LC3 from diffused (LC3I) to discrete punctate (LC3II). It is widely

accepted that the number of LC3 puncta correlates with the number of autophagosomes (Kabeya 2000), Figure 3-5.

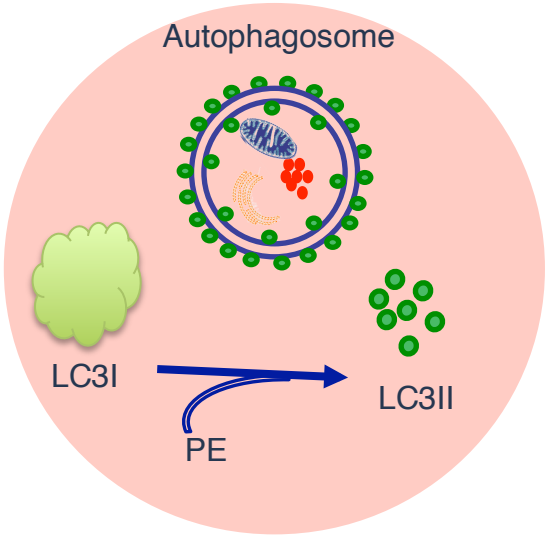

Figure 3-5 Schematic representation of LC3 lipidation

Upon the induction of autophagy, LC3I is lapidated and recruited to the growing autophagosomal membrane leading to a change in its staining pattern from diffused to discrete puncta.

Therefore the first step to elucidate autophagy induction in HPV5 E6 expressing cells following exposure to UVB was to analyse LC3 puncta. This was first explored using a plasmid encoding GFP-LC3 that allows for a quick assessment of LC3II puncta formation. Since PM1 keratinocytes are difficult to transfect, HT1080 cell lines stably expressing HPV5 E6 or pcDNA were chosen. Cells were seeded onto glass coverslips in 60 mm dishes to ~60% confluency. 24 hours later cells were transiently transfected with a plasmid encoding GFP-LC3 using X-tremeGENE 9 at a ratio of 3:1 (X-tremeGENE9: DNA) per dish. The GFP signal was observed 24 hours after transfection. Cells were then irradiated with 10mJ/cm^2 UVB. 8 hrs later cells were fixed with 4% paraformaldehyde and counterstained using DAPI to visualise the nucleus. Coverslips were mounted on glass slides and cells were examined using a fluorescent microscope. Representative images in Figure 3-6 show that untreated HT1080 cells transfected with pcDNA or HPV5 E6 exhibit

diffused GFP-LC3. However, it is observed that following UVB exposure, HPV5 E6 expressing cells start to accumulate LC3 foci, indicating increased numbers of autophagosomes. By contrast empty vector control cells show little foci formation after UVB. These results suggest an increase in autophagy in E6 expressing cells after UVB.

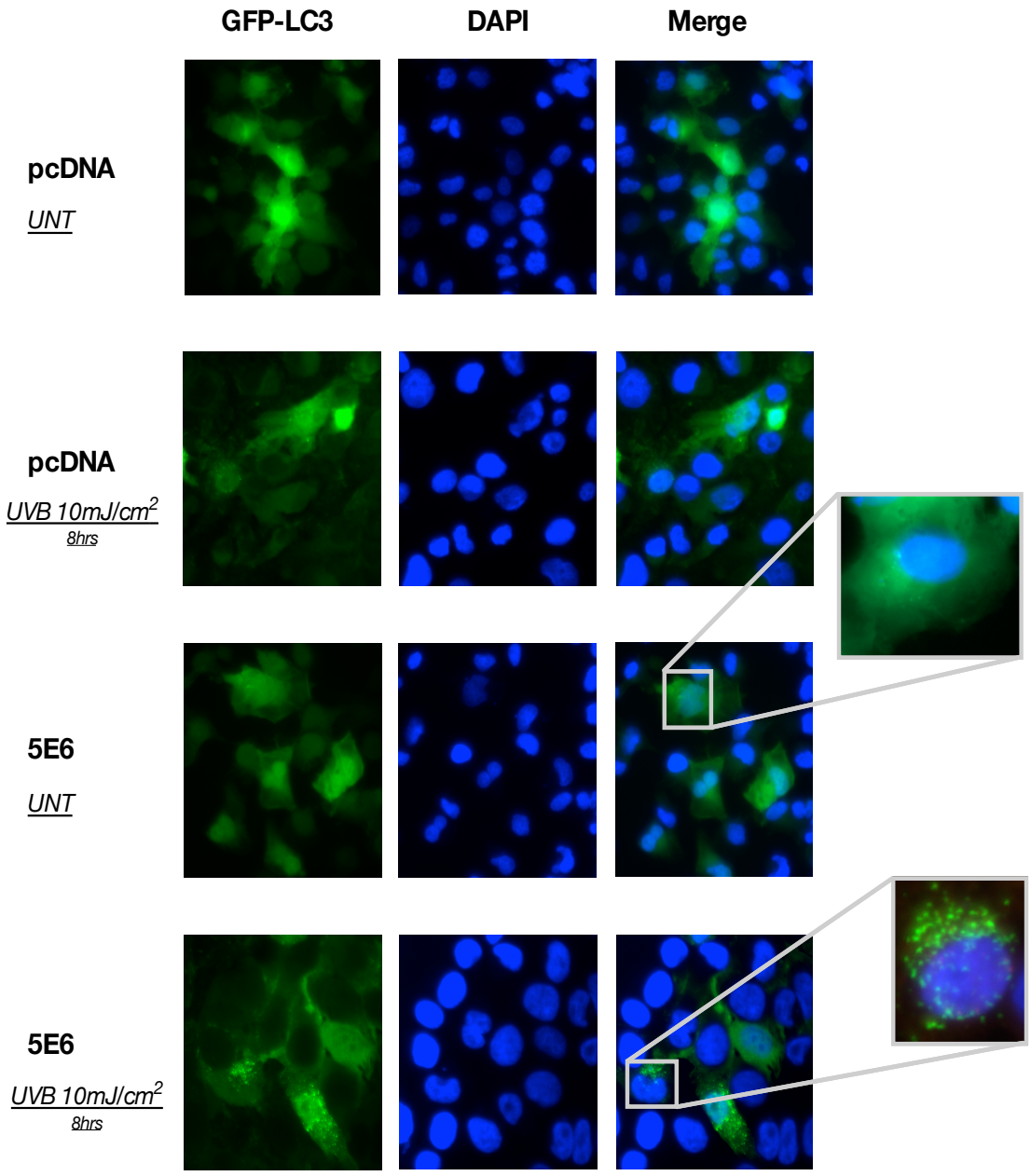

Figure 3-6 GFP-LC3 puncta formation in HT1080 cells

Fluorescent light microscopy images: GFP-LC3 (green) and DAPI (blue) taken at 20x magnification. From the top: HT1080-pcDNA untreated control (UNT), HT1080-pcDNA after 8 hours of 10mJ/cm^2 UVB irradiation, HT1080-HPV5 E6 untreated control (UNT) and HT1080-HPV5 E6 following UVB. Example of diffuse and punctate GFP-LC3 is shown in higher magnification.

3.3.6 Endogenous LC3 foci staining in HT1080 and PM1 keratinocytes in E6 expressing cells

To examine the induction of autophagy after UVB, endogenous levels of LC3 were examined. This offers an advantage over transfected GFP-LC3 which can form aggregates that are indistinguishable from autophagosome associated LC3 foci (Mizushima et al. 2010, Kuma et al. 2007). HT1080 and PM1 cell lines stably expressing HPV5 E6 or control cells were seeded on glass cover-slips to ~70% confluency. Twenty-four hours later, HT1080 cells were irradiated with 10mJ/cm2 UVB whereas PM1 cells were exposed to 15mJ/cm^2. Thapsigargin is an Inhibitor of the sarco/ER Ca2+ ATPase (Thastrup 1990), and was used as positive control to monitor autophagy induction as it increases LC3 puncta accumulation. After 8 hours, cells were fixed with ice-cold methanol, stained for LC3 using an antibody specific to LC3B followed by a 488-Alexa flour secondary antibody. The nuclei were visualised using DAPI. Cells were examined using a scanning confocal microscope and representative images were captured (Figure 3-7A, Figure 3-8A). As previously noted, autophagy is essential for the maintenance of cellular homeostasis. Therefore, when assessing autophagy levels in cells, the average number of foci per cell is a more appropriate indication rather than the percentage of cells with LC3 foci (Mizushima et al. 2010; Klionsky et al. 2014). Thus, to evaluate autophagy levels, the average number of foci/cell was determined by manually counting puncta in 100 cells. Figure 3-7B illustrates that there is a marked increase in LC3 foci/cell in HPV5 E6 expressing cells after UVB irradiation. By contrast pcDNA expressing cells seem to have a smaller increase in the average number of puncta per cell after following UVB damage. These results support the observation in 3.3.4, suggesting that cells expressing HPV5 E6 have higher levels of autophagy after UVB.

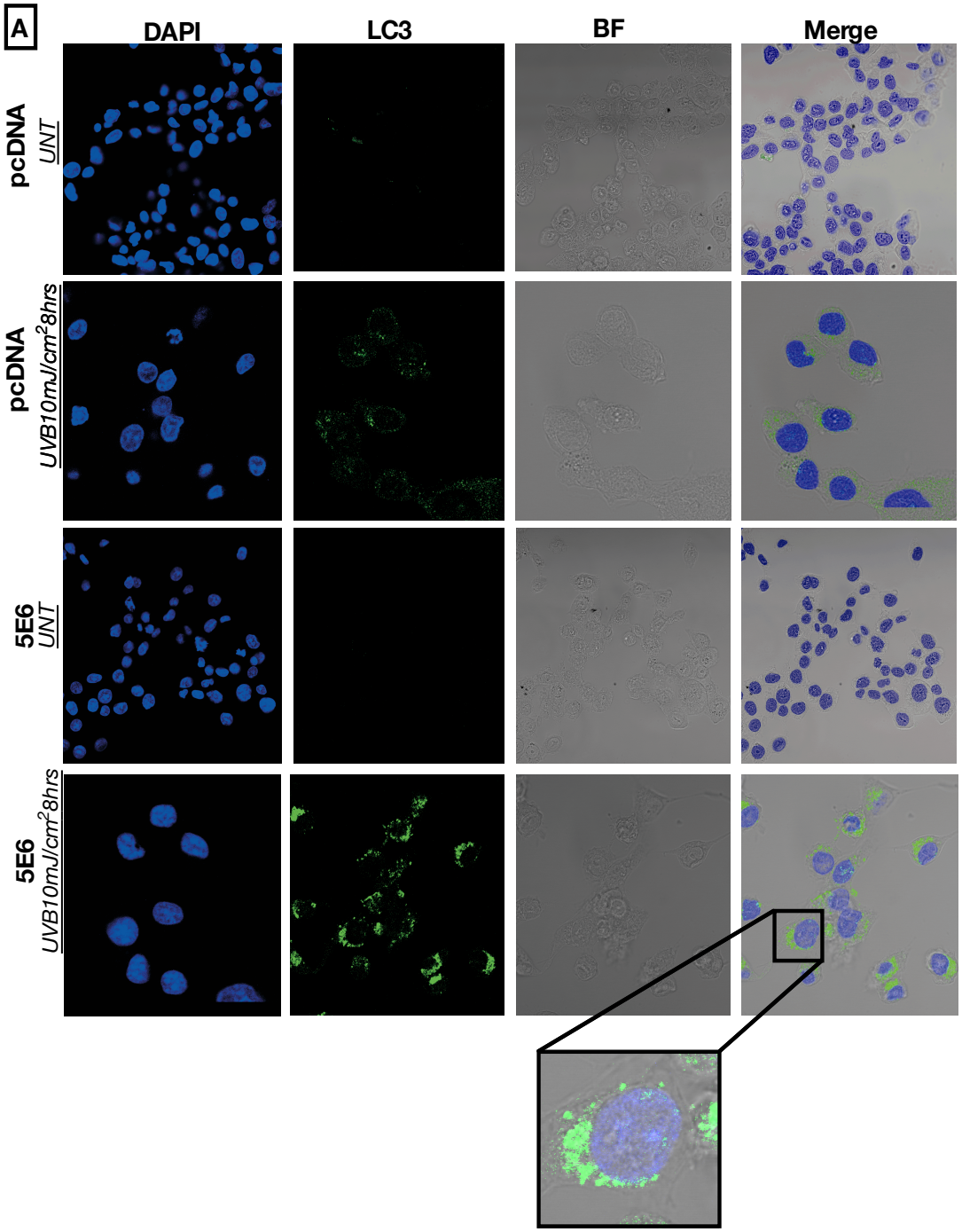
A
DAPI
LC3
BF
Merge
pcDNA
UNT
pcDNA
UVB10mJ/cm2 8hrs
5E6
UNT
5E6
UVB10mJ/cm2 8hrs

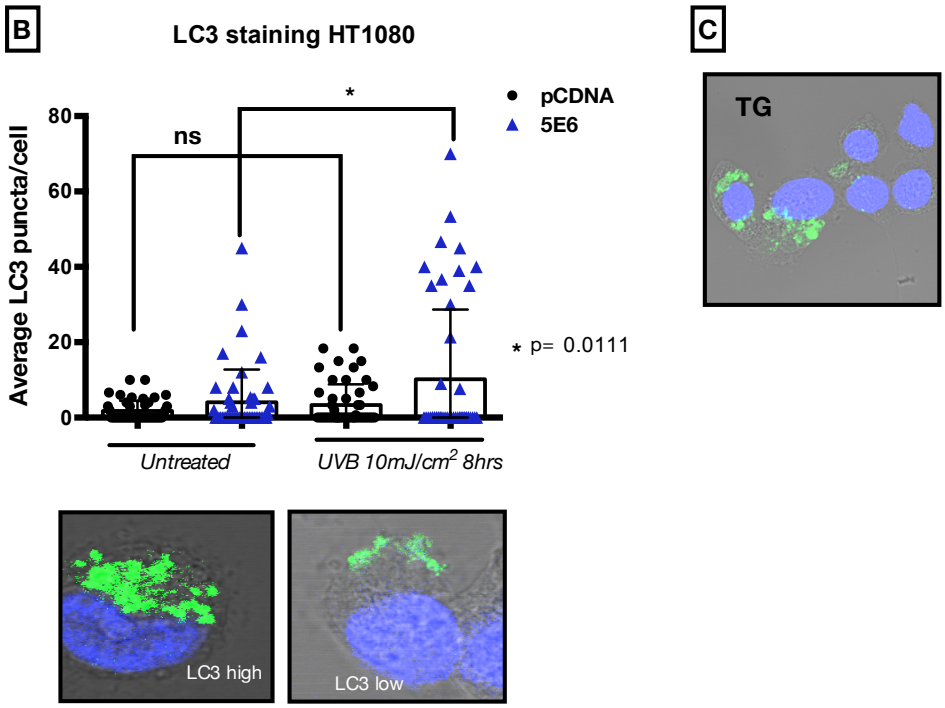

Figure 3-7 LC3 foci formation in HT1080 cells expressing pcDNA, HPV5 E6

HT1080 cells stably expressing pcDNA or 5E6 were exposed to 10mJ/cm^2 after 8 hours; cells were fixed and stained for LC3 (green) and DAPI (blue) for the nucleus. Images were taken on confocal microscope. **A)** From the top panel: HT1080-pcDNA untreated control (UNT), HT1080-pcDNA after 8 hours 10mJ/cm^2 UVB, HT1080-5E6 untreated control and HT1080-5E6 following 8 hours 10mJ/cm^{2}UVB irradiation. **B)** The average number of foci/cell was counted in 100 cells manually on fluorescent microscope. Two-way ANOVA was used to compare different groups, mean with SD. n=3 *p=0.0111. **C)** Example of Thapsigargin control (TG). Examples of high and low LC3 foci are shown.

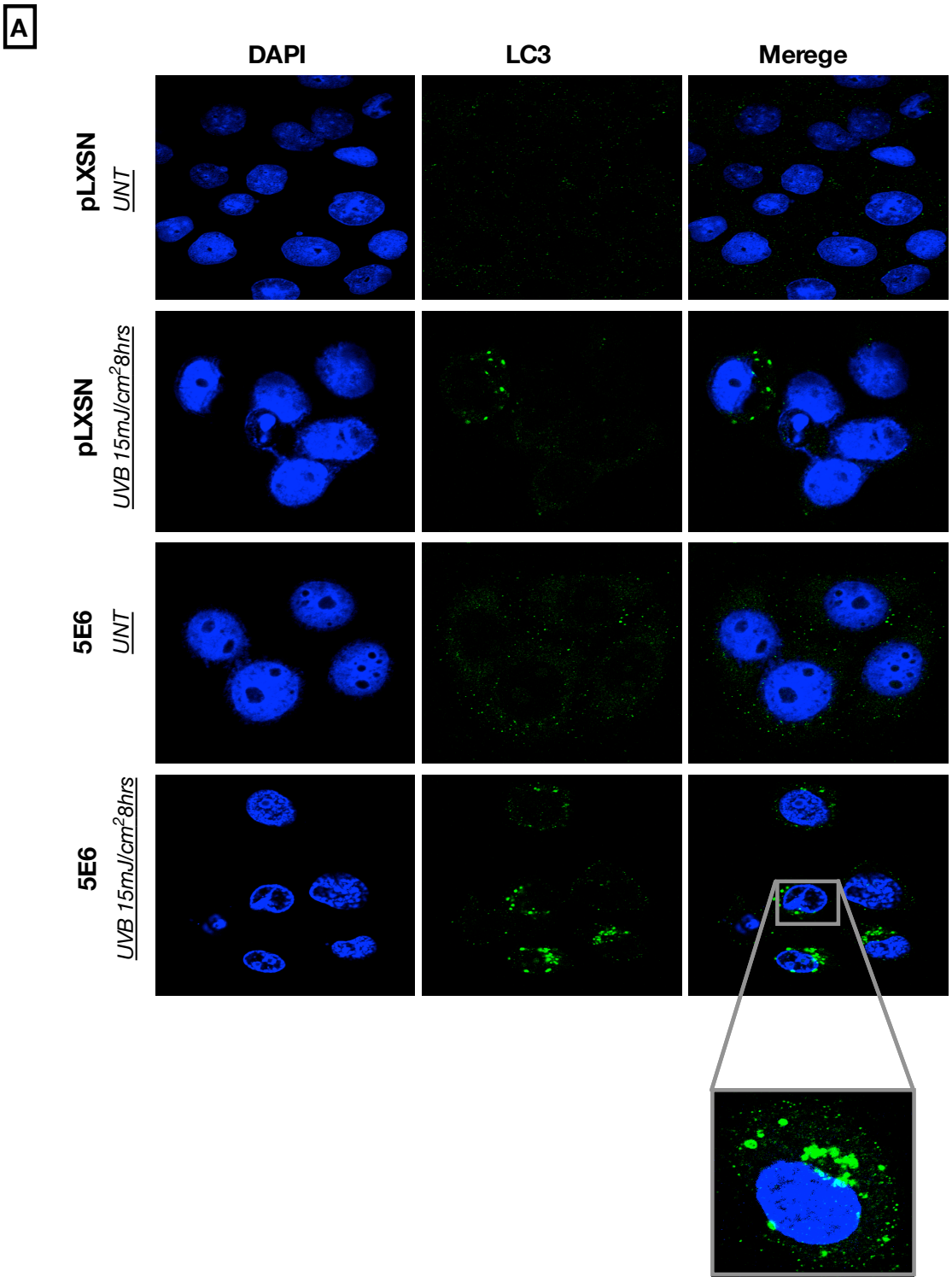
A
DAPI
LC3
Merege
pLXSN
UNT
pLXSN
UVB 15mJ/cm2 8hrs
5E6
UNT
5E6
UVB 15mJ/cm2 8hrs

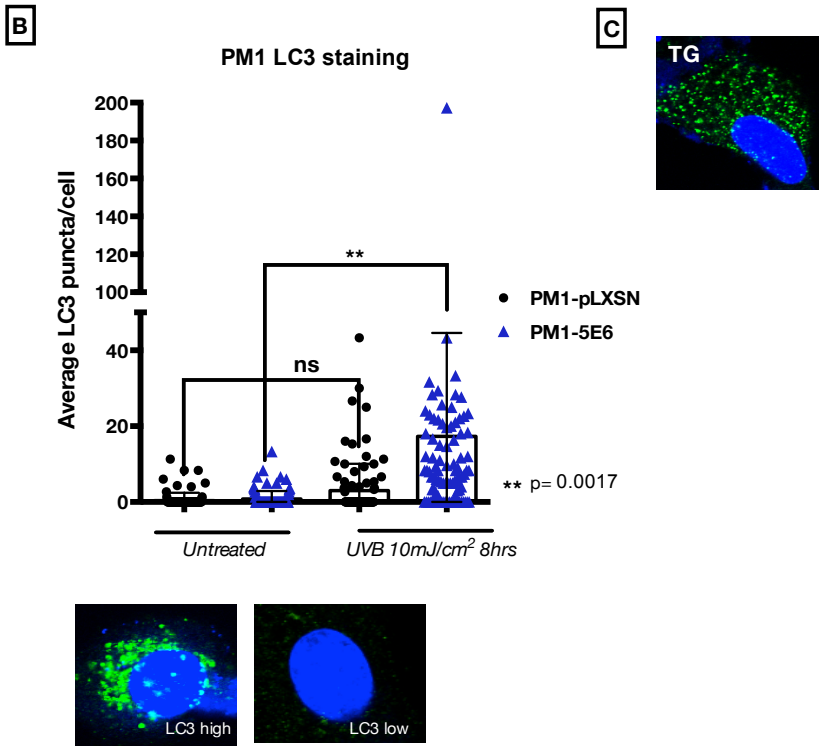

Figure 3-8 LC3 punctate staining in PM1 keratinocytes

PM1 keratinocytes cell line expressing either pLXSN or pLXSN-5E6 stably were irradiated with 15mJ/cm^2. 8 hours later; cells were fixed in ice-cold methanol and stained for LC3 (green) and DAPI (blue) for the nucleus. Images were taken on a confocal microscope. **A)** From the top panel: PM1-pLXSN untreated control (UNT), PM1-pLXSN after 8 hours 15mJ/cm^2 UVB, PM1-5E6 untreated control and PM1-5E6 following 8 hours 15mJ/cm^{2}UVB irradiation. **B)** A scatter plot showing the average number of foci/cell was counted in 100 cells manually on fluorescent microscope. Two-way ANOVA was used to compare different groups, mean with SD. n=3 **p=0.0017. **C)** Example of Thapsigargin control (TG). Examples of high and low LC3 foci are shown.

As previously mentioned, HPVs are strictly epitheliotropic and thus validating autophagy levels in keratinocytes is of great importance. Figure 3-8A shows representative confocal images of LC3 puncta in PM1 keratinocytes expressing pLXSN and HPV5 E6. Similar to previous results, HPV5 E6 expressing cells seem to have a large increase in the average number of puncta per cell, suggesting that keratinocytes expressing HPV5 E6 that are exposed to DNA damage also induce an autophagic response (Figure 3-8B).

3.3.7 Assessing autophagic flux

Autophagy is a dynamic process in which autophagosomes form and fuse with lysosomes for degradation. The balance between the number of autophagosomes formed and cleared by lysosomes is termed the autophagic flux. It can be argued that autophagosome accumulation can be the result of either autophagy induction or an inadequate clearing of the autophagosomes by lysosomes due to lysosomal dysfunction. Thus, to test this, lysosomal inhibitors that block the fusion between autophagosomes and lysosomes such as Bafilomycin A1 or Chloroquine are generally used in autophagy studies (Klionsky et al. 2014).

Bafilomycin A1 is a vacular-ATPase inhibitor that blocks the fusion of the autophagic vacuole with the lysosome (Yamamoto et al. 1998) and was chosen to assess autophagic flux in the two cell line models, by immunofluorescent staining, immunoblotting, and Image Stream analysis of LC3. First, endogenous LC3 staining in PM1 keratinocytes expressing pLXSN or HPV5 E6 was carried out. Cells were seeded on glass coverslips as described previously and 24 hours later exposed to 15mJ/cm^2 UVB. Bafilomycin A1 was added at a 100nM concentration 2 hours prior to fixation. Cells were collected after 8 and 24 hours of UVB, fixed with methanol and stained for LC3 using LC3 specific antibody followed by Alexa Fluor® 488. The nuclei were visualised using DAPI. Coverslips were mounted on glass slides and examined using the confocal microscope and the average number of LC3 foci per cell was counted in 100 cells after 24 hours of UVB. Representative images in Figure 3-8A demonstrate that HPV5 E6 expressing cells accumulate more LC3 puncta that are also larger in size after UVB. The addition of Bafilomycin A1 resulted in a further increase in the number of foci per cell in HPV5 E6 expressing cells following UVB. Figure 3-9B shows a scatter plot representing the average number of puncta per cell in 100 cells. This data suggests that the

autophagosome accumulation in HPV5 E6 expressing cells is due to autophagy induction, leading to high autophagic flux, and is not due to lysosomal dysfunction.

A
pLXSN
5E6
-
+
-
+
Bafilomycin A1
LC3
Nuclei
UNT
UVB 15mJ/cm² 8hrs
UVB 15mJ/cm² 24hrs

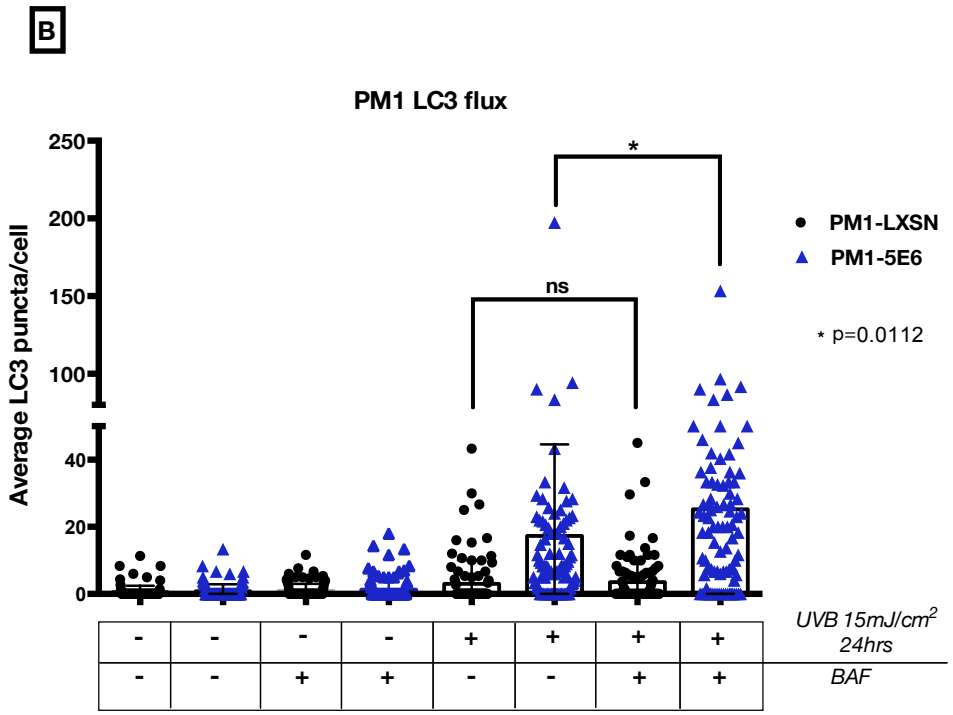

Figure 3-9 Autophagic flux in PM1 keratinocytes

PM1 keratinocytes expressing pLXSN or HPV5 E6 were exposed to UVB 15mJ/cm^2. Bafilomycin A1 (BAF) was added two hours before fixation. **A)** Representative confocal images taken after 8 and 24hrs of UVB. Left panel: PM1-pLXSN and the right panel is PM1-HPV5 E6. Horizontally: untreated control (UNT), UVB 8 hours and UVB 24 hours. **B)** A scatter plot showing the average number of foci/cell was counted in 100 cells manually on fluorescent microscope. Two-way ANOVA was used to compare different groups, mean with SD. n=3 *p=0.012

Second, LC3 levels were assessed in HT1080 and PM1 keratinocytes stably empty vector control or HPV5 E7 using western blots.

The lipid conjugation of LC3I and its conversion to LC3II changes its mobility on a protein gel from 18kDa to 16kDa. This allows the tracking of LC3 turnover, which is a good indicator of autophagy rates and autophagic flux.

HT1080 cells stably expressing pcDNA or HPV5 E6 were seeded as previously described. Twenty-four hours later the cells were irradiated with 10mJ/cm^2 UVB. To assess the autophagic flux, Bafilomycin A1 was added 2 hours prior to harvesting. After 4 and 8 hours of UVB, cells were collected and lysed. Protein levels were determined using Nanodrop and normalized to the sample with the lowest protein concentration. Lysates were then resolved on 16% SDS-PAGE gels and transferred

onto a PVDF membrane. PVDF membranes were then immune probed using anti-LC3 antibody and β−actin was used a loading control. Figure 3-10A demonstrates an increase in LC3II in HT1080-HPV5 E6 over time after UVB. Increased autophagic flux in 5E6 expressing cells is reflected by high LC3 turnover, indicated by higher levels of LC3 after adding Bafilomycin A1.

PM1 keratinocytes transduced with HPV5 E6 or pLXSN were seeded and exposed to 15mJ/cm^2 UVB. Two hours before the indicated time points, Bafilomycin A1 was added Figure 3-9B. Similarly to the results obtained in Figure 3-9A, HPV5 E6 expressing keratinocytes show high autophagic flux after UVB.

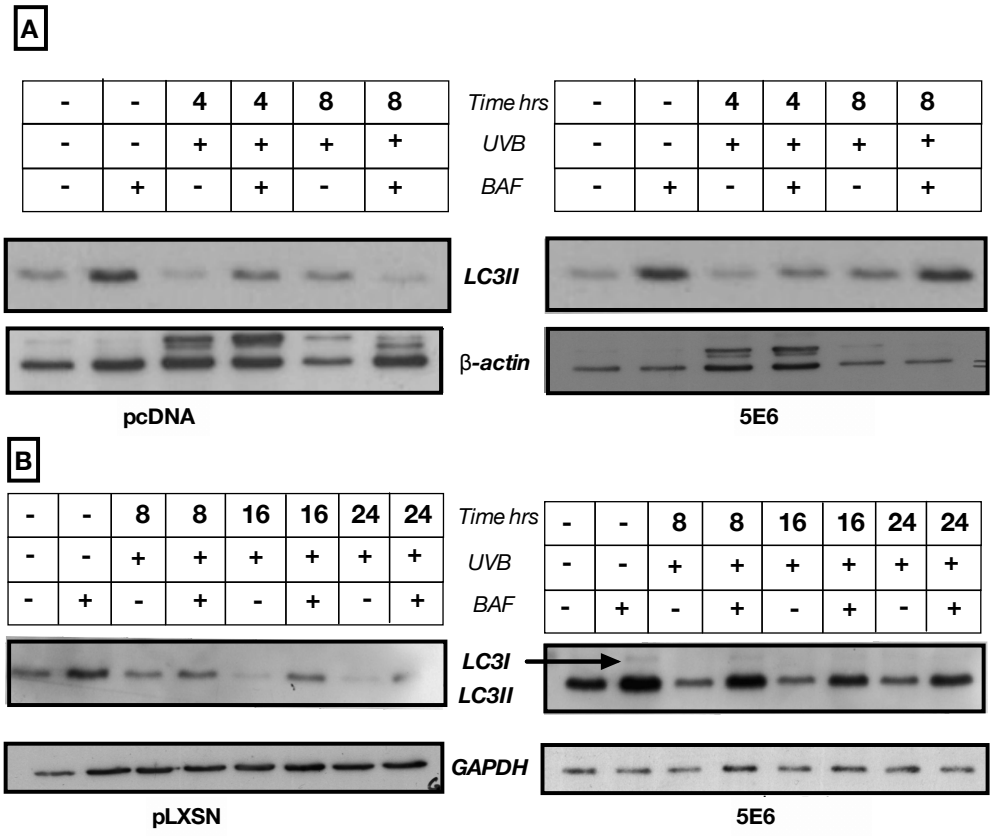

Figure 3-10 LC3II turnover in HT1080 and PM1 cells

A) LC3II immunoblots. HT1080 cells expressing pcDNA or HPV5 E6 were irradiated with 10mJ/cm^2. Bafilomycin A1 (BAF) was added 2 hours prior to indicated time points. Proteins were collected and resolved on 16% SDS-PAGE.

B) PM1 keratinocytes expressing pLXSN or HPV5 E6 were exposed to 15mJ/cm^2 UVB and collected for western blotting at the indicated time points. Bafilomycin A1 was added 2 hours before to assess LC3 turnover.

Third, assessing the levels of autolysosomes using the Image Stream was carried out in PM1 keratinocytes. ImageStream Amnis IS100 is a high throughput technology combining flow cytometry and imaging analysis. The system measures the co-localization intensity of LC3 and lysosome. PM1 keratinocytes expressing pLXSN or HPV5 E6 were seeded in 10cm dishes at a concentration of 2x10^6 per plate. Thapsigargin was used here as a positive control. After twenty-four hours, cells were detached using trypsin. Cells were then washed and stained for lysosomes using Lyso-ID (Enzo life sciences) and for autophagosomes using an antibody against LC3. The results showed a small but significant increase in LC3-

lysosomal co-localization in E6 expressing cells compared to the empty vector control, indicating a higher number of autolysosomes in E6 cells following UV exposure. Taken together, these results suggest that in E6 expressing cells autophagy is induced after UVB DNA damage.

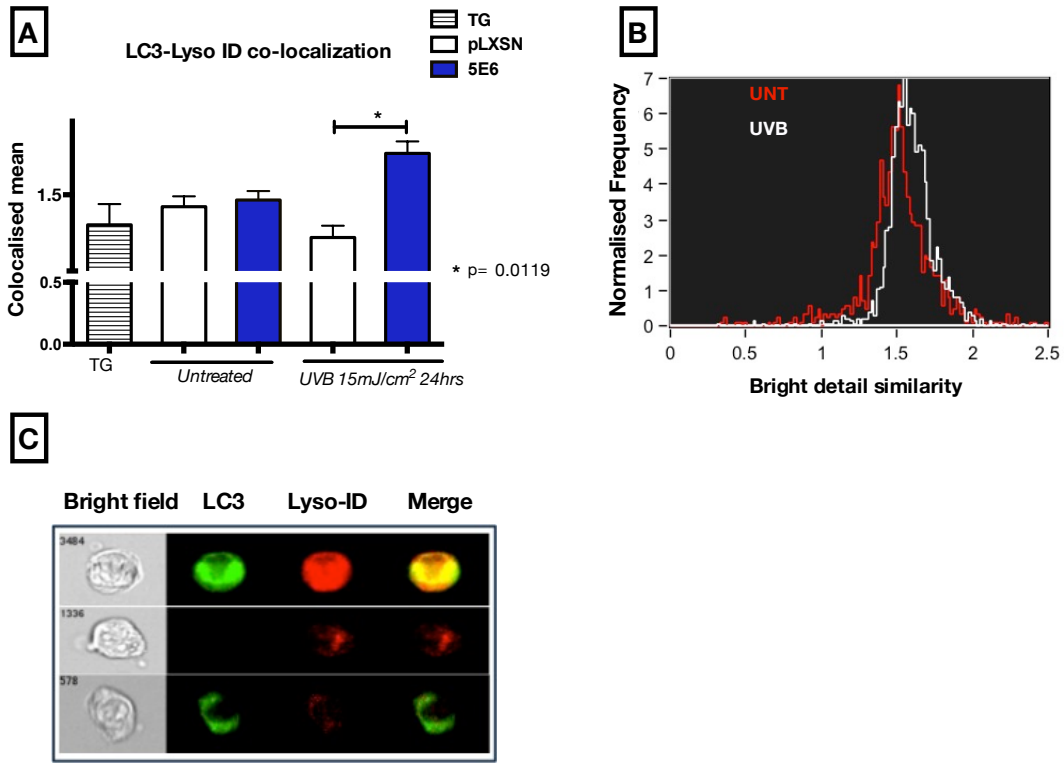

Figure 3-11 Image Stream analysis of autolysosomes

A) Bar graph of the co-localised mean of LC3 and lyso-ID in PM1 keratinocytes expressing pLXSN (clear bars) or 5E6 (blue bars). Unpaired t-test was performed to compare the mean-co-localised of pLXSN and HPV5 E6 after UVB. Mean ± SEM of three biological replicates is shown *p=0.0119. **B)** Bright detail similarity histogram obtained from Image Stream software. **C)** Example images of single cells captured by the Image Stream.

3.3.8 Measuring autophagy levels in HPV5 E7 expressing cells

The oncogenic transformation of HPV is attributed to the multiple functions of E6 and E7. E7's major role in the viral life cycle is to maintain a functional replicative status in terminally differentiated keratinocytes.

A recent study demonstrated that expression of HPV16 E7 in keratinocytes resulted in increased autophagy. Thus, it was crucial to test if UVB genomic stress would induce autophagy in E7 expressing cells. This was tested in HT1080 cells stably expressing HPV5 E7 or pcDNA. Autophagy levels were examined using LC3 immunofluorescence and LC3 turnover using western blots as previously discussed. HPV5 E6 was used for comparison. Fig3-13A shows LC3 foci staining after irradiation with different doses of UVB. Interestingly contrasting to E6, cells expressing the E7 protein seem to accumulate very few LC3 foci after UVB. In Fig3-13B LC3 turnover immunoblots demonstrate that expression of E7 in HT1080 cells has little effect on autophagy levels in the milieu of UVB induced genomic stress.

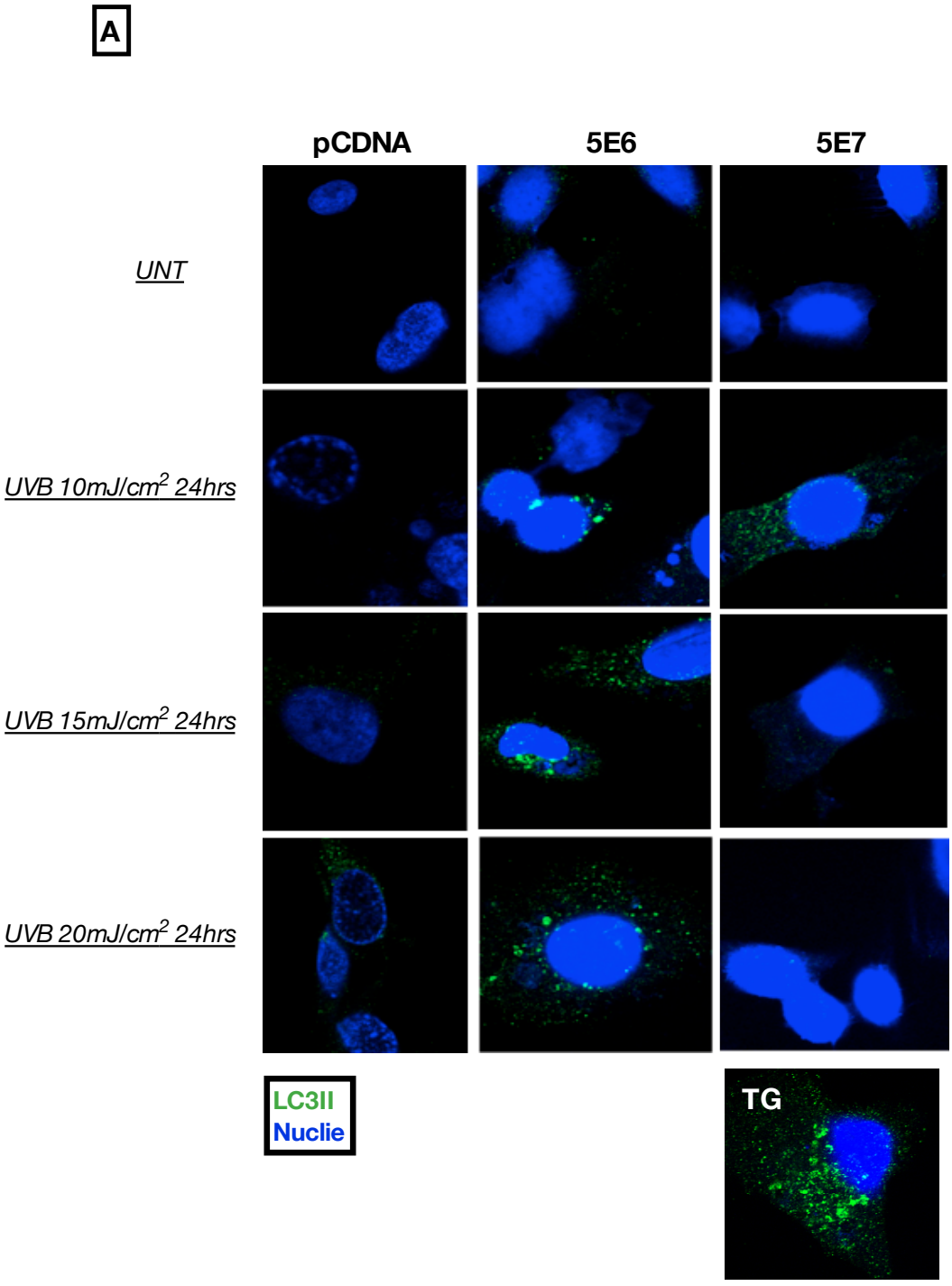
A
pCDNA
5E6
5E7
UNT
UVB 10mJ/cm2 24hrs
UVB 15mJ/cm2 24hrs
UVB 20mJ/cm2 24hrs
LC3II
Nuclie
TG

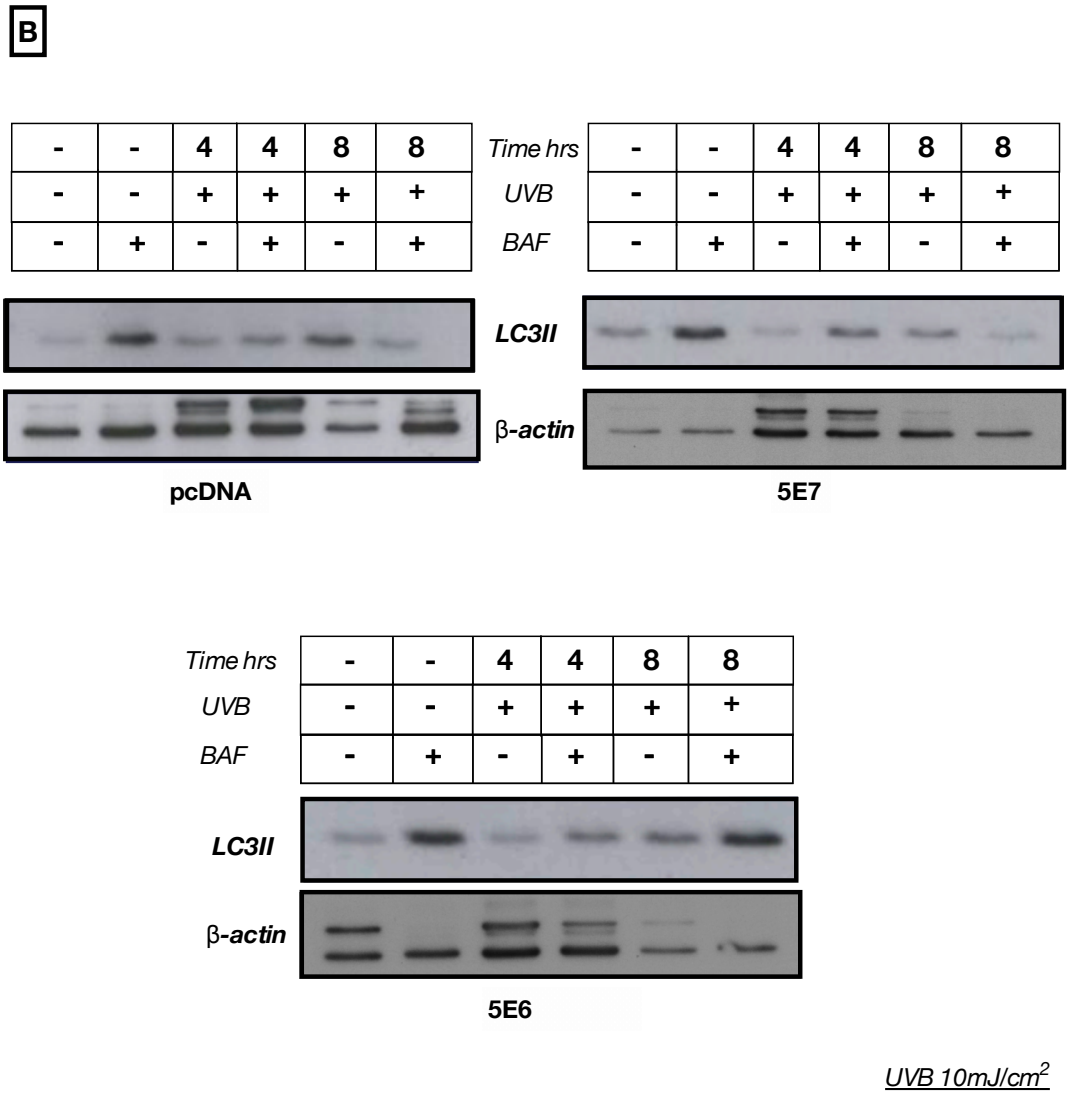

Figure 3-12 Autophagy levels in HT1080-HPV5 E7 cells

A) Confocal images of HT1080 cells stably expressing pcDNA, HPV5 E6 and HPV 5E7 stained for LC3 (green), nuclei (blue). Thapsigargin was used as a positive control

B) Immunoblots of LC3 turnover with Bafilomycin A1 (BAF).

3.3.9 Investigating levels of autophagy related proteins

As discussed in 1.4 the autophagic pathway is orchestrated by a number of autophagy related proteins. Beclin-1 is a Bcl-2-homology (BH)-3 domain only protein that is essential for phagophore formation, the first step of autophagy. The second step of autophagy is elongation; this is conducted by two ubiquitin like

systems. Atg7 is an E1 like protein and is essential for the conjugation of Agt12 and Atg5 (Figure 3-13B). In order to further confirm the induction of autophagy in E6 expressing cells, the levels of Beclin1, atg7 and atg5/12 complex were investigated in PM1 keratinocytes using western blots.

PM1 keratinocytes stably expressing HPV5 E6 or pLXSN were seeded in 60mm dishes. 24 hours later the cells were irradiated with UVB 15mJ/cm^2. Bafilomycin A1 was added two hours prior to harvesting. Cells were collected at 8 and 16 hours, lysed and proteins were resolved by SDS-PAGE electrophoresis. Protein gels were transferred onto a PVDF membrane that was probed for Beclin1, Atg5/12 and Atg7. GAPDH was used a loading control. Figure 3-13A shows that HPV5 E6 expressing keratinocytes have higher levels of Beclin1 after UVB, suggesting an induction of the autophagic pathway at the initial steps. Moreover the levels of Atg5/12 and Atg7 were increased after UVB indicating that undergoing autophagic response is classical macroautophagy depending on Atg7 and 5. Additionally the increase in autophagy related proteins after UVB in 5E6 expressing cells lends further support to the observation that HPV5 E6 increases autophagy levels and autophagic flux in keratinocytes.

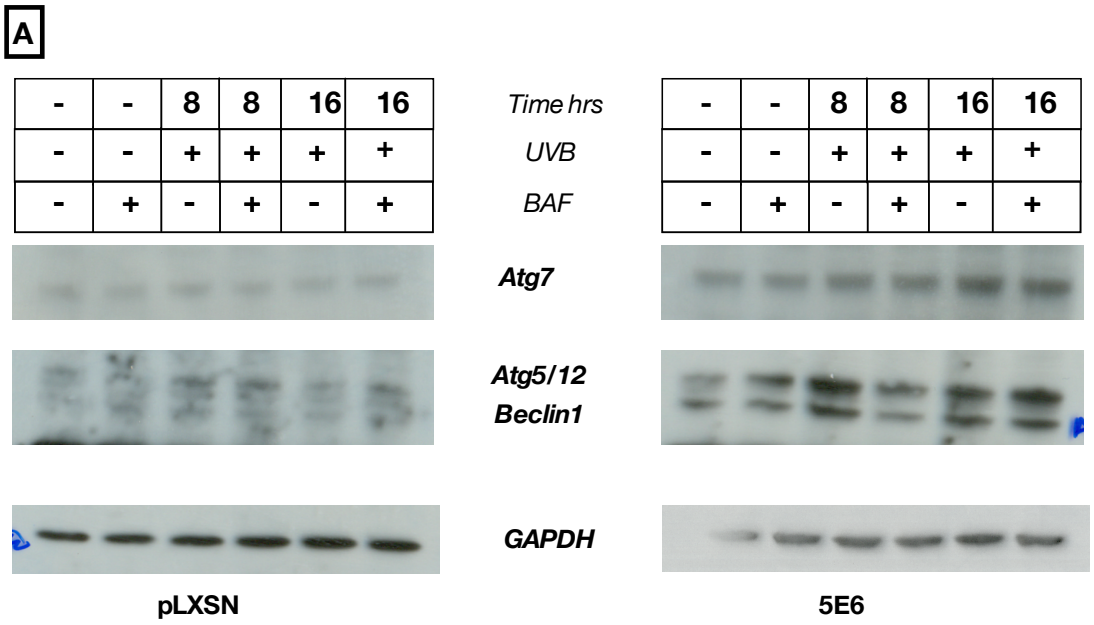

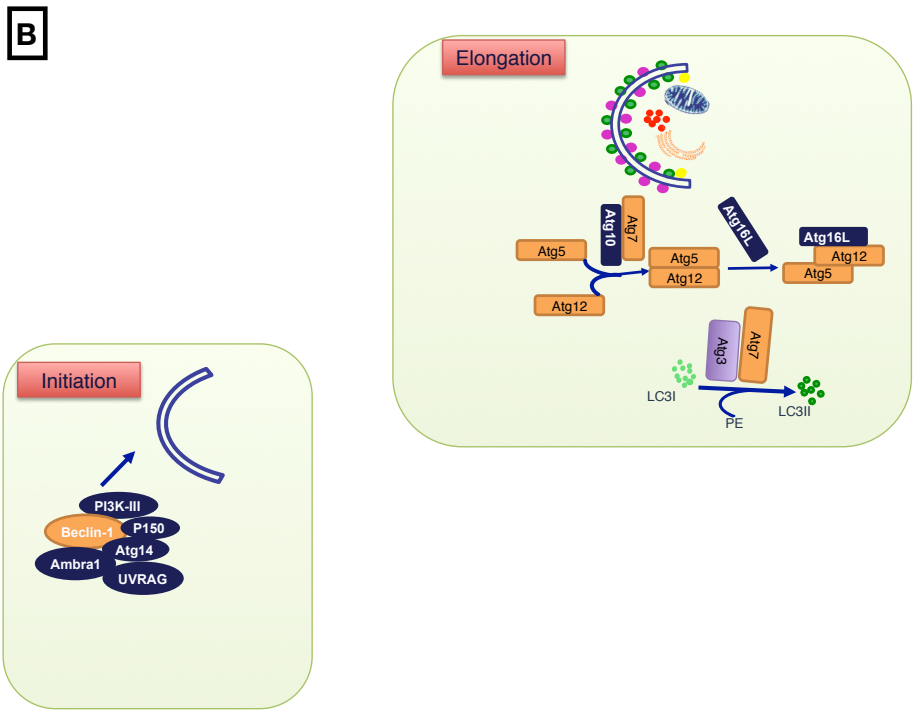

Figure 3-13 Levels of Beclin1, Atg7 and Atg5/12 complex in PM1 keratinocytes

A) Immunoblots of Atg7 (~78 kDa), Atg5/12 complex (~52 kDa) and Beclin1 (~56 kDa) carried out in PM1 keratinocytes expressing pLXSN on the left or HPV5 E6 on the right. GAPDH was used a loading control (~37 kDa).

B) Illustration showing the roles of Beclin1, Atg7 and Atg5/12 in the autophagic pathway.

3.3.10 Investigating autophagy levels in cells expressing E6 from different β-HPV types

The data obtained thus far indicate that there is an increase in autophagy levels and autophagic flux flowing UVB in cells expressing β-HPV5 E6, the main focus of this study. However other HPV types from the cutaneous family have also been implicated in human disease. Alongside HPV5, HPV 38 and 20 are implicated in the development of non-melanoma skin cancer (Astori et al. 1998). However, low risk HPVs such as HPV1 and 4 cause *Verrucae vulgares*, a benign wart lesion of the skin (Ljubojevic & Skerlev 2014). Investigating autophagy in different types of HPV might give an insight as to the potential relevance autophagy on the oncogenic transformation of cells. Therefore, autophagy levels using LC3 turnover was carried out in cells expressing E6 from low risk HPV1 and HPV4 in addition to cancer associated HPV20 and 38 of the beta HPV types. PM1 keratinocytes were retrovirally transduced to express HPV1 E6, HPV4 E6, HPV38 E6, HPV20 E6 or pLXSN. Cells were then seeded and 24 hours later irradiated with 15mJ/cm^2 UVB. As previously described, Bafilomycin A1 was added two hours before harvesting. Cells were collected and proteins were processed for western blots. Interestingly, both 38E6 and 20E6 expressing cells show increased levels of LC3II even in the untreated states, and these levels were further increased after UVB. However, a decrease of LC3II is observed after 16 hours of UV in cells expressing HPV38 E6 and 20 E6, Figure 3-14A suggesting a return to basal autophagy levels.

Contrasting to their high-risk counterparts, expression of E6 protein from HPV type 1 and 4 resulted in decreased autophagy levels, and a decrease in autophagic flux. This indicates that autophagy might play a different role in cells expressing E6 from different HPV types.

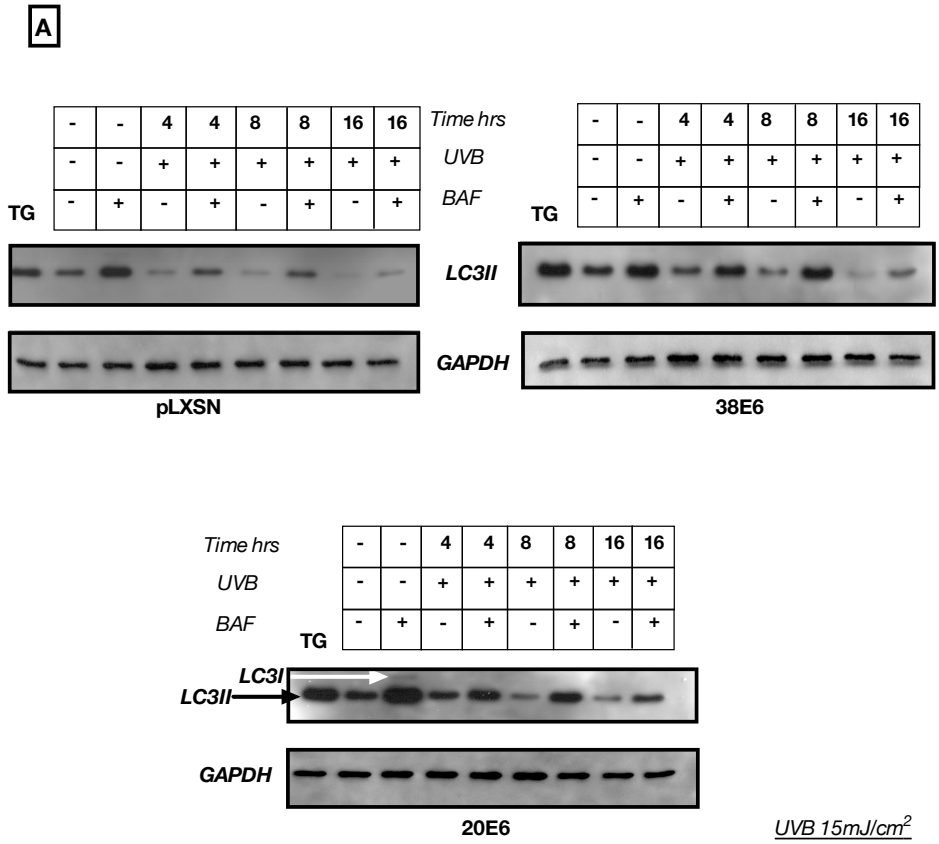
A
Time hrs
UVB
BAF
TG
LC3II
GAPDH
pLXSN
38E6
LC3I
20E6
UVB 15mJ/cm2
B
1E6
4E6

Figure 3-14 Autophagy levels in PM1 keratinocytes expressing E6 from different HPV types

Immunoblots of LC3II (~16kDa) and the loading control GAPDH (~37 kDa). Cells were seeded in 60mm dishes and 24 hours later cells were irradiated and harvested at the indicated times. Bafilomycin A1 was added 2 hours before harvesting. Thapsigargin was used as a positive control (TG).

A) PM1 keratinocytes expressing pLXSN, HPV38 E6 or HPV20 E6.

B) HPV1 E6, HPV4 E6 and pLXSN expressing keratinocytes.

3.3.11 HPV8 E6 induces autophagy in HT1080 and PM1 keratinocytes

HPV5 and HPV8 are closely related, but it was necessary to test if HPV8 E6 can also modulate autophagy.

PM1 keratinocytes cell lines were transduced to express pLXSN-8E6 or transduced with pLXSN and stable cell lines were produced as previously described in 3.3.1. To assess autophagic flux in HPV8 E6 expressing cells, autophagic flux was probed by immunofluorescent staining and immunoblotting. First, endogenous LC3 staining in PM1 keratinocytes transduced with pLXSN or HPV8 E6 was carried out. Cells were seeded on glass coverslips and 24 hours later exposed to 15mJ/cm^2 UVB. Bafilomycin A1 was added at a 100nM concentration 2 hours prior to fixation. Cells were collected after 8, 16 and 24 hours post UVB, fixed with methanol and stained for LC3 as previously described in 3.3.7. Representative images are shown in Figure 3-15A. The results demonstrated that HPV8 E6 expressing cells accumulate more LC3 puncta that are larger in size after UVB, similar to the results obtained with HPV5 E6.

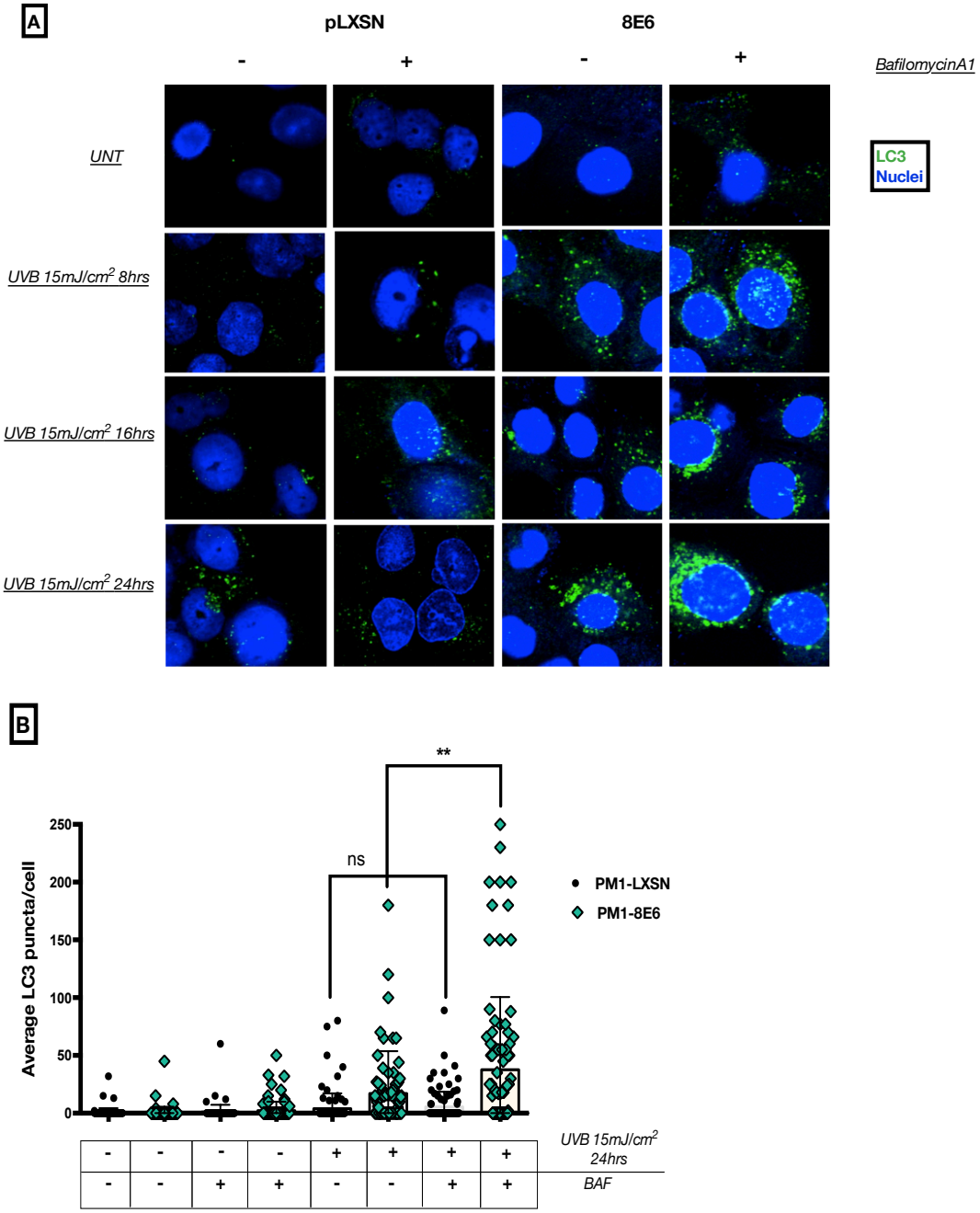

Figure 3-16 Endogenous LC3 staining in PM1 keratinocytes expressing HPV8 E6

PM1 keratinocytes expressing pLXSN or HPV8 E6 were exposed to UVB 15mJ/cm^2. Bafilomycin A1 (BAF) was added two hours before fixation. **A)** Representative confocal images taken after 8, 16 and 24hrs of UVB. Left panel: PM1-pLXSN and the right panel is PM1-HPV8 E6. Horizontally: untreated control (UNT), UVB 8 hours, 16 hours and UVB 24 hours. **B)** A scatter plot showing the average number of foci/cell was counted in 100 cells manually on fluorescent microscope. Two-way ANOVA was used to compare different groups, mean with SD. n=3 **<0.01.

Moreover, Bafilomycin A1 treatment resulted in a further increase in the number of foci per cell in HPV8 E6 expressing cells following UVB. This data suggests that the autophagosome accumulation in HPV8 E6 expressing cells is due to autophagy induction, leading to high autophagic flux.

Second, LC3 turnover using western blot was performed. PM1 keratinocytes transduced with HPV8 E6 or pLXSN were seeded and exposed to 15mJ/cm^2 UVB. Two hours before the indicated time points, Bafilomycin A1 was added to assess autophagy flux. The ER stressor Thapsigargin was used as a positive control for autophagy induction. The results showed that there is a decrease in autophagy in the pLXSN but the levels increased in HPV8 E6 expressing cells and higher autophagy flux was observed.

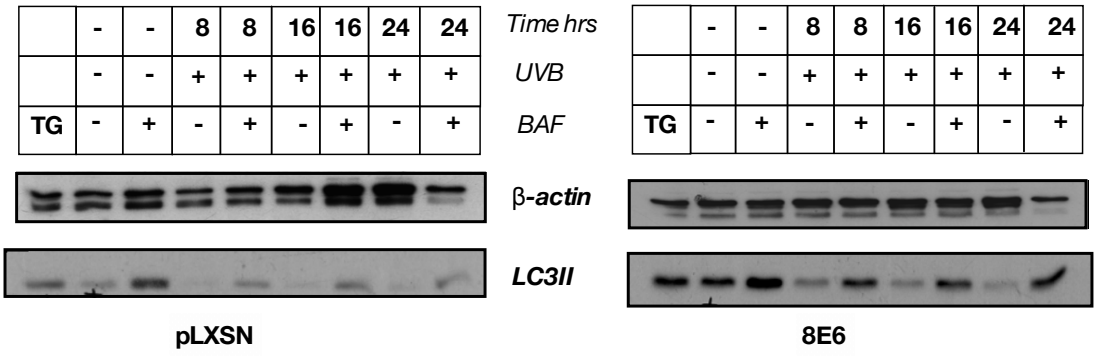

Figure 3-17 LC3II immunoblots in HPV8 E6 expressing cells

PM1 keratinocytes transduced with pLXSN or HPV8 E6 were exposed to 15mJ/cm^2 UVB and two hours before the indicated time Bafilomycin A1 was added, cells were then collected, lysed and resolved on SDS-PAGE. The membranes were then immunoprobed for β-actin as a loading control (~42kDa) and LC3II (~16kDa).

Thus, taken together, these findings support previous studies with HPV5 E6 and suggest that autophagy induction may be a conserved function across high-risk β-HPV types.

3.3.12 Autophagy levels in HT1080 cells expressing high risk alpha E6 protein

Studies showed that HPV E6 of both α and β target BAK for proteolysis and inhibit apoptosis; therefore, it was of interest to investigate the levels of autophagy in cells

expressing E6 of high-risk mucosal HPV types (Thomas & Banks 1999). HT1080 cells were transfected to stably express two of the most common high-risk α-HPV (HPV18 E6 and HPV16 E6). Those lines were probed for autophagy levels using LC3 immunoblots. Interestingly, similarly to HPV E6 protein of the cutaneous type, high LC3II levels in cells expressing E6 from mucosal HPV types 16 and 18 were observed. Additionally, those levels were increased after being exposed to UV DNA damage. These results suggest that the E6 effect on autophagy levels is not restricted to β-HPV types but also to high-risk α-HPV.

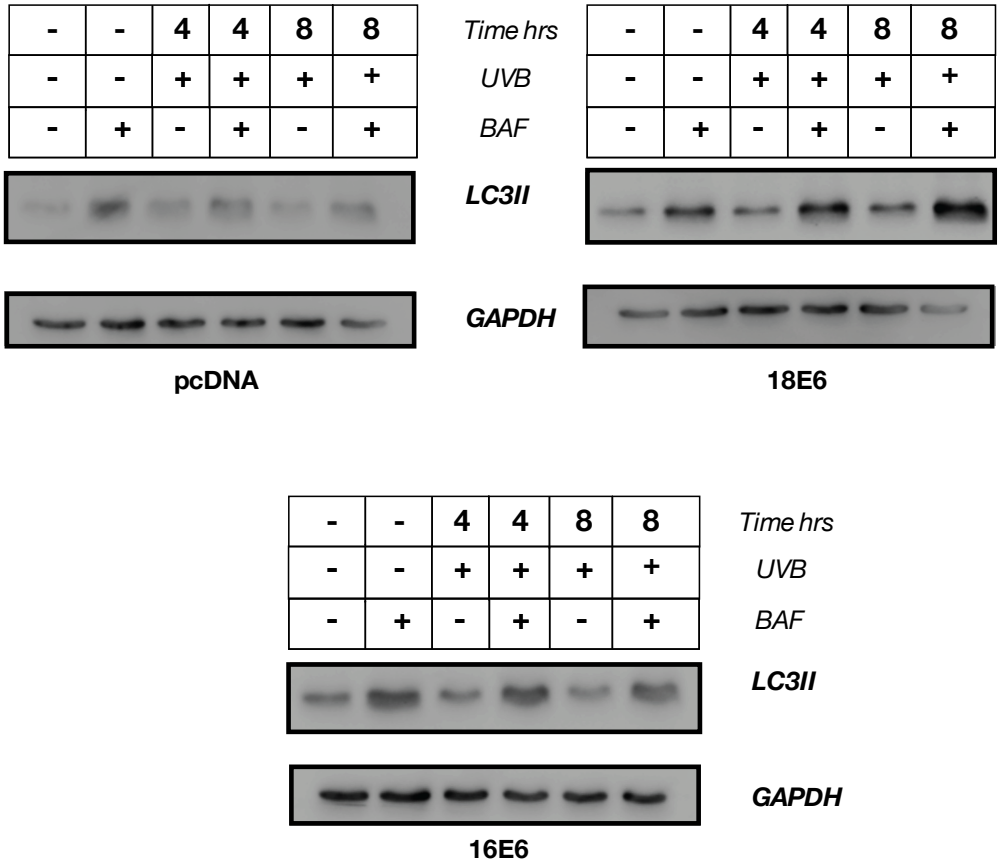

Figure 3-18 LC3 turn over in HT1080 cells expressing high-risk HPV E6

LC3 turn over blots in HT1080 cell line expressing pcDNA, HPV18 E6 or 16E6. Cells were seeded and exposed to 10mJ/cm^2 UVB and harvested after 4 or 8 hours. Bafilomycin A1 (BAF) was added to assess the autophagic flux 2 hours before harvesting. LC3II (~16kDa), the loading control GAPDH is observed at (~37 kDa).

3.3.13 Identifying the region of E6 important for inducing autophagy

Published work from this lab generated and characterised a series of HPV5 E6 mutants, some of which have lost the ability to abrogate UVB triggered apoptosis and degrade BAK (Simmonds & Storey 2008). To assess whether BAK proteolysis is essential for the induction of autophagy by E6 expressing cells, E6 mutants were screened for autophagy levels after UVB. The mutagenesis was made across multiple domains in HPV5 E6 that were either conserved amongst cutaneous HPV types alone or all HPV types (Figure 3-19A). The researchers found that point mutations affected E6's ability to target BAK for proteolysis; however that was not always parallel with the abrogation of UVB induced apoptosis. Table 9 summarizes the activity of the mutants generated, compared to wt HPV5 E6.

Table 9 Summary HPV5 E6 mutants activity

The activity of different E6 mutants compared to wt E6. +++ = strong, ++ = intermediate activity, + = weak activity and - = no activity. Adapted from (Simmonds & Storey 2008)

E6 mutants	Promotes BAK proteolysis	Inhibition of Apoptosis
Wild type	+++	+++
F43Y	+	++
P40A	-	+
L63A	-	++
V70A	-	++
K151A	+	++

Since point mutations affected the functions of E6, it was of interest to screen these mutants for autophagy levels after UVB to try and identify the regions of E6 necessary for autophagy induction.

HT1080 cell lines were transfected with empty vector or plasmid encoding, F43Y, P40A, L63A, K151A and V70A. Stable cell lines were then treated with 10mJ/cm^2

UVB and cells were harvested after, 4, 6, and 8 hours, Bafilomycin A1 was added 2 hours prior to the indicated time points to assess autophagic flux. Autophagy levels were then examined using LC3 western blots (Figure 3-19B).

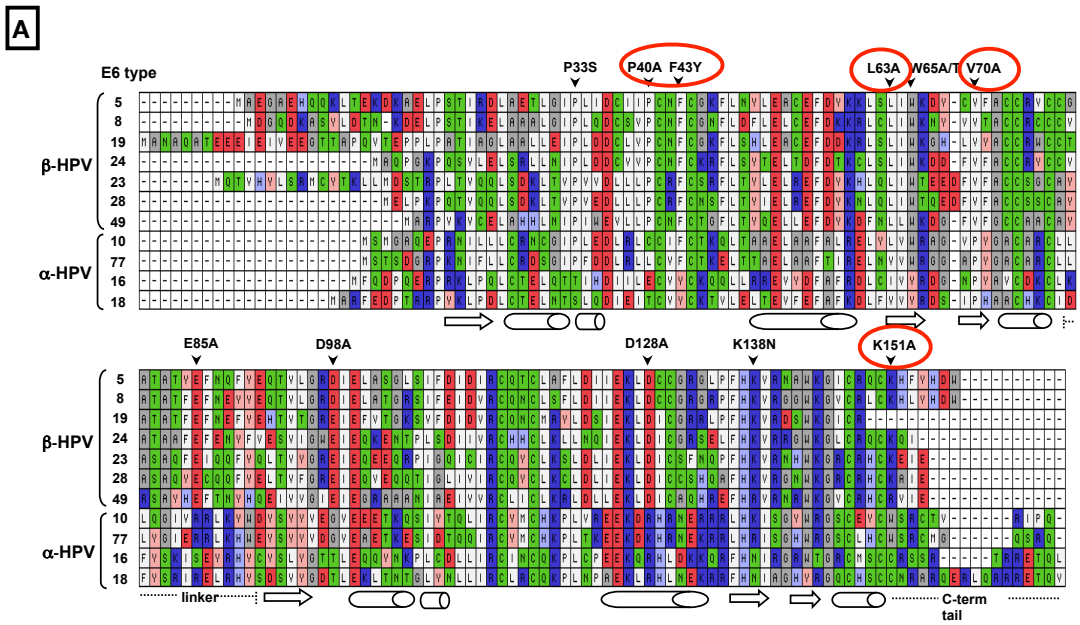

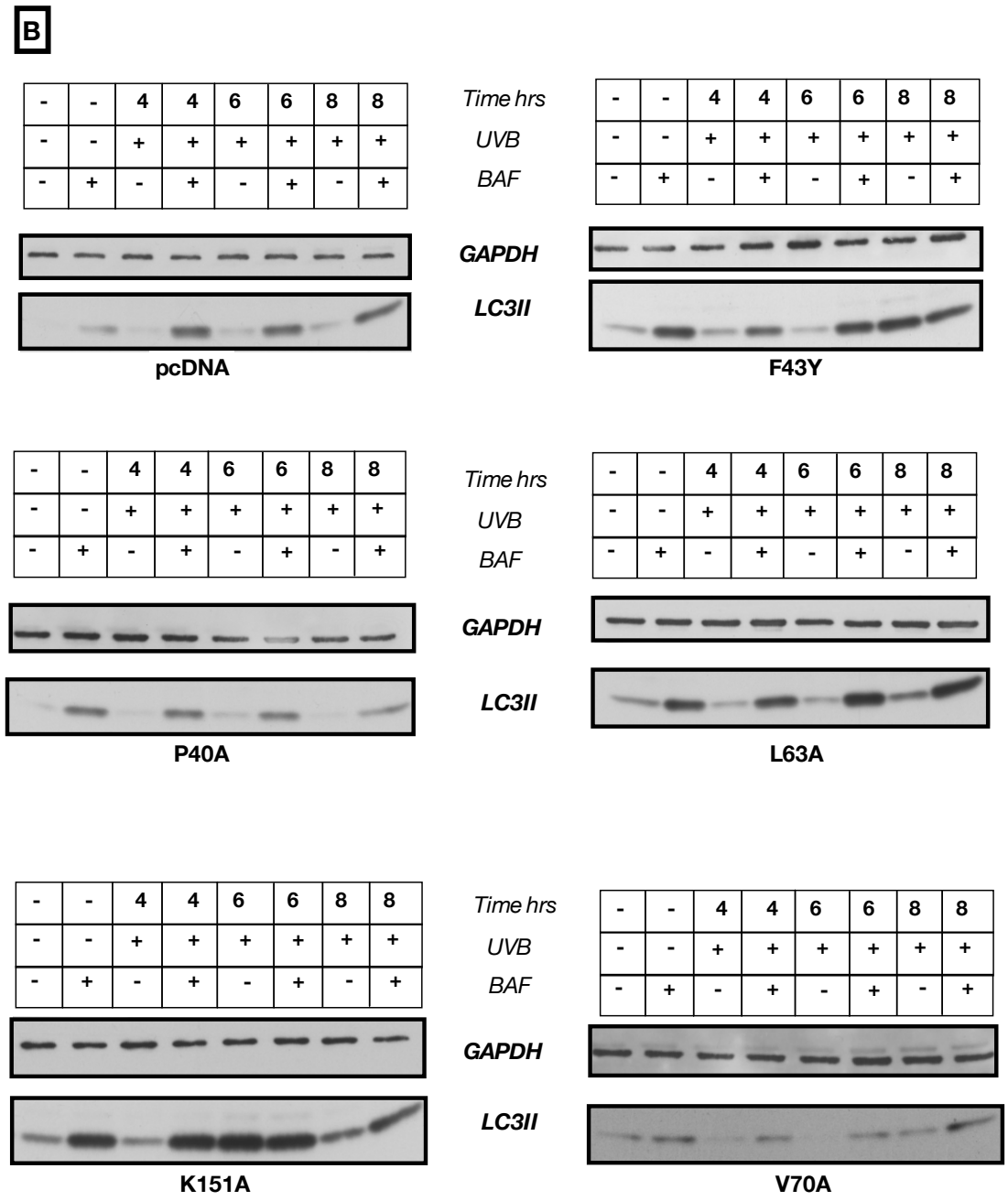

Figure 3-19 Autophagy levels in different HPV5 E6 mutants

A) Mutagenesis of E6, taken from (Simmonds & Storey 2008).

B) HT1080 cell lines stably expressing pcDNA, F43Y, P40A, L63A, K151A and V70A were irradiated with 10mJ/cm^2 UVB and cellular protein were harvested at the indicated time points. Bafilomycin A1 was added 2 hours before harvesting. Protein lysates were resolved on SDS-PAGE and immunoprobed for LC3II levels, GAPDH was used as a loading control.

It is observed that the two E6 mutants V70A and P40A that have lost the ability to degrade BAK completely showed low autophagy levels after UVB damage demonstrated low LC3II levels. However, the L63A E6 mutant which has also lost

the ability to degrade BAK and inhibited apoptosis to some extent, showed autophagy induction after UVB. These results suggests that although the inhibition of apoptosis and BAK degradation might have an impact on autophagy levels after UVB in E6 expressing cells, autophagy induction and BAK degradation are mediated by different regions of the E6 protein.

3.4 Discussion

Cutaneous HPV types have a co-factorial role in the development of NMSC alongside UV, the main etiological agent (Shterzer et al. 2014). It is postulated that in this context HPV plays a role in the initial transformation events. Studies showed that the oncogenic protein E6 from different beta HPV types specifically targets the pro-apoptotic protein BAK for proteolytic degradation after UVB DNA damage, thereby inhibiting apoptosis (Thomas & Banks 1999; Sarah Jackson & Storey 2000; Underbrink et al. 2008). This; was also demonstrated here in Figure 3-3A&B. HT1080 and PM1 cell lines expressing HPV5 E6 harbour low annexin V staining compared to the empty vector control. This Indicates that at the selected UV doses apoptosis is inhibited by E6. Additionally, p53 behaviour was not altered in PM1 keratinocytes at the UVB dose used. As previously described in (3.1.2) a crosstalk exists between autophagy and apoptosis. Moreover, a recent study showed that in mouse embryonic fibroblasts lacking the pro-apoptotic proteins BAK and BAX, DNA damage provoked an autophagic response that delayed cell death (Shimizu et al. 2004). It was then hypothesised that since HPV E6 degrades BAK upon the receipt of a DNA damaging signal, autophagy would be induced. Autophagy levels were investigated in cells expressing E6 after UVB DNA damage initially by monitoring the formation of LC3 puncta using GFP-LC3. It was observed that after 4 hours of UVB damage, HPV5 E6 expressing cells accumulated LC3 puncta, suggesting an activation of the autophagic pathway. Moreover, endogenous LC3

staining in Figure 3-7, Figure 3-8 revealed that after UVB, HPV5 E6 expressing cells show an increase in the number of LC3 puncta per cell, indicating autophagy induction and supporting the initial observation obtained using GFP-LC3. However, autophagy is a dynamic process where autophagosomes are constantly being formed and cleared by the lysosomes (autophagic flux). This means that the accumulation of LC3 puncta can be the result of either an induction of the autophagic pathway or an impairment of lysosomal clearance of the autophagosomes. Here, autophagic flux was assessed by monitoring the increase in LC3 puncta formation after blocking the fusion between the autophagosomes and the lysosomes using Bafilomycin A1 following UVB treatment. Figure 3-9 shows that in HPV5 E6 expressing keratinocytes, the number of LC3 puncta per cell increased after UVB, and that the addition of Bafilomycin A1 resulted in a further increase in LC3 puncta. This suggests that E6 expressing cells have a high autophagic flux after UVB, indicating an induction of the autophagic pathway. Second, LC3 turnover with the addition of Bafilomycin A1 was examined using western blots. In this assay, the difference between LC3II bands before and after Bafilomycin A1 is used as an indication for autophagic flux; an increase in the LC3II band after Bafilomycin A1 treatment suggests active induction of autophagy. Interestingly, it is observed that cells expressing HPV5 E6 have a high autophagic flux in the untreated stress free conditions, and these levels were further increased after UVB Figure 3-10 A and B. Meanwhile control cells seem to have lower autophagy levels after UVB, which could be attributed to the presence of an apoptotic response in these cells. Third, autophagy activity was examined using ImageStream to further confirm the previous results. This technique allows for the assessment of the formation of autolysosomes, a later step in the autophagic pathway. The results in Figure 3-11 shows that PM1 cells expressing E6 show an increase in autolysosomes after UVB suggesting that there are more

autophagosomes formed and fused with the lysosomes and indicating an induction of autophagy after UVB. Contrastingly, autolysosomes levels seem to be decreased in control cells, and this may be due to a decrease in autophagic activity and an increase in apoptosis. These results are parallel to previous results and suggest that after UVB, E6 expressing cells harbour a high autophagic flux and an active autophagy.

Although there is no evidence that HPV E7 can modulate apoptosis after UVB, a recent study showed a link between HPV16 E7 oncoprotein and autophagy. The researchers demonstrated that the expression of HPV16 E7 resulted in an increase in the autophagy marker LC3II and this increase was exacerbated by growth factor deprivation. It was then of interest to assess autophagy levels in E7 expressing cells after genomic stress. In Figure 3-12 western blot analysis and LC3 puncta staining show that HPV E7 expressing cells behave similarly to the control cells, where autophagy levels are maintained at basal levels or decreased after UVB. This suggests that an increase autophagy after DNA damage is a specific effect of E6.

Although assessing autophagy activity by LC3 analysis is considered accurate, it has to be complemented by measuring other proteins involved in the pathway (Mizushima et al. 2010). It was observed that the levels of Beclin-1, one of the key autophagy regulator were increased after UVB in HPV5 E6 expressing cells. This could indicate that E6 might interact with the early stages of autophagy to increase flux. Additionally, in Figure 3-13 the levels Atg7 and Atg5/12 complex seem to be increased in HPV5 E6 expressing cells after UVB. Additionally an increase in levels of Atg5/12 complex lends further support to previous results showing an increase in LC3 puncta after UVB. Moreover, recent studies described an autophagy process that is independent of Atg7 and 5, this type of autophagy was still regulated by Beclin-1, but showed little LC3 puncta formation (Nishida et al. 2009). Therefore the increase in Atg5/12 complex and Atg7 in HPV5 E6 expressing cells

upon UVB irradiation suggests a classical macroautophagy, dependent on Atg7 and Atg5.

The main focus of this study is delineating the relationship between E6 from HPV types 5 and 8 and host autophagy due to their strong involvement in NMSC. However, other types of cutaneous HPV are also implicated in the disease. Different studies detected the presence of HPV38 and 20 DNA in patients with NMSC and solar keratosis. Moreover, a recent study showed that in mice expressing HPV38 E6/E7 on K14 promoter rendered SCC and skin lesion after UVB treatment (Viarisio et al. 2011). Furthermore, it has been demonstrated that E6 from those two types can inhibit UVB induced apoptosis (Underbrink et al. 2008). It was then of interest to test autophagy levels in cells expressing those types. Figure 3-14A shows that similar to HPV5 E6, cells expressing E6 from HPV38 and 20 exhibit high autophagic flux after UVB. Interestingly, at 16 hours, the levels of autophagy seem to be returning to basal levels or lower, suggesting that in cells expressing E6 from HPV38 and 20, respond with high autophagy after UVB but that response might not be sustained for long.

Although the overall structure of E6 from different HPV types is broadly similar, the cellular targets are different. Understanding the different cellular processes that engage E6 and E7 in both high risk and low risk HPVs can help shed the light on the mechanism of oncogenic transformation of those two proteins. Here, levels of autophagy in cells expressing E6 from low risk HPV type 1 and 4 were examined. Interestingly, LC3 turnover with the addition of Bafilomycin A1 was decreased after UVB, suggesting a decrease in autophagy levels or an inhibition of autophagy. There are no studies examining the interplay between E6 from HPV1 and 4 and apoptosis after UVB. However, the observed low autophagy levels in cells

expressing E6 from HPV1 and HPV4, suggest that E6 from different viral types has markedly different effects on the cells.

Unlike cutaneous HPV, the causality between cervical cancer and mucosal HPVs is established. E6 from HPV types 18 and 16 is known to target p53 for degradation (Moody & Laimins 2010); moreover E6 from these types also can also alter the apoptotic response of the cell by targeting BAK for proteolysis after DNA damage (Thomas & Banks 1999). Therefore, autophagy levels were tested in cells expressing HPV16 and 18 E6 by measuring LC3 turn-over. Figure 3-18 shows an increase in autophagic flux after UVB in cells expressing HPV18 E6 and to a lesser extent in HPV16 E6 expressing cells. Previous work showed that expression of HPV16 E6 activated the mTORC1 pathway and promoted protein synthesis in keratinocytes (Münger 2010). These studies postulate that this effect may inhibit autophagy in these cells. However, autophagy can be regulated by an mTORC1 dependent manner, and in the context of genomic stress, E6 might lead to autophagy activation to override the death response of the cell and promote cell survival. The data presented here suggest that the increase in autophagy levels might be a common function across different high-risk HPV types. Additionally, these data indicate the undergoing autophagy process is p53 independent, since E6 from both alpha and beta HPV seem to result in increased autophagic activity and flux after UVB DNA damage.

As discussed in (3.1.1), many viruses including other DNA viruses modulate autophagy and subvert the process mainly for viral life cycle. Little is known about the relationship between HPV and host autophagy; one study revealed an increase in autophagy levels in primary human keratinocytes upon the infection with HPV16 pseudo-virus (Ishii 2013). Furthermore inhibition of autophagy using 3-Methyladenine (3-MA), a class III phosphatidylinositol-inhibitor or shRNA against one of the key autophagy proteins Atg7, dramatically increased the infectivity of

HPV16 pseudo-virus, suggesting a role for autophagy as a host defence mechanism in HPV16 infection (Griffin et al. 2013). Another study demonstrated that HPV16 pseudo-virus interaction with the EGFR signalling activated mTORC1 and AKT signalling which then inhibited autophagy in human keratinocytes before viral entry (Surviladze et al. 2013). The oncogenic transformation of HPV is not attributed to viral entry and infection, but rather to the expression of E6 and E7, the major oncoproteins encoded by the virus genome (Moody & Laimins 2010). Thus understanding the cellular targets of these two proteins can help shed the light on potential mechanisms involved in cellular transformation. The results thus far showed that cells expressing HPV5 E6 have high autophagy levels and high autophagic flux after UVB DNA damage whilst abrogating apoptosis. The induction of autophagy could be a result of a direct interaction of E6 with autophagy regulators or a by-product of apoptosis inhibition in the cells. It can be postulated that through inhibition of apoptosis and induction of autophagy, E6 is capable of determining cell fate leading to cell survival in the background of genomic stress and that may contribute towards tumourigenesis. The role of autophagy in E6 cell survival will be further explored in chapter 4. Additionally HPV E6 might cause a metabolic shift in the cells, which in turn can activate autophagy, this hypothesis will be tested in chapter 4.

Chapter 4 Investigating the role of autophagy in E6 expressing cells

4.1 Introduction

Evidence of a cytoprotective autophagy effect has been described in physiologic nutrient depletion and in diseases such as cancer. The autophagic degradation of cytoplasmic proteins, glycogen granules and lipid droplets upon starvation yields substrates that support the tricarboxylic acid cycle (TCA) and protein synthesis thus allowing the cells to adapt and survive during nutrient scarcity (Rabinowitz & White 2010). Cancer cells are able to utilize the survival and adaptive roles of autophagy. Survival through autophagy was shown in harsh tumour microenvironments for example in hypoxia and in response to chemotherapy and radiation (reviewed in White 2012). Its has been demonstrated that the inhibition of autophagy in radiation resistant cervical cancer and breast cancer cell lines leads to increase in cell death after radiation (Apel et al. 2008). Additionally, the metastatic skin cancer cell line (MET4) showed increased LC3II puncta accumulation, and inhibition of autophagy by 3-methyladinine or specific ATG5 knockdown augmented the cytotoxicity of cisplatin and AKT inhibitors, suggesting a role for autophagy in chemotherapeutic resistance (Claerhout et al. 2010).

The mechanism by which autophagy promotes cell survival in established tumours is not clearly understood, however, research showed that autophagy can support cancer cell metabolism and also aid survival via removal of damaged organelles (Ostenfeld et al. 2008),(Høyer-Hansen & Jäättelä 2008).

Cancer cells exhibit multiple mutations in oncogenes that lead to metabolic dysregulation and this alteration in metabolism is now emerging as one of the hallmarks of cancer (Hanahan & Weinberg 2011). Otto Warburg has described a glycolytic shift in cancer cells that led to an increase in glycolytic rate and lactate production, even at high oxygen levels (Warburg 1956). Additionally, the rapid proliferation and migration of cancer cells is energy demanding and autophagy can

help cancer cells meet these high energy demands by providing metabolites that can be used for ATP production (Rabinowitz & White 2010). For example, the breakdown of lipid droplets by autophagy provides fatty acids for β-oxidation generating acetyl-CoA that supports the TCA cycle(Singh et al. 2009). Moreover, the degradation of proteins contributes to the amino acid pool in the cytoplasm and can also feed into the TCA cycle (Mizushima & Klionsky 2007).

Recently, autophagy was proven to support Ras-driven tumourigenesis by removal of mitochondria to support oxidative phosphorylation in nutrient low conditions. In these tumours, inhibition of autophagy resulted in a decrease of Ras tumourigenic capacity and cell death (J. Y. Guo et al. 2011). Mitophagy, is the specific removal of mitochondria, upon mitochondrial depolarisation PARKIN, a RING-HECT hybrid E3 ubiquitin ligase translocates to the OMM of the damaged mitochondria through the activity of PINK1 (Narendra et al. 2010). This translocation leads to the poly-ubquitinlaytion of several mitochondrial proteins, leading to the recruitment of p62/Sequestosome 1 and the sequestration of damaged mitochondria into the autophagosomes (Geisler et al. 2010). Other proteins have also been demonstrated to translocate to damaged mitochondria, such as BNIP3 and NIX, which are downstream targets of HIF1 alpha. BNIP3 can associate with the OMM and interact with LC3 via its LIR domain, and thereby mediate mitophagy (Zhang & Ney 2009).

The removal of damaged mitochondria by mitophagy was also proven essential for the survival of autophagy addicted melanoma cells. Studies show that knockdown of BNIP3 leads to the accumulation of ROS, and decreases cell viability of melanoma cells *in vitro* (Maes et al. 2014).

4.2 Aims

In the first chapter, evidence was obtained that cells expressing the HPV E6 protein respond to UVB by an increase in autophagy and a high autophagic flux. Given the multiple roles of autophagy, there are several possible roles that E6 may fulfill by inducing autophagy under conditions of UV-induced stress. These could include: promoting cell survival and increasing the pool of metabolites. This chapter aims to explore the role that autophagy plays in cells expressing E6.

4.3 Results

4.3.1 Effect of autophagy on survival of E6 expressing cells

One of the canonical roles of autophagy in cells is to promote cell survival in harsh environmental conditions such as nutrient deprivation and hypoxia. Hence it can be hypothesised that the observed autophagic induction in E6 expressing cells promotes cell survival during genomic stress.

To test this hypothesis, the effect of autophagy inhibition on E6 expressing cells survival was examined by an shRNA-mediated knockdown of ULK1, a key regulator of autophagy. ULK1 is a downstream target of mTORC1 and AMPK. In nutrient rich conditions, mTORC1 phosphorylates ULK1 at the S117 preventing its association with FIP200 and preventing the formation of the ULK1 complex, and therefore inhibiting autophagy (Bach et al. 2011). Recent studies have shown that the energy sensor AMK can directly activate and regulate ULK1, preventing its phosphorylation by mTORC1 (Kim et al. 2011).

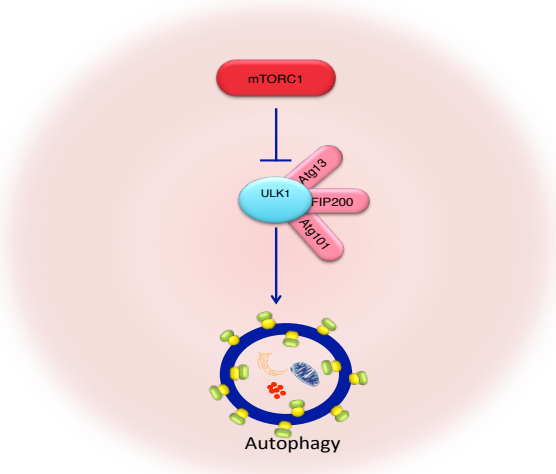

Figure 4-1 ULK1 in the regulation of autophagy

Upon mTORC1 inhibition, ULK1 associates with FIP200, Atg13 and Atg101 leading to autophagy activation.

PM1 cells stably expressing empty vector control or HPV5 E6 were transduced with a lentiviral vector encoding an shRNA against ULK1 tagged with RFP that also carries a doxycycline resistance gene. Cells were then expanded and selected using puromycin for one week. To check for knockdown efficiency, cells were seeded on 100mm dishes and 24 hours later, doxycycline was added at a concentration of 1 μg/ml. A further 24 hours later RFP expression was examined using fluorescent microscopy. Cells were then harvested and protein levels were probed using western blot analyses and mRNA levels were analysed using RT-PCR (Figure 4-2). The results showed that there is good knockdown of ULK1 at both the mRNA and protein levels.

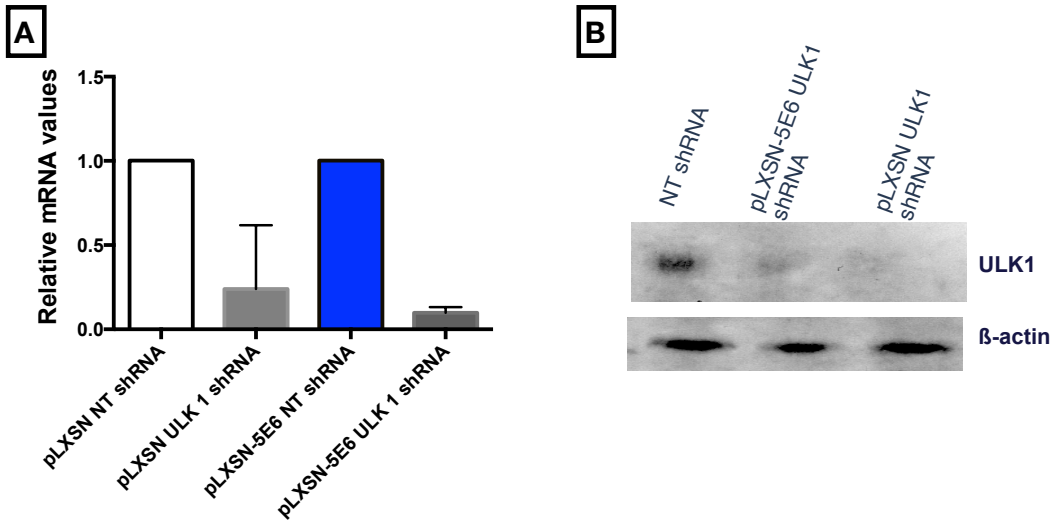

Figure 4-2 shRNA knockdown of ULK1 in PM1 cell line

PM1 keratinocytes transduced with pLXSN or pLXSN-5E6 were transduced with either a non-target shRNA (NT shRNA) or an shRNA against ULK1. After 24 hours of doxycycline treatment, mRNA levels were measured using RT-PCR and protein levels were examined by western blot**. A)** mRNA levels of ULK1 measured by RT-PCR. **B)** Western blot of ULK1 ~150 kDa, actin was used as a loading control.

Having established an inducible shRNA system in the PM1 cell lines, the effect of autophagy inhibition on E6 expressing cell survival was tested by measuring apoptosis levels using annexin V. Cells were seeded in 60mm dishes at $3x10^5$ cells per dish. Twenty-four hours later, doxycycline was added to culture media and a further 24 hours later cells were treated with UVB 10mJ/cm^2 and stained for annexin V to determine apoptosis levels. Cellular viability was also assessed using LIVE/DEAD® Aqua. Note that the UVB dose was decreased in this assay due to the observation that the combination of doxycycline and a 15mJ/cm^2 (the dose previously used to monitor autophagy) was very toxic to E6 expressing cells (preliminary data). Flowcytometric analysis was carried out to measure annexin V and LIVE/DEAD® after gating only on the RFP positive cells that have the ULK1 knockdown. Interestingly, the results revealed that autophagy inhibition abrogated the protection from cell death provided after UVB, this demonstrated by an increase in annexin V levels in pLXSN-5E6 expressing cells (Figure 4-3A). Moreover, the live/dead marker revealed a marked decrease in cell viability after

autophagy inhibition following UVB, even with a UVB dose lower than that used for autophagic studies (Figure 4-3). These results suggest a role for autophagy in the survival of cells expressing E6 after UVB damage.

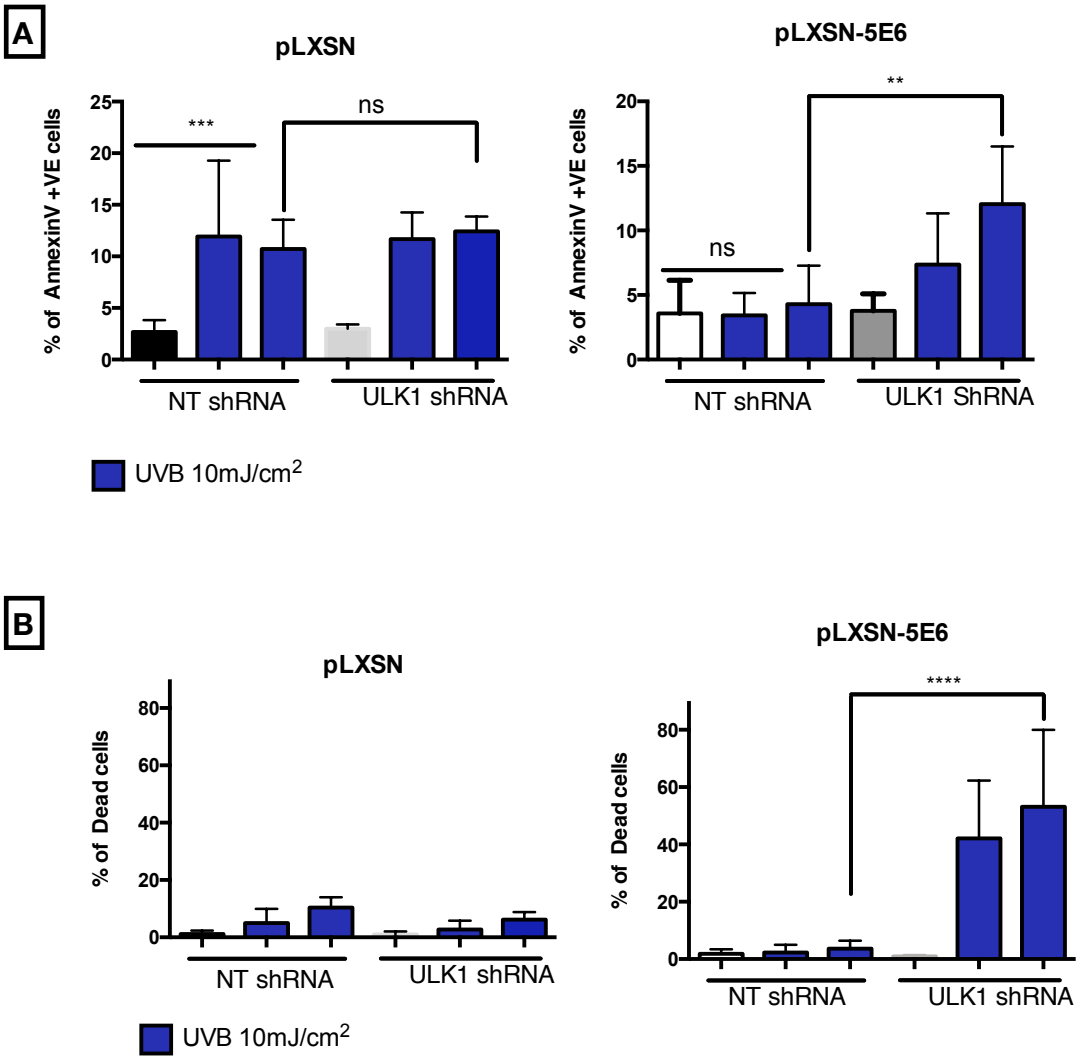

Figure 4-3 Effect of autophagy inhibition on E6 cell survival after UVB

PM1 cells line transduced with pLXSN or pLXSN-5E6 were transduced with a non-target shRNA (NT shRNA) or an shRNA against ULK1. Cells were incubated for 24 hours with a media containing 1µg/ml doxycycline. Cells were then irradiated with UVB and a further 24 hours later, cells were collected and stained for annexinV and Live/Dead Aqua. After gating on RFP, annexin V and LIVE/DEAD® levels were measured. **A)** levels of annexin V positive cells in pLXSN and pLXSN-5E6 PM1 keratinocytes. The blue bars represent the levels after UVB irradiation. **B)** Percentage of cell death measured by LIVE/DEAD® levels in pLXSN and pLXSN-5E6. Statistical analysis was perfumed using one-way ANOVA. S.E.M ± **p<0.01, ***p<0.001 and ****p<0.0001.

The observation that autophagy inhibition decreases the survival of E6 expressing cells after UVB raises the question as to whether E6 expression leads to (autophagy-addiction) during stress. This could suggest that HPV driven tumour cells might have high autophagy levels.

Next pharmaceutical inhibition of autophagy was used to complement the previous observations. This was investigated using Bafilomycin A1, which was used previously to inhibit autophagy and assess autophagic flux.

PM1 keratinocytes transduced with pLXSN or pLXSN-5E6 were exposed to UVB irradiation of 7mJ/cm^2 and Bafilomycin A1 was added to the culture media immediately after irradiation. After twenty-four hours the cells were harvested and stained with annexin V/PI to assess cell death (Figure 4-4). Interestingly, the results revealed that autophagy inhibition using Bafilomycin A1 caused an increase in apoptotic cell death in E6 expressing cells after UVB (Figure 4-4A). However, it was also observed that more than 50% of E6 expressing cells lost viability, this was demonstrated by high levels of PI staining and low annexin V (Figure 4-4B). Examination of FACS scatterplot revealed that E6 expressing cells were taking up more PI than annexin V, demonstrated by an upward shift in the scatterplot quadrants (Figure 4-4C). This could suggest that although a small population of cells undergo apoptotic cell death after autophagy inhibition, the majority of cells die via a different cell death modality.

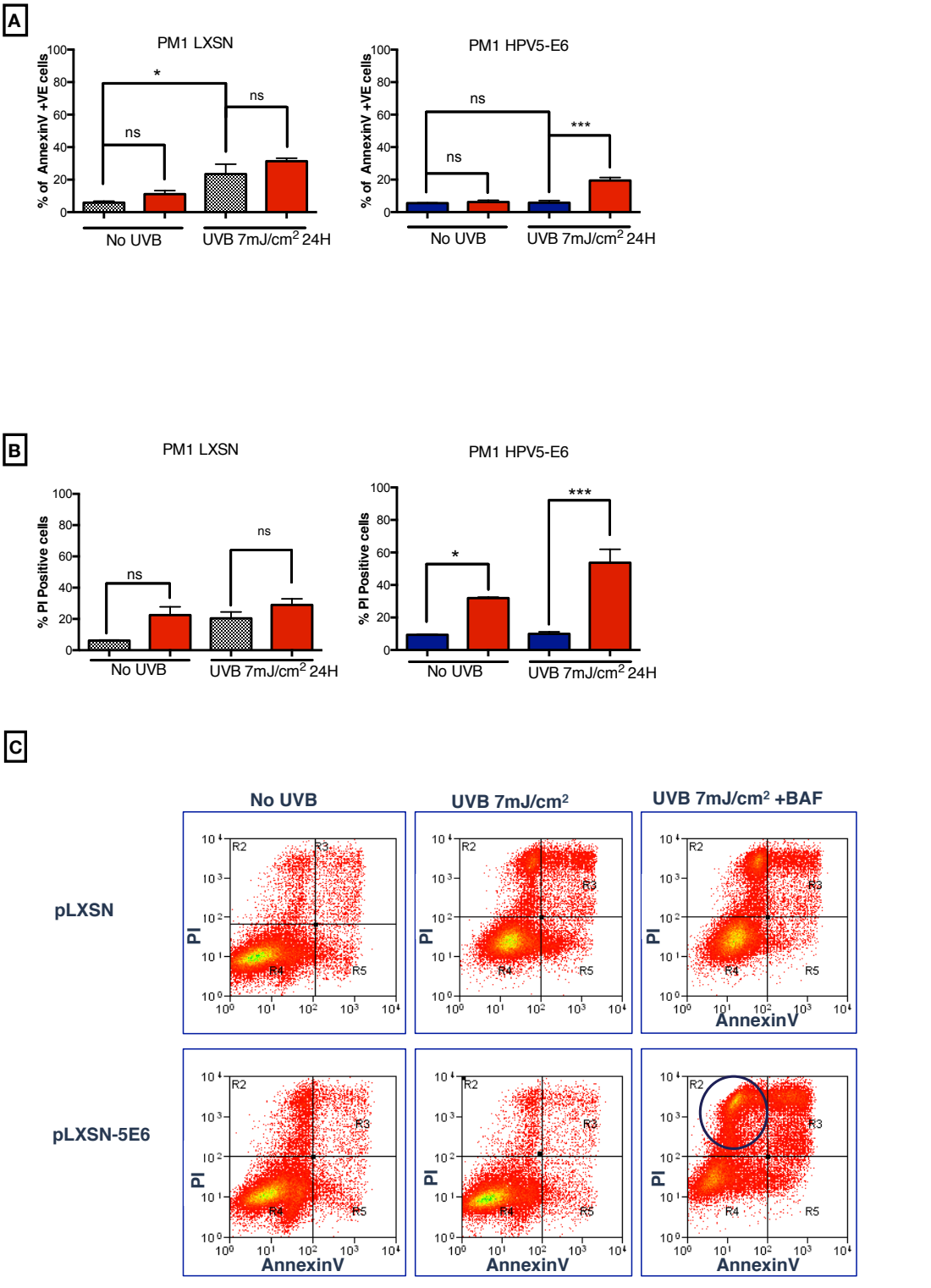

Figure 4-4 Effect of autophagy inhibition using Bafilomycin A1 on cell viability after UVB

PM1 keratinocytes expressing pLXSN-5E6 or empty vector control were irradiated with UVB and Bafilomycin A1 (BAF) was added to the cells immediately after. After 24 hours, the cells were stained using annexin V and PI. **A)** Levels of apoptosis as measured by annexin V in pLXSN and pLXSN-5E6 after UVB. **B)** PI levels in pLXSN and pLXSN-5E6. Red bars in both A and B represent the levels with autophagy inhibition using Bafilomycin A1. **C)** Example of FACS plot obtained. Statistical analysis was performed using one-way ANOVA S.E.M ± **p<0.01, and ***p<0.001. n=3

4.3.2 HPV8 E6 expressing cells depend on autophagy to survive

Results in 4.3.1 showed that cells expressing HPV5 E6 depend on autophagy to survive following UVB DNA damage. This was demonstrated by an increase in cell death after UVB and autophagy inhibition in Bafilomycin A1. To investigate whether HPV8 E6 were also dependent on autophagy for survival after UVB, apoptosis levels were analysed after autophagy inhibition. PM1 keratinocytes transduced with pLXSN or pLXSN-8E6 were exposed to UVB irradiation of 7mJ/cm^2 and Bafilomycin A1 was added to the culture media immediately after irradiation. After twenty-four hours the cells were harvested and stained for annexin V to measure apoptosis and PI was used as a viability indicator. Interestingly, the results revealed that autophagy inhibition using Bafilomycin A1 caused an increase in apoptotic cell death in HPV8 E6 expressing cells after UVB, suggesting that these cells are more dependent on autophagy for survival even under conditions of no DNA damage Figure 4-5. However, similarly to HPV5 E6 expressing cells, more than 50% of HPV8 E6 expressing keratinocytes seem to have undergone a non-apoptotic cell death.

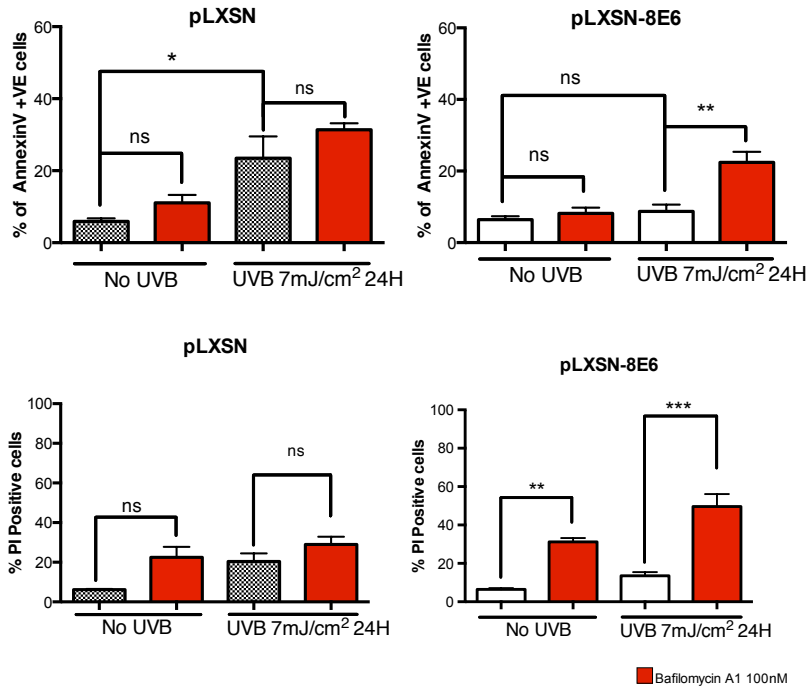

Figure 4-5 Effects of autophagy inhibition on the survival of HPV8 E6 expressing cells

PM1 keratinocytes expressing pLXSN-8E6 or empty vector control were irradiated with UVB and Bafilomycin A1 (BAF) was added to the cells immediately after. After 24 hours, the cells were stained for annexin V and PI. Top graphs show levels of apoptosis as measured by annexin V in pLXSN and pLXSN-8E6 after UVB. Bottom graphs show PI levels in pLXSN and pLXSN-8E6. Red bars represent the levels with autophagy inhibition using Bafilomycin A1. **C)** Statistical analysis was performed using one-way ANOVA S.E.M ± **p<0.01, and ***p<0.001.

4.3.3 Investigating the mechanism of cell death after autophagy inhibition in E6 expressing cells

The increase in annexin V in E6 expressing cells after autophagy inhibition and UVB damage suggested that at least some cells might have died via apoptosis. The apoptotic pathway involves the activation of downstream effector caspases so to investigate if autophagy inhibition leads to caspase mediated cell death, a pan caspase inhibitor z-VAD fmk was used.

pLXSN or pLXSN-5E6 PM1 cells were seeded in a culture media that was supplemented with z-VAD fmk. After 8 hours, the cells were irradiated with UVB, and Bafilomycin A1 was added to inhibit autophagy. Etoposide, a DNA damaging

agent that is known to induce apoptosis, was used as a positive control to confirm z-VAD inhibition of caspase mediated death. The cells were collected after 24 hours following UVB and stained using annexin V and PI (Figure 4-6). The data showed that in E6 expressing cells, z-VAD treatment lead to a small decrease in annexin V staining following UVB irradiation and Bafilomycin A1 inhibition of autophagy. This suggests that a small percentage of cells undergo apoptosis following autophagy inhibition and UVB damage. However, the addition of z-VAD showed very little effect on the percentage of PI positive cells in E6 expressing cells after UVB and autophagy inhibition. These results suggest that the cell death response triggered by the combination of UVB and Bafilomycin A1 in E6 expressing cells is mainly non-apoptotic cell death.

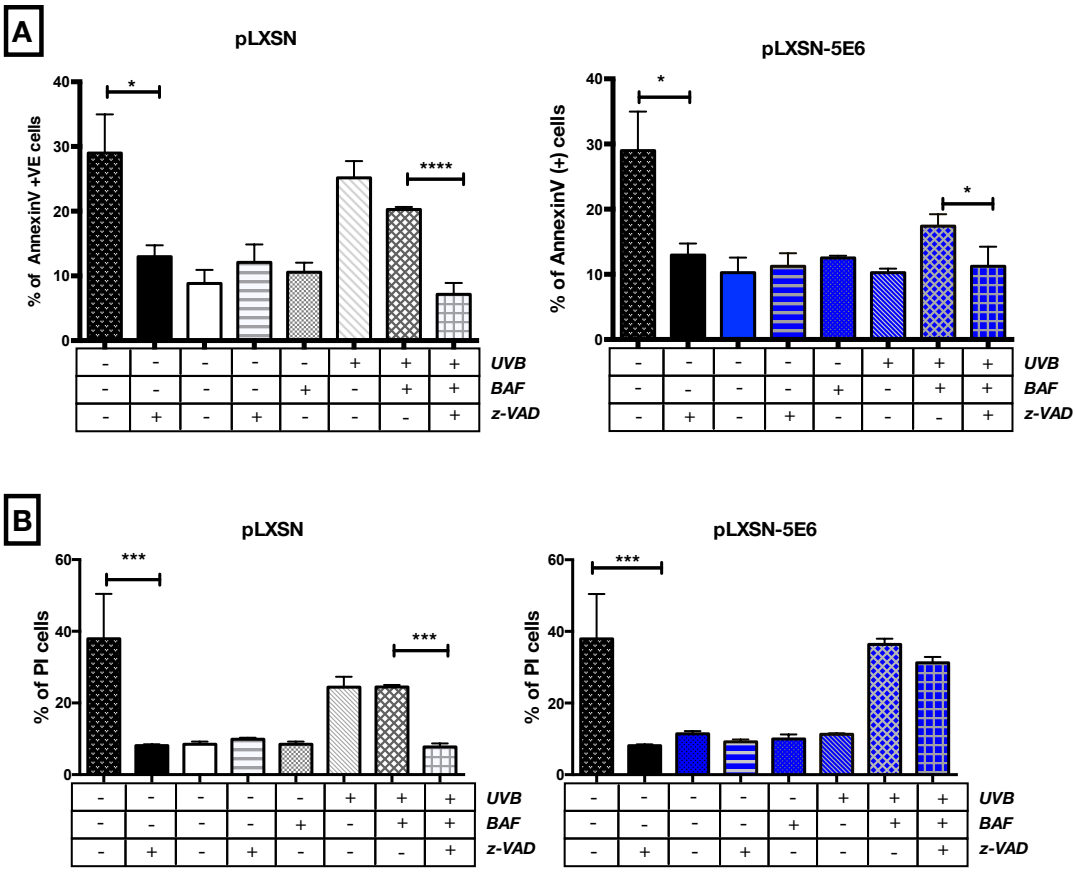

Figure 4-6 Effect of the pan caspase inhibitor on E6 cell viability following UVB and autophagy inhibition

PM1 keratinocytes expressing pLXSN-5E6 or pLXSN were seeded in culture media containing z-VAD fmk. After 8 hours, the cells were irradiated with 7mJ/cm^2 and Bafilomycin A1 was immediately added to the culture media. Twenty-four hours later, the cells were then harvested and stained for annexin V and PI. **A)** Percentage of annexin V cells in pLXSN and pLXSN expressing cells. **B)** Levels of PI positive cells in pLXSN and pLXSN-5E6. Statistical analysis was performed using one-way ANOVA S.E.M ± *p<0.05,**p<0.01, ***p<0.001 and ****p<0.0001. Black bars in both A&B represent Etoposide positive control. n=3

It is well established that the E6 protein from different HPV types abrogate the apoptotic response of cells following a death stimulus such as UVB. This is partly attributed to E6 mediated degradation of the apoptotic regulator BAK (Sarah Jackson & Storey 2000). The results obtained in Figure 4-6 suggested that although a small percentage of E6 expressing cells might undergo apoptosis after UVB and autophagy inhibition, the majority of cells might be dying via a different cell death modality. There are multiple pathways leading to cellular demise, including necroptosis. The key difference between necrosis and apoptosis is the ability to provoke an inflammatory response (Degenhardt et al. 2006). Thus, if autophagy inhibition in E6 expressing cells leads to a release of inflammatory signals, this observation may be of therapeutic benefit.

Necroptosis is an alternative mechanism of programed cell death involving RIPK1(Giampietri et al. 2014). A recent paper by Wallberg et al. described a time-lapse assay to distinguish between necroptosis and apoptosis using annexin V and PI. The principle of this assay is that cells undergoing apoptosis can be identified by annexin V staining first, then the uptake of PI. However, cells undergoing necroptosis are identified by the rapid uptake of both PI and annexin V (double positive) or PI alone (Wållberg et al. 2013).

PM1-pLXSN or PM1-pLXSN-5E6 cells were seeded in glass bottom 4 well dish. After 24 hours, the cells were irradiated with UVB 7mJ/cm^2 and Bafilomycin A1 was added. Annexin V conjugated with FITC was added to the tissue culture media along with PI. A time-lapse series was set up in an environmentally controlled chamber using the DeltaVision imaging system in which 2 fields of view per well randomly were set and images were obtained every hour for 24 hours. The data was analysed by counting the number of annexin V positive, PI positive or double positives in each field of view over time in Fiji (Image J software). H_2O_2 was used as

a positive control to monitor necrosis and Etoposide was used to monitor apoptosis Figure 4-7.

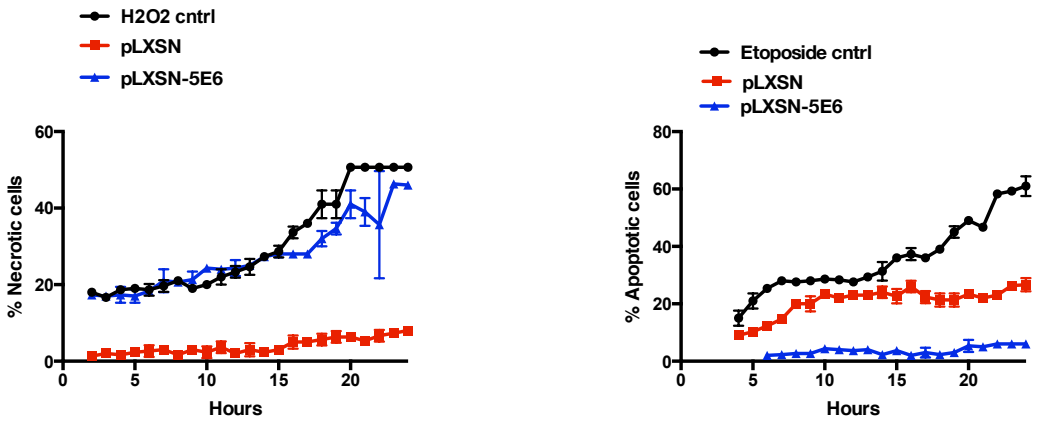

Figure 4-7 Time-Lapse analysis of cell death

pLXSN-5E6 and pLXSN PM1 keratinocytes were seeded in small glass bottom dishes. Cells were irradiated with 7mJ/cm^2 and Bafilomycin A1 was added to the media. The time-lapse series was set to image every hour for 24 hours. The number of apoptotic and the number necrotic cells were counted by counting double positive, PI positive for necrosis and annexin V positive for apoptosis. The graph on the left represents the % of necrotic cells counted. The graph on the right represents the number of apoptotic cells counted. Error bars are SEM.

The results showed that after UVB and Bafilomycin A1 treatment, cells expressing E6 displayed an increase in the number of necroptotic cells defined by an increase in the number of double positive (PI and annexin V) and PI positive cells (Figure 4-7 left graph). Whereas the number of cells showing annexin V positivity alone remained low (Figure 4-7 right graph), suggesting that in E6 expressing cells the inhibition of autophagy during UV stress might lead to nectroptotic cell death.

The previous results suggest that after UVB, autophagy inhibition in E6 expressing cells may result in a necrotic cell death. Both necrosis and apoptosis have distinct morphological features; therefore transmission electron microscopy (TEM) studies were performed to probe in further detail these observations.

PM1 keratinocytes were treated with UVB and Bafilomycin A1 for 16 hours. The cells were then collected and fixed in 4% glutaraldehyde. Pellets were then sent to electron microscopy for analysis and images were obtained by Professor David

Ferguson. Control cells showed normal morphology under no treatment conditions (Figure 4-8A). However, upon UVB irradiation (Figure 4-8B), cells showed increased mitochondria (Figure 4-8B,MT), an increase in keratin filaments was also observed (Figure 4-8B,K), suggesting differentiation after UVB. Apoptotic cells (Figure 4-8B,AP), identified by cellular membrane blebbing and chromatin condensation were also detected in control cells after UVB and Bafilomycin A1 treatment. Interestingly, the expression of E6 seems to alter PM1 keratinocyte morphology under no treatment conditions. The changes observed were mainly in chromatin distribution suggesting that E6 might alter transcription and chromatin packaging in cells (Figure 4-8C, AC). Upon UVB and Bafilomycin A1 treatment, cells showed striking abnormalities morphological features that did not fit either the classical apoptotic morphology nor necrotic. In some cells, the nuclei were lost but the cytoplasm was intact (Figure 4-8C, LC). Additionally cells were heavily vacuolated (Figure 4-8C, VA), likely due to Bafilomycin A1 effects of blocking the degradation of the autophagosomes by the lysosomes, leading to an accumulation of autophagosomes. Dead cells seemed to have cellular membrane rupture and frayed a cytoplasm. These results suggest that autophagy inhibition leads to an atypical form of cell death after UVB in E6 expressing cells.

A
pLXSN
UNT
pLXSN-5E6
UNT
2μm
2μm
AC
1μm
500nm
MT

B

pLXSN

UVB 7mJ/cm^2 16hrs

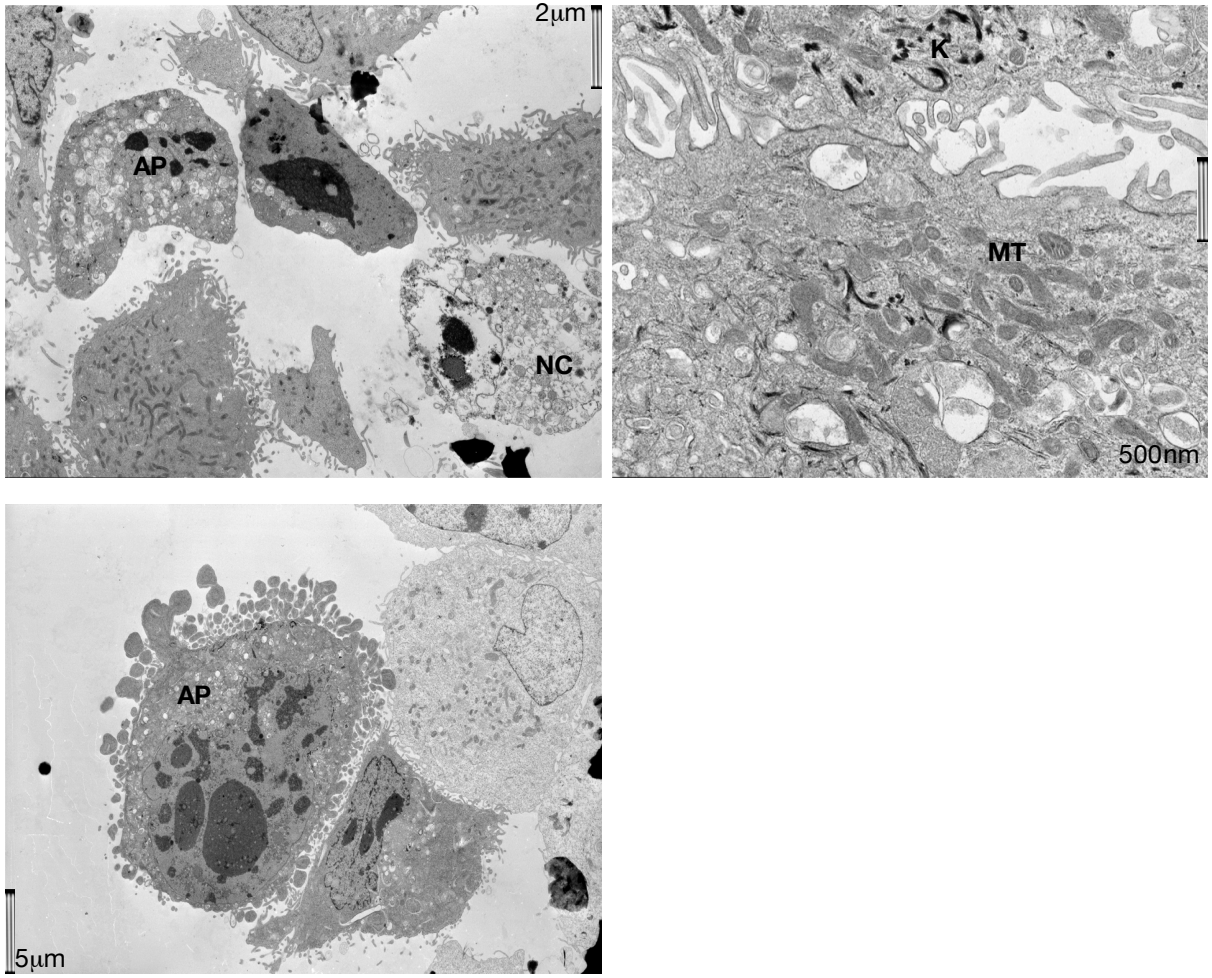

C

pLXSN-5E6

UVB 7mJ/cm^2 16hrs

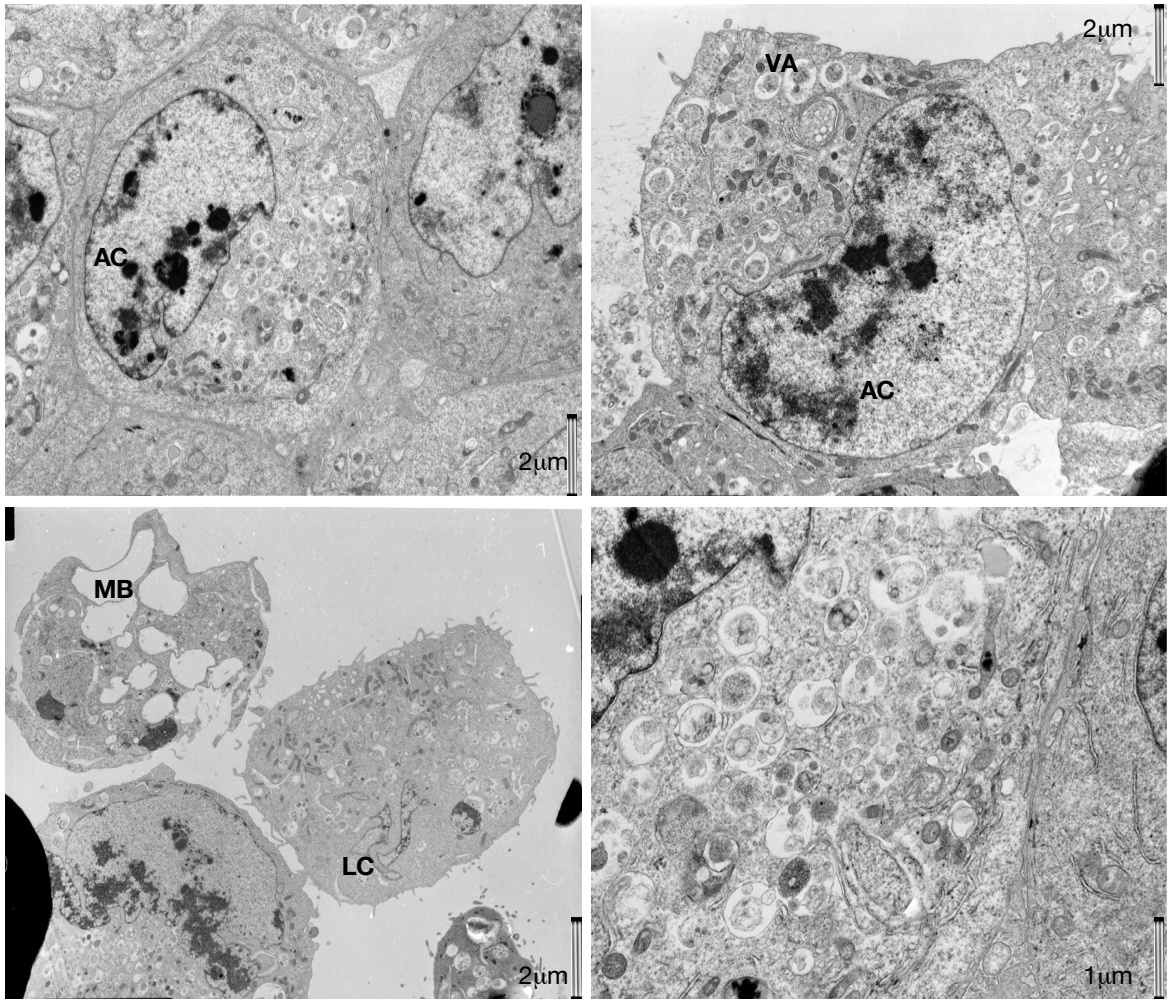

Figure 4-8 Transmission electron micrographs of PM1 keratinocytes after UVB and autophagy inhibition

pLXSN and pLXSN-5E6 PM1 keratinocytes were irradiated with 7mJ/cm^2 and treated with Bafilomycin A1 for 16 hours. Cell pellets were then collected, fixed and sent to EM for analysis. **A)** Electron micrographs of untreated (UNT) pLXSN and pLXSN-5E6. MT: mitochondria. AC: abnormal chromatin. **B)** Electron micrographs of pLXSN after UVB irradiation and Bafilomycin A1. AP: apoptotic cells. NC: necrotic cell. K: keratin filaments. MT: mitochondria. **C)** Electron micrographs of pLXSN-5E6 after UVB irradiation and Bafilomycin A1. LC: loss of nucleus with finger like projections remnants. MB: Cell membrane breakage. AC: abnormal chromatin. VA: vacuoles.

4.3.4 The role of mitochondria in autophagy mediated cell survival in E6 expressing cells

There are many ways in which autophagy can lead to cell survival including eliminating damaged organelles, the accumulation of which might lead to cell death, such is the case for mitophagy where specific mitochondrial elimination occurs by the autophagic machinery. This process is triggered in response to various stress signals including accumulation of reactive oxygen species (ROS) and mitochondrial membrane depolarization. High levels of ROS are known to be toxic to the cells, and some studies have showed that at high doses, UVB can induce ROS generation which in turn damage the mitochondria (Kovacs et al. 2009). Defective clearing of the mitochondria can multiply ROS damage and lead to cytochrome *c* release and cellular demise. Since one of the major roles of E6 is inhibition of apoptosis, it can be postulated that the autophagy induction observed after UVB is to counteract ROS induced apoptosis, and thereby promote cell survival. To test this hypothesis, ROS levels were measured in E6 expressing HT1080 and PM1 keratinocytes using MitoSOX, a super oxide indicator dye.

HT1080 and PM1 cell lines stably expressing HPV5 E6 and control lines were irradiated with UVB and collected at the indicated time points Figure 4-9. Cells were then stained using MitoSOX and ROS levels were analysed using flow cytometry. Antimycin A, an inhibitor of complex III that leads to ROS accumulation was used as a positive indicator for ROS (You & Park 2010). Results in Figure 4-9 reveal a minimal increase in ROS levels after UVB in both HPV5 E6 expressing cells and the empty vector control, questioning the possible role of mitophagy induction due to ROS damage.

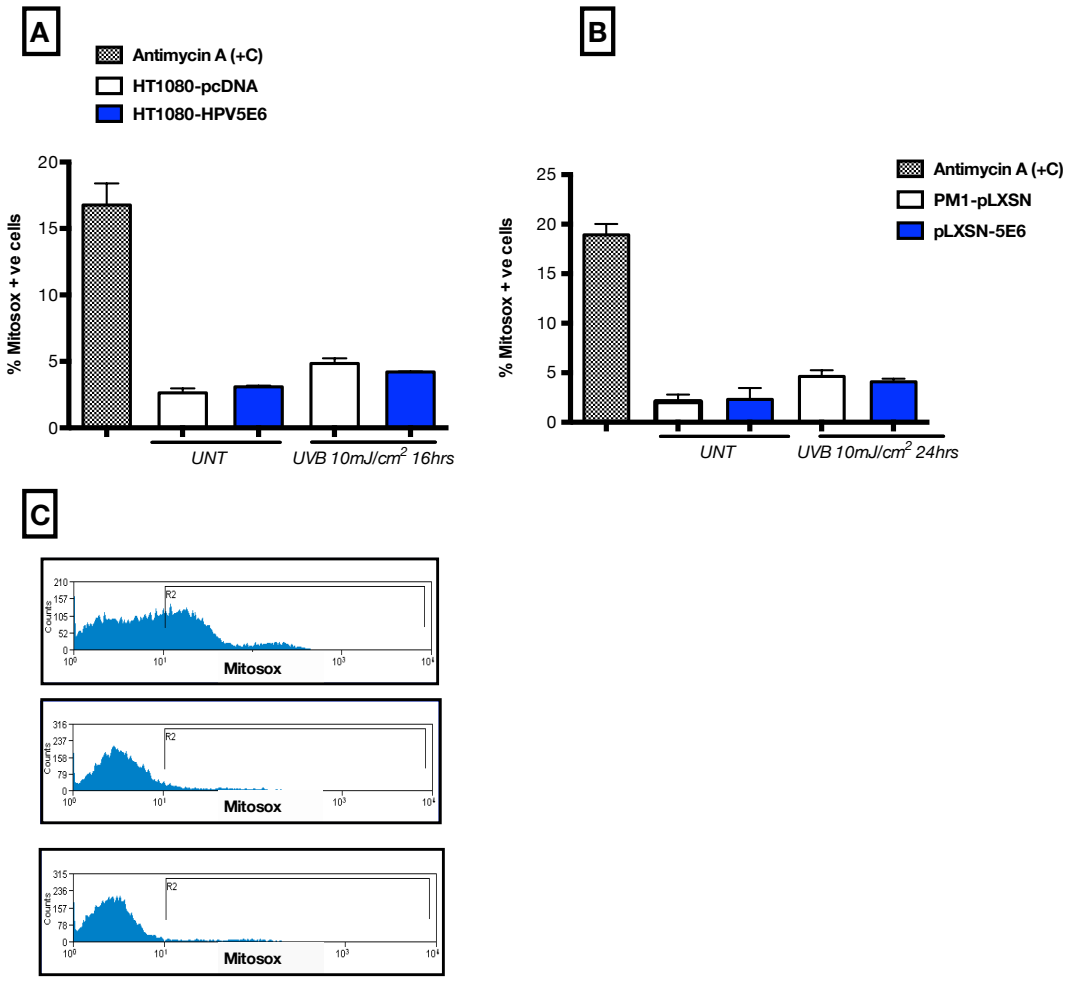

Figure 4-9 ROS levels in HT1080 and PM1 cell lines expressing E6

HT1080 and PM1 cells expressing HPV5 E6 or control lines were seeded in 60mm dishes. Twenty-four hours later, cells were treated with UVB and harvested at the indicated time points. Cells were then stained for ROS using MitoSOX and levels were analysed using flowcytometry. Antimycin A was used as a positive control. **A)** Bar graph showing %MitoSOX in HT0180 cell lines transfected with pcDNA or HPV5 E6. **B)** Bar graph showing %MitoSOX in PM1 cell lines transduced to express pLXSN-5E6 or pLXSN. **C)** Example FACS histograms, top is Antimycin A treated cells, middle empty vector control and bottom are HPV5 E6. UNT= Untreated control. Error bars are S.E.M ± n=3

To further investigate the possibility of mitophagy induction after UVB, co-localisation study between LC3 and mitochondria was conducted in PM1 keratinocytes encoding pLXSN and pLXSN-5E6. Cells were seeded on glass cover-slips as previously described and 24 hours later, cells were exposed to UVB 15mJ/cm^2. Two hours before harvesting, Bafilomycin A1 was added to assess

autophagic flux and enhance LC3 puncta accumulation. After 24 hours of UVB treatment, live cells were stained for mitochondria using MitoTracker® red probe, a cell-permeable dye that contains a mildly thiol reactive chloromethyl moiety, that accumulates in the mitochondria. Cells were then fixed and stained for LC3 puncta. Representative images were taken using a confocal microscope, Figure 4-10. It was observed that there is no co-localisation between LC3 puncta and the mitochondria, suggesting that the mitochondria are not being eliminated by the autophagosomes.

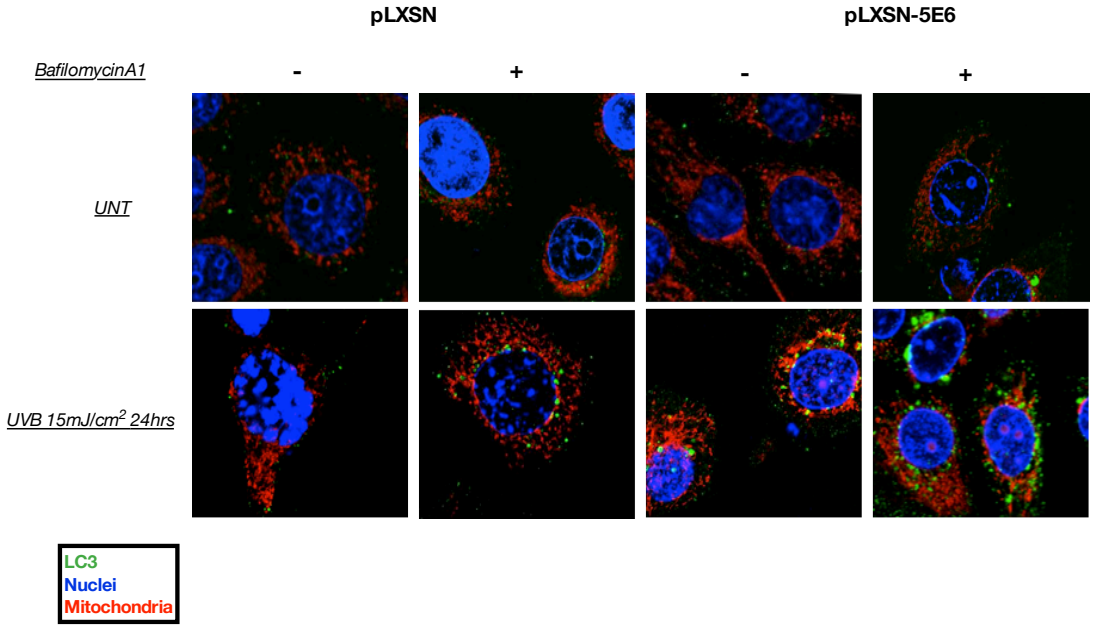

Figure 4-10 LC3-Mitochondria co-localisation in the PM1 cell line expressing HPV5 E6

PM1 cells expressing pLXSN and pLXSN-5E6 were cultured on cover-slips in keratinocytes media with 10% FCS. The cells were then exposed to UVB (15mJ/cm^2). Twenty-four hours after UV the cells were stained with Invitrogen MitoTracker® Red FM (200nM). Cells where then fixed and stained for LC3 foci (green). To enhance LC3 puncta accumulation Bafilomycin A1 was added to the media two hours before harvesting. The nucleus was visualized using DAPI.

Mitochondrial clearing by autophagy can be demonstrated by a decrease in mitochondrial content. Therefore, mitochondrial content was examined using MitoTacker® green in HT1080 cells transfected with pcDNA and pcDNA-5E6. Cells were seeded in 60mm dishes and 24 hours later treated with UVB. Cells were then harvested at the indicated time points and stained using MitoTracker® green for

flowcytometric analysis, Figure 4-11. Surprisingly, the data shows that after UVB, there is a significant increase in the mitochondrial content in both HPV5 E6 expressing and control cells. Suggesting that after UVB there is an increase in mitochondrial activity and this could also suggest an increase in metabolic activity.

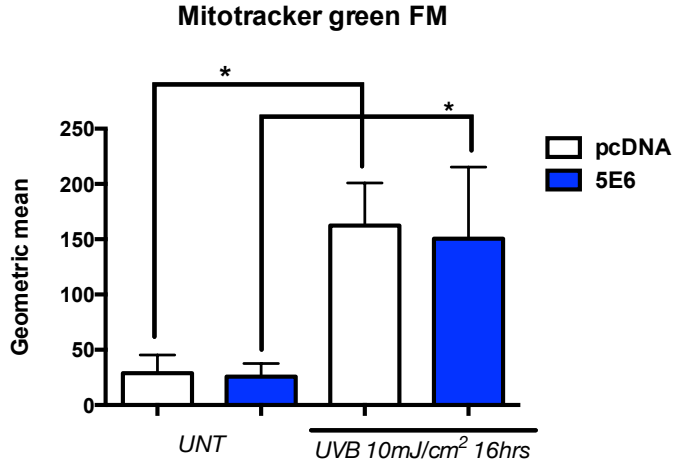

Figure 4-11 Mitochondrial content assessment in HT1080 cell lines after UVB

HT1080 cells expressing HPV5 E6 or empty vector control were seeded in 60mm dishes and 24 hours later cells were exposed to UVB 10mJ/cm^2. Cells were harvested after 16 hours, stained for mitochondria using MitoTracker Green FM and analysed using flowcytometry. Data were analysed using the student t-test. S.E.M ± * $p<0.05$.

The results obtained thus far suggested that in cells expressing E6, the mitochondria are not being targeted for clearance by mitophagy after UVB damage. To further confirm that the undergoing autophagy process is not a result of damaged mitochondria, the content of the autophagosomes were examined using TEM. HT1080 cells transfected with plasmids encoding pcDNA and HPV5 E6 were exposed to UVB, cells were harvested after 8 hours and fixed in 4% glutaraldehyde. Cell pellets were then sent to Electron Microscopy Unit for processing and image analysis by Prof. David Ferguson. Representative images (Figure 4-12) showed more double membrane vesicles in E6 expressing cells, morphologically consistent with autophagosomes. Additionally E6 expressing cells showed a high number of autolysosomes, that are single membrane vacuoles

contains electron dense granules. These observations are consistent with high autophagic flux, but however, this can only be confirmed by using Bafilomycin A1. The Autophagosomes observed in TEM did not contain any specific organelles, the double membrane vesicles were filled with cytoplasm. Additionally, the mitochondria showed intact and healthy morphological features even after UVB exposure in in both E6 and the empty vector control. Taken together these data indicate that the mechanism of survival by E6 mediated autophagy does not involve mitochondrial clearance.

A
pcDNA
UNT
pcDNA 5E6
UNT
2μm
2μm
1μm
1μm
Mitochondria
Mitochondria

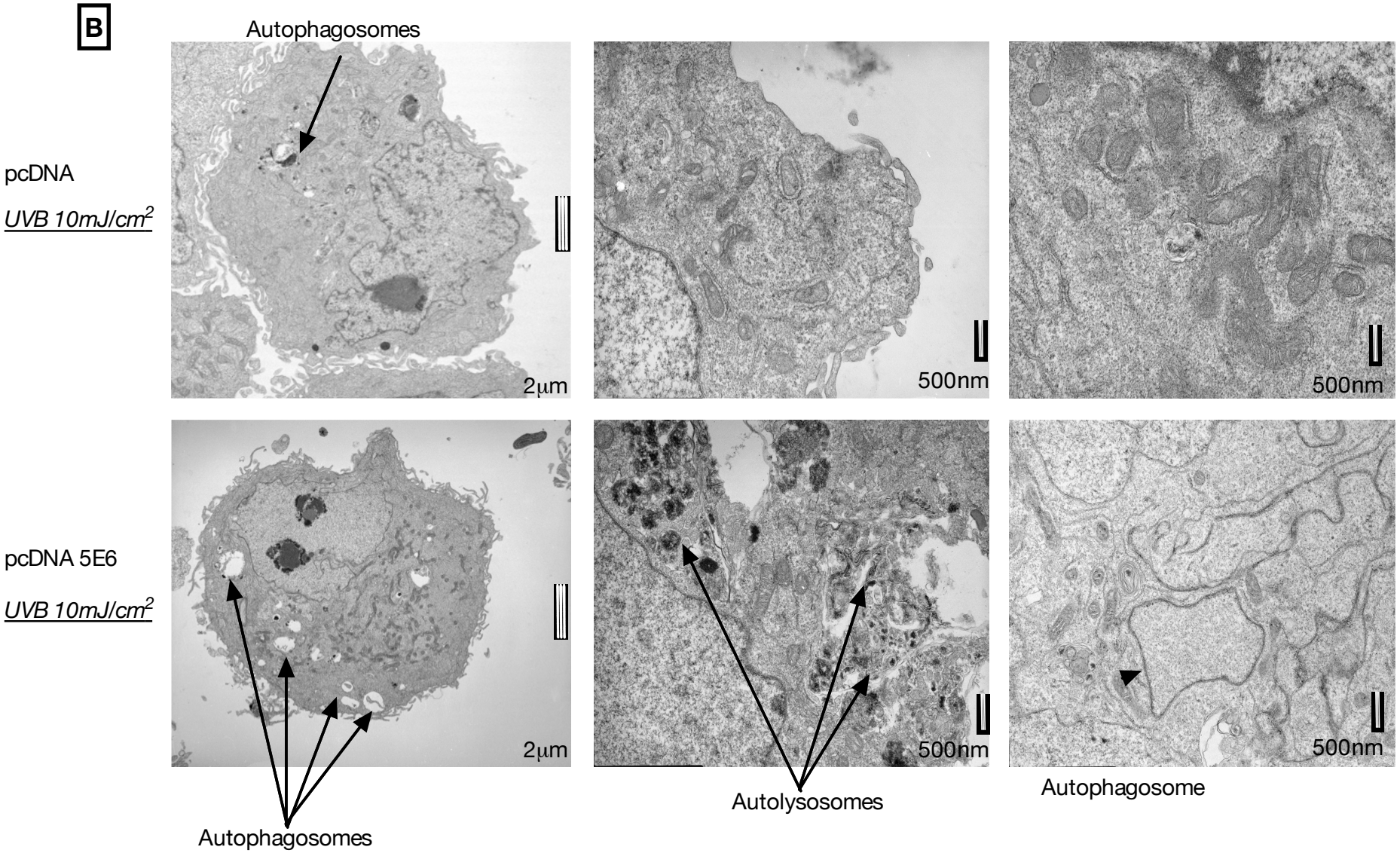
B
Autophagosomes
pcDNA
UVB 10mJ/cm2
2μm
500nm
500nm
pcDNA 5E6
UVB 10mJ/cm2
2μm
500nm
500nm
Autophagosomes
Autolysosomes
Autophagosome

Figure 4-12 Electron micrographs of HT1080 cell lines

HT1080 cells encoding empty vector control or HPV5 E6 were seeded in 100mm dishes. Twenty-four hours later, cells were irradiated with UVB 10mJ/$cm^{2.}$ Cells were then harvested after 8 hours and sent to the EM unit for processing. A) Representative images for untreated (UNT) pcDNA and pcDNA 5E6 showing normal cellular morphology. B) Images of pcDNA and pcDNA 5E6 after 8 hours of UVB. Arrows show examples of autophagosomes and autolysosomes (vacuoles with electron dense granules). Arrowhead showing a classical autophagosomes structure with bulk cytoplasmic material.

4.3.5 Effects of E6 on cellular metabolism

Research suggests that autophagy can support cancer cell metabolism by providing the building blocks that are required for macromolecule synthesis and therefore enhance cell survival in the tumour microenvironment which is low in nutrients (Rabinowitz & White 2010). A recent study demonstrated that HPV16 E6 contributes to the glycolytic shift involving HIF1-α (Y. Guo et al. 2014). The observed increase in mitochondrial content after UVB in Figure 4-11 may suggest an increase in energy demand. It can therefore be postulated that E6 expression might cause a change in cellular metabolism and therefore autophagy is induced to support the increase in energy demand.

To assess metabolic status of E6 expressing cells, glycolysis rates were analysed using the Seahorse™ Bioenergetics analyser. The Seahorse analyser allows for real time measurements of glycolysis by using solid-state sensor probes that are placed in the media 200 microns above the cell monolayer.

Glycolysis rates were measured using the XF Glycolysis stress test kit. During glycolysis cells produce lactate and which leads to the acidification of the surrounding media, this assay measures glycolytic rates by directly measuring the extracellular acidification rate (ECAR). HT1080 cell lines transfected with pcDNA or pcDNA-5E6 were seeded in 60mm dishes. Twenty-four hours later, cells were irradiated with UVB of 10mJ/cm^2 and left to recover for 2 hours. Cells were then lifted and re-seeded in Seahorse 96 well plates and left to attach for 2 hours. The culture media was then aspirated and replaced with Seahorse custom media without glucose and the basal non-glycolytic ECAR was measured by the XF Seahorse analyser. Using special injection ports, a series of 3 injections adds drugs to the media to measure different glycolytic parameters. First, 10mM of glucose is

added to the cells and the rate of glycolysis under basal conditions is measured. Second, Oligomycin, an ATP synthase inhibitor is added to inhibit mitochondrial driven ATP synthesis thus shifting energy production to glycolysis, and this allows for the measurement of the maximum glycolytic capacity of the cells. Finally, glycolysis is inhibited by the addition of the glucose analogue 2-DG, this leads to a drop in ECAR, confirming that ECAR rates measured reflect glycolysis. The difference between the maximum glycolytic capacity and the glycolytic rate is defined as the glycolytic reserve.

Results in Figure 4-13 revealed that E6 expression increased glycolysis in cells even without UVB stress. However, these rates were decreased after UVB in both empty vector control and E6 expressing cells (Figure 4-13B, top left graph). Moreover, E6 expressing cells showed higher levels of glycolytic capacity under no treatment conditions, UVB irradiation resulted in a decrease in glycolytic capacity in both control cells and E6 expressing cells (Figure 4-13B, top right graph). Additionally, there was no change observed in the glycolytic reserve before and after UVB in E6 expressing cells. However, control cells showed a small decrease in glycolytic reserve after UVB (Figure 4-13B, bottom left graph). These results suggest that E6 expression in cells increases glycolysis, however this rate was decreased after UVB.

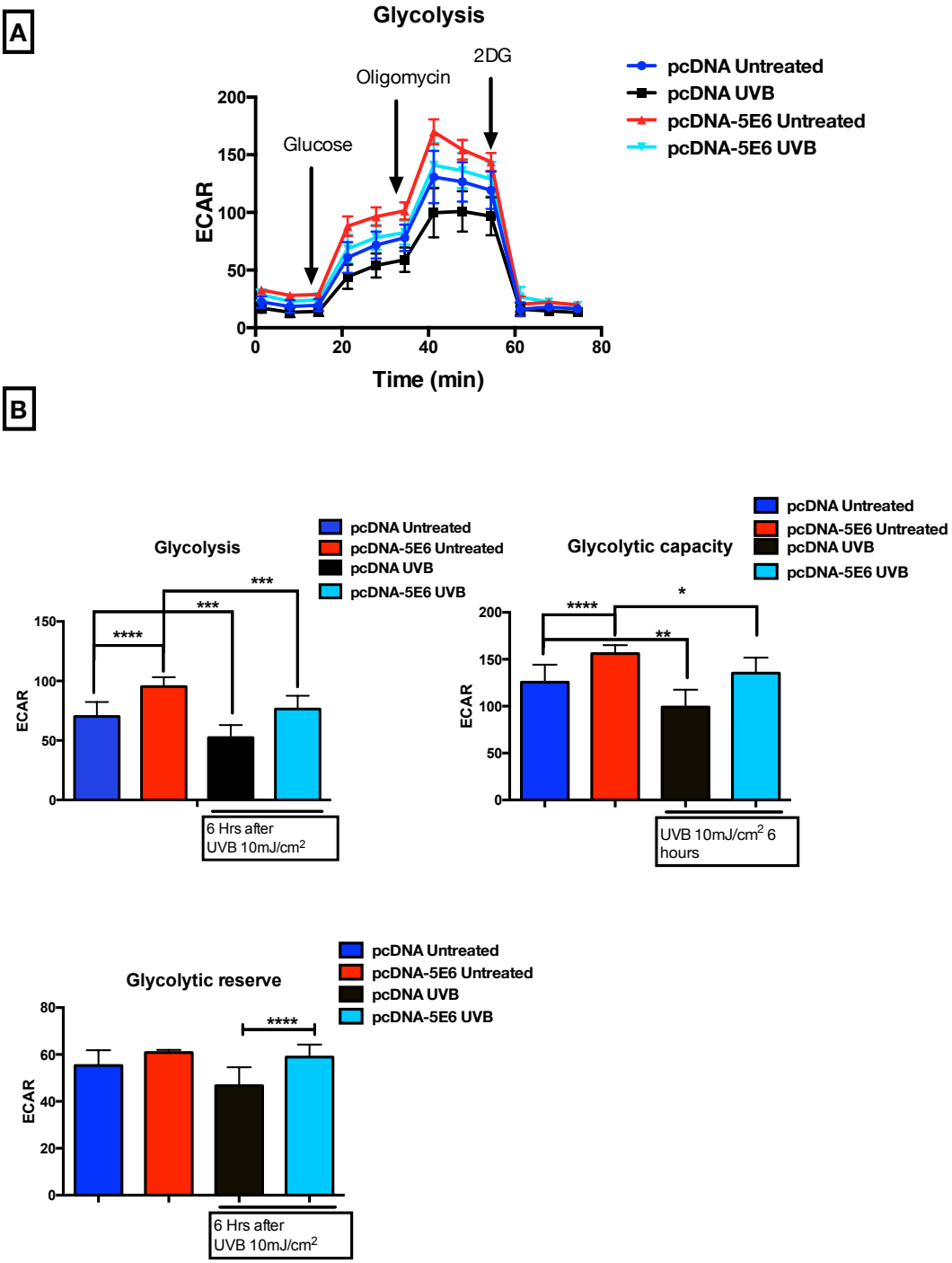

Figure 4-13 Effects of E6 on glycolysis

HT1080 cells expressing pcDNA or pcDNA-5E6 were UVB irradiated in 60mm dishes and then lifted and re-seeded on to Seahorse 96 well plate. The Glycolysis stress test kit was performed by the sequential addition of: glucose 10mM, Oligomycin, and 2-DG. ECAR was measured after 6 hours of UVB. **A)** ECAR levels over time as measured by the Seahorse analyser. **B)** Glycolytic parameters: Glycolysis levels (top left), maximal glycolytic capacity (top right) and glycolytic reserve (bottom left). Statistical analyses was performed using One-way ANOVA, S.E.M ± * $p<0.05$, ** $p<0.01$, and **** $p<0.0001$, n=3.

The observation that E6 expression leads to an increase in glycolysis raised the question as to whether this increase is accompanied by an increase in glucose uptake. The transport of glucose across the cellular membrane is facilitated by a family of proteins known as glucose transporters (GLUT). In humans there are 14 GLUT proteins (GLUTs 1-14 and HMIT) (Mueckler & Thorens 2013). Here, GLUT1 levels were measured and a glucose uptake assay was performed to assess the effect of E6 on glucose uptake.

HT1080 cells transfected with pcDNA or pcDNA-5E6 were seeded and 24 hours later, cells were irradiated with 10mJ/cm^2 UVB and collected after 8 hours. Cells were then incubated in media containing the fluorescent analogue of glucose, 2-NBDG for one hour. Cells were then washed and levels of 2-NBDG were analysed using flowcytometry (Figure 4-14A). For GLUT1 levels, HT1080 cells transfected with pcDNA or pcDNA-5E6 were seeded and 24 hours later, the cells were irradiated with UVB 10mJ/cm2. After 8 hours, the cell culture media was aspirated and the cells were stained for GLUT1 using the Human GLUT1 PerCP conjugated antibody. Cells were then washed and levels analysed by flowcytometry (Figure 4-14B).

The data revealed that E6 expression in HT1080 cells resulted in an increase in glucose uptake under no treatment conditions. However, glucose uptake is decreased after UVB in E6 expressing cells as well as empty vector control. This is in line with glycolysis rates measured by Seahorse Bioenergetics. Interestingly however, this increase in glucose uptake was not accompanied by an increase in GLUT1 (Figure 4-14B).

Taken together these results indicated that under no stress conditions, E6 expressing cells shift energy production to glycolysis and that UVB decreases the glycolytic rates of the cells.

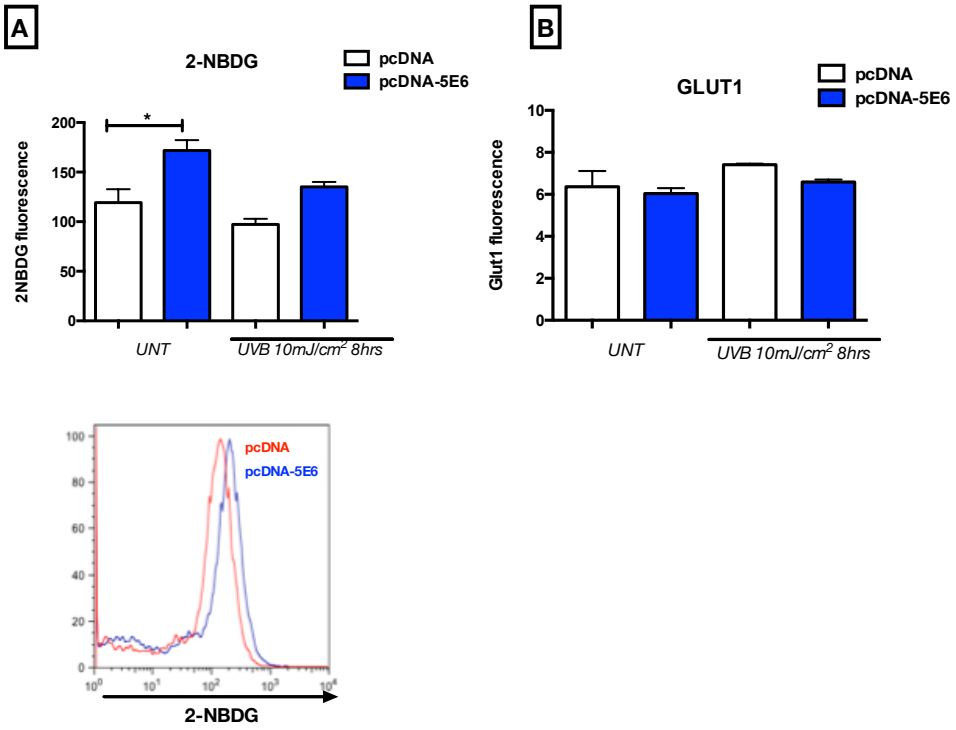

Figure 4-14 Glucose uptake and GLUT1 levels in E6 expressing cells

A) HT1080 cell lines expressing pcDNA-5E6 or pcDNA were irradiated with 10mJ/cm^2 UVB and incubated with 2-NDBG 8 hours later. Statistical analysis was performed using one-way ANOVA. Mean S.E.M ± * $p<0.05$ n=3

The increase in glycolysis observed suggest that E6 expressing cells might exhibit a Warburg effect and have decreased oxidative phosphorylation, this shift in metabolism is one of the hallmarks of cancer cells. It was therefore important to assess mitochondrial respiration status in E6 expressing cells. This was measured using the Seahorse Bioenergetics MitoStress test kit. This assay allows for the real-time measurement of oxygen consumption rates (OCR) using solid-state probes (as previously described in the glycolysis assay). In this assay basal respiration levels are measured first then the cells are metabolically challenged by sequential injection of drugs into the media. The first injection is Oligomycin, which prevents ATP synthesis, OCR levels after this injection allows for the distinction between ATP-linked respiration and proton leak. Second, the mitochondria are uncoupled by injecting Carbonyl cyanide-p- trifluoromethoxyphenylhydrazone (FCCP), this

allows for the measurement of maximal respiration. Additionally, the difference between basal respiration levels and maximal respiration can be used as indicative of cells spare capacity, or the ability to respond to high energy demands. The third injection is of Antimycin A and Rotenone, this leads to a shut down in mitochondrial respiration and thus allowing for the measurement of non-mitochondrial OCR or proton leak. HT1080 cells expressing pcDNA or pcDNA-5E6 were seeded and transferred to Seahorse 96 well plate as previously described for the Glycolysis Stress test. The culture media was replaced with Seahorse custom media supplemented with 5mM glucose and 1mM pyruvate. Surprisingly, the results demonstrate that E6 expression leads to a large increase in basal respiration rates (Figure 4-15A), these basal rates decrease after UVB in E6 expressing cells as well as the controls (Figure 4-15B, top left). This is inline with the observation that glycolysis levels decrease after UVB. Moreover, uncoupling the mitochondria using FCCP revealed that E6 expressing cells have a maximal respiratory capacity comparable to that of the empty vector control. UVB exposure resulted in a decrease in the maximal respiratory capacity in E6 expressing cells (Figure 4-15B, top right). Additionally, E6 cells show high ATP production under no stress conditions; those levels were also decreased after UVB (Figure 4-15B, second row left). Interestingly a negative spare respiratory capacity is demonstrated in both cell lines, more so in E6 expressing cells (Figure 4-15B, second row left). Suggesting that the high demand of energy in E6 expressing cells cannot be sustained for a long duration. Results also show high proton leak in E6 expressing cells, Inline with the observed increase in glycolytic rates in E6 cells under no stress conditions.

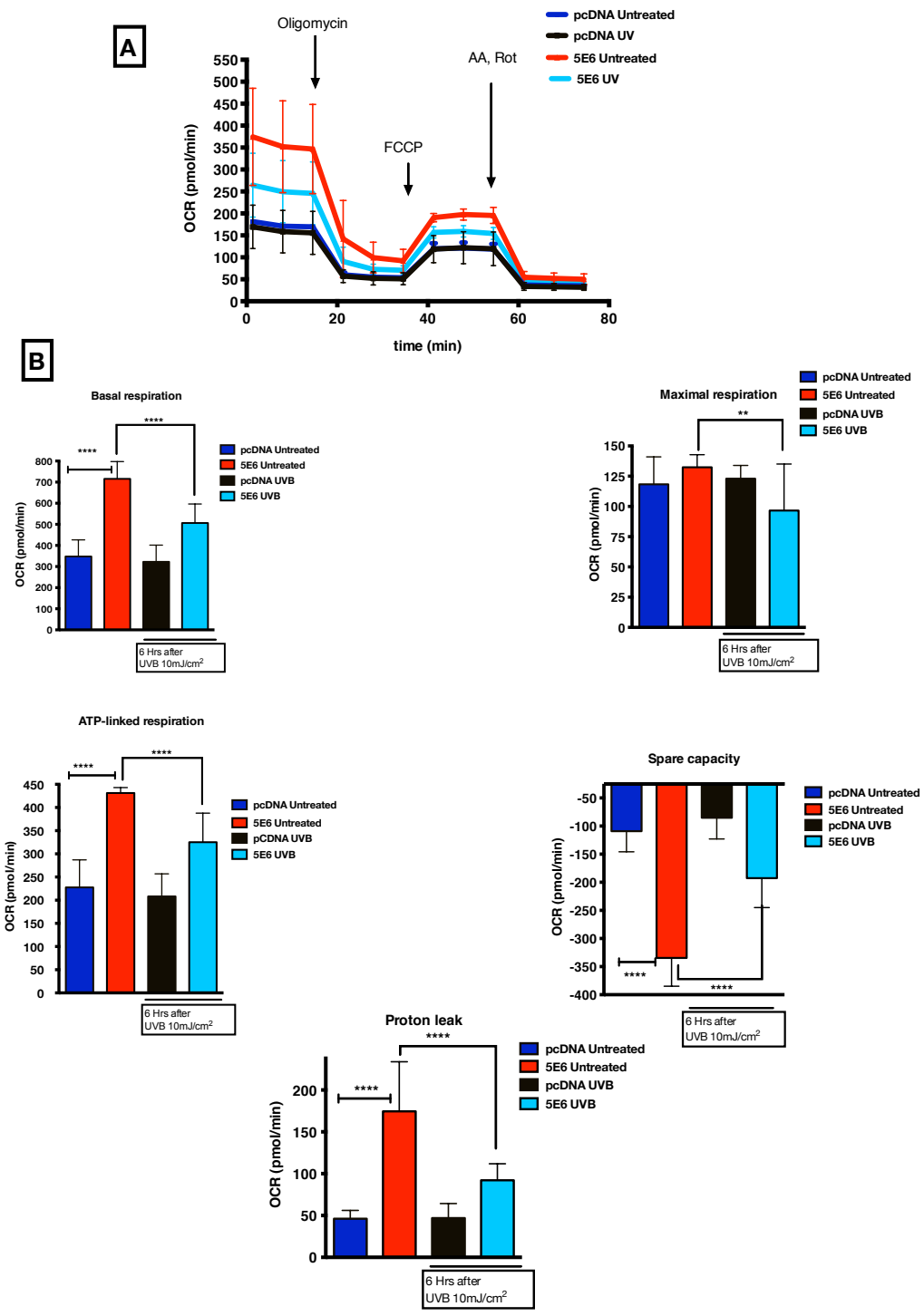

Figure 4-15Mitochondrial respiration status in E6 expressing cells

HT1080 cells transfected with pcDNA or pcDNA 5E6 were seeded onto 60mm dishes and 24 hours later cells were irradiated with 10mJ/cm^2 UVB. Cells were then moved to Seahorse 96 well plate and MitoStress test was performed by the addition of: Oligomycin, FCCP, Antimycin A and rotenone. **A)** Oxygen consumption rates over time (OCR). **B)** Mitochondrial parameters calculated from OCR. Basal respiration (top left), maximal respiration (top right), ATP production (second row left), spare capacity (bottom centre) and proton leak (second row right). Statistical analysis was performed using one-way ANOVA. Mean S.E.M. * p<0.05, ** p<0.01, and ****p<0.0001, n=3.

These results indicate that E6 expression leads to a surge in cellular energy production driven by both glycolysis and mitochondrial respiration. However since the cells cannot sustain such a high energy demand, it is likely that the cells will go through an energy crisis, this could explain the toxicity of high E6 expression on cells over a long period of time. Additionally, it is observed that UVB resulted in a decrease in energy production in both control and E6 expressing cells, suggesting that cells might be moving towards a quiescence or senescence.

4.4 Discussion

Autophagy is mainly described as a cell survival and adaptation pathway that is upregulated in response to different cellular stresses. The role of autophagy in cell survival is has been widely studied in cancer, where autophagy promotes cancer cell survival in hypoxia and nutrient stress (Mathew et al. 2007). Findings showed that autophagy increased cell survival and delayed apoptosis in the breast cancer cell line MCF-7 in response to the DNA damaging agent camptothecin (Abedin et al. 2007). The aim of this chapter was to elucidate the role of autophagy in HPV5 E6 expressing cells after UVB. Interestingly, the data showed that in HPV5 E6 expressing cells, shRNA mediated knockdown of ULK1 resulted in decreased viability and increased apoptosis following UVB damage. Additionally, inhibition of the autophagic pathway at the later stages using Bafilomycin A1, led to a similar decrease in viability and a slight increase in apoptosis after UVB irradiation. It is well established that the evasion of apoptosis is one of the hallmarks of cancer (Hanahan & Weinberg, 2011). Furthermore, studies have showed that deficiency in BAK/BAX blocks apoptosis and promotes tumourigenesis (Degenhardt et al. 2002). E6 is a well-established oncogene and one of the major roles of E6 is the abrogation of stress induced apoptosis. The results obtained thus far suggests that HPV5 E6 expressing cells depend on autophagy to promote cell survival after

DNA damage, whilst at the same time inhibiting apoptosis and this may contribute to tumour development as a consequence of genomic stress.

Autophagy is mainly considered as a cell survival pathway, however a few studies suggest that autophagy is a cell death mechanism known as autophagic cell death (ACD). ACD, is characterised by excessive autophagic flux and sequestration of large portions of the cytoplasm by the autophagosomes, thus leading to cellular demise (Denton et al. 2012) . The evidence supporting ACD in mammals is scarce. In a recent study the knockdown of ATG5 was shown to protect mice from an other wise lethal infection by H5N1 influenza virus, suggesting a role for autophagy in H5N1 lethality (Sun et al. 2012). However, most evidence suggests that autophagy is manifested in cells undergoing programmed cell death (Kroemer & Levine 2008), rather than being a mechanism of cell death. Therefore it is unlikely, that autophagy leads to cell death in E6 expressing cells after UVB.

The inhibition of UVB triggered apoptosis by E6 is well described. Therefore the increase in the number of apoptotic cells in E6 expressing cells after UVB raised a question about the interplay between different cell death modalities in the cells. As discussed in 3.1.2, autophagy is a part of the integrated stress cellular response, and a crosstalk exists between autophagy and apoptosis (Mariño et al. 2014). Autophagy was also demonstrated to converge necrosis, a recent study showed that in immortalized baby mouse kidney epithelial cells (iBMK) that are BAK/BAX knockout, autophagy inhibition leads to cell death via necroptosis (J. Y. Guo et al. 2011). Necroptosis is an alternative cell death mechanism mediated by TNF, Fas ligand and toll like receptors (Giampietri et al. 2014). During necroptosis, cells are characterised by loss of cell membrane permeability, swelling, cell lysis and DNA fragmentation (Giampietri et al. 2014). A recent paper described a method to distinguish apoptosis from necrosis using time-lapse microscopy of annexin V and PI (Wållberg et al. 2013). Using this technique, it was observed that autophagy

inhibition using Bafilomycin A1 in HPV5 E6 cells resulted in an increase in the number of necrotic cells after UVB. This technique however, is not conclusive for the characterisation of necroptotic cell death; studies such as investigation of RIP1 kinase levels can lend further evidence to these results.

More convincing evidence was obtained upon electron microscopy examination. The inhibition of autophagy in E6 expressing cells following UVB damage resulted in marked abnormalities with features such as loss of nuclei and the rupture of cellular membrane. The morphological characteristics of the cell death process observed do not conform to typical necrosis. Other cell death pathways may be involved, such as pyroptosis. Pyropotosis is a cell death pathway that is stimulated by a range of microbial infections and non-infectious stimuli, such as host factors released in myocardial infarction. This pathway is characterised by the release of pro-inflammatory intracellular contents (Lamkanfi 2011). Further work is required to identify the mechanism of cell death. If the undergoing cell death mechanism, can provoke an immune response, then perhaps autophagy inhibition can be utilized to expose HPV infected cells.

Interestingly, TEM examination of PM1 HPV5 E6 expressing cells under no stress conditions cells showed an altered cellular morphology, in particular abnormal chromatin distribution. E6 has been found to localize to the cytoplasm and the nucleus, and it was demonstrated that E6 has the ability to affect gene transcription by interacting with cellular transcription complexes. E6 from both low and high risk mucosal HPVs are able to interact with the TIP60 acetyltransferase resulting in the destabilization of p53 complexes and affecting the regulation of p53 responsive genes (Jha et al. 2010). However, little is known about the effects of β-HPV E6 on cellular transcription. Based on the observation of chromatin re-distribution in the nuclei of E6 expressing cells it can be postulated that E6 from cutaneous HPV

types can modulate transcription. In this case, ChiP-Seq analysis could yield valuable information about the targets of E6 in that can regulate gene transcription.

The mechanism by which autophagy leads to cell survival in stress condition, is not clearly defined. Mitochondria play a major role in cellular metabolism redox control and serve as a hub for the regulation of cell death (Narendra 2011). Therefore mitochondrial quality control by autophagy might impinge on cell survival. For example in melanoma, an increase in mitophagy is observed in aggressive tumours (Maes & Agostinis 2014). It was postulated here that the observed increase in autophagy in HPV5 E6 expressing cells might be the result of increase in mitophagy due to mitochondrial damage by UVB. The results showed low levels of ROS after UVB in both empty vector and HPV5 E6 expressing cells.

Additionally, there was no co-localisation between the autophagosomal marker LC3 and the mitochondria. EM examination showed the autophagosomes as double membrane vesicles with bulk cytoplasmic material and intact mitochondria after UVB in both E6 expressing cells and the empty vector control. However, this was performed on HT1080 cell lines and needs to be confirmed in PM1 keratinocytes. These data imply that the mitochondria might not be targeted for elimination by autophagy after UVB Damage.

As a catabolic process, autophagy provides building blocks for the synthesis of macromolecules required during nutrient stress. Evaluating the respiratory status in HPV E6 expressing HT1080 cell lines showed an increase in glycolysis in E6 expressing under nutrient rich and no stress conditions. The increase in glycolysis was supplemented by an increase in glucose uptake, but surprisingly not an increase in GLUT1. Studies described an increase in glucose uptake and glycolysis in cervical cancer; a recent study described that HPV18 E6 enhances the expression of secondarily active Na^+, glucose co-transporter SGLT1 (Leiprecht et al. 2011). However, little is known about the effect of E6 the beta HPV types on

glycolysis, results presented here suggest an increase in the glycolytic rates in HPV5 E6 expressing cells, indicating that the modulation of cellular metabolism by E6 is conserved amongst alpha and beta HPV types. Interestingly, this increase in glycolysis was accompanied by an increase in oxidative phosphorylation, suggesting high-energy demand by E6. Published work on HPV16 E6 revealed that E6 affects PDK1 and mTORC2 to activate Akt, causing subsequent activation of the mTORC1 pathway to increase protein synthesis (Münger 2010). In this context, an induction of autophagy supports protein synthesis by degrading macromolecules and providing building blocks. It may be that increasing energy metabolism could enhance HPV replication since HPVs replicate in terminally differentiated cells that are likely to have a low nutrient supply (Vande Pol & Klingelhutz 2013).

More studies are required to assess the ratio of glycolysis to oxidative phosphorylation to determine which energy-producing pathway is utilized by E6 expressing cells. It is worth to mention that the metabolic profile obtained here was in HT1080 cell lines, a cancer cell line that might be glycolytic in nature, therefore these findings need to be confirmed in epithelial non-transformed cells. However, it can be inferred that the expression of E6 leads to a surge in energy production through oxidative phosphorylation and glycolysis. Recent work from the lab demonstrated that in human keratinocytes E6 can modulate the integrin pathway leading to increased cellular migration (Holloway & Storey 2014), a process that is known to be dependent on high glycolytic rates (Beckner et al. 1990).

UVB irradiation resulted in decreased glycolysis and oxidative phosphorylation rates in both HPV5 E6 and empty vector control cells. This observation could suggest either that cells are either moving towards a quiescent state or a less metabolically active or that the decrease in oxidative phosphorylation and glycolysis is coupled by increase in fatty acid oxidation. In this scenario an

increased autophagy might serve to release lipids from lipid droplets to support the energy requirements of the cell. Interestingly, on this note, infection with DENV has been shown to increase lipid metabolism and leads to the release of triglycerides from lipid droplets in an autophagy dependent manner (Heaton & Randall 2010). Microarray analysis of primary human keratinocytes expressing pLXSN-5E6 revealed an upregulation of diacylglycerol O-acyltransferase homolog 2 (ACSL1), which is essential for fatty acid oxidation (Soupene & Kuypers 2008).

Overall, the results presented in this chapter suggest that cells expressing HPV E6 are dependent on autophagy to survive after UVB DNA damage and inhibition of autophagy in cells expressing E6 resulted in a marked decrease in cell viability. This decrease in cell viability might be harnessed to probe the role of autophagy in E6 transgenic mouse models.

Chapter 5 Discussion and further data

5.1 General discussion

NMSC is the most common cancer in the fair-skinned population, with more than 100,000 cases in the UK alone. It is a major burden on the health care system. Although the risk of the development of NMSC depends on various factors such as environmental factors, genetic predisposition and HPV infection, the main etiological agent is DNA damage resulting from prolonged exposure to ultraviolet light. This is evidenced by the development of NMSC in sun-exposed body sites and the increased incidence of NMSC in countries with higher UV indices.

The association between a subset of cutaneous HPVs and the development of SCC, in combination with UV, is supported by several lines of evidence, including the cases of *Epidermodysplasia verruciformis* and immunosuppressed transplant patients, epidemiological studies, and investigations into viral activities. However, the mechanisms of viral tumourigenesis have not been fully described, in contrast to the well-characterised association between cervical cancer and high-risk mucosal HPVs.

E6 is a known potent oncoprotein that can impinge on many of the defined hallmarks of cancer, such as inhibition of apoptosis and prevention of differentiation, both of which may contribute to the promotion of NMSC alongside UV. The work presented in this thesis aims to further the understanding of the effects of E6 on the cell after UV DNA damage. This may shed the light on the oncogenic transformation by E6.

The results obtained showed for the first time that the expression of β-HPV5 E6 oncoprotein increases autophagy levels and autophagic flux following UVB damage in two different cell line models, PM1 and HT1080. This increase in autophagy was

paralleled by a decrease in apoptotic markers. In early studies, HPV types 5 and 8 were identified in 90% of squamous cell carcinomas (SCC) from EV individuals. Additionally, infection with HPV types 5 and 8 increased the risk of carcinoma development (Orth, 1986; Pfister, 2003; Pfister & Ter Schegget, 1997). Moreover, the functions of E6 from HPV types 5 and 8 are conserved such as the abrogation of UV triggered apoptosis and the secretion of IL-8 (Akgül et al. 2009). Investigating the levels of autophagy after UV irradiation in HPV8 E6 expressing keratinocytes revealed an increase in autophagy and autophagic flux, similar to that seen in HPV5 E6 expressing cells.

Other high-risk β-HPV types that were identified in SCC of the skin, such as HPV20 and 38, also showed an increase in autophagy levels following UV DNA damage. However, keratinocytes expressing E6 from low-risk HPV types such as HPV1 and 4 displayed a decrease in autophagy levels after UV damage. These results indicate that the increased level of autophagy after UV is characteristic of the high-risk β-HPV types, and that autophagy might contribute to tumour development.

Although E6 proteins from different HPV types have different cellular targets, some targets are similar, one example being BAK. E6 from different types of α- and β-HPVs is able to specifically target activated BAK for proteolysis after DNA damage. Here, the modulation of autophagy was demonstrated to also be a conserved function amongst E6 from high-risk β- and α-HPV, underscoring the significance of autophagy induction to tolerate genomic stress after UV. The induction of autophagy by mucosal high-risk HPV types also suggests that the undergoing autophagy process is independent of p53.

HPV E7 oncoprotein is known to play a critical role in cervical cancer, however little is known on the cellular targets of the cutaneous HPV E7 protein. A recent study

showed that growth factor deprivation in HPV16 E7 expressing keratinocytes triggered an autophagy-related process. In this thesis however, examining levels of autophagy in HPV5 E7 expressing cells revealed low autophagy after UVB, suggesting that the increase in autophagy is a unique feature of E6 and further confirming the difference of behaviors of high-risk β- and α-HPVs.

E6 from various HPV types targets the pro-apoptotic protein BAK for degradation following UV DNA damage. Given the cross talk between autophagy and apoptosis, the increase in autophagy observed was postulated to be a consequence of BAK degradation. However, examining a series of HPV5 E6 mutants that have lost the ability to degrade BAK after UV implied that the induction of autophagy by HPV E6 and the degradation of BAK are mediated by distinct regions of the E6 protein.

The increase in autophagy after UV damage in cells expressing E6 from high-risk HPVs is interesting, given that increased autophagy levels are currently under investigation for cancer therapy. Increased LC3 levels are observed in a number of epithelial cancers including colon, pancreatic and gastrointestinal (S. Yang et al. 2011). Additionally, high autophagy levels in melanoma are correlated with poor prognosis. In these cancers, autophagy acts as a cell survival and stress adaptation pathway.

Here, interestingly, the inhibition of autophagy by an shRNA mediated knockdown of ULK1, a key regulator of autophagy, resulted in a marked increase in cell death and a decrease in cell viability of cells expressing HPV5 E6. Moreover, inhibiting the completion of the autophagic pathway by Bafilomycin A1 also resulted in a significant increase of cell death in cells expressing E6 from HPV types 5 and 8, indicating that HPV E6 expressing cells utilise autophagy to survive during genomic stress. Cell survival mediated by autophagy is exemplified in a study showing that autophagy increased cell survival and delayed apoptosis in the breast cancer cell

line MCF-7 in response to the DNA damaging agent camptothecin (Abedin et al. 2007).

As described in 1.1.2, all of the early proteins encoded by HPV act to facilitate the life cycle of the virus. It can be postulated that; during the HPV's life cycle the modulation of autophagy by E6 may be essential to maintain the cells to produce viral progeny after DNA damage.

Interrogating the cell death mechanism revealed that the majority of E6 expressing cells die via a cell death modality that morphologically was not consistent with neither apoptosis nor necroptosis. Still, the mechanism of cell death following autophagy inhibition remains unexplained. Further studies are required to identify the mechanism of cell death such as: 1) inhibition of necroptosis using necroststin1, 2) RIPK immunoblots 3) pro-caspase 1 and IL1- β immunoblots.

After establishing the role of autophagy in the survival of E6 expressing cells following UVB, experiments were initiated to investigate the underlying mechanism of cell survival. Interestingly, the observed increase in autophagy was not a result of damaged mitochondria or accumulation of ROS.
Metabolic profile analysis showed that the expression of E6 drives cellular energy demands by increasing the glycolytic and the oxidative phosphorylation pathway. Surprisingly, UVB irradiation resulted in a decrease in energy demands, suggesting senescence or quiescence. Therefore, cell cycle analysis after UV and β-galactosidase assays are required.

As previously described, the literature is filled with evidence on the association of β-HPV types 5 and 8 with the development of NMSC, in particular SCC in both the

immunocompromised and the immunocompetent individuals (Pfister, 2003; Quint et al. 2015).

Currently, removal of NMSC by surgery is usually the most successful course of action, and in a large number of cases, this is usually sufficient. If surgery is unsuitable or results in incomplete removal, radiotherapy is used. Chemotherapy, photodynamic therapy or immunotherapy may also be used. Treatment of SCC is often successful and results in low mortality. However NMSC has a high morbidity owing to invasion of surrounding tissue and damage from treatment. Lastly, treatment of SCC is a large burden on healthcare resources – the cost of care for NMSC in America is the 5th highest for all cancers (Housman et al. 2003, Nguyen and Ho, 2002). In England it is estimated that each case of NMSC costs the National Health Service approximately £1,000 (Morris et al. 2009, Vallejo-Torres et al. 2011). Thus there is a need for better and more cost-effective treatment for NMSC.

The results presented in this thesis identify autophagy as a novel pathway targeted by the oncoprotein HPV E6 after DNA damage. Since autophagy inhibitors are being investigated for cancer therapy, we can harness the modulation of autophagy by HPV E6 in treatment of NMSC and other HPV-driven tumours. To investigate the potential use of autophagy in the treatment of HPV-driven tumours, preliminary *in vivo* work was conducted and is presented in the following section.

5.2 Investigating the role of autophagy in HPV driven tumours

The carcinogenic potential of HPV8 was demonstrated in a transgenic mouse model expressing the complete early region (CER). It was observed that 91% of HPV8 CER transgenic mice developed sporadic papillomas within 90 days without

being exposed to chemical or physiological stress and 25% of the papillomas displayed dysplastic features ranging from moderate to severe. Additionally, 6% of the developed tumours progressed to SCC of the skin (Schaper et al. 2005). Moreover, exposure to UV and wounding accelerated papilloma formation in HPV8 transgenic mice to three weeks after damage (Marcuzzi et al. 2009). Furthermore, after UV irradiation of HPV8 transgenic mice, the mRNA levels of HPV8 E6 increased after one day and reached their highest levels by 4 days. Moreover, siRNA-mediated knockdown of HPV8 E6 resulted in delayed papilloma formation and decreased the incidence of papilloma development (Hufbauer et al. 2010). Additionally, vaccination against HPV8 E6 in HPV8 transgenic mice protected the mice from papilloma development in about 40% of the cases (Marcuzzi et al. 2014). Interestingly, the same group also showed that HPV8 E6 transgenic mice showed a similar phenotype to HPV8 CER mice displaying papilloma formation and SCC development after UV (Marcuzzi et al. 2009).

As a cellular degradation and homeostasis pathway, defects in the autophagy pathway are implicated in many pathological conditions. Recently, the role of autophagy in cancer development and prevention has been the focus of many studies.

High autophagy levels in HPV8 E6 expressing cells and the dependence on autophagy to survive after UVB led to the hypothesis that autophagy might play a significant role in promoting cell survival after UVB damage *in vivo* and it may, therefore, facilitate tumour development. This hypothesis was tested in HPV8 E6 transgenic mouse models described in earlier. This work was done in collaboration with Dr. Baki Akgül and Dr. Martin Hufbauer. Please note that the mouse work was performed in the Institute for Virology, Köln, Germany.

HPV8 E6 transgenic mice were generated so that they express the E6 gene under the control of the keratin-14 promoter, which limits expression of this gene to basal keratinocytes (Marcuzzi et al. 2009).

Since the levels of E6 were shown to increase even after one day of UV in mouse models (Hufbauer et al. 2010), it was of interest to assess autophagy levels in skin lysates of those mice. HPV8 E6 mice and FVB WT mice were irradiated over a 4 cm^2 area with UV (10J UVA and 1J UVB/ cm^2). Skin extracts from the UV irradiated area were collected and lysed. Lysates were then separated in SDS-PAGE electrophoresis and immunoprobed for LC3 levels. Figure 5-1 revealed that under no stress condition E6 mice seem to have a higher level of LC3II compared to the wild type mice.

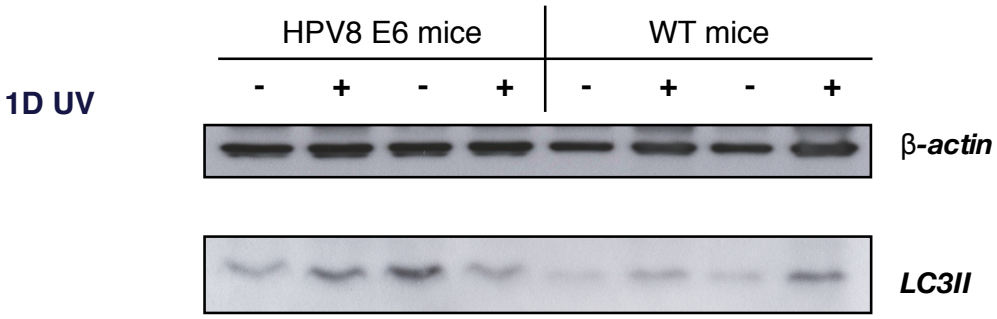

Figure 5-2 Levels of LC3 in UV irradiated HPV8 E6 transgenic mouse skin lysates

A 4 cm^2 dorsal area was irradiated with UV (10J UVA and 1J UVB/ cm^2) in 2 WT mice and 2 HPV8 E6 transgenic mice. Skin extracts were collected after 1 day of UV and lysed and resolved on SDS-PAGE. The membranes were then immunoprobed fore β-actin as a loading control (~42kDa) and LC3II (~16kDa).

In one HPV8 E6 and one WT mice, LC3 levels were increased after 1 day of UV. However, the second HPV8 E6 mouse showed a decrease of LC3 levels, but this decrease might be attributed to high autophagic flux. These results are inconclusive and need to be repeated and complemented by flux analysis.

In vivo, p62 is used to determine autophagic flux in many human and mouse cancer tissues. p62 is a multifunctional protein that is targeted for degradation by

autophagy and therefore p62 levels are inversely proportional to autophagy activity (Moscat & Diaz-Meco, 2012).

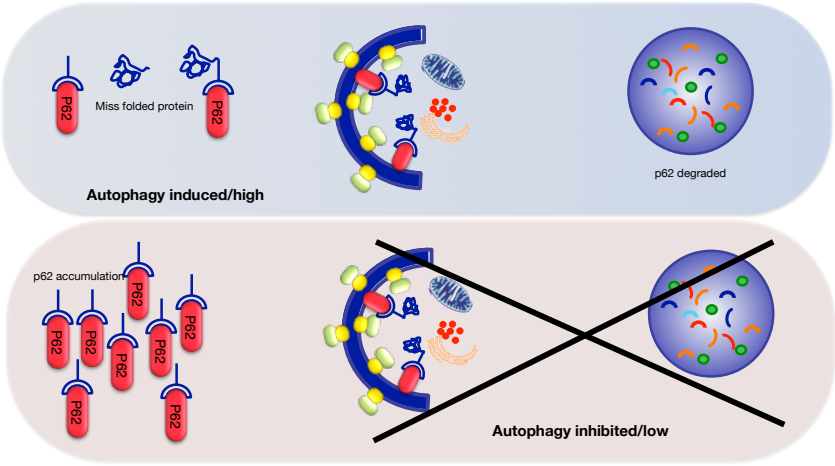

Figure 5-3 p62 in autophagy

Schematic representation of the role of p62 in autophagy. Upon induction of autophagy p62 is recruited to the autophagosome and is degraded. When autophagy is inhibited or autophagy levels are low, p62 is accumulated in the cytoplasm

HPV8 E6 transgenic and WT mice were irradiated with UVA/UVB (10 and 1J/cm^2). After 5 days and 24 days the tumours were collected, embedded and sectioned as described in 2.12. The tissue sections were stained with p62 antibody and to determine autophagy levels and scored by Dr. Ioannis Roxannis (Consultant Pathologist, John Radcliffe Hospital). The staining of p62 was scored from 0-3 (0=negative/weak, 1=moderate, 2=strong, 3=very strong), and the extent of staining or the proportion was scored from 1-4 (1=1-10%, 2= 11-50%, 3= 51-80% and 4=80-100% of cells stained). A final score was obtained by multiplying the score by the proportion. The p62 staining scoring was performed for each cell layer separately. This is because different cells are at different stages of the cell cycle and differentiation and thus may respond differently to UV irradiation.

Figure 5-3A shows p62 scores in different cell layers. In basal cells, WT mice (grey bars) showed slightly higher p62 levels than HPV8 E6 mice (pink bars). Five days after UV, p62 levels decreased in both HPV8 E6 transgenic mice and WT mice, and the levels decreased further after 24 days of UV irradiation. As p62 is degraded by autophagy, the decrease in p62 staining suggests an increase in autophagy levels after UV, in both WT and HPV8 E6 mice. Interestingly, the response was different in the middle cell layer, where basal levels of p62 were slightly elevated in HPV8 E6 transgenic mice, suggesting low autophagy. After 5 days of UV exposure, there was a marked increase in p62 levels in both mice, indicating decreased autophagy levels. Twenty-four days after UV, levels of p62 in WT mice returned to basal levels, and levels in HPV8 E6 transgenic mice were slightly lower than basal levels. This suggests that 5 days after UV exposure, the middle cell layer has decreased autophagy levels and those levels returned to basal after 24 days. The granular cell layer showed increased p62 levels after 5 days of UV exposure in WT mice, similar to the middle cell layer, suggesting decreased autophagy. The granular cell layer of HPV8 E6 transgenic mice showed a decrease in p62 levels after UV, suggesting increased autophagy. Generally, autophagy levels in HPV8 E6 and WT were increased with an increase in cell proliferation and papilloma formation. Examples of p62 staining in mouse skin sections are shown in Figure 5-3 B, C.

A

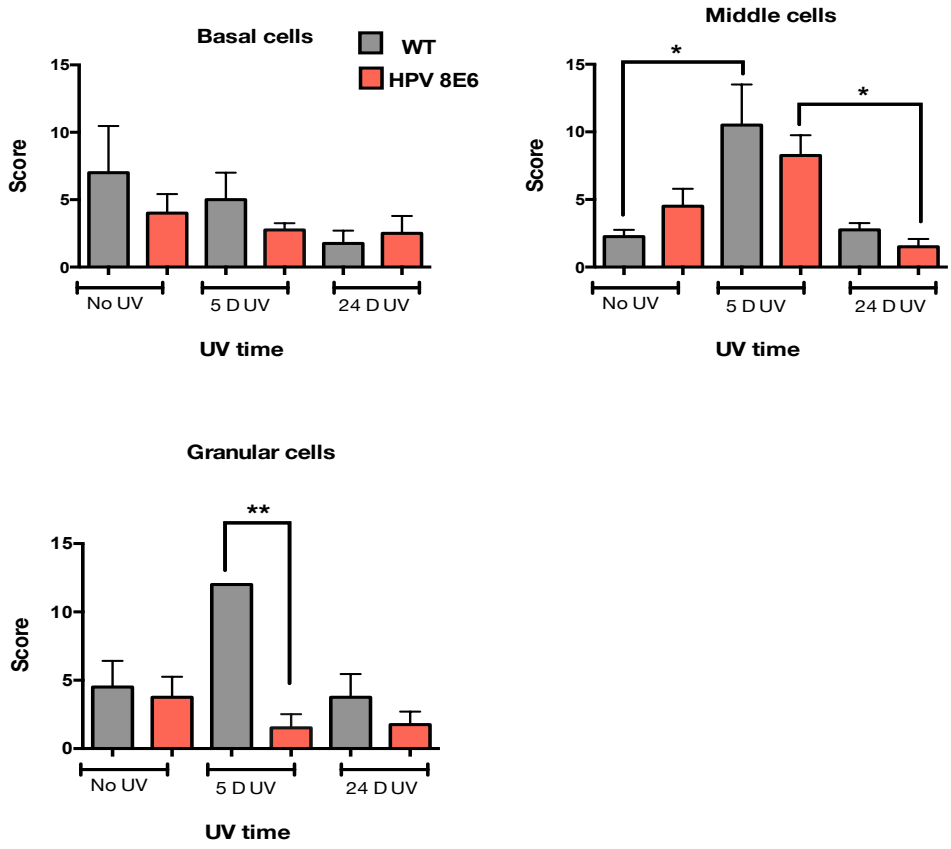

B p62 staining from WT mice

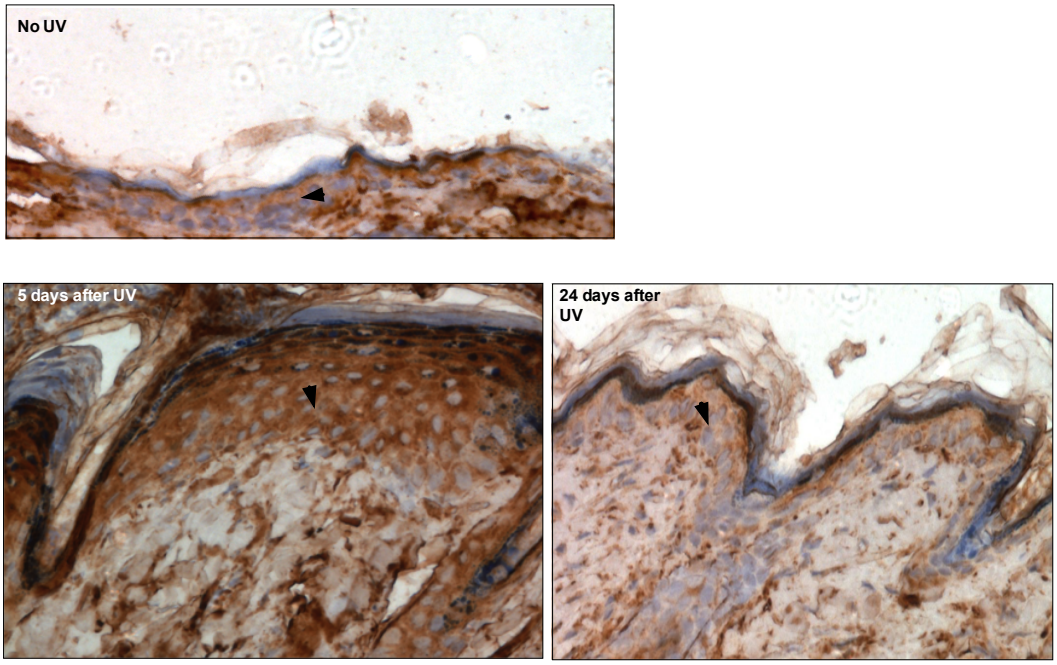

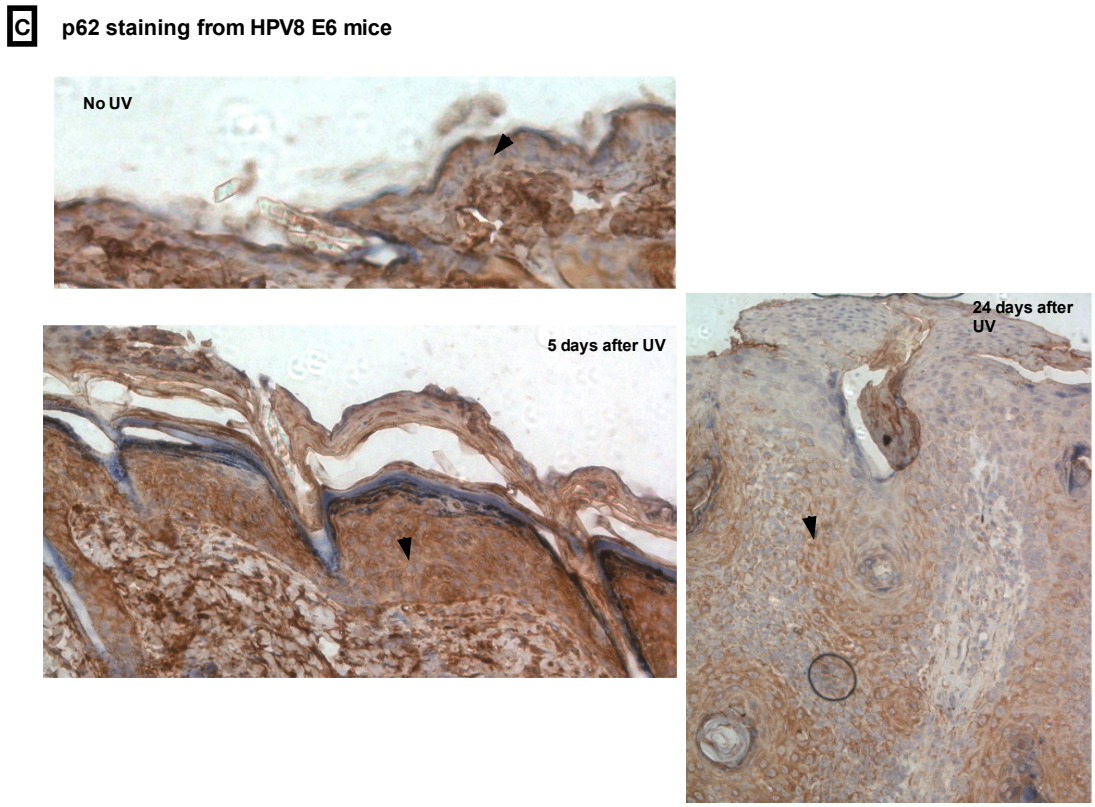

Figure 5-4 p62 staining in WT mice and HPV8E6 transgenic mice

The skin was shaved and the mice were irradiated with 10J UVA and 1J UVB/cm^2.

The tumours were observed for growth and after 5 and 24 days the tumours were harvested imbedded and sectioned. The sections were then stained for p62 and counterstained with haematoxylin to visualise the nuclei. The levels of p62 are inversely proportional to autophagy levels. The staining of p62 was scored from 0-3 (0=negative/ weak, 1=moderate, 2=strong, 3=very strong), and the extent of staining or the proportion was scored from 1-4 (1=1-10%, 2= 11-50%, 3= 51-80% and 4=80-100% of cells stained). **A)** Bar graph showing p62 scores in WT mice and HPV8 E6 transgenic mice, error bars are SEM and n=4 per time point. Statistical analysis was performed using two-way ANOVA and *p<0.1 and **p<0.01. **B)** Examples of p62 staining in WT mice. **C)** Examples of p62 staining HPV8 E6 transgenic mice. Arrows indicate the area of the sections that were scored.

5.2.1 The effect of autophagy inhibition on tumour development in HPV8 E6 transgenic mice

To test the effect of autophagy inhibition on HPV8 E6 mediated tumours, the autophagy inhibitor Chloroquine was used. Chloroquine is an anti-malarial drug that blocks the fusion between the autophagosome and the lysosomes by disrupting the acidification of the lysosomes.

Four HPV8 E6 transgenic mice and four WT mice were pre-treated with Chloroquine for 3 days at a concentration of 40mg/kg/d. The mice were then UV irradiated (10J UVA and 1J UVB/cm^2), and Chloroquine treatment continued until 24 days after UV exposure. The tumour formation was observed and pictures were taken after 24 days. Figure 5-4 A shows gross tumour appearance in Chloroquine treated HPV8 E6 transgenic mice in comparison to WT and no Chloroquine treatment. UV irradiation of WT mice resulted in hyper-proliferation and a wound healing response that regressed and returned to normal after 24 days. Surprisingly, it was observed that in all 4 WT mice, the use of Chloroquine resulted in prolonged hyperplasia and delayed wound-healing persisting after 24 days. As expected, UV irradiation of HPV 8 E6 transgenic mice showed papilloma formation, of which a subset could potentially progress to carcinoma. Chloroquine treatment resulted in tumour regression in 2 mice of the 4 treated HPV8 E6 mice, whereas the other two showed tumours that were more aggressive in comparison to the tumours formed in the HPV8 E6 mice exposed to UV alone. The tumours from these mice were obtained and stained for p62 to evaluate the autophagy levels. Figure 5-4 B shows that Chloroquine decreased autophagy levels *in vivo*, demonstrated by an increase in p62 staining.

A

24 days after UV

	WT	HPV 8E6
-CQ		
+CQ	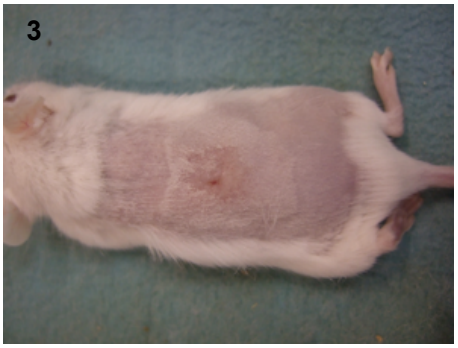	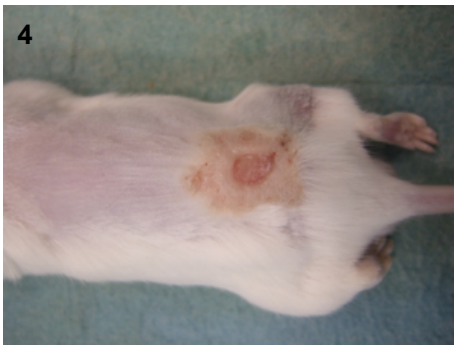
		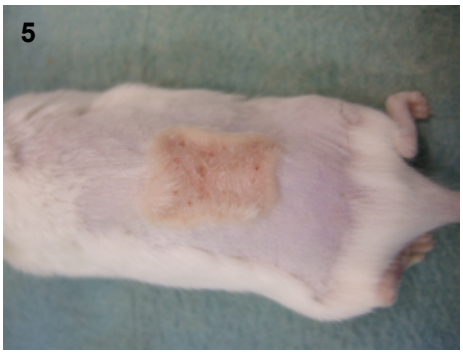

B

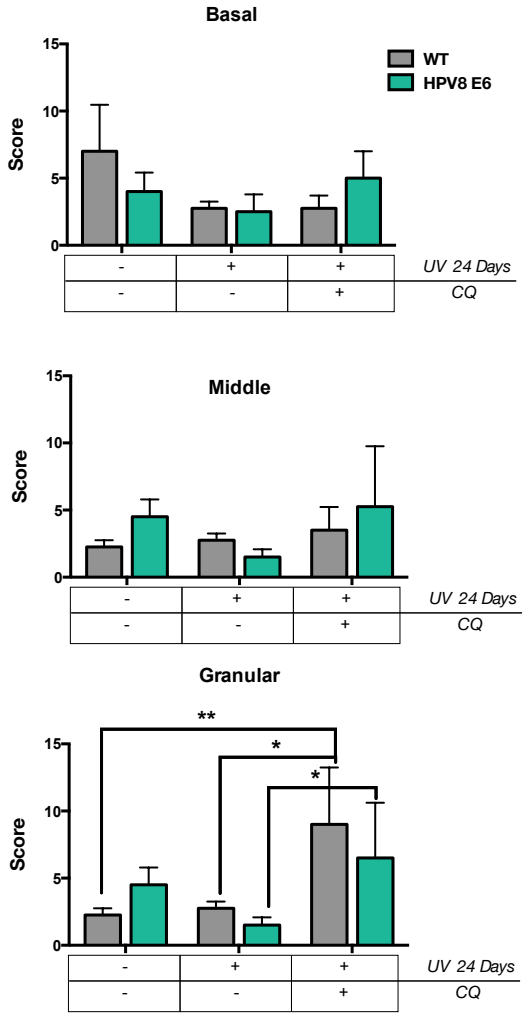

Figure 5-5 Effect of Chloroquine on HPV8 E6 transgenic mice

A) Gross appearance of tumour formation after UV irradiation. CQ= Chloroquine

1) WT mice 24 days after UV exposure. 2) HPV8 E6 mice 24 days after UV exposure. 3) WT mice treated with Chloroquine 24 days after UV irradiation. 4) HPV8 E6 transgenic mice treated with Chloroquine after 24 days of UV, showing a more aggressive tumour. 5) Tumour regression with Chloroquine in HPV8 E6 transgenic mice 24 days after UV irradiation.

B) Bar graph of p62 staining scoring by IHC. n=4 mice per treatment, statistical analysis was performed using two-way ANOVA *p<0.1 and **p<0.01.

5.2.2 The levels of autophagy in SCC

To test if autophagy is upregulated in SCC, patient SCC biopsies that were HPV positive were stained with p62 and levels were compared to HPV negative tumours (courtesy of Dr. Ingo Nindl). HPV DNA was detected using PCR and the HPV genotyping was performed using reverse-line-blotting (RLB). Since different HPV types can infect at the same time, some samples were positive for more than one type of HPV.

Table 10 Summary of HPV types in 8 patient samples

Sample	Diagnosis	PCR	Cut.HPV-RLB results
1	SCC	++	4,96
2	SCC	++	neg
3	SCC	+++	4,48
4	SCC	+	5,8,12,14,20
5	SCC	+++	neg
6	SCC	+++	neg
7	SCC	++	20,48
8	SCC	+++	92

It is important to note that during surgical excision, a part of the surrounding normal tissue is also removed. Therefore, p62 staining was scored in the tumour and normal surrounding tissue of each sample for comparison. Interestingly, sections from both HPV positive and negative samples revealed an increase in p62 levels in the normal thin epithelium, indicating low autophagy levels. Contrastingly, the carcinoma tissue showed very low p62 levels, suggesting active or high

autophagy (**Error! Reference source not found.**A). An example of p62 staining is shown in Figure 5-5B.

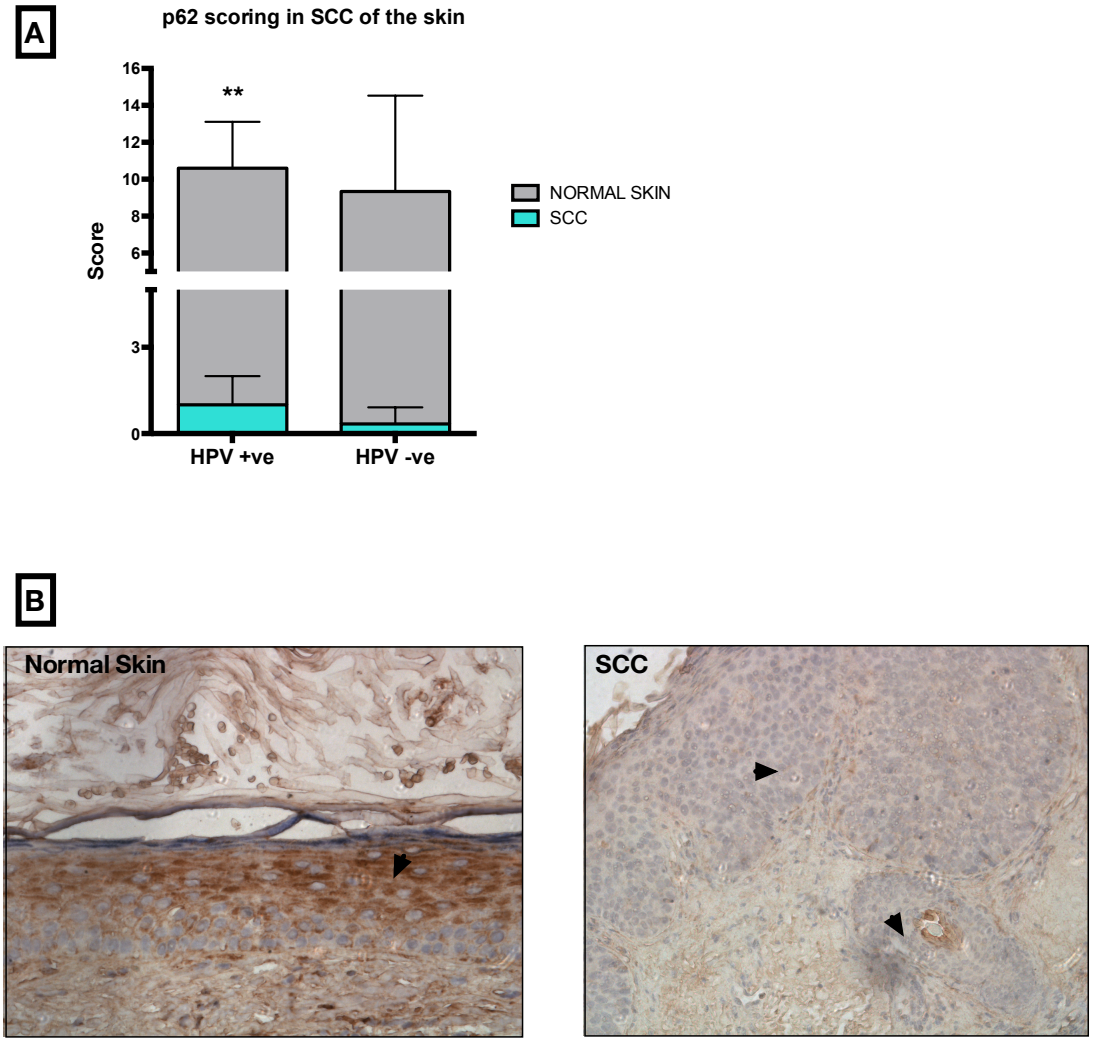

Figure 5-6 p62 levels in HPV positive SCC of the skin

The slides were stained for p62 and counterstained with haematoxylin to visualise the nuclei. The levels of p62 are inversely proportional to autophagy levels. n=5 HPV positive tumours and 3 HPV negative tumours. Statistical analysis was performed using two-way ANOVA **p<0.01. Arrows indicate the areas of the section scored for p62.

5.2.3 The levels of autophagy in cervical cancer

The results obtained in 2.12 suggested that the increase in autophagy levels is conserved among different HPV types including those of the α-HPV type 16 and 18, which are mainly detected in cervical cancer. Therefore, it was of interest to assess autophagy levels in cervical cancer samples.

Three tissue microarrays were obtained from Protein Biotechnologies (TMA 2218, 2219 and 2220). The microarrays had three different diagnoses: cervical polyp, carcinoma *in situ* (CIS) and SCC. This allows for the assessment of autophagy levels during progressive stages of disease development. The biopsies were stained for p62 as previously described and counterstained with haematoxylin.

In contrast to the results obtained from skin SCC, there was no significant change observed in p62 levels in the carcinoma compared to normal epithelium. Interestingly however, CIS showed the lowest levels of p62 suggesting an increase of autophagy levels in CIS.

A

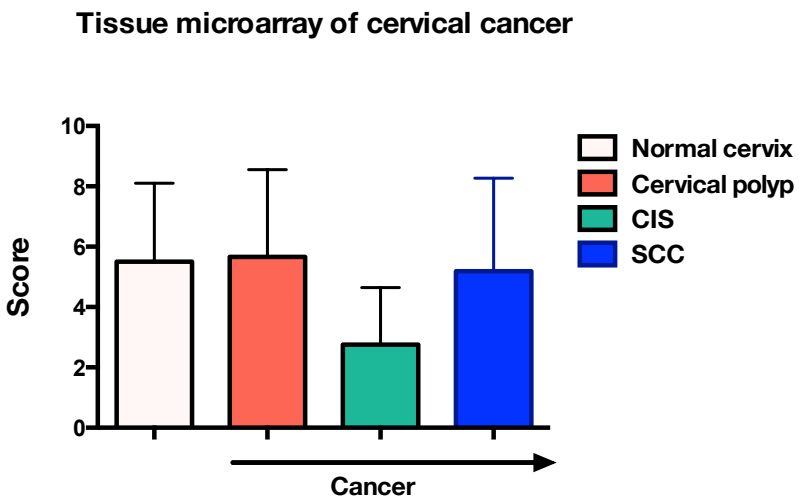

Figure 5-7 Levels of p62 in cervical cancer samples

The slides were stained for p62 and counterstained with haematoxylin to visualise the nuclei. The levels of p62 are inversely proportional to autophagy levels. n=24 normal, n=117 SCC. Statistical analysis was performed using two-way ANOVA =non significant

5.2.4 Discussion

Transgenic mouse models suggest a strong role for HPV E6 in the development of tumours and skin cancer after UV irradiation. The best described pathways that are modulated by β-HPV E6 are apoptosis and DDR, both of which contribute to genomic instability and perhaps transformation (Sarah Jackson & Storey 2000; Wallace et al. 2012). The data presented in Chapter 3 showed that in cells expressing E6 from HPV types 5 and 8, autophagy levels are increased following UV DNA damage. The role of autophagy in tumour development and suppression is currently being investigated in tumours arising from different body sites (Chandra B Lebovitz & Gorski et al. 2012). However, there are few studies on autophagy in HPV-related cancer. In order to examine the role of autophagy in HPV8 E6-driven tumours, the levels of autophagy were assessed in tumours arising in HPV8 E6 transgenic mice after UV irradiation. The results showed that after 5 days of UV exposure, the upper and more differentiated layers of the epithelium (middle and granular) demonstrated an increase in p62 staining, indicative of low autophagy. However, the basal cell layer (the proliferative cell layer) of the epidermis showed a decrease in p62 levels after 5 and 24 days of UV irradiation, suggesting an increase in autophagy after UV exposure in both HPV8 E6 transgenic mice and WT mice. The difference in autophagy levels between the different layers of the epidermis was mainly observed after 5 days of UV irradiation. This may indicate that *in vivo* there is a slower autophagic response than that observed *in vitro*. A general observation was that after 24 days of UV autophagy levels were lower than basal levels, and this may indicate active autophagy. Taken together these results suggest a role for autophagy in keratinocytes in response to UV irradiation in WT and HPV8 E6 mice. However, in contrast to the cell line models, there was no

significant difference between WT mice and HPV8 E6 transgenic mice. This could indicate that the increase in autophagy in E6 expressing cells after UV is a cell line effect. However, assessing autophagy levels using more markers is required to confirm these observations.

As previously described, autophagy can be a tumour suppressor, but can also promote tumour growth in stress conditions. Generally, in apoptosis competent cells, autophagy allows for cell survival under sub-lethal stress conditions and functions as quality control for cell mitigating damage (Mizushima et al. 2010). However, in apoptosis defective cells autophagy promotes cell survival (Lum et al. 2005) and this may contribute towards tumourigenicity under stress conditions.
Since HPV E6 abrogates DDR and DNA-damage mediated apoptosis, it was postulated that the observed survival upon autophagy induction would contribute towards tumour formation in HPV8 E6 transgenic mice after UV damage. It was then hypothesised that inhibition of autophagy could stop tumour formation in HPV8 E6 mice. To test this hypothesis, Chloroquine was used to inhibit autophagy in these mice.
Surprisingly, it was observed that the inhibition of autophagy by Chloroquine resulted in the formation of tumours that had a more aggressive gross appearance in two out of four mice. However, the other two mice showed tumour regression, making these results inconclusive. One of the major drawbacks of using Chloroquine is off-target effects, which may explain the confounding results obtained. Additionally, in some cases Chloroquine can induce skin photosensitivity that can lead to photosensitive dermatoses. This could explain the delayed wound healing response observed in WT mice treated with Chloroquine and the more aggressive tumours in HPV8 E6 mice (Prabhakara et al. 1996). To better

characterise the role of autophagy in this context, the experiment would need to be repeated with more mice.

To further explore whether autophagy plays a role in HPV tumours, autophagy levels were examined using p62 in SCC of the skin. Interestingly, both HPV negative and HPV positive SCC showed a marked decrease in p62 levels, indicating high autophagy levels in these lesions. In contrast, the surrounding normal epithelium showed very high p62 levels, indicating low autophagy levels.

Although the sample number is limited, these results suggest that SCC of the skin have high autophagy levels.

In NMSC, E6 is proposed to have a hit and run role and is not required for the sustainability of the disease (Pfister et al. 2003). Therefore, caution must be taken when analysing samples from advanced disease that are negative for HPV, those lesions might have been HPV positive in the past. As discussed in 1.2, early stages of skin cancer are treated by surgical excision. However, advanced tumours are usually resistant to chemotherapeutic agents, which correlates with poor prognosis. Studies on autophagy levels in SCC of the skin are limited. Recently one study showed that in SCC cell lines derived from lymph node metastasis (MET4) showed an increase in autophagy levels, demonstrated by an increase in LC3. That increase was correlated with enhanced resistance to cisplatin. The researches showed that inhibition of autophagy by Atg5 knockdown enhanced cisplatin-mediated cytotoxicity, suggesting a therapeutic potential of targeting autophagy in advanced SCC of the skin (Claerhout et al. 2010).

Autophagy inhibitors are currently being investigated in more than 20 clinical trials as a potential therapeutic strategy for multiple ‘autophagy-addicted’ cancers. The most common autophagy inhibitor used is hydroxychloroquine (HCQ).

One of the challenges facing the establishment of a casual relationship between β-HPV and NMSC is the absence of HPV in every cancer cell. However, α-HPV types

16 and 18 are found in nearly 80% of cervical cases. The results obtained in 3.3.11 showed that cells expressing E6 from HPV 16 and 18 have high autophagy levels in response to DNA damage. Albeit there is no evidence of DNA damage in cervical carcinomas, the induction of autophagy in these tumours might be in response to different forms of stress. IHC p62 analysis of cervical cancer TMAs showed a decrease of p62 levels, indicating low autophagy levels in CIS compared to normal tissue. However, established carcinomas showed p62 levels similar to normal tissue. Few studies exist on the relationship of the development of cervical cancer. In a study by Wang et. al the levels of LC3 and Beclin-1 were decreased in cervical cancer, which correlated to increase high-risk HPV infection (H.-Y. Wang et al. 2014). Additionally, another study that examined the expression of Beclin-1 in normal cervix, CIN and SCC, showed that Beclin-1 expression was negatively correlated with cancer differentiation, with CIN showing levels similar to the normal epithelium (Cheong et al. 2012). These results suggest that contrastingly to SCC of the skin, cervical carcinomas may have low autophagy levels where as CIS and perhaps low-grade tumours have high autophagy levels. This may indicate that autophagy plays a role in the early development of tumours, whereas in established tumours, autophagy levels return to basal.

5.3 Conclusions and future work

In conclusion, the work presented here shows for the first time that cells expressing E6 from different high-risk cutaneous HPV types show high autophagy levels and active autophagic flux after UV DNA damage. These results suggest a role for autophagy in the development of HPV associated NMSC.

Inhibition of autophagy in E6 expressing cells after UV irradiation triggered a non-apoptotic cell death, which resulted in a marked decrease in cell viability. These

findings indicate that E6 expressing cells depend on autophagy to survive in the background of genomic stress, allowing for genetic mutations to accumulate. In infected skin, this may contribute to tumour development.

Autophagy facilitates tumour cell survival in many cancers. Normal cells have low basal levels of autophagy that are upregulated by a multitude of external and internal stimuli such as starvation and ROS accumulation. Contrastingly, cancer cells have high basal levels of autophagy even in nutrient rich conditions. Studies demonstrated a link between changes in autophagy and multiple tumour associated physiological changes such as survival and proliferation, genomic instability and angiogenesis (Chandra B Lebovitz & Gorski, 2012). Pancreatic primary tumours and cancer cell lines show a marked increase in autophagy levels, and pharmaceutical inhibition of autophagy results in a decrease in tumour progression of xenograft models (S. Yang et al. 2011). Moreover, tumours with activated RAS are highly dependent on autophagy to survive in stress conditions. Knockdown of autophagy essential genes impairs RAS oncogenicity in mice models (J. Y. Guo et al. 2011). RAS mutations significantly increase the risk of skin cancer development and are found in the skin, characteristically seen at codons 12, 13 and 6. These are all localised opposing to UV-sensitive CC sites (Boukamp, 2005).

Furthermore, autophagy-mediated survival under hypoxic conditions is indispensable for cancer growth and progression of various cancer cells including melanoma (Lozy & Karantza et al. 2012). Additionally, in glioblastomas, hypoxia induced autophagy allows for cell survival and resistance to anti-angiogenic treatment (Hu et al. 2012). The mechanism of HIF1 induced autophagy involved the Bcl-2 protein BNIP3. Recently, a study identified a role for BNIP3 in keratinocyte differentiation (Moriyama et al. 2014). The skin is naturally hypoxic and

recently mass-spec studies identified HIF1-α as a target for HPV8 E6. Therefore, the observed autophagy levels might be the result of HIF1 activity.

Autophagy was also proven essential for the survival of breast cancer cell lines after exposure to the DNA damaging agent Etoposide. In skin infected with HPV, E6 might activate autophagy to allow for cell survival and override the natural apoptotic response. This may contribute to tumour formation.

5.3.1 Future work

1) Screen more HPV5 E6 mutants to identify the region required for autophagy induction

2) Elucidate the cell death mechanism occurring after autophagy inhibition:

-RIPK immunoblot

-Inhibit necrosis using necrostatin1

- Pro-caspase 1 immunoblot

-IL1-beta immunoblot and ELIZA assay

3) Using Seahorse Bioanalyser to determine which of the two pathways, glycolysis or oxidative phosphorylation, is preferred by E6

- Following UV irradiation measure β-oxidation

4) Analyse the cell cycle after UV irradiation

5) Run β-galactosidase assay to identify if the cells are undergoing senescence after UV

6) Using the transgenic mouse model for HPV8 E6, inhibit autophagy by tattooing siRNA against ULK1

7) Stain HPV positive SCC for autophagy markers

8) Stain EV samples for autophagy markers

Appendix and supplementary data

HT1080 cell line validation

HT1080 cell lines were validated by LGC Standards using Cell Line Authentication 16 Loci Service and was proven to have good profile characteristics.

***PowerPlex*® 16 HS 16 Loci Service**	**Results table reference**
Amelogenin	Amel
CSF1PO	CSF1
D13S317	D13
D16S539	D16
D18S51	D18
D21S11	D21
D3S1358	D3
D7S820	D5
D8S1179	D7
FGA	D8
Penta D	FGA
Penta E	PeD
TH01	PeE
TPOX	TH01
vWA	TPOX

Definitions of terms used in this report:

Peak Area Difference (PAD):

Refers to a heterozygous peak imbalance.Two alleles at a single locus should amplify in a similar manner; and therefore produce peaks of similar height and area. Peaks which are above threshold (50 rfu) but are not of similar area, within 50% of each other, are referred to as a PAD. Due to their nature cell lines do not amplify in the same manner as a sample taken from a fresh buccal swab. PAD is far more common in cell line samples.

Stutter:

A stutter peak is a small peak which occurs immediately before the true peak. It is defined as being a single repeat unit smaller than the true peak. The stutter peak should be less than 15% of the true peak. The stutter is caused by the polymerase.

+4 Peak:

A +4 is similar to a stutter but occurs immediately after the true peak. A stutter peak should be less than 5% for a homozygous and 10% for a heterozygous.

Below Threshold Peak(s):

Cell lines can produce unusual profiles and occasionally a peak will amplify poorly and be below threshold. Where we find a below threshold peak which we believe is valid we indicate it as a below threshold peak. Our cell line analysis criteria, Homozygous and Heterozygous peaks must be equal to or above the set height threshold for it to be considered a true peak.

Ladder/ Off Ladder Peak(s):

The allelic ladder consists of most or all known alleles in the population and allows for precise assignment of alleles. Those which do not align are termed ‘off ladder.’

ATCC reference CCL-121	Customer sample HT1080
X,Y	X,Y
	16,16
6,6	6,6
	28,30
	12,18
	5,15
11,13	11,13
12,14	12*,14
9,10	9,10
9,12	9,12
12,12	12,12
	9,12
14,19	14,19
	13,14
8,8	8,8
	22,25

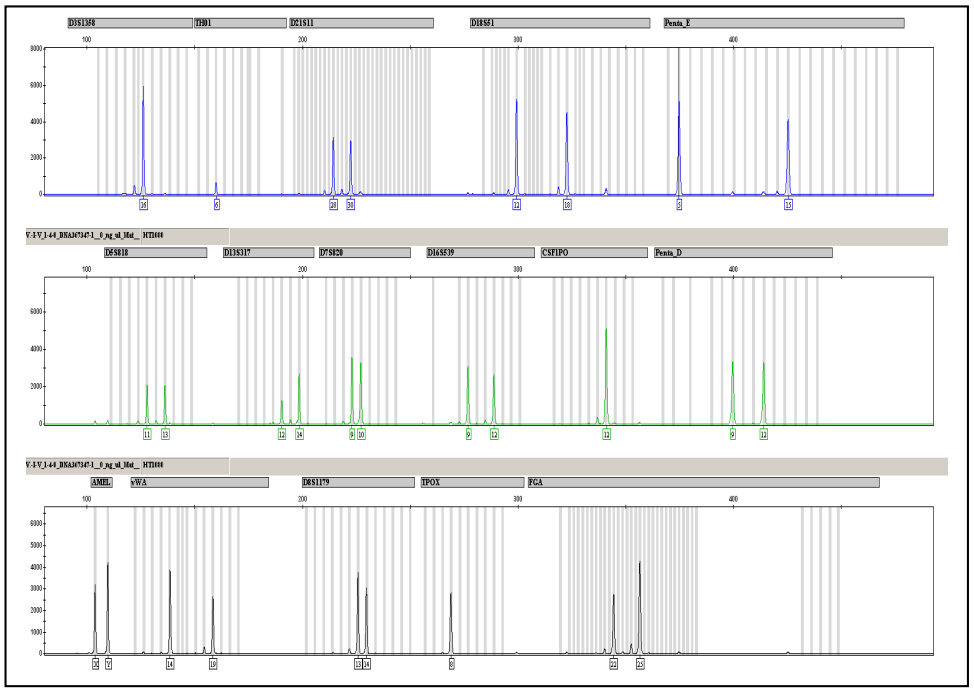

fference
shold peak

9 loci profile, here LGC Standards has profiled those same 9 plus 7 others.
e 5 for terms used.

atches all of the 8 reference STR loci (plus Amelogenin) available from ATCC for CCL-121.

Optimisation of Seahorse assay

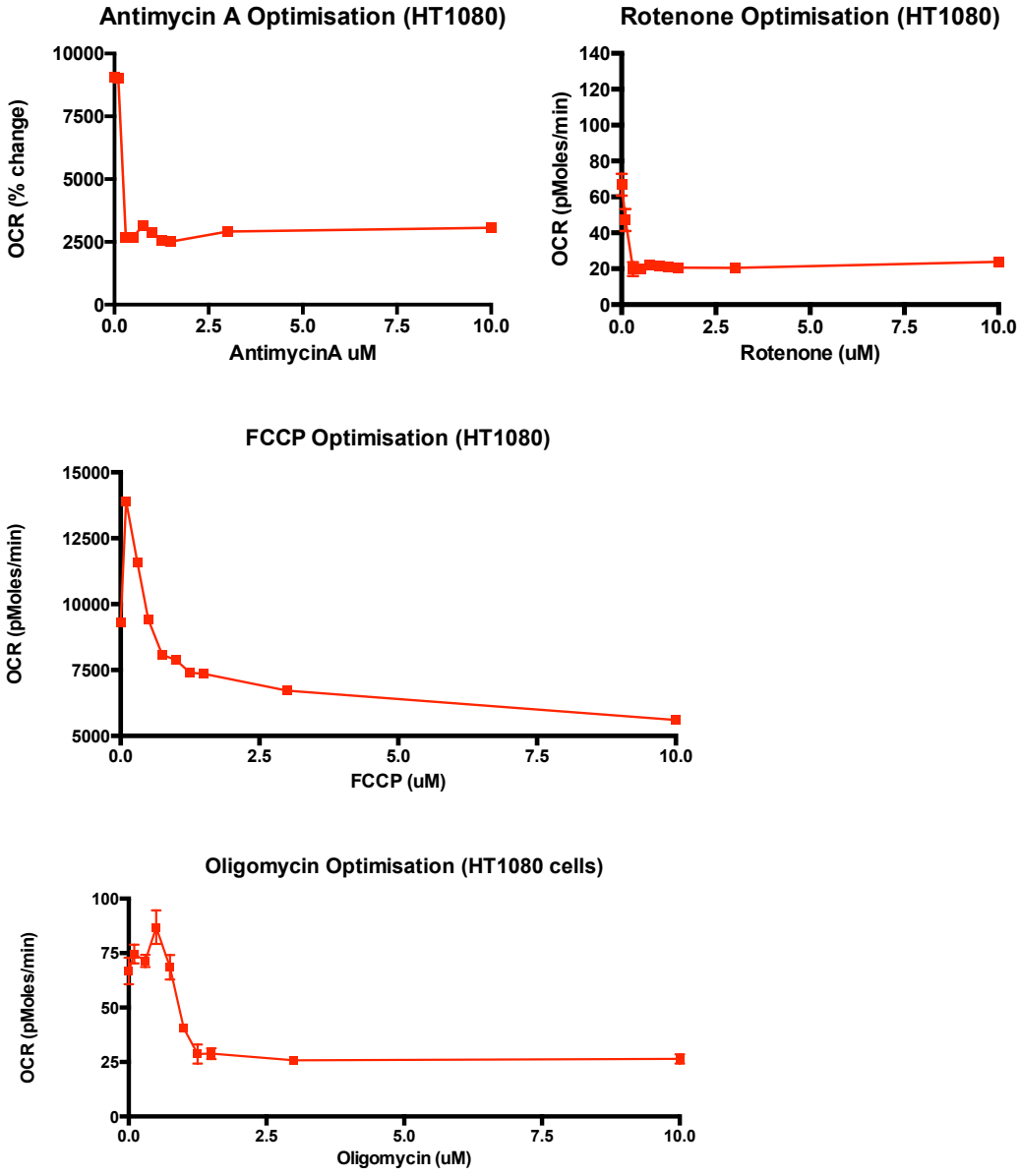

Optimisation of drug concentration for the MitoStress Test.

Bibliography

Abedin, M.J. et al., 2007. Autophagy delays apoptotic death in breast cancer cells following DNA damage. *Cell Death & Differentiation*, 14(3), pp.500–510.

Agar, N.S. et al., 2004. The basal layer in human squamous tumors harbors more UVA than UVB fingerprint mutations: a role for UVA in human skin carcinogenesis. *Proceedings of the National Academy of Sciences*, 101(14), pp.4954–4959.

Akgül, B., Bostanci, N., Westphal, K., Nindl, I., Navsaria, H., Storey, A., & Pfister, H. (2010). Human papillomavirus 5 and 8 E6 downregulate interleukin-8 secretion in primary human keratinocytes. Journal of General Virology, 91(4), 888–892. doi:10.1099/vir.0.016527-0

Akgül, B. et al., 2005. The E7 protein of cutaneous human papillomavirus type 8 causes invasion of human keratinocytes into the dermis in organotypic cultures of skin. *Cancer Research*, 65(6), pp.2216–2223.

Apel, A. et al., 2008. Blocked autophagy sensitizes resistant carcinoma cells to radiation therapy. *Cancer Research*, 68(5), pp.1485–1494.

Arron, S.T. et al., 2011. Transcriptome sequencing demonstrates that human papillomavirus is not active in cutaneous squamous cell carcinoma. *The Journal of investigative dermatology*, 131(8), pp.1745–1753.

Ashrafi, G.H. et al., 2006. E5 protein of human papillomavirus 16 downregulates HLA class I and interacts with the heavy chainvia its first hydrophobic domain. *International Journal of Cancer*, 119(9), pp.2105–2112.

Astori, G. et al., 1998. Human papillomaviruses are commonly found in normal skin of immunocompetent hosts. *Journal of Investigative Dermatology*, 110(5), pp.752–755.

Axe, E.L. et al., 2008. Autophagosome formation from membrane compartments enriched in phosphatidylinositol 3-phosphate and dynamically connected to the endoplasmic reticulum. *The Journal of cell biology*, 182(4), pp.685–701.

Azad, A. & Storey, A., 2013. BAK multimerization for apoptosis, but not bid binding, is inhibited by negatively charged residue in the BAK hydrophobic groove. *Molecular Cancer*, 12(1), p.65.

Bach, M. et al., 2011. The serine/threonine kinase ULK1 is a target of multiple phosphorylation events. *Autophagy, mitochondria and oxidative stress: cross-talk and redox signalling*, 440(2), pp.283–291.

Bastien, N. & McBride, A.A., 2000. Interaction of the Papillomavirus E2 Protein with Mitotic Chromosomes. *Virology*, 270(1), pp.124–134.

Bavinck, J.N.B. et al., 2010. Multicenter Study of the Association between Betapapillomavirus Infection and Cutaneous Squamous Cell Carcinoma. *Cancer Research*, 70(23), pp.9777–9786.

Beckner, M.E. et al., 1990. Glycolysis as primary energy source in tumor cell chemotaxis. *Journal of the National Cancer Institute*, 82(23), pp.1836–1840.

Bergant Marušič, M. et al., 2012. Human papillomavirus L2 facilitates viral escape from late endosomes via sorting nexin 17. *Traffic (Copenhagen, Denmark)*, 13(3), pp.455–467.

Bernard, H.-U. et al., 2010. Classification of papillomaviruses (PVs) based on 189 PV types and proposal of taxonomic amendments., 401(1), pp.70–79.

Bhambri, S. & Del Rosso, J.Q., 2010. Bowen's Disease: A Four-Year Retrospective Review of Epidemiology and Treatment at a University Center. *Yearbook of Dermatology and Dermatologic Surgery*, 2010, pp.352–353.

Bjørkøy, G. et al., 2005. p62/SQSTM1 forms protein aggregates degraded by autophagy and has a protective effect on huntingtin-induced cell death. *The Journal of cell biology*, 171(4), pp.603–614.

Borgogna, C. et al., 2014. Improved detection reveals active β-papillomavirus infection in skin lesions from kidney transplant recipients. *Modern pathology : an official journal of the United States and Canadian Academy of Pathology, Inc*, 27(8), pp.1101–1115.

Boukamp, P., 2005. Non-melanoma skin cancer: what drives tumor development and progression? *Carcinogenesis*, 26(10), pp.1657–1667.

Bratton, S.B. & Salvesen, G.S., 2010. Regulation of the Apaf-1-caspase-9 apoptosome. *Journal of cell science*, 123(Pt 19), pp.3209–3214.

Bravo, I.G., Alonso, A. & Auvinen, E., 2013. Human papillomavirus type 16 E5 protein. *Papillomavirus Report*, 15(1), pp.1–6.

Brimer, N. et al., 2012. Cutaneous papillomavirus E6 oncoproteins associate with MAML1 to repress transactivation and NOTCH signaling. *Oncogene*.

Buck, C.B. & Trus, B.L., 2012. The papillomavirus virion: a machine built to hide molecular Achilles' heels. *Viral Molecular Machines*.

Buck, C.B. et al., 2008. Arrangement of L2 within the papillomavirus capsid. *Journal of virology*, 82(11), pp.5190–5197.

Buck, C.B., Day, P.M. & Trus, B.L., 2013. The papillomavirus major capsid protein L1. *Virology*, 445(1-2), pp.169–174.

Chan, E.Y.W., Kir, S. & Tooze, S.A., 2007. siRNA screening of the kinome identifies ULK1 as a multidomain modulator of autophagy. *Journal of Biological Chemistry*, 282(35), pp.25464–25474.

Chandra B Lebovitz, S.B.B. & Gorski, S.M., 2012. Here, there be dragons: charting autophagy-related alterations in human tumors. *Clinical cancer research : an official journal of the American Association for Cancer Research*, 18(5), pp.1214–1226.

Chang, Y.-Y. & Neufeld, T.P., 2009. An Atg1/Atg13 complex with multiple roles in

TOR-mediated autophagy regulation. *Molecular biology of the cell*, 20(7), pp.2004–2014.

Chen, G. & Stenlund, A., 2002. Sequential and ordered assembly of E1 initiator complexes on the papillomavirus origin of DNA replication generates progressive structural changes related to melting. *Molecular and Cellular Biology*, 22(21), pp.7712–7720.

Chinnaiyan, A.M. et al., 1995. FADD, a novel death domain-containing protein, interacts with the death domain of Fas and initiates apoptosis. *Cell*, 81(4), pp.505–512.

Chipuk, J.E. et al., 2010. The BCL-2 Family Reunion. *Molecular cell*, 37(3), pp.299–310.

Claerhout, S. et al., 2010. Concomitant inhibition of AKT and autophagy is required for efficient cisplatin-induced apoptosis of metastatic skin carcinoma. *International Journal of Cancer*, 127(12), pp.2790–2803.

Cornet, I. et al., 2012. Comparative analysis of transforming properties of E6 and E7 from different beta human papillomavirus types. *Journal of virology*, 86(4), pp.2366–2370.

Côté-Martin, A. et al., 2008. Human papillomavirus E1 helicase interacts with the WD repeat protein p80 to promote maintenance of the viral genome in keratinocytes. *Journal of virology*, 82(3), pp.1271–1283.

Crighton, D., Wilkinson, S., O'Prey, J., Syed, N., Smith, P., Harrison, P.R., Gasco, M., Garrone, O., Crook, T. & Ryan, K.M., 2006a. DRAM, a p53-induced modulator of autophagy, is critical for apoptosis. *Cell*, 126(1), pp.121–134.

Crighton, D., Wilkinson, S., O'Prey, J., Syed, N., Smith, P., Harrison, P.R., Gasco, M., Garrone, O., Crook, T. & Ryan, K.M., 2006b. DRAM, a p53-induced modulator of autophagy, is critical for apoptosis. *Cell*, 126(1), pp.121–134.

Culp, T.D. et al., 2006. Keratinocyte-secreted laminin 5 can function as a transient receptor for human papillomaviruses by binding virions and transferring them to adjacent cells. *Journal of virology*, 80(18), pp.8940–8950.

Davy, C.E. et al., 2005. Human Papillomavirus Type 16 E1◦E4-Induced G2 Arrest Is Associated with Cytoplasmic Retention of Active Cdk1/Cyclin B1 Complexes. *Journal of virology*, 79(7), pp.3998–4011.

Day, P.M. et al., 1998. The papillomavirus minor capsid protein, L2, induces localization of the major capsid protein, L1, and the viral transcription/replication protein, E2, to PML oncogenic domains. *Journal of virology*, 72(1), pp.142–150.

de Gruijl, F.R., van Kranen, H.J. & Mullenders, L.H.F., 2001. UV-induced DNA damage, repair, mutations and oncogenic pathways in skin cancer. *Journal of Photochemistry and Photobiology B: Biology*, 63(1-3), pp.19–27.

de Koning, M.N.C. et al., 2009. Prevalence and associated factors of betapapillomavirus infections in individuals without cutaneous squamous cell

carcinoma. *Journal of General Virology*, 90(7), pp.1611–1621.

Degenhardt, K. et al., 2006. Autophagy promotes tumor cell survival and restricts necrosis, inflammation, and tumorigenesis. *Cancer cell*, 10(1), pp.51–64.

Degenhardt, K., Chen, G. & White, E., 2002. BAX and BAK mediate p53-independent suppression of tumorigenesis. *Cancer cell*, 2(3), pp.193–203.

Denton, D., Nicolson, S. & Kumar, S., 2012. Cell death by autophagy: facts and apparent artefacts. *Cell Death & Differentiation*, 19(1), pp.87–95.

Dewson, G. et al., 2008. To trigger apoptosis, Bak exposes its BH3 domain and homodimerizes via BH3:groove interactions. *Molecular cell*, 30(3), pp.369–380.

DiMaio, D. & Petti, L.M., 2013. The E5 proteins. *Virology*, 445(1-2), pp.99–114.

Dong, W. et al., 2005. Skin hyperproliferation and susceptibility to chemical carcinogenesis in transgenic mice expressing E6 and E7 of human papillomavirus type 38. *Journal of virology*, 79(23), pp.14899–14908.

Doorbar, J., 2013. The E4 protein; structure, function and patterns of expression. *Virology*, 445(1-2), pp.80–98.

Doorbar, J. & Gallimore, P.H., 1987. Identification of proteins encoded by the L1 and L2 open reading frames of human papillomavirus 1a. *Journal of virology*, 61(9), pp.2793–2799.

Doorbar, J. et al., 2012. The Biology and Life-Cycle of Human Papillomaviruses. *Vaccine*, 30, pp.F55–F70.

Du, C., Fang, M. & Li, L., 2000. Smac, a mitochondrial protein that promotes cytochrome c–dependent caspase activation by eliminating IAP inhibition. *Cell*.

Eckhart, L. et al., 2013. Cell death by cornification. *Biochimica et Biophysica Acta (BBA) - Molecular Cell Research*, 1833(12), pp.3471–3480.

Elias, P.M. et al., 2002. Origin of the Epidermal Calcium Gradient: Regulation by Barrier Status and Role of Active vs Passive Mechanisms. *Journal of Investigative Dermatology*, 119(6), pp.1269–1274.

English, L. et al., 2009. Autophagy enhances the presentation of endogenous viral antigens on MHC class I molecules during HSV-1 infection. *Nature immunology*, 10(5), pp.480–487.

Esclatine, A., Chaumorcel, M. & Codogno, P., 2009. Macroautophagy signaling and regulation. *Current topics in microbiology and immunology*, 335, pp.33–70.

Eskes, R. et al., 2000. Bid induces the oligomerization and insertion of Bax into the outer mitochondrial membrane. *Molecular and Cellular Biology*, 20(3), pp.929–935.

Fang, L. et al., 2006. The human papillomavirus type 11 E1^E4 protein is not essential for viral genome amplification. *Virology*, 351(2), pp.271–279.

Feng, H. et al., 2008. Clonal Integration of a Polyomavirus in Human Merkel Cell Carcinoma. *Science*, 319(5866), pp.1096–1100.

Feng, Y. et al., 2014. The machinery of macroautophagy. *Cell Research*, 24(1), pp.24–41.

Fernández-Figueras, M.T. et al., 2014. Actinic keratosis with atypical basal cells (AK I) is the most common lesion associated with invasive squamous cell carcinoma of the skin. *Journal of the European Academy of Dermatology and Venereology*, pp.n/a–n/a.

Filippova, M., Parkhurst, L. & Duerksen-Hughes, P.J., 2004. The human papillomavirus 16 E6 protein binds to Fas-associated death domain and protects cells from Fas-triggered apoptosis. *Journal of Biological Chemistry*, 279(24), pp.25729–25744.

Finnen, R.L. et al., 2003. Interactions between papillomavirus L1 and L2 capsid proteins. *Journal of virology*, 77(8), pp.4818–4826.

Forman, D. et al., 2012. Global Burden of Human Papillomavirus and Related Diseases. *Vaccine*, 30, pp.F12–F23.

Fox, J. et al., 2011. “Licensed to kill”: tyrosine dephosphorylation and Bak activation. *Cell Cycle*, 10(4), pp.598–603.

Fuchs, E. & Raghavan, S., 2002. GETTING UNDER THE SKIN OF EPIDERMAL MORPHOGENESIS. *Nature Reviews Genetics*, 3(3), pp.199–209.

Fujii, T. et al., 2001. High and Low Levels of Cottontail Rabbit Papillomavirus E2 Protein Generate Opposite Effects on Gene Expression. *Journal of Biological Chemistry*, 276(2), pp.867–874.

Fujita, N. et al., 2008. The Atg16L complex specifies the site of LC3 lipidation for membrane biogenesis in autophagy. *Molecular biology of the cell*, 19(5), pp.2092–2100.

Gao, W., Shen, Z. & Shang, L., 2011. Upregulation of human autophagy-initiation kinase ULK1 by tumor suppressor p53 contributes to DNA-damage-induced cell death. *Cell Death & Differentiation*, 18(10), pp.1598–1607.

Garnett, T.O., Filippova, M. & Duerksen-Hughes, P.J., 2006. Accelerated degradation of FADD and procaspase 8 in cells expressing human papilloma virus 16 E6 impairs TRAIL-mediated apoptosis. *Cell Death & Differentiation*, 13(11), pp.1915–1926.

Geisler, S. et al., 2010. PINK1/Parkin-mediated mitophagy is dependent on VDAC1 and p62/SQSTM1. *nature cell biology*, 12(2), pp.119–131.

Giampieri, S. & Storey, A., 2004. Repair of UV-induced thymine dimers is compromised in cells expressing the E6 protein from human papillomaviruses types 5 and 18. *British journal of cancer*, 90(11), pp.2203–2209.

Giampietri, C. et al., 2014. Necroptosis: Molecular Signalling and Translational Implications. *International Journal of Cell Biology*, 2014(6), p.490275. Available

at:
http://eutils.ncbi.nlm.nih.gov/entrez/eutils/elink.fcgi?dbfrom=pubmed&id=24587805&retmode=ref&cmd=prlinks.

Giglia Mari, G. & Sarasin, A., 2003. TP53 mutations in human skin cancers. *Human mutation*, 21(3), pp.217–228.

Gillison, M.L. et al., 2013. Eurogin Roadmap: Comparative epidemiology of HPV infection and associated cancers of the head and neck and cervix. *International Journal of Cancer*, 134(3), pp.497–507.

Giri, I. & Yaniv, M., 1988. Structural and mutational analysis of E2 trans-activating proteins of papillomaviruses reveals three distinct functional domains. *The EMBO journal*, 7(9), pp.2823–2829.

Goldstein, J.C. et al., 2000. The coordinate release of cytochrome c during apoptosis is rapid, complete and kinetically invariant. *nature cell biology*, 2(3), pp.156–162.

Gonzalez, S.L. et al., 2001. Degradation of the retinoblastoma tumor suppressor by the human papillomavirus type 16 E7 oncoprotein is important for functional inactivation and is separable from proteasomal degradation of E7. *Journal of virology*, 75(16), pp.7583–7591.

Griffin, L.M., Cicchini, L. & Pyeon, D., 2013. Human papillomavirus infection is inhibited by host autophagy in primary human keratinocytes. *Virology*, 437(1), pp.12–19.

Guo, J.Y. et al., 2011. Activated Ras requires autophagy to maintain oxidative metabolism and tumorigenesis. *Genes & Development*, 25(5), pp.460–470.

Guo, K. et al., 2001. Hypoxia induces the expression of the pro-apoptotic gene BNIP3. *, Published online: 11 April 2001; | doi:10.1038/sj.cdd.4400810*, 8(4), pp.367–376.

Guo, Y. et al., 2014. Human Papillomavirus 16 E6 Contributes HIF-1α Induced Warburg Effect by Attenuating the VHL-HIF-1α Interaction. *International journal of …*.

Hanahan, D. & Weinberg, R.A., 2011a. Hallmarks of cancer: the next generation. *Cell*, 144(5), pp.646–674.

Hanahan, D. & Weinberg, R.A., 2011b. Hallmarks of cancer: the next generation. *Cell*, 144(5), pp.646–674.

Hayashi-Nishino, M. et al., 2009. A subdomain of the endoplasmic reticulum forms a cradle for autophagosome formation. *nature cell biology*, 11(12), pp.1433–1437.

Häcker, G., 2000. The morphology of apoptosis. *Cell and Tissue Research*, 301(1), pp.5–17.

He, C. & Levine, B., 2010. The Beclin 1 interactome. *Current Opinion in Cell Biology*, 22(2), pp.140–149.

Heaton, N.S. & Randall, G., 2010. Dengue Virus-Induced Autophagy Regulates Lipid Metabolism. *Cell host & microbe*, 8(5), pp.422–432.

Hill, L.L., 1999. Fas Ligand: A Sensor for DNA Damage Critical in Skin Cancer Etiology. *Science*, 285(5429), pp.898–900.

Holloway, A. & Storey, A., 2014. A conserved C-terminal sequence of high-risk cutaneous beta-human papillomavirus E6 proteins alters localization and signalling of β1-integrin to promote cell migration. *The Journal of general virology*, 95(Pt 1), pp.123–134.

Holloway, A. et al., 2014. Resistance to UV-Induced Apoptosis by Beta HPV5 E6 Involves Targeting of Activated BAK for Proteolysis by Recruitment of the HERC1 Ubiquitin Ligase. *International Journal of Cancer*, pp.n/a–n/a.

Hongmei, Z., 2012. Extrinsic and Intrinsic Apoptosis Signal Pathway Review. In T. Ntuli, ed. *Apoptosis and Medicine*. InTech.

Hosokawa, N. et al., 2009. Nutrient-dependent mTORC1 Association with the ULK1-Atg13-FIP200 Complex Required for Autophagy. *Molecular biology of the cell*, 20(7), pp.1981–1991.

Housman, T. S., Feldman, S. R., Williford, P. M., Fleischer, A. B., Jr., Goldman, N. D., Acostamadiedo, J. M. & Chen, G. J. 2003. Skin cancer is among the most costly of all cancers to treat for the Medicare population. J Am Acad Dermatol, 48, 425-9.

Hou, S. Y., Wu, S. Y. & Chiang, C. M. 2002. Transcriptional activity among high and low risk human papillomavirus E2 proteins correlates with E2 DNA binding. J Biol Chem, 277, 45619-29.

Hufbauer, M. et al., 2010. Enhanced human papillomavirus type 8 oncogene expression levels are crucial for skin tumorigenesis in transgenic mice. *Virology*, 403(2), pp.128–136.

Hufbauer, M. et al., 2013. Expression of betapapillomavirus oncogenes increases the number of keratinocytes with stem cell-like properties. *Journal of virology*, 87(22), pp.12158–12165.

Hughes, F.J. & Romanos, M.A., 1993. E1 protein of human papillomavirus is a DNA helicase/ATPase. *Nucleic Acids Research*, 21(25), pp.5817–5823.

Huh, K. et al., 2007. Human Papillomavirus Type 16 E7 Oncoprotein Associates with the Cullin 2 Ubiquitin Ligase Complex, Which Contributes to Degradation of the Retinoblastoma Tumor Suppressor. *Journal of virology*, 81(18), pp.9737–9747.

Huibregtse, J.M., Scheffner, M. & Howley, P.M., 1991. A cellular protein mediates association of p53 with the E6 oncoprotein of human papillomavirus types 16 or 18. *The EMBO journal*, 10(13), pp.4129–617.

Huibregtse, J.M., Scheffner, M. & Howley, P.M., 1993. Cloning and expression of the cDNA for E6-AP, a protein that mediates the interaction of the human papillomavirus E6 oncoprotein with p53. *Molecular and Cellular Biology*, 13(2),

pp.775–784.

Høyer-Hansen, M. & Jäättelä, M., 2008. Autophagy: an emerging target for cancer therapy. *Autophagy*, 4(5), p.574.

Iannacone, M.R., Gheit, T., Pfister, H., Giuliano, A.R., Messina, J.L., Fenske, N.A., Cherpelis, B.S., Sondak, V.K., Roetzheim, R.G., Silling, S., Pawlita, M., Tommasino, M. & Rollison, D.E., 2014a. Case-control study of genus-beta human papillomaviruses in plucked eyebrow hairs and cutaneous squamous cell carcinoma. *International Journal of Cancer*, 134(9), pp.2231–2244.

Iannacone, M.R., Gheit, T., Pfister, H., Giuliano, A.R., Messina, J.L., Fenske, N.A., Cherpelis, B.S., Sondak, V.K., Roetzheim, R.G., Silling, S., Pawlita, M., Tommasino, M. & Rollison, D.E., 2014b. Case–control study of genus-beta human papillomaviruses in plucked eyebrow hairs and cutaneous squamous cell carcinoma. *International Journal of Cancer*, 134(9), pp.2231–2244.

Ishii, Y., 2013. Electron microscopic visualization of autophagosomes induced by infection of human papillomavirus pseudovirions. 433(4), pp.385–389.

Itakura, E., Kishi-Itakura, C. & Mizushima, N., 2012. The Hairpin-type Tail-Anchored SNARE Syntaxin 17 Targets to Autophagosomes for Fusion with Endosomes/Lysosomes. *Cell*, 151(6), pp.1256–1269.

Jackson, S. & Storey, A., 2000. E6 proteins from diverse cutaneous HPV types inhibit apoptosis in response to UV damage. *Oncogene*, 19(4), pp.592–598.

Jha, S. et al., 2010. Destabilization of TIP60 by human papillomavirus E6 results in attenuation of TIP60-dependent transcriptional regulation and apoptotic pathway. *Molecular cell*, 38(5), pp.700–711.

Johnson, K.M. et al., 2009. Role of Heparan Sulfate in Attachment to and Infection of the Murine Female Genital Tract by Human Papillomavirus. *Journal of virology*, 83(5), pp.2067–2074.

Jones, P.H. & Watt, F.M., 1993. Separation of human epidermal stem cells from transit amplifying cells on the basis of differences in integrin function and expression. *Cell*, 73(4), pp.713–724.

Kabeya, Y., 2000. LC3, a mammalian homologue of yeast Apg8p, is localized in autophagosome membranes after processing. *The EMBO journal*, 19(21), pp.5720–5728.

Kabeya, Y. et al., 2000. LC3, a mammalian homologue of yeast Apg8p, is localized in autophagosome membranes after processing. *The EMBO journal*, 19(21), pp.5720–5728.

Kang, M.-I. et al., 2012. Targeting of Noncanonical Wnt5a Signaling by AP-1 Blocker Dominant-Negative Jun When It Inhibits Skin Carcinogenesis. *Genes & cancer*, 3(1), pp.37–50.

KarlMunger, B.W.N.D.W.C.P.E.H. & Howley, P., 1991. Complex formation of human papillomavirus E7 proteins withtheretinoblastomatumor suppressor gene product

. *The EMBO journal*, 8, pp.pp.4099–4105.

Kerr, J.F., Wyllie, A.H. & Currie, A.R., 1972. Apoptosis: a basic biological phenomenon with wide-ranging implications in tissue kinetics. *British journal of cancer*, 26(4), pp.239–257.

Kessis, T.D. et al., 1993. Human papillomavirus 16 E6 expression disrupts the p53-mediated cellular response to DNA damage. *Proceedings of the National Academy of Sciences of the United States of America*, 90(9), pp.3988–3992.

Kim, J. et al., 2011. AMPK and mTOR regulate autophagy through direct phosphorylation of Ulk1. *nature cell biology*, 13(2), pp.132–141.

Kines, R.C. et al., 2009. The initial steps leading to papillomavirus infection occur on the basement membrane prior to cell surface binding. *Proceedings of the National Academy of Sciences*, 106(48), pp.20458–20463.

Kiyono, T. et al., 1998. **Both Rb/p16^{INK4a} inactivation and telomerase activityare required to immortalize human epithelial cells**

. *Nature*, pp.1–5.

Klingelhutz, A.J., Foster, S.A. & McDougall, J.K., 1996. Telomerase activation by the E6 gene product of human papillomavirus type 16. *Nature*, 380(6569), pp.79–82.

Klionsky, D.J. et al., 2014. Guidelines for the use and interpretation of assays for monitoring autophagy in higher eukaryotes. *Autophagy*, 4(2), pp.151–175. Available at: http://eutils.ncbi.nlm.nih.gov/entrez/eutils/elink.fcgi?dbfrom=pubmed&id=18188003&retmode=ref&cmd=prlinks.

Knight, G.L. et al., 2011. A cyclin-binding motif in human papillomavirus type 18 (HPV18) E1^E4 is necessary for association with CDK–cyclin complexes and G2/M cell cycle arrest of keratinocytes, but is not required for differentiation-dependent viral genome amplification or L1 capsid protein expression. *Virology*, 412(1), pp.196–210.

Koster, M.I. & Roop, D.R., 2007. Mechanisms Regulating Epithelial Stratification. *Annual Review of Cell and Developmental Biology*, 23(1), pp.93–113.

Kouroku, Y. et al., 2006. ER stress (PERK/eIF2α phosphorylation) mediates the polyglutamine-induced LC3 conversion, an essential step for autophagy formation. *Cell Death & Differentiation*, 14(2), pp.230–239.

Kovacs, D. et al., 2009. Keratinocyte growth factor down-regulates intracellular ROS production induced by UVB. *Journal of dermatological science*, 54(2), pp.106–113.

Köchl, R. et al., 2005. Microtubules Facilitate Autophagosome Formation and Fusion of Autophagosomes with Endosomes. *Traffic (Copenhagen, Denmark)*, 7(2), pp.129–145.

Kraemer, K.H., 1997. Sunlight and skin cancer: another link revealed. *Proceedings*

of the National Academy of Sciences, 94(1), pp.11–14.

Kroemer, G. & Levine, B., 2008. Autophagic cell death: the story of a misnomer. *Nature Reviews Molecular Cell Biology*, 9(12), pp.1004–1010.

Kroemer, G., Mariño, G. & Levine, B., 2010. Autophagy and the Integrated Stress Response. *Molecular cell*, 40(2), pp.280–293.

Kuma, A., Matsui, M. & Mizushima, N., 2007. LC3, an Autophagosome Marker, Can be Incorporated into Protein Aggregates Independent of Autophagy: Caution in the Interpretation of LC3 Localization. *dx.doi.org*, 3(4), pp.1–242.

Lamkanfi, M., 2011. Emerging inflammasome effector mechanisms. *Nature reviews. Immunology*, 11(3), pp.213–220.

Lazarczyk, M. et al., 2012. EVER Proteins, Key Elements of the Natural Anti-Human Papillomavirus Barrier, Are Regulated upon T-Cell Activation. *PloS one*, 7(6), p.e39995.

Lazarczyk, M. et al., 2008. Regulation of cellular zinc balance as a potential mechanism of EVER-mediated protection against pathogenesis by cutaneous oncogenic human papillomaviruses. *The Journal of experimental medicine*, 205(1), pp.35–42.

Lechler, T. & Fuchs, E., 2005. Asymmetric cell divisions promote stratification and differentiation of mammalian skin. *Nature*, 437(7056), pp.275–280.

Lee, H.K. et al., 2007. Autophagy-dependent viral recognition by plasmacytoid dendritic cells. *Science*, 315(5817), pp.1398–1401.

Lee, S.S. et al., 2000. Multi-PDZ domain protein MUPP1 is a cellular target for both adenovirus E4-ORF1 and high-risk papillomavirus type 18 E6 oncoproteins. *Journal of virology*, 74(20), pp.9680–9693.

Leiprecht, N. et al., 2011. Regulation of Na+-coupled glucose carrier SGLT1 by human papillomavirus 18 E6 protein. 404(2), pp.695–700.

Li, H. et al., 1998. Cleavage of BID by caspase 8 mediates the mitochondrial damage in the Fas pathway of apoptosis. *Cell*, 94(4), pp.491–501.

Li, Y. et al., 2004. TSC2: filling the GAP in the mTOR signaling pathway. *Trends in biochemical sciences*.

Ljubojevic, S. & Skerlev, M., 2014. HPV-associated diseases. *Clinics in dermatology*, 32(2), pp.227–234.

Lomas, A., Leonardi-Bee, J. & Bath-Hextall, F., 2012. A systematic review of worldwide incidence of nonmelanoma skin cancer. *British Journal of Dermatology*, 166(5), pp.1069–1080.

Lu, Z. et al., 2004. Human papillomavirus 16 E6 oncoprotein interferences with insulin signaling pathway by binding to tuberin. *Journal of Biological Chemistry*, 279(34), pp.35664–35670.

Lustbader, E.D. et al., 1992. Segregation analysis of cancer in families of childhood soft-tissue-sarcoma patients. *American journal of human genetics*, 51(2), pp.344–356.

Madan, V., Lear, J.T. & Szeimies, R.-M., 2010. Non-melanoma skin cancer. *The Lancet*, 375(9715), pp.673–685.

Maes, H. & Agostinis, P., 2014. Autophagy and mitophagy interplay in melanoma progression. *Mitochondrion*.

Maes, H. et al., 2014. Dynamic interplay between autophagic flux and Akt during melanoma progression in vitro. *Experimental dermatology*, 23(2), pp.101–106.

Maglennon, G.A., McIntosh, P. & Doorbar, J., 2011. Persistence of viral DNA in the epithelial basal layer suggests a model for papillomavirus latency following immune regression. *Virology*, 414(2), pp.153–163.

Majewski, S. & Jabłońska, S., 1995. Epidermodysplasia Verruciformis as a Model of Human Papillomavirus—Induced Genetic Cancer of the Skin. *Archives of Dermatology*, 131(11), pp.1312–1318.

Malladi, S. et al., 2009. The Apaf-1*procaspase-9 apoptosome complex functions as a proteolytic-based molecular timer. *The EMBO journal*, 28(13), pp.1916–1925.

Mammucari, C. et al., 2007. FoxO3 controls autophagy in skeletal muscle in vivo. *Cell metabolism*, 6(6), pp.458–471.

Marcuzzi, G.P. et al., 2009. Spontaneous tumour development in human papillomavirus type 8 E6 transgenic mice and rapid induction by UV-light exposure and wounding. *The Journal of general virology*, 90(Pt 12), pp.2855–2864.

Marcuzzi, G.P. et al., 2014. Tumor prevention in HPV8 transgenic mice by HPV8-E6 DNA vaccination. *Medical Microbiology and Immunology*, 203(3), pp.155–163.

Mariño, G. et al., 2014. Self-consumption: the interplay of autophagy and apoptosis. *Nature Reviews Molecular Cell Biology*, 15(2), pp.81–94.

Mathew, R., Karantza-Wadsworth, V. & White, E., 2007. Role of autophagy in cancer. *Nature Publishing Group*, 7(12), pp.961–967.

Mavromatis, K.O. et al., 1997. The carboxyl-terminal zinc-binding domain of the human papillomavirus E7 protein can be functionally replaced by the homologous sequences of the E6 protein. *Virus Research*, 52(1), pp.109–118.

McBride, A.A., 2008. Chapter 4 Replication and Partitioning of Papillomavirus Genomes. In Advances in Virus Research. Elsevier, pp. 155–205.

McBride, A.A., 2013. The Papillomavirus E2 proteins. *Virology*, 445(1-2), pp.57–79.

McBride, A.A., Bolen, J.B. & Howley, P.M., 1989. Phosphorylation sites of the E2 transcriptional regulatory proteins of bovine papillomavirus type 1. *Journal of virology*, 63(12), pp.5076–5085.

McFarlane, S. et al., 2011. Early induction of autophagy in human fibroblasts after infection with human cytomegalovirus or herpes simplex virus 1. *Journal of virology*, 85(9), pp.4212–4221.

Mesri, E.A., Feitelson, M.A. & Münger, K., 2014. Human viral oncogenesis: a cancer hallmarks analysis. *Cell host & microbe*, 15(3), pp.266–282.

Meyers, J.M. & Münger, K., 2013. The human papillomavirus type 8 E6 protein interferes with NOTCH activation during keratinocyte differentiation. *Journal of virology*, 87(8), pp.4762–4767.

Mizushima, N., 2010. The role of the Atg1/ULK1 complex in autophagy regulation. *Current Opinion in Cell Biology*.

Mizushima, N. & Klionsky, D.J., 2007. Protein Turnover Via Autophagy: Implications for Metabolism*. *Annu Rev Nutr*.

Mizushima, N., Yoshimori, T. & Levine, B., 2010. Methods in Mammalian Autophagy Research. *Cell*, 140(3), pp.313–326.

Moody, C.A. & Laimins, L.A., 2010. Human papillomavirus oncoproteins: pathways to transformation. *Nature Reviews Cancer*, 10(8), pp.550–560.

Morris, S., Cox, B. & Bosanquet, N. 2009. Cost of skin cancer in England. Eur J Health Econ,10, 267-73.

Morin, G. et al., 2011. A conserved amphipathic helix in the N-terminal regulatory region of the papillomavirus E1 helicase is required for efficient viral DNA replication. *Journal of virology*, 85(11), pp.5287–5300.

Moriyama, M. et al., 2014. BNIP3 plays crucial roles in the differentiation and maintenance of epidermal keratinocytes. *The Journal of investigative dermatology*, 134(6), pp.1627–1635.

Morselli, E. et al., 2011. p53 inhibits autophagy by interacting with the human ortholog of yeast Atg17, RB1CC1/FIP200. *Cell Cycle*, 10(16), pp.2763–2769.

Moscat, J. & Diaz-Meco, M.T., 2012. p62: a versatile multitasker takes on cancer. *Trends in biochemical sciences*, 37(6), pp.230–236.

Mueckler, M. & Thorens, B., 2013. The SLC2 (GLUT) family of membrane transporters. *Molecular Aspects of Medicine*, 34(2-3), pp.121–138.

Mukhopadhyay, S. et al., 2014. Autophagy and apoptosis: where do they meet?, 19(4), pp.555–566.

Münger, K., 2010. The human papillomavirus type 16 E6 oncoprotein activates mTORC1 signaling and increases protein synthesis. *Journal of virology*, 84(18), pp.9398–9407. Available at: http://jvi.asm.org/cgi/doi/10.1128/JVI.00974-10.

Muñoz, N., 2000. Human papillomavirus and cancer: the epidemiological evidence. *Journal of Clinical Virology*, 19(1-2), pp.1–5.

Nagata, S. & Golstein, P., 1995. The Fas death factor. *Science*, 267(5203),

pp.1449–1456.

Nakagawa, S. & Huibregtse, J.M., 2000. Human scribble (Vartul) is targeted for ubiquitin-mediated degradation by the high-risk papillomavirus E6 proteins and the E6AP ubiquitin-protein ligase. *Molecular and Cellular Biology*, 20(21), pp.8244–8253.

Nakahara, T. et al., 2002. Modulation of the cell division cycle by human papillomavirus type 18 E4. *Journal of virology*, 76(21), pp.10914–10920.

Narendra, D.P., 2011. Mechanisms of mitophagy. *Nature Reviews Molecular Cell Biology*, 12(1), pp.9–14.

Narendra, D.P. et al., 2010. PINK1 is selectively stabilized on impaired mitochondria to activate Parkin. *PLoS biology*, 8(1), p.e1000298.

Nasseri, M. et al., 1987. A human papilloma virus type 11 transcript encoding an E1^E4 protein. *Virology*, 159(2), pp.433–439.

Nechushtan, A., Smith, C.L. & Lamensdorf, I., 2001. Bax and Bak coalesce into novel mitochondria-associated clusters during apoptosis. *The Journal of cell …*.

Nishida, Y. et al., 2009. Discovery of Atg5/Atg7-independent alternative macroautophagy. *Nature*, 461(7264), pp.654–658.

Nominé, Y. et al., 2006. Structural and functional analysis of E6 oncoprotein: insights in the molecular pathways of human papillomavirus-mediated pathogenesis. *Molecular cell*, 21(5), pp.665–678.

Ogier-Denis, E. et al., 2000. Erk1/2-dependent Phosphorylation of G -interacting Protein Stimulates Its GTPase Accelerating Activity and Autophagy in Human Colon Cancer Cells. *Journal of Biological Chemistry*, 275(50), pp.39090–39095.

Oh, S.T., Kyo, S. & Laimins, L.A., 2001. Telomerase activation by human papillomavirus type 16 E6 protein: induction of human telomerase reverse transcriptase expression through Myc and GC-rich Sp1 binding sites. *Journal of virology*, 75(12), pp.5559–5566.

Olivier, M. et al., 2004. TP53 mutation spectra and load: a tool for generating hypotheses on the etiology of cancer. *IARC scientific publications*, (157), pp.247–270.

Orsi, A. et al., 2012. Dynamic and transient interactions of Atg9 with autophagosomes, but not membrane integration, are required for autophagy. *Molecular biology of the cell*, 23(10), pp.1860–1873.

Orth, G. et al., 1978. Characterization of two types of human papillomaviruses in lesions of epidermodysplasia verruciformis. *Proceedings of the National Academy of Sciences*, 75(3), pp.1537–1541.

Orvedahl, A. et al., 2010. Autophagy protects against Sindbis virus infection of the central nervous system. *Cell host & microbe*, 7(2), pp.115–127.

Ostenfeld, M.S. et al., 2008. Anti-cancer agent siramesine is a lysosomotropic detergent that induces cytoprotective autophagosome accumulation. *Autophagy*, 4(4), pp.487–499.

Pankiv, S. et al., 2007. p62/SQSTM1 Binds Directly to Atg8/LC3 to Facilitate Degradation of Ubiquitinated Protein Aggregates by Autophagy. *Journal of Biological Chemistry*, 282(33), pp.24131–24145.

Peng, Y.C. et al., 2000. AMF-1/Gps2 binds p300 and enhances its interaction with papillomavirus E2 proteins. *Journal of virology*, 74(13), pp.5872–5879.

Perfettini, J.-L., Kroemer, R.T. & Kroemer, G., 2004. Fatal liaisons of p53 with Bax and Bak. *nature cell biology*, 6(5), pp.386–388.

Pfeifer, G.P. & Besaratinia, A., 2012. UV wavelength-dependent DNA damage and human non-melanoma and melanoma skin cancer. *Photochemical & Photobiological Sciences*, 11(1), pp.90–97.

Pfister, H., 2003. Human papillomavirus and skin cancer.

Phelps, W.C. et al., 1992. Structure-function analysis of the human papillomavirus type 16 E7 oncoprotein. *Journal of virology*, 66(4), pp.2418–2427.

Pincelli, C. & Marconi, A., 2010. Keratinocyte stem cells: Friends and foes. *Journal of cellular physiology*, 225(2), pp.310–315.

Prabhakara, V.G. et al., 1996. Chloroquine-induced photosensitive dermatoses. *Indian journal of dermatology, venereology and leprology*, 62(3), pp.165–166.

Pratt, Z.L. & Sugden, B., 2012. How Human Tumor Viruses Make Use of Autophagy. *Cells*, 1(3), pp.617–630.

Proby, C.M. et al., 2011. A case-control study of betapapillomavirus infection and cutaneous squamous cell carcinoma in organ transplant recipients. *American journal of transplantation : official journal of the American Society of Transplantation and the American Society of Transplant Surgeons*, 11(7), pp.1498–1508.

Proby, C.M. et al., 2000. Spontaneous keratinocyte cell lines representing early and advanced stages of malignant transformation of the epidermis. *Experimental dermatology*, 9(2), pp.104–117.

Pustišek, N. & Šitum, M., 2011. UV-radiation, apoptosis and skin. *Collegium antropologicum*.

Quint, K.D. et al., 2015. Human Beta-papillomavirus infection and keratinocyte carcinomas. *The Journal of pathology*, 235(2), pp.342–354.

Rabinowitz, J.D. & White, E., 2010. Autophagy and metabolism. *Science*, 330(6009), pp.1344–1348.

Ramoz, N. et al., 1999. A susceptibility locus for epidermodysplasia verruciformis, an abnormal predisposition to infection with the oncogenic human papillomavirus type 5, maps to chromosome 17qter in a region containing a

psoriasis locus. *Journal of Investigative Dermatology*, 112(3), pp.259–263.

Ramoz, N. et al., 2002. Mutations in two adjacent novel genes are associated with epidermodysplasia verruciformis. *Nature Genetics*, 32(4), pp.579–581.

Rasheed, S. et al., 1974. Characterization of a newly derived human sarcoma cell line (HT-1080). *Cancer*, 33(4), pp.1027–1033.

Ravikumar, B. et al., 2010. Plasma membrane contributes to the formation of pre-autophagosomal structures. *nature cell biology*, 12(8), pp.747–757.

Roman, A. & Münger, K., 2013. The papillomavirus E7 proteins. *Virology*, 445(1-2), pp.138–168.

Rubinsztein, D.C., BRINDA RAVIKUMAR, S.S.J.E.D.M.F.M.G.-A.Z.W.G.-T.M.J.-S.V.I.K.M.L.S.L.D.C.O.M.F.M.M.K.M.U.N.M.R.F.H.S.B.R.U.A.R.W. & Ravikumar, B., 2010. Regulation of mammalian autophagy in physiology and pathophysiology. *Physiological Reviews*, 90(4), pp.1383–1435.

Sarah Jackson, C.H.M.T.L.B. & Storey, A., 2000. Role of Bak in UV-induced apoptosis in skin cancer and abrogation by HPV E6 proteins. *Genes & Development*, 14(23), pp.3065–3073.

Scaffidi, C. et al., 1999. The role of c-FLIP in modulation of CD95-induced apoptosis. *Journal of Biological Chemistry*, 274(3), pp.1541–1548.

Schaper, I.D. et al., 2005. Development of skin tumors in mice transgenic for early genes of human papillomavirus type 8. *Cancer Research*, 65(4), pp.1394–1400.

Scheffner, M. et al., 1990. The E6 oncoprotein encoded by human papillomavirus types 16 and 18 promotes the degradation of p53. *Cell*, 63(6), pp.1129–1136.

Schiffman, M. & Kjaer, S.K., 2003. Chapter 2: Natural History of Anogenital Human Papillomavirus Infection and Neoplasia. *JNCI Monographs*, 2003(31), pp.14–19.

Schiller, J.T. & Lowy, D.R., 2012. Understanding and learning from the success of prophylactic human papillomavirus vaccines. *Nature reviews. Microbiology*, 10(10), pp.681–692.

Schiller, J.T., Day, P.M. & Kines, R.C., 2010. Current understanding of the mechanism of HPV infection. *Gynecologic oncology*, 118(1 Suppl), pp.S12–7.

Schneider, J.L. & Cuervo, A.M., 2014. Autophagy and human disease: emerging themes. *Current opinion in genetics & development*, 26C, pp.16–23.

Schneider-Brachert, W., Heigl, U. & Ehrenschwender, M., 2013. Membrane trafficking of death receptors: implications on signalling. *International Journal of Molecular Sciences*, 14(7), pp.14475–14503.

Sessler, T. et al., 2013. Structural determinants of DISC function: new insights into death receptor-mediated apoptosis signalling. *Pharmacology & therapeutics*, 140(2), pp.186–199.

Shen, S., Kepp, O. & Kroemer, G., 2014. The end of autophagic cell death?

dx.doi.org.

Shimizu, S., Kanaseki, T., Mizushima, N., Mizuta, T., Arakawa-Kobayashi, S., Thompson, C.B. & Tsujimoto, Y., 2004a. Role of Bcl-2 family proteins in a non-apoptotic programmed cell death dependent on autophagy genes. *nature cell biology*, 6(12), pp.1221–1228.

Shimizu, S., Kanaseki, T., Mizushima, N., Mizuta, T., Arakawa-Kobayashi, S., Thompson, C.B. & Tsujimoto, Y., 2004b. Role of Bcl-2 family proteins in a non-apoptotic programmed cell death dependent on autophagy genes. *nature cell biology*, 6(12), pp.1221–1228.

Shterzer, N. et al., 2014. Human papillomavirus types detected in skin warts and cancer differ in their transforming properties but commonly counteract UVB induced protective responses in human keratinocytes. *Virology*, 468-470(C), pp.647–659.

Simmonds, M. & Storey, A., 2008. Identification of the regions of the HPV 5 E6 protein involved in Bak degradation and inhibition of apoptosis. *International Journal of Cancer*, 123(10), pp.2260–2266.

Singh, R. et al., 2009. Autophagy regulates lipid metabolism. *Nature*, 458(7242), pp.1131–1135.

Sinha, R.P. & Häder, D.-P., 2002. UV-induced DNA damage and repair: a review. *Photochemical & Photobiological Sciences*, 1(4), pp.225–236.

Slominski, A. et al., 2003. The skin as a model for the immunodulatory effects of corticotropin-releasing hormone. *… inflammation by the …*.

Soupene, E. & Kuypers, F.A., 2008. Mammalian long-chain acyl-CoA synthetases. *Experimental biology and medicine*, 233(5), pp.507–521.

Sprick, M.R. et al., 2002. Caspase-10 is recruited to and activated at the native TRAIL and CD95 death-inducing signalling complexes in a FADD-dependent manner but can not functionally substitute caspase-8. *The EMBO journal*, 21(17), pp.4520–4530.

Steger, G. & Pfister, H., 1992. In vitro expressed HPV 8 E 6 protein does not bind p 53. *Archives of Virology*, 125(1-4), pp.355–360.

Steger, G., Ham, J. & Yaniv, M., 1996. E2 proteins: Modulators of papillomavirus transcription and replication. In *RNA Polymerase and Associated Factors, Part B*. Methods in Enzymology. Elsevier, pp. 173–185.

Stockman, J.A., III, 2006. Regression of Low-Grade Squamous Intra-epithelial Lesions in Young Women. *Yearbook of Pediatrics*, 2006, pp.20–22.

Stransky, N. et al., 2011. The mutational landscape of head and neck squamous cell carcinoma. *Science*, 333(6046), pp.1157–1160.

Struijk, L. et al., 2008. Specific betapapillomaviruses associated with squamous cell carcinoma of the skin inhibit UVB-induced apoptosis of primary human keratinocytes. *Journal of General Virology*, 89(9), pp.2303–2314.

Sun, Y. et al., 2012. Inhibition of autophagy ameliorates acute lung injury caused by avian influenza A H5N1 infection. *Science Signaling*, 5(212), p.ra16.

Surviladze, Z. et al., 2013. Cellular entry of human papillomavirus type 16 involves activation of the phosphatidylinositol 3-kinase/Akt/mTOR pathway and inhibition of autophagy. *Journal of virology*, 87(5), pp.2508–2517.

Suzuki, M., Youle, R.J. & Tjandra, N., 2000. Structure of Bax: coregulation of dimer formation and intracellular localization. *Cell*.

Suzuki, Y. et al., 2001. A serine protease, HtrA2, is released from the mitochondria and interacts with XIAP, inducing cell death. *Molecular cell*, 8(3), pp.613–621.

Tait, S.W.G. & Green, D.R., 2010. Mitochondria and cell death: outer membrane permeabilization and beyond. *Nature Reviews Molecular Cell Biology*, 11(9), pp.621–632.

Tait, S.W.G. & Green, D.R., 2013. Mitochondrial Regulation of Cell Death. *Cold Spring Harbor Perspectives in Biology*, 5(9), p.a008706.

Tan, M.J.A. et al., 2012. Cutaneous β-human papillomavirus E6 proteins bind Mastermind-like coactivators and repress Notch signaling. *Proceedings of the National Academy of Sciences of the United States of America*, 109(23), pp.E1473–80.

Terenzi, F., Saikia, P. & Sen, G.C., 2008. Interferon-inducible protein, P56, inhibits HPV DNA replication by binding to the viral protein E1. *The EMBO journal*, 27(24), pp.3311–3321.

Tessman, I., Liu, S.K. & Kennedy, M.A., 1992. Mechanism of SOS mutagenesis of UV-irradiated DNA: mostly error-free processing of deaminated cytosine. *Proceedings of the National Academy of Sciences*, 89(4), pp.1159–1163.

Thastrup, O., 1990. Role of Ca2+-ATPases in regulation of cellular Ca2+ signalling, as studied with the selective microsomal Ca2+-ATPase inhibitor, thapsigargin. *Agents and Actions*, 29(1-2), pp.8–15.

Thomas, M. & Banks, L., 1999. Human papillomavirus (HPV) E6 interactions with Bak are conserved amongst E6 proteins from high and low risk HPV types. *The Journal of general virology*, 80 (Pt 6), pp.1513–1517.

Titolo, S. et al., 2000. Identification of domains of the human papillomavirus type 11 E1 helicase involved in oligomerization and binding to the viral origin. *Journal of virology*, 74(16), pp.7349–7361.

Tjon Pian Gi, R.E.A. et al., 2014. Clinical course of recurrent respiratory papillomatosis: Comparison between aggressiveness of human papillomavirus-6 and human papillomavirus-11. *Head & Neck*, pp.n/a–n/a.

Tooze, S.A. & Yoshimori, T., 2010. The origin of the autophagosomal membrane. *nature cell biology*, 12(9), pp.831–835.

Tsujimoto, Y. et al., 1985. Involvement of the bcl-2 gene in human follicular lymphoma. *Science*, 228(4706), pp.1440–1443.

Underbrink, M.P. et al., 2008. E6 Proteins from Multiple Human Betapapillomavirus Types Degrade Bak and Protect Keratinocytes from Apoptosis after UVB Irradiation. *Journal of virology*, 82(21), pp.10408–10417.

Valencia, S.M. & Hutt-Fletcher, L.M., 2012. Important but differential roles for actin in trafficking of Epstein-Barr virus in B cells and epithelial cells. *Journal of virology*, 86(1), pp.2–10.

Vallejo-Torres, L., Morris, S., Kinge, J., Poirier, V. & Verne, J. 2011. Cost of skin cancer in England. The Economics of Cancer Workshop. The Ambassadors Bloomsbury,Upper Woburn Place, London.

Vande Pol, S.B. & Klingelhutz, A.J., 2013. Papillomavirus E6 oncoproteins. *Virology*, 445(1-2), pp.115–137.

Venuti, A. et al., 2011. Papillomavirus E5: the smallest oncoprotein with many functions. *Molecular Cancer*, 10, p.140.

Verhagen, A.M. et al., 2000. Identification of DIABLO, a mammalian protein that promotes apoptosis by binding to and antagonizing IAP proteins. *Cell*, 102(1), pp.43–53.

Vessoni, A.T., Muotri, A.R. & Okamoto, O.K., 2012. Autophagy in Stem Cell Maintenance and Differentiation. *Stem Cells and Development*, p.120118064452007.

Viarisio, D. et al., 2011. E6 and E7 from beta HPV38 cooperate with ultraviolet light in the development of actinic keratosis-like lesions and squamous cell carcinoma in mice. P. Lambert, ed. *PLoS Pathogens*, 7(7), p.e1002125.

Vucic, D., Dixit, V.M. & Wertz, I.E., 2011. Ubiquitylation in apoptosis: a post-translational modification at the edge of life and death. *Nature Reviews Molecular Cell Biology*, 12(7), pp.439–452.

Walczak, M. & Martens, S., 2013. Dissecting the role of the Atg12-Atg5-Atg16 complex during autophagosome formation. *Autophagy*, 9(3), pp.424–425.

Wallace, N.A. et al., 2012. HPV 5 and 8 E6 Abrogate ATR Activity Resulting in Increased Persistence of UVB Induced DNA Damage. *PLoS Pathogens*, 8(7), p.e1002807.

Wang, J.W. & Roden, R.B.S., 2013. L2, the minor capsid protein of papillomavirus. *Virology*, 445(1-2), pp.175–186.

Warburg, O., 1956. On the origin of cancer cells. *Science*.

Wållberg, F., Tenev, T. & Meier, P., 2013. Time-Lapse Imaging of Necrosis. In *Methods in Molecular Biology*. Totowa, NJ: Humana Press, pp. 17–29.

Weidberg, H. et al., 2010. LC3 and GATE-16/GABARAP subfamilies are both essential yet act differently in autophagosome biogenesis. *The EMBO …*.

Wen, H.-J. et al., 2010. Enhancement of Autophagy during Lytic Replication by the Kaposi's Sarcoma-Associated Herpesvirus Replication and Transcription

Activator. *Journal of virology*, 84(15), pp.7448–7458.

White, E., 2012. Deconvoluting the context-dependent role for autophagy in cancer. *Nature Reviews Cancer*, 12(6), pp.401–410.

Wiley, S.R. et al., 1995. Identification and characterization of a new member of the TNF family that induces apoptosis. *Immunity*, 3(6), pp.673–682.

Wilson, R. et al., 2007. The full-length E1^E4 protein of human papillomavirus type 18 modulates differentiation-dependent viral DNA amplification and late gene expression. *Virology*, 362(2), pp.453–460.

Wilson, V.G. et al., 2002. Papillomavirus E1 proteins: form, function, and features. *Virus genes*, 24(3), pp.275–290.

Wirawan, E. et al., 2011. Autophagy: for better or for worse. *Cell Research*, 22(1), pp.43–61.

Wolter, K.G. et al., 1997. Movement of Bax from the cytosol to mitochondria during apoptosis. *The Journal of cell biology*, 139(5), pp.1281–1292.

Yamamoto, A. et al., 1998. Bafilomycin A1 prevents maturation of autophagic vacuoles by inhibiting fusion between autophagosomes and lysosomes in rat hepatoma cell line, H-4-II-E cells. *Cell structure and function*, 23(1), pp.33–42.

Yang, S. et al., 2011. Pancreatic cancers require autophagy for tumor growth., 25(7), pp.717–729.

Yang, Z. & Klionsky, D.J., 2010a. Mammalian autophagy: core molecular machinery and signaling regulation. *Current Opinion in Cell Biology*, 22(2), pp.124–131.

Yang, Z. & Klionsky, D.J., 2010b. Mammalian autophagy: core molecular machinery and signaling regulation. *Current Opinion in Cell Biology*, 22(2), pp.124–131.

You, B.R. & Park, W.H., 2010. The effects of antimycin A on endothelial cells in cell death, reactive oxygen species and GSH levels. *Toxicology in Vitro*, 24(4), pp.1111–1118.

Zhang, J. & Ney, P.A., 2009. Role of BNIP3 and NIX in cell death, autophagy, and mitophagy. *Cell Death & Differentiation*, 16(7), pp.939–946.

Zhou, F., Yang, Y. & Xing, D., 2011. Bcl-2 and Bcl-xL play important roles in the crosstalk between autophagy and apoptosis. *FEBS Journal*, 278(3), pp.403–413.

Zmijewski, M.A. & Slominski, A.T., 2011. Neuroendocrinology of the skin. *dx.doi.org*, 3(1), pp.3–10.